

# Macroreticular Resins. III. Formation of Macroreticular Styrene- Divinylbenzene Copolymers

KENNETH A. KUN and ROBERT KUNIN, *Research Laboratories,  
Rohm and Haas Company, Philadelphia, Pennsylvania*

## Synopsis

Experimental evidence is presented that describes the mechanism of formation of macroreticular styrene-divinylbenzene copolymers in which phase separation occurs during a suspension polymerization. The mode of formation of the macroreticular structure is described as a three-stage process in which each droplet of the organic phase behaves as an individual in a bulk polymerization that results in a bead of copolymer. Macroreticular structure formation is described by changes in copolymer swelling ratios, infrared absorption spectra of vinyl groups pendent to the polymeric matrices, surface area, total porosity, and pore-size distribution. The proposed mechanism of formation is also substantiated by electron micrographs of the copolymers during various stages of the copolymerization.

## INTRODUCTION

The development of a new polymerization technique by Meitzner and Oline<sup>1</sup> has provided novel matrices for a series of new ion-exchange resins,<sup>2-5</sup> synthetic adsorbents,<sup>6</sup> and oxidation-reduction polymers.<sup>7,8</sup> The materials differ from the older, corresponding copolymers that are characterized as essentially crosslinked gels of polyelectrolytes, whose pores are defined as the distances between polymeric chains. Such a structure may also be described as "gel-phase molecular porosity" and be considered *microreticular*. *Macroreticular* resins, by contrast, contain a significant nongel porosity in addition to the conventional gel porosity. The nongel interstices of the styrene-divinylbenzene macroreticular resins are channels between agglomerates of minute spherical gel particles. Electron micrographs show the conventional gel resins to be a nonporous, continuous polymeric phase, whereas the macroreticular resins are agglomerates of randomly packed microspheres with a continuous nongel structure or a continuous gel structure permeated with holes and channels similar to those found in bone char or alumina. The gel phase of a macroreticular structure may be continuous or discontinuous.<sup>4</sup>

Other workers in the field of synthetic ion-exchange resins also have prepared by various techniques macroreticular styrene-divinylbenzene

matrices with a variety of structures. Millar et al.<sup>9-12</sup> prepared expanded microreticular, or gel-phase, structures and macroreticular, or macroporous, structures by varying the proportions of styrene, divinylbenzene, and solvent in solutions of monomers prior to polymerization. Seidl, Malinsky, and Dusek,<sup>13-19</sup> Lyustgarten et al.,<sup>20</sup> Abrams,<sup>21,22</sup> Bortel,<sup>23</sup> and Tevlina and Sadova<sup>24</sup> describe the formation of macroreticular polymers by copolymerizations with solvents for the monomers and copolymerizations in the presence of nonpolymerizing materials.

Since the first reports describing the effects produced by phase separation during suspension polymerization<sup>1</sup> both the mechanism of formation and the structure of macroreticular resins have been of constant interest. In previous publications the nongel pore structure of macroreticular ion exchangers<sup>4,5</sup> and redox polymers<sup>7,25,26</sup> are described. The purpose of this study is to provide an experimental basis for the mechanism of formation of the macroreticular structure during a polymerization involving phase separation.

## PLAN OF STUDY

The polymerization procedure of Meitzner and Oline<sup>27,28</sup> was used, in which only the styrene-divinylbenzene ratio was changed. The polymerization temperature was kept constant at 80°C. Three levels of crosslinking were examined, so that at least one level would show significant changes in properties during the polymerization. Levels of 3, 10, and 20% divinylbenzene were used to give structures that were lightly and highly crosslinked.

The experimental procedure for following the formation of the macroreticular structures during suspension polymerizations involved the removal of a series of aliquots from the suspension mixture as the reaction proceeded. Each sample was immediately quenched in a large excess of methanol containing hydroquinone, so as to terminate the polymerization and precipitate the polymer. Only the insoluble, or crosslinked, copolymers were examined. The crosslinked fractions were isolated, washed free of monomers, extender, and soluble polymers, and dried *in vacuo* to constant weight. The physical and chemical properties of the fractions were then examined.

## RESULTS AND DISCUSSION

### Swelling Ratios

Swelling ratios of crosslinked copolymers are an indirect measure of crosslinking. As the degree of crosslinking increases, the relative extent of swelling in a particular "good swelling liquid" decreases. Following changes in the swelling ratio as a function of polymerization time can be used as a measure of the physical changes taking place in the polymeric matrices, i.e., the changes in the degree of crosslinking. Figure 1 shows the

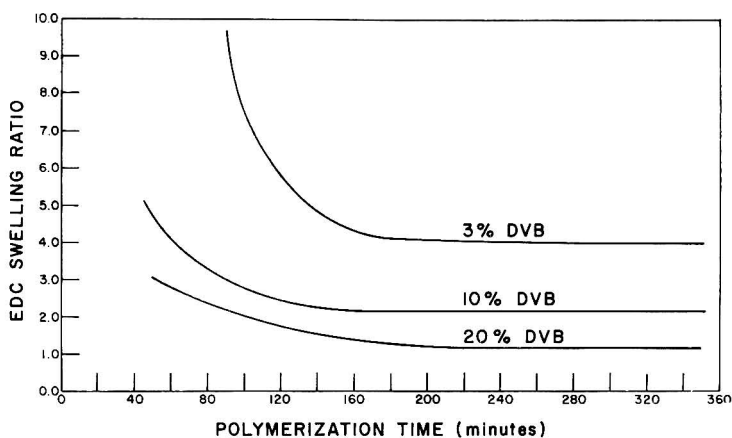


Fig. 1. Ethylene dichloride swelling ratio of polymer fractions at various divinylbenzene levels.

changes in ethylene dichloride swelling ratios of copolymers containing 3, 10, and 20% divinylbenzene in the initial monomer formulations. The most significant changes in structure take place within the first 180 min. of the polymerization cycle. The physical appearances of the various fractions in ethylenedichloride clearly show the transition from a very loose, amorphous gel, through a series of stages, to spherical beads having a macroreticular structure. Figure 2 shows the transformation of the resins from the gel stage to the milk-white stage characteristic of macroreticular

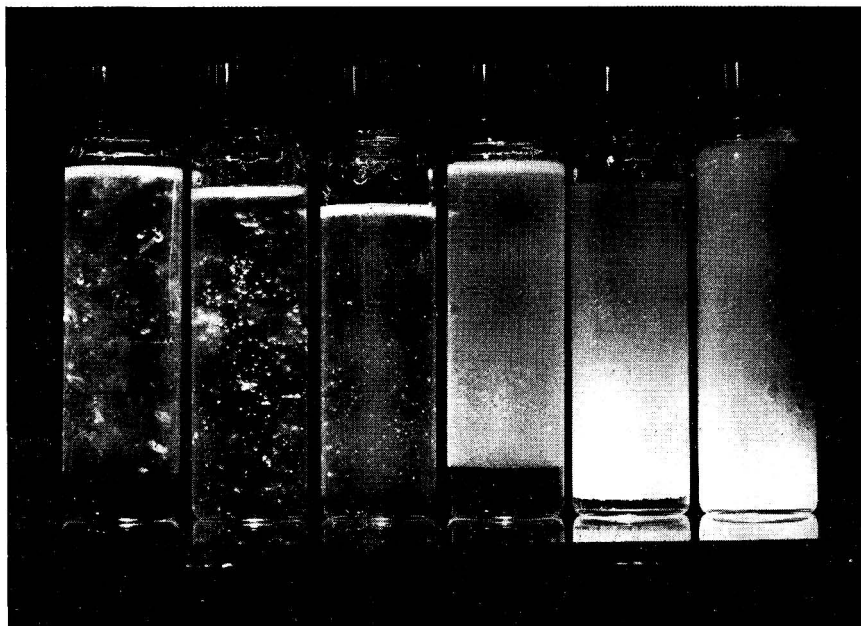


Fig. 2. Transformation of gel-like structure to macroreticular structure.

copolymers of 3% divinylbenzene formulation. Clear and translucent beads are characteristic of the conventional gel structures and are indications that the materials have negligible surface areas and porosities. The opaque, white appearance of the copolymer is characteristic of macroreticularity. Similar patterns may be seen, but not as dramatically, at the 10 and 20% divinylbenzene levels; here the isolated beads have macroreticular structures even at the very early stages of polymerization.

### Infrared Absorption Spectra of Pendent Vinyl Groups

The infrared absorption spectra of the crosslinked copolymers at the early stages of polymerization showed significant absorption in the region characterized by vinyl groups. Since the vinyl groups are part of the polymeric matrix, they must be the unreacted or pendent vinyl groups of the divinylbenzene units that are incorporated in the copolymer. The infrared spectra of polymers isolated during the polymerizations at the 10 and 20% divinylbenzene levels were obtained, and the relative concentrations of pendent vinyl groups were measured from the ratios of transmittance at 9.75 and 10.15  $\mu$ . Plots of these ratios versus polymerization time are shown in Figure 3. The absorption at 9.75  $\mu$  is a characteristic peak found in polystyrenes and therefore is used as the reference peak for the absorption at 10.15  $\mu$ , one of the peaks associated with a monosubstituted vinyl group. Ratios of these absorption peaks show that the relative concentration of pendent vinyl groups decreases as the polymerization proceeds. This, of course, is expected. The kinetics of the styrene-divinylbenzene polymerization indicates that there is a greater relative concentration of divinylbenzene in the copolymer in the early stages of the polymerization than in the late stages.<sup>29</sup> During the early stages of

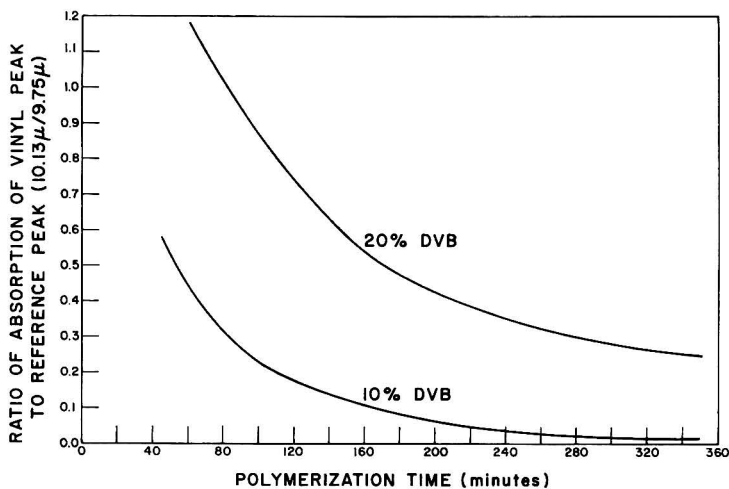


Fig. 3. Relative rate of loss of vinyl groups pendent to polymeric matrix during a copolymerization.

the polymerization the gel structure is very lightly crosslinked and, as the polymerization proceeds, the pendent vinyl groups react with monomers and other growing polymer chains. The curves in Figure 3 indicate that the fractional rate of loss of pendent vinyl groups is not appreciably affected by divinylbenzene concentrations of more than 10% and that the structures containing high concentrations of divinylbenzene are sufficiently rigid to "freeze in" some pendent vinyl groups. These data indicate that a homogeneous or a uniform distribution of crosslinks does not exist in the styrene-divinylbenzene copolymer matrix. This is true of both microreticular and macroreticular structures. This conclusion has a significant bearing on the theoretical ion-exchange selectivity and rate measurements of ion exchange resins prepared from all styrene-divinylbenzene copolymers.

### Surface Areas

Macroreticular structures are characterized by having unusually large surface areas compared with those of the conventional gel structures. By measuring changes in the surface area of the copolymer during the polymerization cycle the formation of macroreticular structures was followed at various crosslinker concentrations. Figure 4 shows the relationship between surface area and polymerization time at two divinylbenzene levels. At the 20% divinylbenzene level the first isolated, crosslinked copolymer sample had a surface area of 1.5 m.<sup>2</sup>/g. During the next 22 min. of polymerization the surface area rapidly increased to 38.7 m.<sup>2</sup>/g. and then slowly increased to 48.8 m.<sup>2</sup>/g. at 162 min. after the beginning of polymerization. The surface area then did not change significantly until the 258 min. mark, where a slight decrease was observed. At the termination of the polymerization cycle (348 min.) the surface area fell to 37.7 m.<sup>2</sup>/g. A similar pattern was observed in the polymerization with 3% divinylbenzene. Because of the very low degree of crosslinking in the samples the first copolymer sample isolated at the 90 min. mark had a

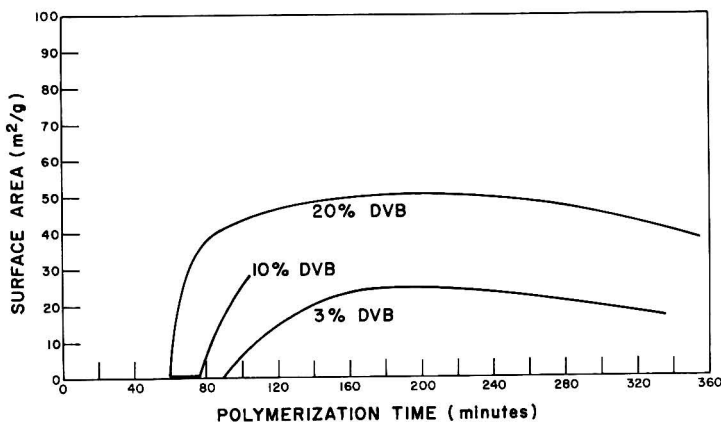


Fig. 4. Surface area changes of copolymer during polymerization.

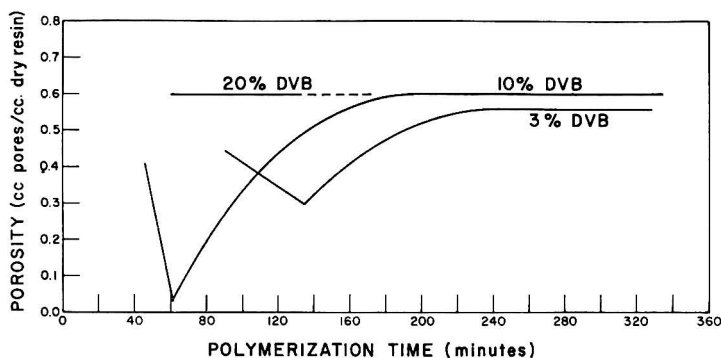


Fig. 5. Total porosity changes in copolymer during polymerization.

surface area of less than  $1 \text{ m}^2/\text{g}$ . The surface area of this material increased to  $9.2 \text{ m}^2/\text{g}$  at 105 min. and approached a maximum of  $24.5 \text{ m}^2/\text{g}$  at 165 min. As in the polymerization with 20% divinylbenzene, the surface area remained more or less constant to the 225 min. mark and then slowly decreased to  $16.7 \text{ m}^2/\text{g}$  at the end of the polymerization cycle.

Plots of surface area versus polymerization time, Figure 4, show increases in surface area during the formation of the macroreticular structure and also indicate a change in structure on continued heating. The change in structure appears to be characterized by a decrease in surface area at about 225 min. after the beginning of polymerization. In both the 3% and the 20% divinylbenzene polymerization series the surface area started to decrease at about the same time during the polymerization cycle, and the rate of decrease appeared to be similar in both cases.

### Total Porosity

The total porosity values for the macroreticular copolymers were determined from the apparent and skeletal densities of copolymers, taken during the polymerizations at 3, 10, and 20% divinylbenzene levels. Plots of changes in total porosity as a function of polymerization time are shown in Figure 5. A comparison of the total porosity values of the three series indicates that the first polymer isolated in the 20% divinylbenzene suspension already had a porosity of  $0.6 \text{ cm}^3$  of pores per cubic centimeter of copolymer, and the remaining samples were in the same range for the entire polymerization at the 20% crosslinker level. The isolated fractions from this series have a constant nongel porosity while the surface area is increasing from 1.5 to  $48.8 \text{ m}^2/\text{g}$ . In the series containing 10% crosslinker a decrease in nongel porosity, followed by an increase, is observed. The crosslinker copolymer isolated after 45 min. has a nongel porosity of  $0.41 \text{ cm}^3$  of pores per cubic centimeter of copolymer. At 60 min. the nongel porosity falls to  $0.03 \text{ cm}^3$ , and then it increases:  $0.17 \text{ cm}^3$  at 75 min.,  $0.29 \text{ cm}^3$  at 95 min., and so on, until it reaches  $0.60 \text{ cm}^3$  at 165 min., at which it remains to the end of the polymerization cycle.

A similar pattern is observed in the polymerization containing 3% divinylbenzene. Here also decreases followed by increases in nongel porosity are taking place while the surface area of the copolymer beads are continually increasing. It must be remembered that the isolated polymeric fractions are not "finished" copolymers such as normally found in the final product. These copolymers, at the very early stages in the polymerization, are loose gel structures resembling a large mesh network. Such structures have significant porosities but very low surface areas. As the polymerization proceeds, macrogelation takes place, giving finite beads, within which the macroreticular structure is forming.

### Mode of Pore-Structure Formation

The mode of formation of the macroreticular structure can be now described as a three-stage process in which each droplet of the organic phase behaves as an individual bulk polymerization that results in a bead of copolymer. Each droplet is composed of a solution of monomers, the initiator and the extender; it is suspended in an aqueous solution. During the early stages of the polymerization a polymer is formed that is composed of straight chains with pendent vinyl groups. Continued polymerization yields intramolecularly crosslinked microgels and higher molecular weight linear chains that are soluble in the monomer-extender solvent system. The reaction temperature, crosslinker concentration, and extender concentration determine when the polymer-phase separation occurs. This separation gives a copolymer-rich phase and an extender phase with a very low polymer concentration, the monomers being distributed between the two phases. Since solvated and very lightly crosslinked copolymers can behave, in some respects, like a liquid, the interfacial tension on the polymer-rich phase gives it the low-energy spherical form, and the polymer separates as a mass of microspheres. At a certain conversion of monomer to polymer macrogelation occurs and gives a gel type of bead composed of an agglomeration of microgels. The first stage in the formation of a macroreticular structure is the production and agglomeration of gel microspheres such that they make a bead of copolymer. As the polymerization and formation of microspheres continue, the microspheres are bound together by the polymerization of the monomers solvating the microspherical polymers.

The second stage in pore-structure formation is the binding together of the microspheres while the polymerization continues. It is during this stage that the macroreticular structure is actually forming. Though the characteristics of the pore are dependent upon the formation of microspheres in the first stage, the nongel structure is not formed until the second stage. During the second stage there are compositional changes, in which the concentration of monomers in the extender are decreasing, the ratio of crosslinker to monomer is varying according to the reactivity of the growing radicals to various types of vinyl compound, i.e., styrene or divinylbenzene, and the extender concentration is increasing.

Late in the polymerization cycle, in the third stage, the macroreticular structure is formed, and the concentration of monomer in the extender phase is low. During this stage the rate of polymerization has decreased; however, when the reaction mixture is heated and the extender removed by steam distillation, the rate of polymerization is increased again. The reconcentration of monomer through the removal of the extender drives the unreacted monomer into the polymer phase, where this monomer then polymerizes.

### Pore-Structure Changes during Copolymer Synthesis

The changes in pore structure during the formation of macroreticular structures can be observed by the examination of thin sections (about 500 Å.) of these resins with an electron microscope. Figure 6 shows three electron micrographs that represent the three stages of pore formation during the polymerization of a styrene-divinylbenzene (3%) formulation

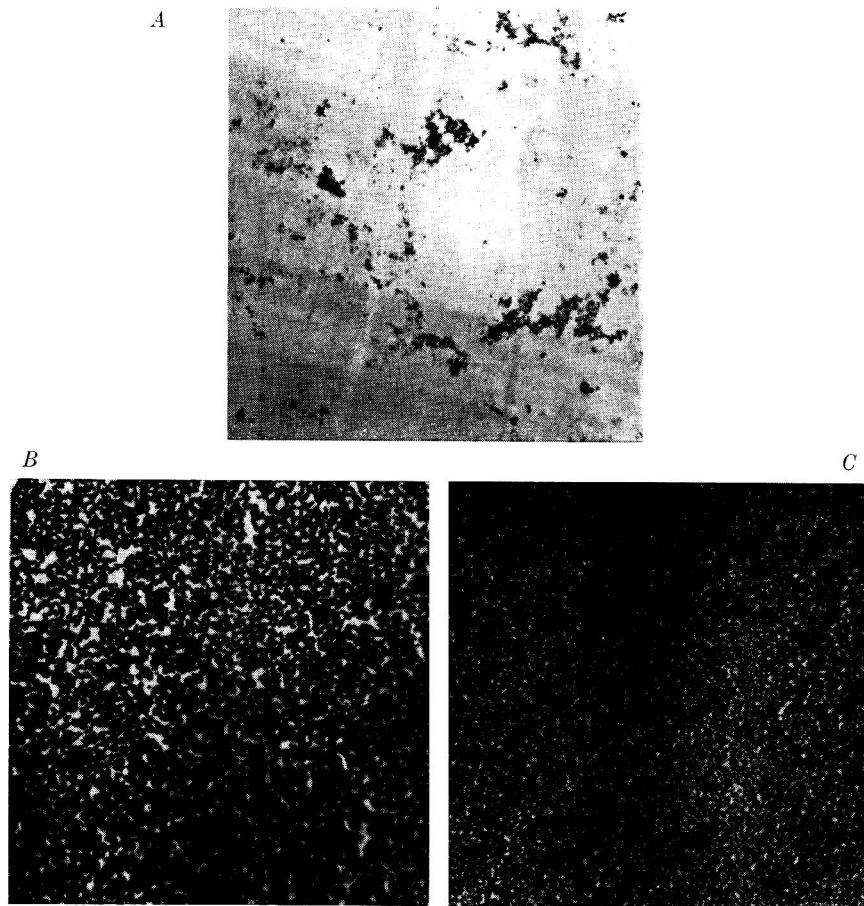


Fig. 6. Electron micrographs of thin sections at various stages in a 3% divinylbenzene-styrene copolymerization.

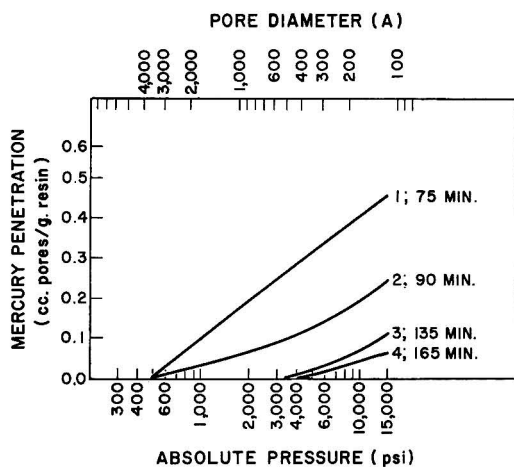


Fig. 7. Pore-structure changes during agglomeration of microspheres.

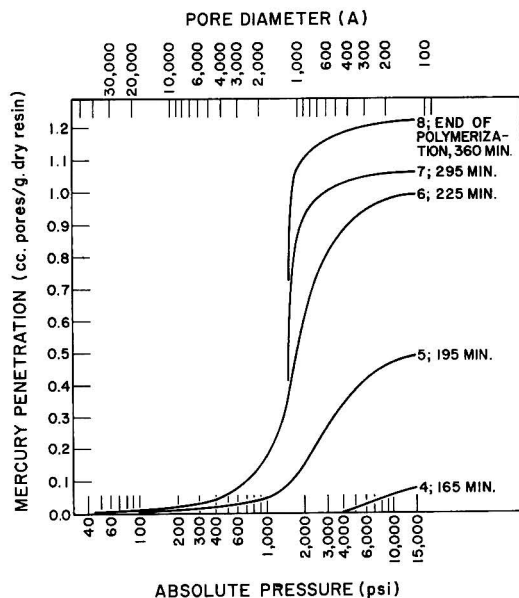


Fig. 8. Pore-structure changes during formation of macroreticular structure.

of monomers. Figure 6A shows the first stage, in which a large continuous gel phase contains small areas of agglomerates of microspheres. Figure 6B shows the second stage, in which the macroreticular structure has pores with very large diameters. Figure 6C shows the third stage, in which the finished copolymer has pores of smaller diameters and a fairly uniform pore-size distribution.

Using the previously described methods of determining pore size, pore-size distribution, and total porosity from apparent and skeletal densities<sup>4</sup> the changes in pore-structure characteristics during the polymerization

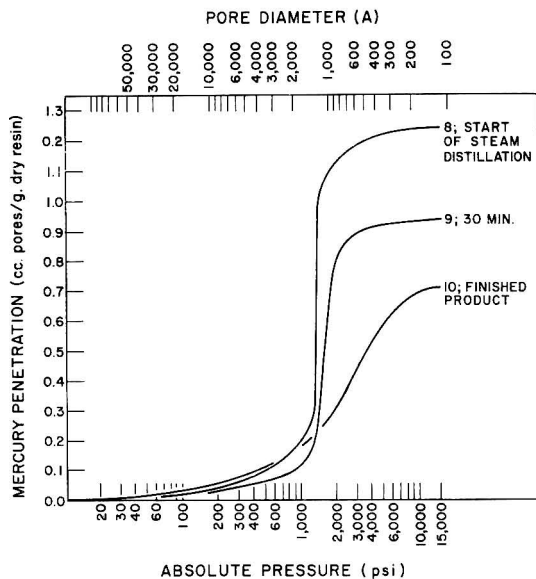


Fig. 9. Pore-structure collapse during "solvent-nonsolvent" removal.

were determined. Figures 7, 8, and 9 show the changes in pore structure by a series of pore-size distribution spectra. During the early part of the polymerization agglomerates of lightly crosslinked microspheres are forming. Figure 7 shows the pore spectra of the copolymer when the agglomeration is increasing from a loose grouping of highly swollen microgels having a random pore-size distribution (curve 1) to a material composed of tightly packed, lightly crosslinked gel masses (curve 4). At 75 min. after the initiation of the polymerization the beads of copolymer have a random pore size range from  $<120$  to 4000 A. and a total porosity of  $0.58 \text{ cm}^3$  of pores per gram of dry resin. As the polymerization continues, the pores are filled with lightly crosslinked material. After 90 min. the pore size is still from  $<120$  to 500 A. with a total porosity of  $0.17 \text{ cm}^3$  of pores per gram of dry resin.

Continued polymerization inside the individual gel masses of the agglomerates results in the shrinkage of the individual polymer particles. Figure 8 shows the changes in the pore spectra of the copolymer fractions as the individual particles shrink and the voids between these polymeric masses increase. At 195 min., curve 5, the pore diameter range has increased from  $<120$  to about 30,000 A. with a total porosity of  $0.46 \text{ cm}^3$  of pores per gram of dry resin. This rapid increase in both pore-size range and porosity continues as the polymerization goes to higher monomer conversion levels. The randomness of the pore-size distribution has decreased at this stage, and the pore spectra changes indicate that the material is approaching a narrow pore-size distribution. At 225 min., curve 6, the pore spectrum indicates that the pore-size range is now from 130 to 20,000 A. with a total porosity of  $0.99 \text{ cm}^3$  of pores per gram of dry resin and that

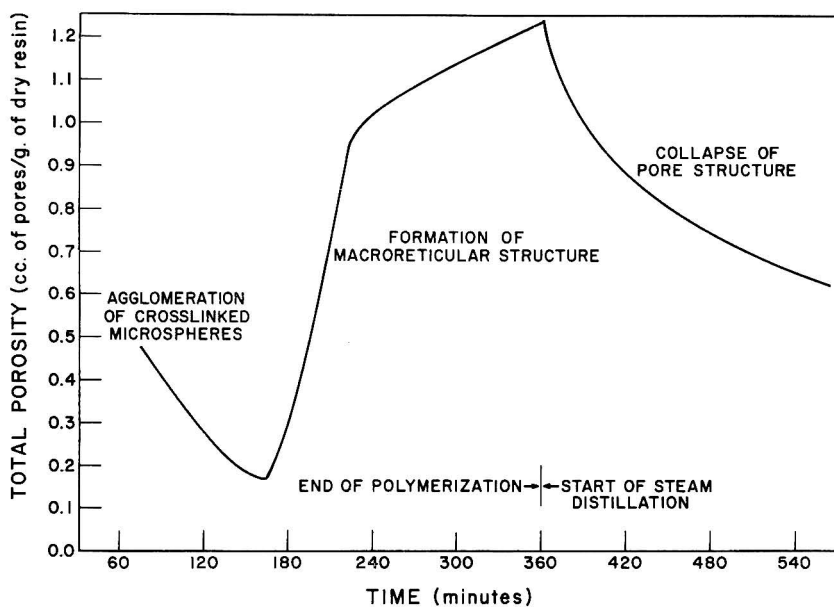


Fig. 10. Pore-volume changes during copolymer synthesis.

most of the pores have diameters of about 1000 Å. This trend of increasing porosity and narrowing pore-size range continues to the end of the polymerization cycle. The macroreticular copolymer at this stage in the synthesis has a total porosity of 1.25 cm.<sup>3</sup> of pores per gram of dry resin, a pore diameter range of 400–20,000 Å., and an average pore diameter of approximately 1200 Å.

Distillation of the phase extender from the copolymer causes a shrinkage of the individual polymeric particles. This causes a corresponding shrinkage or "collapse" of the macroreticular structure. Figure 9 shows the changes in the pore-size distribution during the third stage. At 30 min. after the start of distillation the total porosity of the copolymer has fallen from 1.25 to 0.95 cm.<sup>3</sup> of pores per gram of dry resin, and the entire pore spectrum has shifted slightly to smaller pore diameters. At the completion of this particular 4 hr. distillation the total porosity of the final product was 0.61 cm.<sup>3</sup> of pores per gram of resin, with an average pore diameter of 600 Å. and a pore-diameter range from 130 to 10,000 Å.

Changes in total porosity during the synthesis of the copolymer reflect the structural changes that lead to the macroreticular resins. Figure 10 graphically summarizes the relationship between porosity and polymerization time for a particular set of synthesis conditions. The mode of pore structure formation, however, would be the same for polymerizations in which the crosslinker concentration, the "solvent-nonsolvent" diluent concentration, and the reaction temperature are varied. The marked effects of the nature of the solvent or the phase extender on the nature of the pore structure of the final crosslinked copolymer have been described

by Meitzner and Oline,<sup>27,28</sup> Lloyd and Alfrey,<sup>30</sup> and Seidl et al.<sup>31</sup> in a recent excellent review.

## EXPERIMENTAL

The suspension polymerizations were run in a 5-liter, four-necked, round-bottomed flask fitted with a stirrer, a thermometer connected to a thermostat, a reflux condenser with a gas inlet at the top joint, and a sample outlet reaching into the suspension mixture. With the exception of the extra inlet and outlet tubes the apparatus is of the type used in standard suspension polymerizations. The gas inlet tube is connected to a nitrogen source. During the run the reaction flask was vented, at the inlet tube, to the atmosphere by a line to a three-way stopcock in the nitrogen line. When a sample is taken during the polymerization cycle, the three-way stopcock is turned to close the vent to the atmosphere and opened to a nitrogen tank. The nitrogen pressure forces the suspension up the sample outlet tube and out into a graduated cylinder. When the desired quantity of material is collected, the nitrogen pressure is released, and the reaction flask is vented to the atmosphere again.

A solution of styrene (570.2 g.), technical-grade divinylbenzene (29.8 g. containing 60.5% divinylbenzene), *t*-amyl alcohol (520.0 g.), and benzoyl peroxide (7.0 g.) was combined in the 5-liter flask with a solution of the ammonium salt of a high molecular weight styrene-maleic anhydride copolymer (11.3 g.) and Pharmagel (0.4 g.) in 1.8 liters of water. The mixture was agitated, until the organic components were dispersed as fine droplets, and then heated at 80°C.

When the temperature reached 80°C., an aliquot of the reaction mixture was removed, and subsequent aliquots were removed at set intervals throughout the polymerization and the steam distillation for removal of the solvent-nonsolvent mixture. The aliquots were immediately quenched in 250 ml. of 2B ethanol containing approximately 2% hydroquinone. After cooling to room temperature the precipitated polymeric material was filtered, washed three times with water, and then washed three times with 2B alcohol, once with benzene, once again with cold 2B alcohol. This washing procedure removed unreacted monomers, solvents, and non-crosslinked polymeric materials. The purified, crosslinked polymer fractions were placed in a steam oven to remove organic solvents and then dried overnight at 110°C.

The authors wish to express their appreciation to Bayard T. Storey for his helpful discussions during the course of this work, Raymond Wilkins and Miss Ann Thomas for the electron micrographs, and Edgar Cloeren and Eric Isacoff for their technical assistance.

## References

1. E. F. Meitzner and J. A. Oline, Union of S. Africa Pat. Appl. 59/2393.
2. R. Kunin, E. F. Meitzner, and N. Bortnick, *J. Am. Chem. Soc.*, **84**, 305 (1962).
3. R. Kunin, E. F. Meitzner, J. A. Oline, S. Fisher, and N. Frisch, *Ind. Eng. Chem. Prod. Res. Develop.*, **1**, 140 (1962).
4. K. A. Kun and R. Kunin, *J. Polymer Sci. B*, **2**, 587, 389 (1964).
5. K. A. Kun and R. Kunin, *J. Polymer Sci. B*, **2**, 389, 587 (1964).
6. *Amberlite XAD-1 and Amberlite XAD-2*, Rohm and Haas Company, Philadelphia, Pa.
7. K. A. Kun, *J. Polymer Sci. A*, **3**, 1833 (1965).
8. H. G. Cassidy and K. A. Kun, *Oxidation-Reduction Polymers*, Interscience, New York, 1965.
9. J. R. Millar, D. G. Smith, W. E. Marr, and T. R. E. Kressman, *J. Chem. Soc.*, **1963**, 218.
10. J. R. Millar, D. G. Smith, W. E. Marr, and T. R. E. Kressman, *J. Chem. Soc.*, **1963**, 2779.
11. J. R. Millar, D. G. Smith, W. E. Marr, and T. R. E. Kressman, *J. Chem. Soc.*, **1964**, 2740.
12. J. R. Millar, D. G. Smith, and T. R. E. Kressman, *J. Chem. Soc.*, **1965**, 304.
13. J. Seidl and J. Malinsky, in *Anomalous Processes in Ion Exchange*, Akademie-Verlag, Berlin, 1962.
14. K. Dusek, *Chem. Prumysl*, **11**, 439 (1961).
15. K. Dusek, *Collection Czech. Chem. Commun.*, **27**, 2841 (1963).
16. J. Seidl and J. Malinsky, *Chem. Prumysl*, **13**, 100 (1963).
17. K. Dusek, *Collection Czech. Chem. Commun.*, **28**, 2512 (1963).
18. J. Seidl, J. Malinsky, and K. Dusek, *Soviet Plastics*, **1964**, 10.
19. K. Dusek, *J. Polymer Sci. B*, **3**, 209 (1965).
20. E. I. Lyustgarten, V. P. Li, A. B. Pashov, N. B. Shakal'skaya, T. I. Davydova, and M. A. Zhukov, *Soviet Plastics*, **1965**, 11.
21. I. M. Abrams, *Ind. Eng. Chem.*, **48**, 1469 (1956).
22. I. M. Abrams, *Can. Pat.* 625,989 (1961).
23. E. Bortel, *Przemysl Chem.*, **44**, 255 (1965).
24. A. S. Tevlina and S. F. Sadova, *Zh. Prikl. Khim.*, **38**, 1643 (1965).
25. K. A. Kun, *J. Polymer Sci. A*, **4**, 859 (1966).
26. K. A. Kun and R. Kunin, in *Macromolecular Chemistry*, IUPAC, Prague (*J. Polymer Sci. C*, **16**) 1457 (1967).
27. E. F. Meitzner and J. A. Oline, Brit. Pat. 932,125 (1963).
28. E. F. Meitzner and J. A. Oline, Brit. Pat. 932,126 (1963).
29. B. T. Storey, *J. Polymer Sci. A*, **3**, 265 (1965).
30. W. G. Lloyd and T. Alfrey, *J. Polymer Sci.*, **62**, 301 (1962).
31. J. Seidl, J. Malinsky, K. Dusek, and W. Heitz, *Advan. Polymer Sci.*, **5**, 113 (1957).

Received August 21, 1967

Revised October 12, 1967

## Polymerization of Ethylene Catalyzed by Diethylaluminum Chloride and Titanium(III) Acetylacetonate

W. R. WATT, F. H. FRY, and H. POBINER, *American Can Company,  
Princeton Laboratory, Princeton, New Jersey 08540*

### Synopsis

Catalysts for the polymerization of ethylene were prepared from titanium(III) acetylacetonate and diethylaluminum chloride. Titanium(III) acetylacetonate is of interest because it is soluble in hydrocarbon solvents used as polymerization media. As its oxidation product oxobisacetylacetonatotitanium(IV) is also hydrocarbon-soluble, this system provides a vehicle for studying the effects of a change in valence on catalyst activity without an accompanying change of state, as occurs with titanium halides. Relatively high molar ratios ( $>20:1$ ) of aluminum alkyl to titanium compound were required to give active catalysts. Precipitates generally formed in the catalyst mixtures, although dilute catalyst solutions in which no precipitate was visible still initiated polymerization. Catalyst mixtures were observed to undergo certain changes on standing. Light-scattering studies indicated an increase in catalyst particle size, and a gas identified as ethane was evolved. These changes were accompanied by a reduction in activity of the catalyst. Parallel polymerization tests were run for a comparison of catalysts prepared from titanium(III) acetylacetonate and catalysts prepared from oxobisacetylacetonatotitanium(IV). There was essentially no difference in yield or properties of polymer prepared using the two catalyst systems. The evidence suggests that both the trivalent and tetravalent titanium compounds yield the same catalytic intermediate when reacting with diethylaluminum chloride.

### INTRODUCTION

Despite the large number of publications on the subject of olefin polymerization with Ziegler catalysts the only trivalent titanium compound on which extensive studies have been reported is titanium trichloride. This may be due to the difficulties encountered in the preparation of trivalent titanium compounds which, in general, are very unstable to moisture and oxygen. We have recently prepared and studied a trivalent titanium compound, titanium(III) acetylacetonate, which gives active catalysts for the polymerization of ethylene.

Titanium(III) acetylacetonate [hereinafter referred to as  $\text{Ti}(\text{acac})_3$ ] was first synthesized by Chakravarti<sup>1</sup> in 1958. Its use as a cocatalyst in olefin polymerization has not been reported, although the broad claims of some patents include titanium acetylacetonates in general as possible components of Ziegler catalysts.<sup>2,3</sup>

Unlike titanium trichloride,  $\text{Ti}(\text{acac})_3$  is readily soluble in benzene and hydrocarbons used as polymerization media. In combination with alkylaluminum compounds it initiates rapid polymerization of ethylene at low pressures and temperatures. Polymerization occurs in the absence of any solid phase in the catalyst mixture, and these catalysts may therefore be classified as "soluble." Although ethylene polymerizes readily in the presence of these catalysts, attempts to polymerize propylene under the same conditions have been unsuccessful.

$\text{Ti}(\text{acac})_3$  is readily oxidized in solution to oxobisacetylacetonato titanium(IV) without precipitating. This provides an opportunity for comparison of catalysts prepared from trivalent and tetravalent titanium compounds without interference due to changes in solubility.

We have investigated the catalytic activity of  $\text{Ti}(\text{acac})_3$  in the polymerization of ethylene as a function of the molar ratio of diethylaluminum chloride (DEAC) to  $\text{Ti}(\text{acac})_3$ , catalyst age, and oxidative state of the titanium. The polymers obtained were characterized as to solubility, inherent viscosity, and melting point, to determine the effect of changes in the catalyst on these properties.

## EXPERIMENTAL

### Preparation of Titanium(III) Acetylacetonate

$\text{Ti}(\text{acac})_3$  is very sensitive to air and moisture and must be prepared and stored in an inert atmosphere such as dry nitrogen. Synthesis was carried out in a four-necked, 500 ml. flask with a coarse fritted-glass filter and stop-cock sealed to the bottom. The reactor was oven-dried, assembled hot, and flushed with nitrogen. Anhydrous benzene was added, followed by hydrogen-reduced titanium trichloride (Stauffer Chemical Company's H grade).

A solution containing a calculated quantity of sodium acetylacetonate in methanol, which had been dried by distilling from sodium methylate immediately before use, was added dropwise with stirring to the suspension of  $\text{TiCl}_3$  in benzene. The mixture was stirred for 3 hr. at room temperature and then warmed to  $50^\circ\text{C}$ . and filtered rapidly through the glass filter in the bottom of the reaction flask.

Solvent was removed from the filtrate under reduced pressure, leaving a dark-blue residue, which was further dried by gentle heating under high vacuum. This residue was purified by sublimation ( $150^\circ\text{C}$ . at 0.1 mm.) and gave the following analysis (%): Ti 14.1 and 14.2, C 52.0 and 52.0, H 6.13, 6.50, and 6.52. Calcd. for  $\text{Ti}(\text{C}_5\text{H}_7\text{O}_2)_3$  (%): Ti 13.9, C 52.2, H 6.14. Cryoscopic molecular weight determination in benzene (0.6033 g./l.) gave the value 333; formula weight, 345.

### Polymerization Procedure

Polymerization was carried out in 200 ml. polymer bottles with crown caps under 40 psig of ethylene. The bottles were loaded with benzene

and catalyst in a drybox under nitrogen and then capped and immersed in a constant-temperature bath. Monomer (ethylene, Matheson C.P. grade) was introduced directly from the cylinder through  $1/16$ -in. hypodermic tubing penetrating a Buna N self-sealing gasket underneath a  $1/8$ -in. hole in the crown cap. The polymerization mixture was agitated by means of a magnetic stirrer. Multiple tests could be run simultaneously.

The polymer was recovered by pouring the polymerization mixture into a threefold excess of isopropanol and filtering. The polymer was washed twice with methanol in a Waring Blendor and dried at  $60^{\circ}\text{C}$ . under vacuum for 17 hr.

### Characterization of Polymers

Polymers prepared by the technique described above were examined for branching, melting point, solubility in heptane, and inherent viscosity.

Branching was determined by infrared spectrophotometry. An infrared spectral calibration was established for a series of polyethylene standards of known methyl group concentration ranging from 1 to 30 methyl groups per 1000 carbon atoms. The absorbance ratio at  $1370:712\text{ cm}^{-1}$  for  $(\text{C}-\text{CH}_3)/(-\text{CH}_2-)_x$  served as an index of methyl group concentration. Calibrations and analyses of both KBr pellets and pressed films were obtained with a Perkin-Elmer 521 infrared spectrophotometer.

Melting points were determined by differential thermal analysis (DTA) with a du Pont Model 900 differential thermal analyzer at a heating rate of  $20^{\circ}\text{C}/\text{min}$ . To ensure that all samples had the same thermal history they were run up to  $150^{\circ}\text{C}$ . in the DTA cell under nitrogen, cooled to room temperature at a uniform rate, and then heated again. The melting point observed on the second heating cycle was used in each case.

Solubility was determined by extracting 2 g. samples in a bituminous extractor with boiling heptane for 24 hr.

Inherent viscosities were obtained in tetrahydronaphthalene at  $135^{\circ}\text{C}$ . Cannon-Fenske ASTM viscometers in a constant-temperature bath regulated to  $0.1^{\circ}\text{C}$ . were used.

### Gas Evolution Measurements

Benzene solutions of diethylaluminum chloride (DEAC) and  $\text{Ti}(\text{acac})_3$  were loaded into separate compartments of a special flask in a drybox under nitrogen. The flask was removed from the drybox, cooled in a mixture of solid carbon dioxide and acetone, evacuated, and connected to a manometer. The reactants were allowed to come to equilibrium at  $26^{\circ}\text{C}$ ., and the pressure at this temperature was read. The reactants were then mixed and the pressure noted as a function of time.

### Light Scattering Measurements

A Bryce-Phoenix Model 2000-D light-scattering photometer and the square turbidity cell were used for these measurements. A specially

designed Micarta cap was constructed to provide an airtight closure for the cell. This was necessary to protect the air-sensitive solutions from the atmosphere during measurements. The Micarta cap was fitted with two hypodermic needle mountings for nitrogen inlet and exhaust. A tube fitted with a vaccine stopper for the addition of solvent and catalyst solutions was mounted in the cap.

Distilled benzene was pipetted into the cell and purged with nitrogen, and the scattering ratio at  $546\text{ m}\mu$  was determined. The DEAC solution was added by pipet after a purging with nitrogen for 1 min. The cell was sealed and a scattering ratio obtained. The  $\text{Ti}(\text{acac})_3$  solution was similarly added. Thereafter scattering ratios were obtained at 3–5 min. intervals, until a steady state was reached, or until the calculated absolute turbidity  $\tau$  exceeded  $500 \times 10^{-4}$ . The solutions were agitated by bubbling nitrogen through for 1 min. before each measurement.

## RESULTS AND DISCUSSION

$\text{Ti}(\text{acac})_3$  was tested in combination with triethylaluminum, DEAC, and ethylaluminum dichloride for its ability to initiate the polymerization of ethylene. Under the conditions of testing much higher yields of polymer were obtained with DEAC than with either of the other two aluminum compounds, as shown in Table I.

TABLE I  
Comparison of Catalysts Containing Various Aluminum Alkyls  
in Combination with  $\text{Ti}(\text{acac})_3$ : Polymerization of Ethylene in 100 ml.  
of Benzene for 4 hr. at  $40^\circ\text{C}$ . and 40 psig

Aluminum alkyl		Al/Ti	Polymer, g.	M.P., $^\circ\text{C}$ . (DTA)	$\eta_{\text{inh}}$ , dl./g.
Type	Amt., mmoles				
Triethylaluminum	5.8	120	0.8	130	2.89
Diethylaluminum chloride	5.7	117	9.7	125	2.60
Ethylaluminum dichloride	5.7	117	1.9	118	1.63

When  $\text{Ti}(\text{acac})_3$  and DEAC were mixed at low concentrations (less than  $3 \times 10^{-4}$  mole of  $\text{Ti}(\text{acac})_3$  per liter of benzene), clear solutions were obtained. At higher concentrations a brown precipitate formed. The mixture initiated polymerization of ethylene, whether or not any solid phase was present at the time the monomer was introduced.

Separation of the two phases in a concentrated mixture of  $\text{Ti}(\text{acac})_3$  and DEAC, by centrifugation, and a subsequent testing of the two phases showed that only the clear supernatant initiated polymerization. The brown residue, resuspended in benzene, did not initiate. Some differences were noted, however, between polymer prepared with only the

clear supernatant and polymer prepared with catalyst mixtures from which the residue had not been removed. The complete catalyst mixture gave a higher yield of polymer than the supernatant, and the polymer had a larger heptane-insoluble fraction (see Table II).

TABLE II  
Comparison of Soluble and Insoluble Fractions  
of a Mixture of DEAC and  $\text{Ti}(\text{acac})_3$ :<sup>a</sup> Polymerization of Ethylene for 4 hr.  
at 40°C. and 40 psig

Catalyst	Polymer, g.	Heptane- insol., %	M.P., °C. (DTA)	$\eta_{inh}$ , dl./g.
Complete mixture, DEAC + $\text{Ti}(\text{C}_5\text{H}_7\text{O}_2)_3$	13.1	81.3	127	7.77
Supernatant only	6.8	71.9	126	3.74
Residue only	nil	—	—	—

<sup>a</sup> 5.72 mmoles of DEAC and 0.326 mmoles of  $\text{Ti}(\text{C}_5\text{H}_7\text{O}_2)_3$  stirred in 100 ml. of benzene for 1 hr. at room temperature and then centrifuged 10 min. at 2000 rpm.

These differences could have been the result of additional handling of the supernatant to remove the insoluble residue, although similar results were obtained in several tests. In none of these tests did the residue initiate polymerization.

### Effect of Aluminum-to-Titanium Ratio (Al/Ti)

The molar ratio of aluminum alkyl to transition-metal compound in Ziegler catalysts is known to have profound effects on both the yield and the properties of a polymer. Ziegler claimed that in catalysts containing tetravalent titanium salts 8–12 moles of aluminum alkyl to one of titanium salt proved advantageous, but in the special case in which the transition-metal compound is an acetylacetonate molar ratios of aluminum to transition-metal compound of the order of 16–24 were preferable.<sup>2</sup> Others have found that catalysts containing titanium halides show activity at molar ratios of aluminum alkyl to titanium halide of about 2:1 or 3:1.<sup>4–7</sup>

In the case of DEAC– $\text{Ti}(\text{acac})_3$  catalysts the polymerization took place only when DEAC was present in large excess. The exact ratio of DEAC to  $\text{Ti}(\text{acac})_3$  required for polymerization varied with the concentration of  $\text{Ti}(\text{acac})_3$ ; see Figure 1. In general, catalysts containing less than 20 moles of DEAC per mole of  $\text{Ti}(\text{acac})_3$  produced no polymer.

Polymers prepared at high Al/Ti ratios contained large fractions of low molecular weight material, as indicated by the percentage solubility in heptane.

Because of the tendency of some titanium compounds to dimerize, high Al/Ti ratios are needed to disturb the dimerization equilibrium. This has been used to explain the high Al/Ti ratios required in catalysts prepared from titanium alkoxides.<sup>2</sup> Similar reasoning probably cannot be applied to catalysts containing  $\text{Ti}(\text{acac})_3$ , however, because this compound

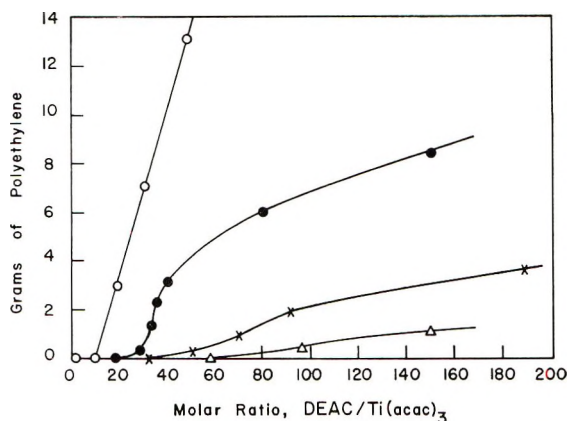
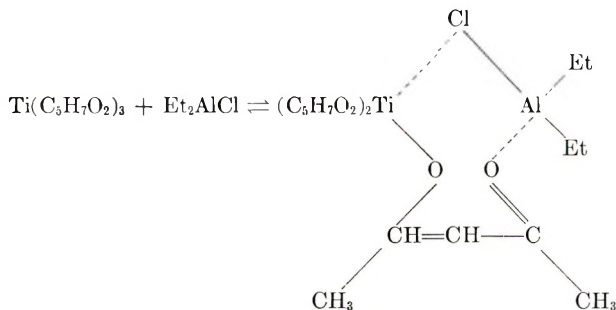


Fig. 1. Effect of molar ratio DEAC/Ti(acac)<sub>3</sub> on polymer yield: polymerization of ethylene at 40°C. and 40 psig in 100 ml. of benzene for 90 min. Millimoles of Ti(acac)<sub>3</sub>: (O) 0.306, (●) 0.0765, (x) 0.0306, (Δ) 0.0153.

has been shown to be monomeric in solution.<sup>8</sup> A possible explanation is that, since the chelate is very stable, a large excess of DEAC is needed to break loose one  $\beta$ -diketone or one end of a  $\beta$ -diketone:



### Effect of Catalyst Age

Experiments in which mixtures of DEAC and Ti(acac)<sub>3</sub> were allowed to react for various lengths of time before ethylene was introduced showed that the catalyst's age influences its activity (see Table III). The highest yields of polymer were obtained when monomer was introduced immediately after mixing of the catalyst. The loss of activity was more rapid at 40°C. than at 25°C. (compare Tables III and VII). Danusso and Sianesi noted a similar effect of temperature on the rate at which trialkylaluminum-TiCl<sub>4</sub> catalysts lost activity.<sup>6</sup> A loss of activity with age has been observed in other related catalyst systems.<sup>5,7,9-11</sup>

A possible explanation of the loss of activity of the catalyst on aging is that the titanium compound is reduced beyond its valence of maximum activity, although there is evidence this does not occur. Ludlum et al.<sup>12</sup> showed that for catalysts that are reduced below the valence of maximum activity a plot of catalyst activity versus molar ratio of aluminum to ti-

TABLE III  
Effect of Aging DEAC-Ti(acac)<sub>3</sub> Catalyst at 25°C.:  
Polymerization of Ethylene at 25°C. and 40 psig for 180 min. with  
5.82 mmoles of DEAC and 0.0759 mmoles of Ti(acac)<sub>3</sub> in 100 ml. of Benzene

Cat- alyst age, hr.	Polymer, g.	M.P., <sup>a</sup> °C. (DTA)	Heptane- insol., %	$\eta_{inh}$ , <sup>b</sup> dl./g.	Branch- ing, <sup>b</sup> CH <sub>3</sub> per 1000 C
0	13.4	122	63.6	5.9	2.8
1	11.7	123	64.1	5.8	<1
3	9.3	124	67.9	7.3	<1
5	8.4	126	68.5	4.5	<1
24	4.9	128	77.1	4.4	<1
46	5.5	130	78.9	4.9	<1
65	4.0	132	78.2	4.9	<1
96	2.1	128	72.6	5.5	<1

<sup>a</sup> Of crude polymer before heptane extraction.

<sup>b</sup> Of heptane-insoluble fraction of polymer.

tanium compound goes through a maximum.<sup>4</sup> Schnecko et al. have shown similar plots. The curves shown in Figure 1 do not pass through a maximum, indicating that DEAC does not overreduce Ti(acac)<sub>3</sub> even at very high Al/Ti ratios.

Observation of mixtures of DEAC and Ti(acac)<sub>3</sub> in benzene with a Bryce-Phoenix light-scattering photometer showed an increase in scattering ratio with time. Two types of behavior were noted, depending on the concentration of Ti(acac)<sub>3</sub>. Dilute solutions, less than  $3 \times 10^{-4}M$  with respect to Ti(acac)<sub>3</sub>, showed a continuous increase in  $\tau$  throughout the entire period of observation (200 min.). In the case of more concentrated solutions the scattering ratio passed through a maximum (see Table IV and Figures 2 and 3).

TABLE IV  
Change in Turbidity of DEAC-Ti(acac)<sub>3</sub> Mixtures on Aging at 25°C.

Ti(acac) <sub>3</sub> , moles/l. $\times 10^4$	Molar ratio Al/Ti	Condition	Change in $\tau$ during aging for 200 min.
2.5	59	soluble <sup>a</sup>	continuous increase
4.4	118	heterogeneous	maximum at 50 min.
4.3	121	heterogeneous	maximum at 33 min.
4.9	125	heterogeneous	maximum at 20 min.
0.6	236	soluble <sup>a</sup>	continuous increase

<sup>a</sup> Transparent to unaided eye.

The observed decrease in scattering ratio of more concentrated solutions after 20–50 min. is believed due to precipitation of suspended particles, reducing the number of scattering centers. Solutions in which the concentration of Ti(acac)<sub>3</sub> was less than  $3 \times 10^{-4}M$  remained clear to

the unaided eye, but visible precipitates formed in more concentrated mixtures.

The light-scattering studies indicate an increase in particle size even in cases in which no visible precipitate occurs. This may explain the observed loss of catalyst activity in clear solutions as well as in those containing precipitates.

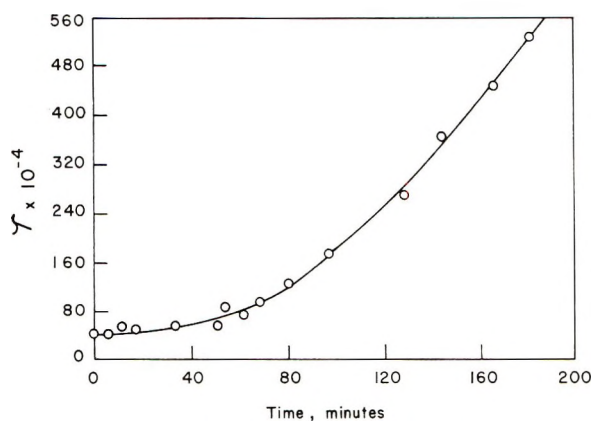


Fig. 2. Absolute turbidity  $\tau$  of catalyst systems in benzene as a function of time: 0.398 mmoles of DEAC and 0.00676 mmoles of  $\text{Ti}(\text{acac})_3$  in 27 ml. of benzene.

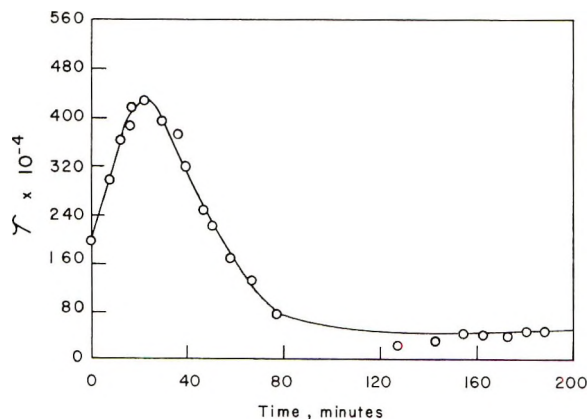


Fig. 3. Absolute turbidity  $\tau$  of catalyst systems in benzene as a function of time: 1.59 mmoles of DEAC and 0.0124 mmoles of  $\text{Ti}(\text{acac})_3$  in 31 ml. of benzene.

During aging of the  $\text{DEAC-Ti}(\text{acac})_3$  catalyst a gas is evolved. This gas was identified as ethane from its infrared spectrum. The moles of ethane evolved per mole of  $\text{Ti}(\text{acac})_3$  were found to vary with the  $\text{Al/Ti}$  molar ratio. No ethane evolution was observed for an  $\text{Al/Ti}$  ratio of less than 1. When the  $\text{Al/Ti}$  ratio was greater than 1, the amount of ethane increased, as the ratio increased, for two different experiments, as shown in Table V.

TABLE V  
Evolution of Ethane on Mixing of DEAC with  $\text{Ti}(\text{acac})_3$   
in 30 ml. of Benzene at 26°C.

DEAC, moles ( $\times 10^{-3}$ )	$\text{Ti}(\text{acac})_3$ , moles ( $\times 10^{-3}$ )	Molar ratio Al/Ti	Moles ethane per mole $\text{Ti}(\text{acac})_3$
0.43	0.54	0.8	None
5.7	0.60	9.5	1.2
8.58	0.60	14.2	3.2

Evolution of a gas accompanying a loss of catalyst activity has been noted in other olefin polymerization catalysts. Friedlander and Oita, studying the polymerization of ethylene initiated by mixtures of alkyl-lithium and titanium tetrachloride, observed that polymerization took place only if monomer was present during mixing of the catalyst components.<sup>10</sup> This phenomenon was associated with the instability of an active titanium organometallic complex. When ethyllithium and titanium tetrachloride were mixed in an inert atmosphere, ethane was evolved. The evolution of ethane was taken to indicate breakdown of the titanium organometallic complex.<sup>10</sup>

Bawn and Symcox found with  $\text{AlR}_3\text{-Ti}(\text{OR})_4$  catalysts a falling off in rate of polymerization with catalyst age and a simultaneous evolution of ethane.<sup>7</sup> Loss of activity of the catalyst was attributed to thermal instability of the active intermediate.

In the case of  $\text{DEAC-Ti}(\text{acac})_3$  catalysts, as in the other cases noted above, evolution of ethane must arise from instability of an active intermediate. We have tried to find a correlation between the rate of gas evolution and loss of catalyst activity on aging. The rate of gas evolution was determined by the increase in pressure over mixtures of DEAC and  $\text{Ti}(\text{acac})_3$ . Plots of  $\log (P_\infty - P)$  versus time were linear over a few half-lives. Rate constants for the evolution of ethane at various molar ratios of DEAC to  $\text{Ti}(\text{acac})_3$  are shown in Table VI.

To calculate a rate constant for the loss of catalyst activity, it was assumed that the polymer yield was directly proportional to the concentration of the active catalyst intermediate. On the basis of the data of Table III the initial slope of a plot of the logarithm of grams of polymer versus time gives a value of  $2.03 \times 10^{-3} \text{ min.}^{-1}$ , in fair agreement with the con-

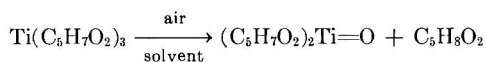
TABLE VI  
Rates of Evolution of Ethane from Mixtures  
of DEAC and  $\text{Ti}(\text{acac})_3$  in 30 ml. of Benzene at 26°C.

DEAC, mmoles	$\text{Ti}(\text{acac})_3$ , mmoles	Al/Ti	Rate constant, $\text{min.}^{-1} (\times 10^{-3})$
8.58	0.15	58	6.2
8.58	0.30	29	8.4
8.58	0.45	19	4.0

stants for the rate of evolution of ethane. Lack of better agreement may indicate that other factors, such as catalyst aggregation, are also affecting catalyst activity.

### Effect of Oxidation

$\text{Ti}(\text{acac})_3$  is readily oxidized to oxobisacetylacetonatotitanium (IV).<sup>1,8</sup>



On exposure to air the dark-blue crystals of  $\text{Ti}(\text{acac})_3$  turn orange in a few hours. Benzene solutions, which remain blue indefinitely, if protected from the atmosphere, rapidly turn orange or yellow in contact with air. The oxidation products remain in solution, and this system provides a vehicle for observing the effects of a change in valence of titanium without the complication of changes in state occurring in the case of titanium halides and esters.

TABLE VII

Comparison of  $\text{Ti}(\text{acac})_3$  and Oxobisacetylacetonatotitanium(IV): Polymerization of Ethylene at 40°C. and 40 psig for 150 min. with 5.72 mmoles of DEAC and 0.0670 mmoles of Titanium Compound in 106 ml. of Benzene; Al/Ti = 85.4

Titanium compound	Catalyst age	Polymer, g.	M.P., °C. (DTA)	Heptane-insol., %	$\eta_{\text{inh}}$ , dl./g. (tetralin, 135°C.)
$\text{Ti}(\text{acac})_3$	0	11.1	126	50.2	4.7
$\text{TiO}(\text{acac})_2$	0	10.8	126	55.9	5.7
$\text{Ti}(\text{acac})_3$	30 min.	11.7	131	70.8	9.5
$\text{TiO}(\text{acac})_2$	30 min.	11.9	130	66.4	12.5
$\text{Ti}(\text{acac})_3$	65 min.	8.2	129	60.8	11.4
$\text{TiO}(\text{acac})_2$	65 min.	8.3	129	58.8	10.7
$\text{Ti}(\text{acac})_3$	100 min.	7.1	130	68.0	10.4
$\text{TiO}(\text{acac})_2$	100 min.	6.9	130	71.0	10.3
$\text{Ti}(\text{acac})_3$	120 min.	6.2	128	54.5	10.9
$\text{TiO}(\text{acac})_2$	120 min.	6.2	128	51.6	8.7
$\text{Ti}(\text{acac})_3$	180 min.	5.6	129	56.1	10.5
$\text{TiO}(\text{acac})_2$	180 min.	5.6	129	55.0	11.3
$\text{Ti}(\text{acac})_3$	240 min.	2.2	127	52.9	10.0
$\text{TiO}(\text{acac})_2$	240 min.	3.1	127	52.3	10.3
$\text{Ti}(\text{acac})_3$	16 hr.	1.1	124	51.7	10.5
$\text{TiO}(\text{acac})_2$	16 hr.	1.9	128	52.1	10.8
$\text{Ti}(\text{acac})_3$	43 hr.	Nil	—	—	—
$\text{TiO}(\text{acac})_2$	43 hr.	Nil	—	—	—

The effect of oxidation on the catalytic activity of  $\text{Ti}(\text{acac})_3$  was investigated. A standard solution of  $\text{Ti}(\text{acac})_3$  in benzene was divided into two parts. One part was protected from the atmosphere and retained its blue color, while the other was exposed to air for several hours and showed the characteristic color change accompanying oxidation of the  $\text{Ti}(\text{acac})_3$ .

to oxobisacetylacetonatotitanium(IV). The two solutions were then tested for catalytic activity in parallel polymerization tests.

Whether the catalyst was prepared from  $\text{Ti}(\text{acac})_3$  or its oxidation product made no significant difference in either the amount of polymer produced or its properties; see Table VII.

### CONCLUSIONS

The DEAC- $\text{Ti}(\text{acac})_3$  system gives effective catalysts for the low-pressure polymerization of ethylene. The catalytic activity is associated with the soluble phase of the reaction mixture.

The time elapsed between mixing of the catalyst and introduction of monomer affects both the rate of polymerization and the properties of the polymer. A loss of activity of the catalyst with aging is the result of changes in the catalyst, giving rise to evolution of ethane and the aggregation of catalyst.

The fact that no significant difference in catalytic activity was observed between  $\text{Ti}(\text{acac})_3$  and its oxidation product strongly suggests that reaction with DEAC yields a single catalytic species. This is reasonable in view of the high molar ratio of DEAC to titanium compound required to form the catalyst.

### References

1. B. N. Chakravarti, *Naturwissenschaften*, **45**, 286 (1958).
2. K. Ziegler, U.S. Pat. 3,231,515 (1966), Belg. Pat. 533,362 (1958).
3. G. Natta, I. Pasquon, and E. Giachetti, U.S. Pat. 3,073,811 (1963).
4. H. Schnecko, M. Reimoller, K. Weirauch, and W. Kern, in *Macromolecular Chemistry, Paris 1963* (*J. Polymer Sci. C*, **4**), M. Magat, Ed., Interscience, New York, 1964, p. 71.
5. A. Orzechowski, *J. Polymer Sci.*, **34**, 65 (1959).
6. F. Danusso and D. Sianesi, *Chim. Ind.*, **40**, 450 (1958).
7. C. E. H. Bawn and R. Symcox, *J. Polymer Sci.*, **34**, 139 (1959).
8. M. Cox, J. Lewis, and R. S. Nyholm, *J. Chem. Soc.*, **1965**, 2840.
9. C. G. Overberger and P. A. Jarovitzky, in *Perspectives in Polymer Science* (*J. Polymer Sci. C*, **12**), E. S. Proskauer, E. H. Immergut, and C. E. Overberger, Eds. Interscience, 1966, p. 3.
10. H. N. Friedlander and K. Oita, *Ind. Eng. Chem.*, **49**, 1885 (1957).
11. G. Natta, P. Pino, G. Mazzanti, and P. Longi, *Gazz. Chim. Ital.*, **87**, 549 (1957).
12. D. B. Ludlum, A. W. Anderson, and C. E. Ashby, *J. Am. Chem. Soc.*, **80**, 1380 (1958).

Received August 21, 1967

Revised October 19, 1967

## Synthesis and Investigation of Properties of Repeatedly Grafted Copolymers (Pemosors)

V. V. KORSHAK, K. K. MOZGOVA, and YU. V. EGOROVA, *Institute of Organo-Element Compounds, Moscow, U.S.S.R.*

### Synopsis

Repeatedly grafted copolymers (pemosors) were obtained by grafting one and the same or different vinyl monomers onto heterochain polymers in a radical reaction. As starting polymers films of polyethylene terephthalate and poly- $\epsilon$ -caproamide were used. Styrene and methyl methacrylate were the grafted vinyl monomers. It has been shown that pemosors could be formed in yields of 500–1000% (of the starting sample weight) by multiple grafting on vinyl polymer. Pemosors differ in appearance both from the starting polymers and the single-graft copolymers. Investigations of pemosor samples by electron microscope showed that the morphological structure of the surface was appreciably affected, the changes being more significant with increasing content of the grafted polymer. X-Ray studies and NMR data on pemosors showed that multiple grafting of vinyl monomers does not change the crystal structure of the starting polymers, affecting only the supermolecular structure of the outer layer. Pemosors are polymers of a new type, differing in their properties from the starting polymers and the single-graft copolymers. The grafting character and penetration depth of the grafted monomer depend on the packing compactness of the supermolecular structure of the polymeric base as well as on the chemical nature of the starting polymers and monomers. Pemosors possess considerable chemical resistance and withstand prolonged boiling in 40% alkali solution.

Graft copolymers obtained by grafting various monomers on polymers activated in different ways have been described by several investigators.<sup>1–5</sup> Attention has been devoted chiefly to studying the process of grafting, the mechanism of the reaction, and the structure and properties of the resultant products of single-graft copolymers. Only a few records of attempts at double grafting are to be found in the literature.<sup>6–10</sup> The possibility of multiple grafting of various monomers or of one and the same monomer has not been demonstrated until now. It might be anticipated that multiple graftings of the same or another vinyl monomer would lead to greater changes in the properties of the initial materials than single graftings and would result in polymers of a new type, with properties differing from both the initial polymers and the single-graft copolymers.

This communication gives an outline of results obtained in the course of synthesizing and investigating some properties of repeatedly grafted copolymers, which are termed "pemosors."

Multiple grafting of monomers was carried out by the block method on

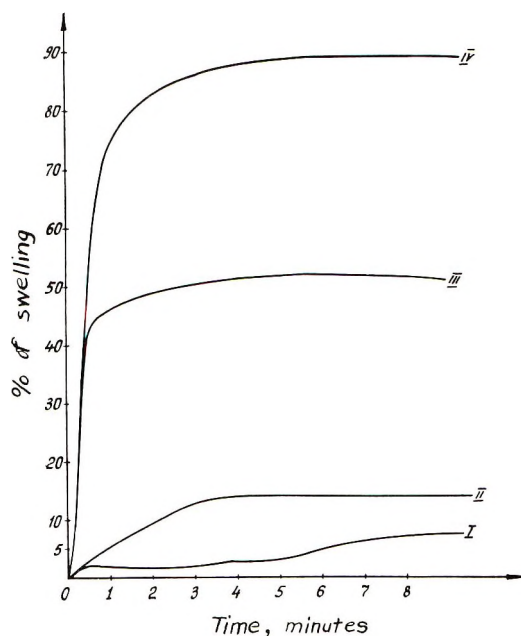


Fig. 1. Swelling of polyethyleneterephthalate and poly- $\epsilon$ -caproamide film in methyl methacrylate film at 20°C: (I) poly- $\epsilon$ -caproamide film with grafted polystyrene (increase in weight: 28%); (II) polyethyleneterephthalate film with grafted polystyrene (increase in weight: 30%); (III) polyethyleneterephthalate film with twice grafted polystyrene (increase in weight: 30%; 155%); (IV) poly- $\epsilon$ -caproamide film with twice grafted polystyrene (increase in weight: 12.7; 10.7%).

poly- $\epsilon$ -caproamide and on polyethylene terephthalate.<sup>11</sup> The activation method was kept unchanged.

It has been found that, of the many monomers, styrene and methyl methacrylate are the most successfully grafted and the yield of the grafted vinyl polymer is higher on polyester films than on polyamide films. For example, after five graftings of styrene on polyethylene terephthalate, the weight of the grafted polystyrene exceeded that of the initial sample by more than eleven times. At the same time, under similar conditions, we obtained from a polyamide film only a fivefold yield of grafted polystyrene.

The difference in yield apparently may be explained by the differences in chemical nature between the polymers and by their dissimilar physical structures, which unquestionably affects the capacity for diffusion of the air oxygen and the monomers.

The process is also considerably influenced by the difference in stability upon thermal treatment between the hydroperoxide groups in these two polymers.

The high yield of a repeatedly grafted vinyl polymer is linked with the fact that the initial polymers used were films with an already grafted layer of a vinyl polymer, which swelled more readily in vinyl monomers than did the ungrafted polymers. Figure 1 shows how the swelling capacity of poly-

$\epsilon$ -caproamide films improves in styrene after polystyrene has already been grafted on them. Polyethylene terephthalate films behaved in exactly the same way.

The process of multiple grafting of a vinyl monomer occurs in such a way that at first the initial rate of absorption of the monomer and that of the formation of a vinyl polymer are almost equal, but in the course of the reaction the formation of the graft polymer gradually slows down. Multiple grafting of a monomer leads, as primary grafting, to the formation in the film of a considerably greater amount of the graft polymer than of homopolymer, as may be seen from Figure 2. The substantial predominance of the reaction of grafting over homopolymerization may be explained by the high viscosity of the reaction system (the gel effect).

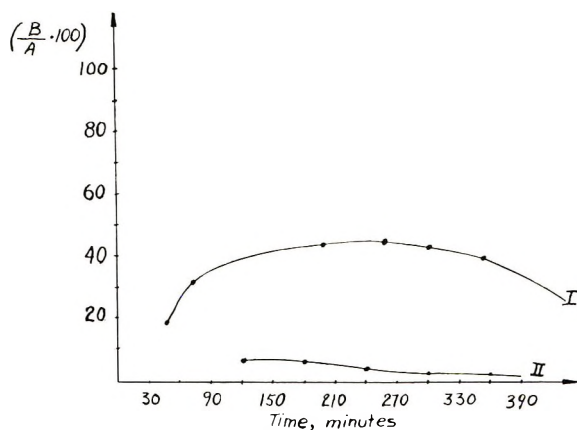


Fig. 2. Dependence of the yield of grafted polystyrene (I) and styrene homopolymer (II), as percentage of the weight of the monomer absorbed by the film ( $B/A \cdot 100$ ), on the duration of copolymerization at 80°C.

We have previously ascertained that the active centers formed in polymers upon their being heated in air serve as initiators of the reaction of graft copolymerization.<sup>12</sup>

The course of the process is also appreciably influenced by the reaction of chain transfer, first through the initial polymer and then through the grafted one.

Some supplementary data obtained by examining samples of graft copolymers by the velocity sedimentation method point to the existence of the two mechanisms of the reaction of graft copolymerization.<sup>13</sup>

Poly- $\epsilon$ -caproamide films with single-graft polymethyl methacrylate or polystyrene were used for the investigation. Simultaneously, a sample of a film containing successively grafted polystyrene and polymethyl methacrylate was also investigated.

To remove the homopolyamide, the samples were boiled for a long time in hydrochloric acid, after which the undissolved part, the vinyl polymer or the copolymer, was thoroughly washed with water and dried.

A benzene solution of 0.5% concentration was used for the sedimentation studies.

The graft copolymer consisting of successively grafted polystyrene and polymethyl methacrylate was first investigated as obtained in the reaction. Then either polystyrene or polymethyl methacrylate was separated from it by means of selective solvents, and the insoluble residue was subjected to sedimentation.

From all the samples of polymethyl methacrylate a bimodal curve with two peaks oriented in different directions was obtained. We made certain that the polymethyl methacrylate contained no admixtures. To account for the presence of two peaks on the sedimentation curve, we made the assumption that they represented the existence of two reactions of initiation of the process of graft copolymerization, occurring at different rates. As a consequence of these two different reactions polymethyl methacrylate is formed with two different degrees of polymerization. One of the initiation reactions is the decomposition of the hydroperoxide groups in the initial polymer; the other is due to chain transfer. Since the two reactions proceed at different rates, it is natural that the resultant chains of polymethyl methacrylate have different degrees of polymerization and different molecular weights.

When samples of grafted polystyrene were examined, only one peak was observed on the curve of sedimentation.

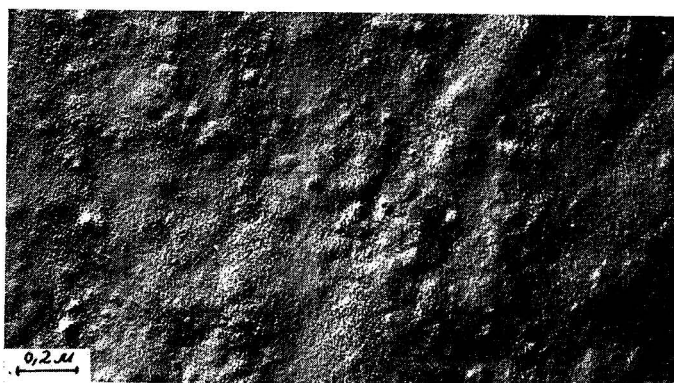
The experimental data so obtained have made it possible to calculate the sedimentation constants, as shown in Table I.

The resultant pemosors differ considerably in appearance from both the initial polymers and the single-graft copolymers. There is a substantial increase in the thickness of the films (by a factor of 5-10) which after several successive gratings may reach 250-300  $\mu$  (the thickness of the initial films is from 30 to 60  $\mu$ ). The linear dimensions of the films likewise in-

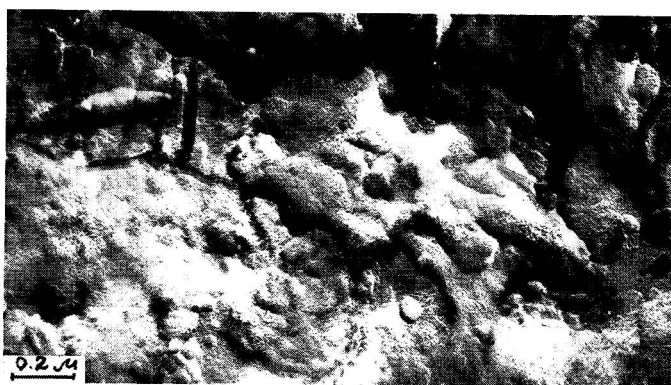
TABLE I  
Calculated Sedimentation Constants

No.	Characteristics of sample <sup>a</sup>	Yield of grafted vinyl polymer or copolymer, %, based on original sample weight	Sedimentation constant ( $\times 10^{-13}$ )	
			$S_2$ (2nd peak)	$S_1$ (1st peak)
1	Grafted part consisting of successively grafted PSt (I) and PMM (II)	43.0 (I) 50.0 (II)	4.9	7.9
2	PMM extracted from grafted part consisting of PSt and PMM	50.0 (II)	3.4	6.0
3	Grafted PMM (single grafting)	25.0	3.8	7.5
4	PSt extracted from grafted part consisting of PSt (I) and PMM (II)	43.0 (I)	4.6	
5	Grafted PSt (single grafting)	43.0	4.9	

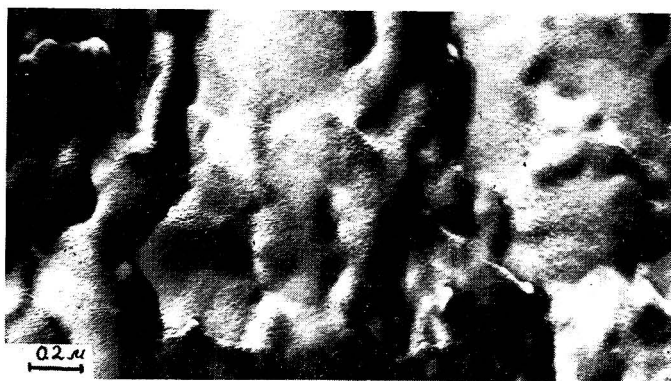
<sup>a</sup> PSt, polystyrene; PMM, polymethyl methacrylate.



(a)



(b)



(c)

Fig. 3. Electron microscope photographs of the surface of poly- $\epsilon$ -caproamide films before and after grafting vinyl monomers: (a) initial poly- $\epsilon$ -caproamide; (b) poly- $\epsilon$ -caproamide with polystyrene (175%), grafted four times; (c) poly- $\epsilon$ -caproamide with polystyrene and polymethylmethacrylate polymers (540%) grafted alternately four times.

crease, especially if the latter (for instance, the polyamide film) is oriented in one direction only.

We studied the change in the surface of the sample by means of an electron microscope (magnification 2400).<sup>14</sup> It has been found that the initial films possess a slightly developed relief. Bands and projections are visible only in some sections of the samples, and their formation may be due to the process of making a film from the polymer.

After the grafting of vinyl monomers the morphological structure of the surface of the sample changes substantially, the changes increasing in proportion to the amount of the grafted polymer. Figure 3 shows such

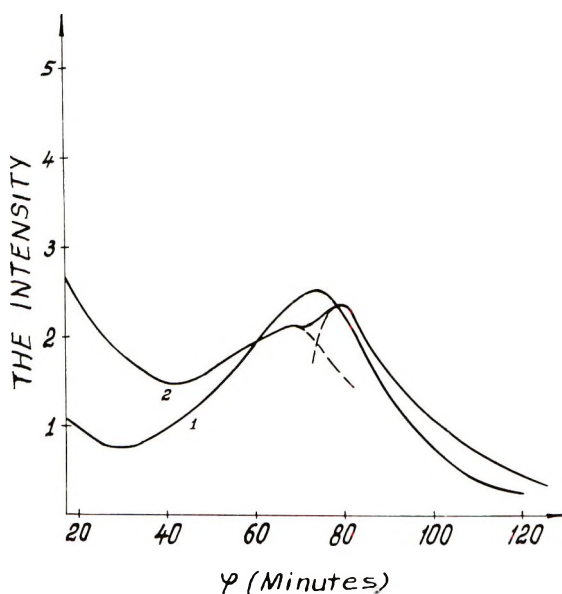


Fig. 4. Curves of small-angle scattering: (1) poly- $\epsilon$ -caproamide with grafted polystyrene (10%); (2) poly- $\epsilon$ -caproamide with grafted polystyrene (20%).

changes, due to the grafting of styrene on films of poly- $\epsilon$ -caproamide. The grafted polystyrene primarily becomes arranged in terraces forming projections with clearly pronounced boundaries.

X-Ray examination of the samples of pemosors has shown that even with large yields of grafting, whose weights are several times that of the initial sample of film, the crystal structure is preserved, although an amorphous halo typical of a vinyl polymer appears in the x-ray pattern.<sup>15</sup>

The x-ray data were corroborated by the results of investigating the samples of grafted films by the nuclear magnetic resonance method. As the width of the lines and the second moment of the nuclear magnetic resonance remained unchanged with an increase in weight of the vinyl polymer over that of the initial sample of 2-300%, it may be assumed that the structure of the polymer remains unchanged after grafting.

After grafting an examination of the samples by the method of small-angle scattering of x-rays permitted the detection of some changes in the supermolecular structure of the polymers.<sup>16</sup>

Figure 4 is a curve of distribution of intensity for samples of poly- $\epsilon$ -caproamide containing 10 and 20% grafted polystyrene. It may be seen that when the yield of grafted polystyrene amounts to 20%, there appears a second maximum and a new long period in addition to the basic maximum ( $d = 78 \text{ \AA}$ ). This points to certain changes in the supermolecular structure, which appear in the outer layer of the polymer under the influence of grafting styrene. The formation of the outer-layer maximum was first observed by Sella<sup>17</sup> in studying samples of polyethylene to which 180% styrene was grafted by the radiation method.

We studied the nature of formation of the structure of pemosors by determining the changes in density of the samples. Additional application was made of the method of light microscopy, by means of which cross sections of the samples were investigated.

The changes in density were measured with a density gradient column at  $25 \pm 0.01^\circ\text{C}$  within  $0.0005 \text{ g/cm}^3$ .<sup>11</sup> They were determined from the difference between the experimental and calculated values of the specific volume. The calculated data were obtained by adding the specific volumes

TABLE II  
Dependence of Density of Polyethylene Terephthalate and Poly- $\epsilon$ -caproamide Samples on Amount of Grafted Polystyrene and Polymethyl Methacrylate<sup>a</sup>

Characteristics of sample <sup>b</sup>	Yield of vinyl lym., %	Density $d$		Spec. vol. $\rho$	
		Exptl.	Calcd.	Exptl.	Calcd.
PET biaxially oriented, grafted with PMM	10.6	1.3440	1.3449	0.7440	0.7435
	27.2	1.2665	1.2730	0.7895	0.7632
	279.0	1.2130	1.2135	0.8244	0.8240
	606.0	1.1925	1.1929	0.8385	0.8382
PET biaxially oriented, grafted with PSt	5	1.3290	1.3347	0.7524	0.7492
	17.0	1.3005	1.2960	0.7689	0.7716
	95.0	1.2355	1.1767	0.8186	0.8498
	107.0	1.1845	1.1674	0.8442	0.8566
	183	1.1335	1.1316	0.8822	0.8837
	1120	1.0580	1.0544	0.9454	0.9484
PET uniaxially oriented, grafted with PSt	30.9	1.2895	1.2905	0.7770	0.7749
	97.08	1.2045	1.2050	0.8802	0.8299
PC grafted with PMM	11.9	1.1200	1.1273	0.8920	0.8868
	85.0	1.1430	1.1468	0.8748	0.8719
PC grafted with PSt	11.4	1.1255	1.1175	0.8884	0.8948
	200	1.0705	1.0634	0.9341	0.9784
	725	1.05	1.0445	0.9505	0.9574

<sup>a</sup> Density  $d$  of initial polyethylene terephthalate, 1.3545; of polymethylmethacrylate homopolymer, 1.1700; of polystyrene homopolymer, 1.0340; of initial poly- $\epsilon$ -caproamide, 1.1280.

<sup>b</sup> PET, polyethylene terephthalate; PMM, polymethyl methacrylate, PSt, polystyrene; PC, poly- $\epsilon$ -caproamide.

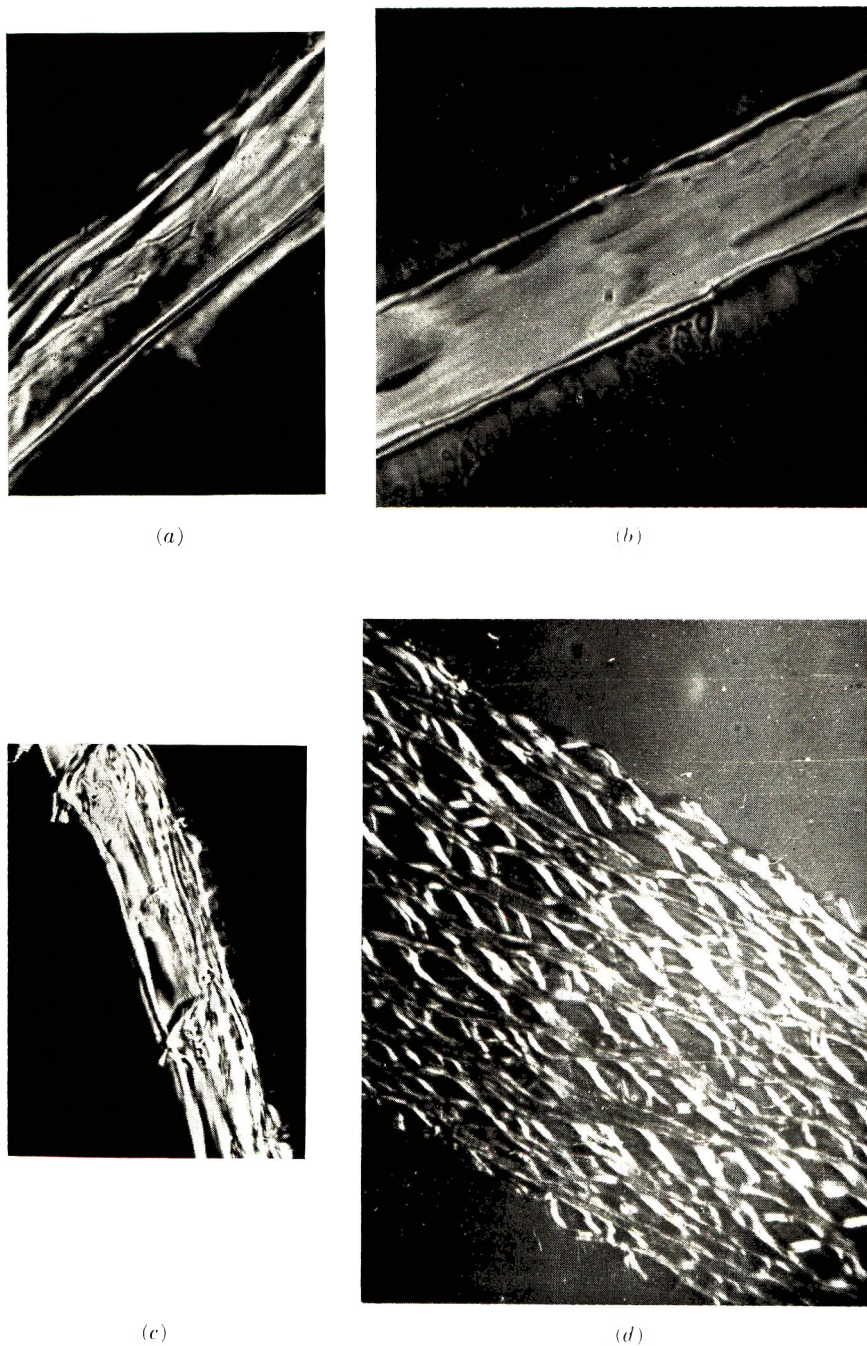


Fig. 5. Microphotographs of transverse cuts of initial and grafted poly- $\epsilon$ -caproamide and polyethyleneterephthalate films: (a) initial poly- $\epsilon$ -caproamide (magnification  $\times 400$ ); (b) poly- $\epsilon$ -caproamide with polymethylmethacrylate (30%) (magnification  $\times 400$ ); (c) initial polyethyleneterephthalate (magnification  $\times 200$ ); (d) polyethyleneterephthalate with polystyrene (200%), grafted three times; (magnification  $\times 400$ ).

of the homopolymer components of a graft copolymer of a certain composition.

The results are presented in Table II, which shows that, after being grafted on polyethylene terephthalate or poly- $\epsilon$ -caproamide, the methyl methacrylate somewhat loosens the surface of the initial film (the density diminishes). With greater yields of grafting (of the order of hundreds of per cent) there are no considerable changes in the structure of the polymers. The grafting of styrene in small amounts (up to 20%) likewise loosens somewhat the surface of the initial sample.

The results are in agreement with observations of cross sections of the samples in polarized light.

It has been found that methyl methacrylate is grafted on poly- $\epsilon$ -caproamide only at the surface (Fig. 5*a* and *b*). This monomer likewise is grafted in exactly the same way on polyethylene terephthalate (a biaxially oriented film was used for the investigation).

The grafting of styrene on polyamide film is accompanied by a slight penetration of the vinyl polymer, which is in agreement with the previously obtained data on the change in density.

If styrene is grafted on a biaxially oriented film of polyethylene terephthalate, only surface grafting is recorded in the case of small yields of grafted polystyrene (up to 25%). As the yield of grafted polystyrene increases up to 100%, it is possible to observe a penetration of the polystyrene into the depth of the polyester film and, as the yield increases to 200%, volume-grafted polystyrene is obtained (Fig. 5*c* and *d*). The volume grafting probably is due to the large number of microdefects and microcavities formed in the film in the course of biaxial orientation.

Operating under the same conditions with a uniaxially oriented polymer, we obtained only a surface-grafted copolymer. A section of the resultant sample was very similar to the one shown in Figure 5*b*.

Thus, the depth of penetration of a grafted monomer on a polymer depends, not only on the chemical nature of the initial polymer and monomer, but also on the degree to which the inner surface of the initial polymer is developed.

All the resultant pemosors could be dissolved in cresol and so had no crosslinked structure. The reduced viscosity of many of the samples so obtained was very high, which pointed to the great molecular weight of the grafted chains. For example, the reduced viscosity of a pemosor of poly- $\epsilon$ -caproamide and of successively grafted polystyrene and polymethyl methacrylate (the increase in weight amounts to 540%) was equal to 12.60. The molecular weight of polystyrene extracted from a graft copolymer was about 1000000.

The change in polydispersity of the samples after multiple grafting of vinyl monomers was determined by turbidimetric titration of a cresol solution of the pemosors. *n*-Heptane was used as a precipitating agent. Figures 6*a* and 6*b* show the turbidimetric curves obtained for samples of polyamide and polyester films to which styrene and methyl methacrylate

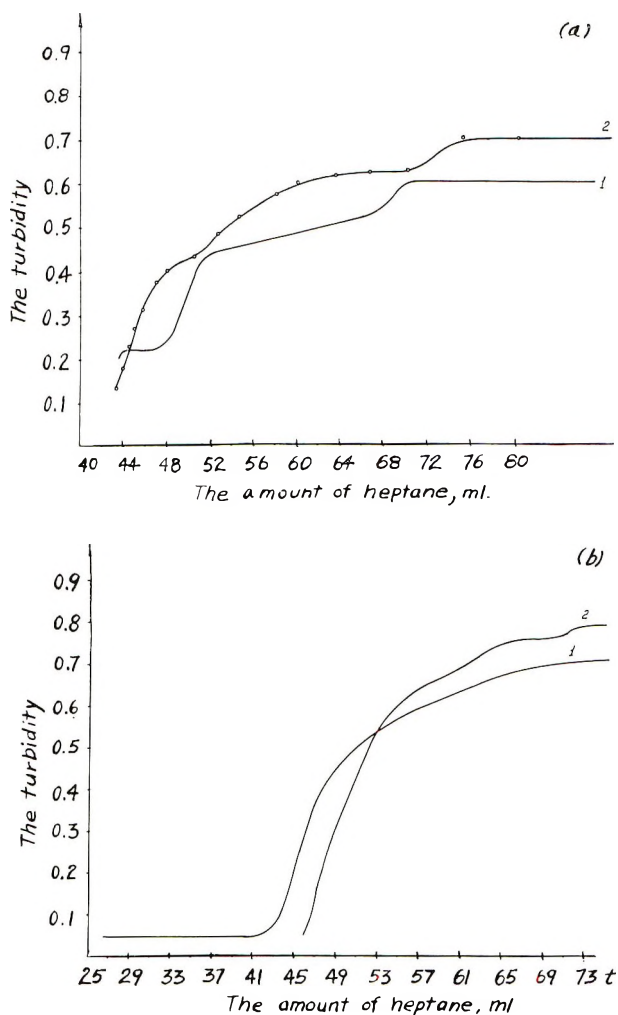


Fig. 6. Curves of turbidimetric titration: (a1) polyethyleneterephthalate with polystyrene and polymethylmethacrylate polymers alternately grafted four times (840%); (a2) poly- $\epsilon$ -caproamide with polystyrene and polymethylmethacrylate polymers alternately grafted four times (540%); (b1) polyethyleneterephthalate with grafted polymers consisting of a polystyrene and polymethylmethacrylate mixture (180%); (b2) poly- $\epsilon$ -caproamide with grafted polymers consisting of a polystyrene and polymethylmethacrylate mixture (30%).

were grafted. The monomers were grafted either as a mixture in one procedure (Fig. 6a) or successively, first styrene and then methyl methacrylate (Fig. 6b). It is evident that the curves appreciably differ from one another. If a mixture of monomers was grafted in one procedure, the curve did not exhibit any bends typical of each of the monomers. In the case of successive grafting of the same monomers these bends were clearly noticeable. Hence, by successively grafting different monomers on films it is

possible to obtain polymers that qualitatively differ from those containing the same monomers grafted as a mixture in one procedure.

Multiple grafting of vinyl monomers substantially enhances the resistance of the initial films to the action of aggressive media. For instance, an initial polyethylene terephthalate quickly dissolved in concentrated sulfuric acid, but its dissolution required many days after a considerable amount of styrene had been grafted on it.

When a polyester film was boiled with twice-grafted polystyrene (200% of the weight of the film) with a 40% solution of KOH for 100 hr, the loss in weight amounted to about 8%. An initial film of polyethylene terephthalate became fully dissolved in this solution of alkali in a few hours.

### Experimental

To obtain pemosors use was made of the method we described previously.<sup>4</sup>

The initial films were thoroughly washed with benzene and dried *in vacuo* at 40–60°C to a constant weight.

A specimen of the film was weighed on an analytical balance and then activated by being heated in air at 110°C for 3 min. For this purpose the specimen was placed in a cylindrical glass vessel equipped with a calcium chloride tube and heated to the desired temperature by means of a thermostat.

After activation, the monomer was added in an amount to cover the film with the liquid. The apparatus was attached to a reflux condenser, and nitrogen was induced through an inlet tube at the rate of one or two bubbles per second (the nitrogen had been deoxygenated and dried). The apparatus was then placed in the thermostat for the graft copolymerization. The duration and temperature of the reaction changed with the experimental conditions (the thermostat temperature was kept within an error of  $\pm 0.1^\circ\text{C}$ ). After the reaction was finished, the specimen of film was taken out, washed with solvents that dissolved the homopolymer to remove the monomer and homopolymer, and boiled in the same solvents to remove the homopolymer completely. The specimen was then dried *in vacuo* at 40–60°C to a constant weight.

The percentage yield of the grafted vinyl polymer then was determined.

The single-graft copolymer so obtained was used for subsequent graftings of vinyl monomers by the method described.

The change in the capacity of the film for swelling in monomers was studied at 20 and 80°C. In the latter case the determination was made in the presence of hydroquinone, which retarded the beginning of polymerization of the monomer.

Investigation of the samples of films by the sedimentation method was carried out by means of an ultracentrifuge of the  $\Gamma$ -110 type, MOM Company, Hungary (40000–50000 revolutions) 20°C. The average experiment lasted 90 min.

The surface of the samples of the films was studied with a UEMV-100 electron microscope with screen magnification of 24000.

For a study of crystalline long periods the distribution of intensity along the meridian of a small-angle x-ray pattern was investigated. The curve of distribution of intensity was obtained in a small-angle camera with a collimator of the Kratky type with a copper source and a nickel filter. The linear beam was perpendicular to the axis of the texture. The half-width of the beam amounted to about 2' of a degree.

The cross sections of the samples of grafted films were examined in polarized light by means of a MKU-I microscope.

The turbidimetric titration of the samples of polymers was done with a modernized photometer.

### Conclusions

(1) Multiple-graft copolymers, or pemosors, were obtained by multiple grafting of the same or different vinyl monomers on heterochain polymers.

(2) By multiple grafting it is possible to produce pemosors with a high yield of a vinyl polymer having 500–1000% the weight of the initial sample.

(3) Multiple grafting of vinyl monomers does not bring about any changes in the crystalline part of the initial polymers. Changes are recorded in the supermolecular structure of the outer layer.

(4) The nature of the grafting and the depth of penetration of the grafted monomer depend on the density of packing of the supermolecular elements of the polymeric base structure and also on the chemical nature of the initial polymers and monomers.

(5) It has been proved that pemosors are polymers of a new type, differing in their properties from ordinary polymers and from single-graft copolymers.

The authors wish to express their profound gratitude to S. A. Pavlova and G. L. Berestneva for carrying out a number of investigations into the properties of pemosors and for their help in discussing the results.

### References

1. I. Burlant and A. Hoffmann, *Block and Graft Copolymers*, Foreign Literature Publishing House, Moscow, 1963 (Russ.).
2. R. Cereza, *Block and Graft Copolymers*, Mir Publishing House, Moscow, 1963 (Russ.).
3. V. V. Korschak and K. K. Mozgova, *Izv. SSSR, Akad. Nauk Otd. Khim. Nauk*, **1958**, 61.
4. V. V. Korschak, K. K. Mozgova, and M. A. Shkolina, *Vysokomolekul. Soedin.*, **2**, 957 (1960).
5. V. V. Korschak, K. K. Mozgova, and M. A. Shkolina, *J. Polymer Sci.*, **58**, 753 (1962).
6. Swiss Pat. 386383, *Ref. Zh. Khim.*, **1966**, 10 C, 887.
7. E. B. Trostyanskaya and A. S. Tevlina, *Vysokomolekul. Soedin.*, **5**, 44 (1963).
8. D. Anastasios and P. Remp, *Compt. Rend. Acad. Sci.*, **256**, 4443 (1963).
9. G. Smets, W. Winter, and G. Delzenne, *J. Polymer Sci.*, **55**, 767 (1961).
10. I. Hamellers and G. Smets, *Makromol. Chem.*, **47**, 7 (1961).
11. V. V. Korschak, K. K. Mozgova, and Yu. V. Egorova, *Vysokomolekul. Soedin.*, **6**, 571 (1964).

12. B. V. Lokshin, V. V. Korschak, K. K. Mozgova, and Yu. V. Egorova, *Dokl. Akad. Nauk SSSR*, **166**, 118 (1966).
13. S. A. Pavlova, V. V. Korschak, Yu. V. Egorova, and K. K. Mozgova, *Dokl. Akad. Nauk SSSR*, **177**, 589 (1967).
14. V. V. Korschak, K. K. Mozgova, Yu. V. Egorova, E. M. Belavtseva, and K. Z. Gumargaliyeva, *Vysokomolekul. Soedin.*, **8**, 1365 (1966).
15. V. V. Korschak, D. Y. Tsvankin, and S. P. Krukovsky, *Dokl. Akad. Nauk SSSR*, **146**, 1347 (1962).
16. D. Y. Tsvankin, K. K. Mozgova, and Yu. V. Egorova, *Vysokomolekul. Soedin.*, **9**, 145 (1967).
17. C. Sella, *J. Polymer Sci.*, **48**, 207 (1960).
18. V. V. Korschak, G. L. Berestneva, K. K. Mozgova, and Yu. V. Egorova, *Vysokomolekul. Soedin.*, in press.

Received October 31, 1967

Revised March 5, 1968

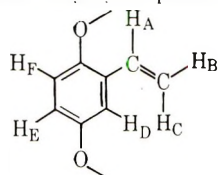
## Electron-Transfer Polymers. XXIX. Copolymerizability of Vinylhydroquinone Derivatives

KEIKICHI UNO, MUTSUKO OHARA, and HAROLD G. CASSIDY,  
*Sterling Chemistry Laboratory, Yale University, New Haven,  
Connecticut 06520*

### Synopsis

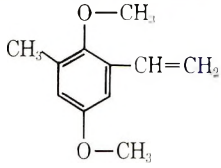
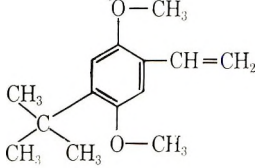
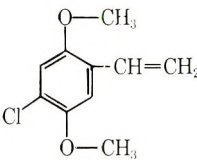
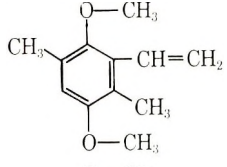
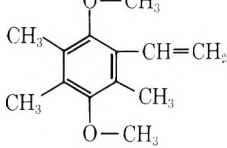
Ten vinylhydroquinone and one vinyl resorcinol derivatives are compared, particularly with respect to NMR spectra and copolymerizability with styrene. They are vinylhydroquinone dimethyl ether (I), vinyl-*O,O'*-bis(1-ethoxyethyl)hydroquinone (II), vinylhydroquinone di(2-pentyl)ether (III), 4-vinyl resorcinol bismethoxymethyl ether (IV), 2-vinyl-5-methylhydroquinone dimethyl ether (V), 2-vinyl-5-methyl-*O,O'*-bis(1-ethoxyethyl)hydroquinone (VI), 2-vinyl-6-methylhydroquinone dimethyl ether (VII), 2-vinyl-5-*tert*-butylhydroquinone dimethyl ether (VIII), 2-vinyl-5-chlorohydroquinone dimethyl ether (IX), 2-vinyl-3,6-dimethylhydroquinone dimethyl ether (X), and 2-vinyl-3,5,6-trimethylhydroquinone dimethyl ether (XI). All the vinyl protons have almost the same coupling constants. Though subtle distinctions are found among all the spectra, they can in general be put into two groups on the basis of the chemical shifts. Let the hydrogen on carbon-1 of the vinyl group be A, the hydrogen *cis* to A be B the hydrogen *trans* to A be C, then in the first group, (I) through (IX), the chemical shifts ( $\tau$ ) are (A)  $3.02 \pm 0.08$ , (C)  $4.41 \pm 0.05$ , and (B)  $4.87 \pm 0.07$ , and in the second group, (X) and (XI), they are (A)  $3.30 \pm 0.03$ , (C)  $4.49 \pm 0.01$ , and (B)  $4.59 \pm 0.03$ . It is supposed that in (X) and (XI) the vinyl group is out of the plane of the ring, because of the two *ortho* substituents, and this conformation is reflected in the NMR data. Ultraviolet spectra are consonant with this interpretation, since the  $\lambda_{\max}$  of (X) and (XI) correspond closely with those of nonvinyl reference compounds, while those of (II), (V), and (VIII) are shifted to longer wavelengths. When these compounds are copolymerized separately with styrene, the behaviors are classifiable into the following three groups, where  $r_1$  and  $r_2$  are monomer reactivity ratios with styrene as the first monomer: (i)  $r_1 < 1$  and  $r_2 < 1$  for compounds (II) and (III) and the reference compound *O,O'*-dibenzoylvinylhydroquinone, (ii)  $r_1 < 1$  and  $r_2 > 1$  for compounds (I), (V), (VII), (VIII), (IX), and (iii)  $r_1 > 1$  and  $r_2 = 0$  for compounds (X) and (XI). These behaviors are correlated with the effect of electronegativity of groups on the stability of the radical at the growing end of the chain and with the simultaneous effects of steric hindrance.

This paper reports a further step<sup>1,2</sup> toward the synthesis of polymers in which redox functional groups are spaced out along polymer chains. When fully oxidized and fully reduced polyvinylhydroquinone redox polymers are mixed in solution, a sequence of changes takes place that reflects the exchange of electrons and protons between the functional groups.<sup>1,3</sup> These changes are indicated by spectral changes of the charge-transfer type that serve as internal indicators of the interactions and are a function of the intramolecular distance between the redox groups.<sup>1,3,4</sup> The observed

TABLE I  
 NMR Data on Vinylhydroquinone Derivatives


Compound no. and structure	Hydrogen <sup>a</sup>					
	H <sub>A</sub>	H <sub>B</sub>	H <sub>C</sub>	H <sub>D</sub>	H <sub>E</sub>	H <sub>F</sub>
I 	2.99 11, 18	4.83 2, 11	4.36 2, 18	3.05	3.36	3.40
II 	2.94 11, 18	4.83 2, 11	4.34 2, 18	2.91	3.15	
III 	2.90 11, 18	4.80 2, 11	4.32 2, 18	2.96	3.23	
IV 	3.05 11, 18	4.93 2, 11	4.46 2, 18	3.27 1, 2, 5	3.42 2, 5, 8	2.74 1, 8
V 	3.05 11, 18	4.91 2, 11	4.44 2, 18	3.23	—	3.51
VI 	3.00 11, 18	4.86 2, 11	4.43 2, 18	2.90	—	3.22

TABLE I *continued*

Component no. and structure	Hydrogen <sup>a</sup>					
	H <sub>A</sub>	H <sub>B</sub>	H <sub>C</sub>	H <sub>D</sub>	H <sub>E</sub>	H <sub>F</sub>
VII 	2.92 11, 18	4.69 2, 11	4.25 2, 18	3.12	3.34	—
VIII 	3.01 11, 18	4.88 2, 11	4.41 2, 18	3.12	—	3.27
IX 	3.10 11, 18	4.82 2, 11	4.40 2, 18	3.08	—	3.23
X 	3.27 11, 18	4.56 2, 11	4.48 2, 18	—	3.57	—
XI 	3.33 11, 18	4.62 2, 11	4.50 2, 18	—	—	—

<sup>a</sup> The first figure given is  $\tau$ ; the second two figures are  $J_{\text{cps}}$ .

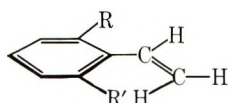
shifts in absorption maxima and changes in intensity provide a new tool with which to examine the behavior of polymer molecules in solution. In the course of copolymerizability studies made to obtain monomer reactivity ratios certain correlations appeared. These are reported since they deal with new compounds and may be of general interest.

## RESULTS AND DISCUSSION

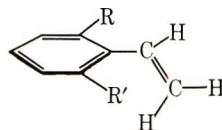
### NMR and Ultraviolet Absorption Spectra

Formulas and NMR data for the substances discussed in this report are collected in Table I; ultraviolet absorption data for several compounds and two reference compounds are collected in Table II. The compounds in Table II fall into two classes: compounds (II), (V), and (VIII) have absorption maxima above 300 m $\mu$ ; compounds (X) and (XI), close to

290 m $\mu$ . In the first class the vinyl group can lie in the plane of the benzene ring, and the resulting conjugation provides the increased delocalization path that is reflected in the longer wavelength of maximum absorption; see the accompanying scheme. In the second class the bulky R groups



Compounds (I)–(IX)  
R = OCH<sub>3</sub>  
R' = H



Compounds (X) and (XI)  
R = OCH<sub>3</sub>  
R' = CH<sub>3</sub>

In compounds (I)–(IX), where R = OCH<sub>3</sub> and R' = H, the vinyl group may lie in the plane of the ring. This is not possible with compounds (X) and (XI), where R = OCH<sub>3</sub> and R' = CH<sub>3</sub>, for there are bulky groups on both sides of the vinyl position.

*ortho* to the vinyl (see the scheme) prevent it from lying coplanar with the ring, thus preventing the conjugation: the absorption maxima lie in the same position as those of the nonvinyl reference compounds hydroquinone dimethyl ether and ethylhydroquinone dimethyl ether.

Two classes are reflected also in the NMR data, Table I. It is well known that in vinyl compounds the coupling constants of *trans* protons, *cis* protons, and *geminal* protons are approximately 18, 11, and 2 cps, respectively. On the basis of such a relation all of the signals of vinyl protons of compounds (I)–(XI) were assigned as shown in Table I. Here two classifications can be found: for compounds (I)–(IX)  $\tau$  is  $3.02 \pm 0.08$ ,  $4.08 \pm 0.07$ , and  $4.41 \pm 0.05$ , and for compounds (X) and (XI), with two bulky substituents *ortho* to vinyl, it is  $3.30 \pm 0.03$ ,  $4.59 \pm 0.03$ , and  $4.49 \pm 0.01$ .

Signals of phenyl protons also assigned. In aromatic compounds, if two protons are in the position *ortho* or *meta* to each other, the coupling constant is of the order of 8–3 cps, but if they are in the *para* position, it is very small. Although these coupling interactions are not always observed, by fortunate circumstance they were clearly evident in the spectrum of compound (IV), and this permitted assignment of the signals to the phenyl protons. If the protons that give signals in the lowest, the middle, and the highest magnetic fields are labeled D, E, and F, respectively (Table I), then

TABLE II  
Ultraviolet Absorption Data in Methanol

Compound no.	$\lambda_{\max}$
II	308
V	316
VIII	321
X	289
XI	292
Hydroquinone dimethyl ether	290
Ethylhydroquinone dimethyl ether	292

the following relations may be deduced. F and D are in the *para* relation to each other, F and E are in the *ortho*, and D and E are in the *meta*. Therefore, D corresponds to the proton *ortho* to the vinyl group, E to the proton *ortho* both to F and an oxymethylene, and D to the proton between the two oxymethylene groups. The signal of the proton *ortho* to the vinyl is at unusually low magnetic field. This would be explained by the influence of the local magnetic field of the vinyl, with the consideration that the vinyl group is in the same plane as the ring. This behavior is found in compounds (I)–(IX).

### Copolymerization of Vinylhydroquinone with Styrene

The results of copolymerizing compounds (I)<sup>5</sup>–(XI) separately with styrene and also the reference compound *O,O'*-dibenzoylvinyhydroquinone<sup>6</sup> are shown in Table III. The values in this table were calculated by the Fineman-Ross method.<sup>7</sup>

TABLE III  
Monomer Reactivity Ratios of Substituted Vinylhydroquinones<sup>a</sup>

Compound	$r_1$	$r_2$	$\log 1/r_1$
Group (i):			
<i>O,O'</i> -Dibenzoylvinyhydroquinone	0.22	0.43	0.66
II	0.90	0.50	0.05
III	0.96	0.20	0.02
Group (ii):			
I	0.77	1.13	0.11
V	0.88	1.30	0.05
VII	0.88	1.30	0.05
VIII	0.60	1.20	0.22
IX	(0.59) <sup>b</sup>		(0.22) <sup>b</sup>
Group (iii):			
X	3.5	0	−0.54
XI	3.0	0	−0.49

<sup>a</sup> M<sub>1</sub>, styrene; M<sub>2</sub>, vinylhydroquinone; reaction temperature, 60°C, solvent, benzene.

<sup>b</sup> Parentheses indicate some uncertainty in the values.

On the basis of their copolymerization behavior with styrene, *O,O'*-dibenzoylvinyhydroquinone and compounds (I)–(XI) are classifiable as three groups, in which  $r_1$  and  $r_2$  are monomer reactivity ratios of the vinylhydroquinones, where styrene is the first monomer, M<sub>1</sub>:

(i) The group in which  $r_1 < 1$  and  $r_2 < 1$ . *O,O'*-Dibenzoylvinyhydroquinone, compounds II and III belong in this group.

(ii) The group in which  $r_1 < 1$  and  $r_2 > 1$ . This group contains compounds (I), (V), (VII), (VIII), and (IX).

(iii) The group in which  $r_1 > 1$  and  $r_2 = 0$ . The compounds (X) and (XI) belong in this group. Once again, compounds (X) and (XI) fall into a separate category.

It is common in examining for correlations between structure and rate of reaction of organic compounds to separate functional group effects into three types: inductive, resonance, and steric effects.<sup>8</sup> Walling et al.<sup>9</sup> in a study of the copolymerization behavior of *para*-substituted styrenes ( $M_2$ ) with styrene ( $M_1$ ) found a linear relation between  $\log 1/r_1$  and Hammett  $\sigma$  values of the substituents (Fig. 1) with a  $\rho$  value of 0.502. The Hammett equation, source of the  $\sigma$  and  $\rho$  parameters, gives excellent results with *meta*- and *para*-substituted molecules but generally fails with *ortho*-substituted ones,<sup>10a</sup> for steric effects are not taken into account in the equation.

Suppose that a  $\sigma$  value for *ortho*-methoxy is taken as  $-0.39$ <sup>10b</sup> and that  $\Sigma\sigma$  is plotted against  $\log 1/r_1$ . It is then found that the monomers, except (VII), are separated into two groups: compounds (I), (II), (III), (V),

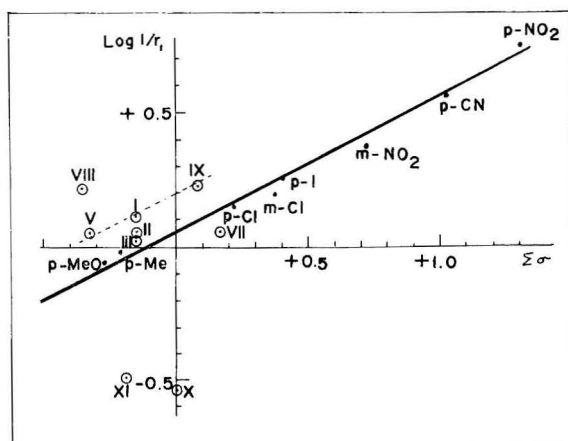


Fig. 1. Arrangement of data on a Walling-Briggs-Wolfstirn-Mayo plot of  $\sigma$  versus  $\log 1/r_1$ .<sup>9</sup>

(VIII), and (IX) form a cluster above the  $\rho = 0.502$  line, and (X) and (XI) fall close together well below the line. Compound (VII) presents an interesting problem in interpretation. The methoxy *ortho* to vinyl is further hindered by a methyl on the other side. The conjugation of its oxygen with the ring may well be blocked. It is then not reasonable to give it a  $\sigma$  value of  $-0.39$ , but the (unconjugated substituent) *meta* value  $+0.115$  becomes defensible. The point then falls close to the straight line in Figure 1. It must be pointed out that in radical polymerization  $\log (k_0/k_p)$  is very nearly equal to zero. The effect of methoxyl is very nearly the same, whether *ortho* or *para* to the reactive ( $sp^2$ ) carbon at the growing end of the chain; nevertheless the interpretation of the behavior of (VII) does represent a considerable extrapolation.

Should a dimethoxy vinyl monomer become the terminal unit of a growing polymer chain, the radical that is present is stabilized by resonance.

Thus, monomer (I) can react with any terminal radical more easily than can styrene, and monomer reactivity ratios become  $r_1 < 1$  and  $r_2 > 1$ . Compound (III), group (i), has two 2-pentyloxy groups, and the effect of these substituents on the benzene ring is considered to be nearly the same as with the methoxy group. But the copolymerization behavior of the compound is quite different from that of compound (I); that is,  $r_1 < 1$  and  $r_2 < 1$ . This behavior is interpreted as due to steric hindrance by the bulky pentyloxy group. The copolymerization behavior of compounds (II) and (III) appears the same as that of *O,O'*-dibenzoylvinylhydroquinone, but one must consider the electronegativity of the benzoyl group as contributing to the behavior of that monomer.

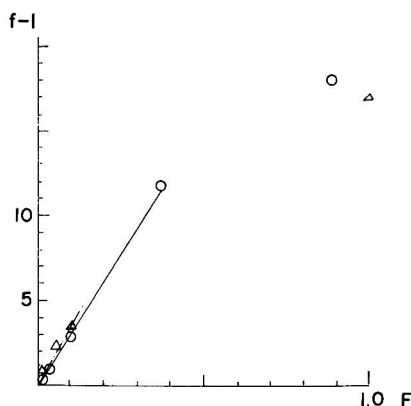


Fig. 2. Mole ratio  $F$  of styrene to monomer in reaction mixture versus mole ratio  $f$  of styrene to monomer in copolymer obtained in a limited period of reaction: ( $\Delta$ ), compound (X); (O) compound (XI).

Compounds (X), and (XI), which show no appreciable conjugation between the vinyl group and the ring, are characterized by the values  $r_1 > 1$  and  $r_2 = 0$  in copolymerization with styrene. Should one of these monomers become a terminal unit on a growing chain, the reactivity of the radical must be decreased very much by the steric hindrance of the substituents R and R' on the ring.

Figure 2 is a plot of  $f - 1$  versus  $F$ . Here  $F$  is the molar ratio of styrene to monomer (X) or (XI) in a reaction mixture, and  $f$  is the molar ratio of styrene to monomer (X) or (XI) in the corresponding copolymer. With monomer (XI) versus styrene a slope of 3.0 is obtained between  $f - 1 = 0$  and  $f - 1 = 11$ . The same tendency and nearly the same slope are found in the copolymerization of monomer (X) with styrene. In both cases straight lines pass through the origin; thus  $r_2 = 0$ . Moreover, the linear relation between  $F$  and  $f - 1$  up to a large value of  $f - 1$  seems to indicate very little remote effect of (X) or (XI) radical (penultimate or prepenultimate effect) on the growing chain end, in spite of the large repulsion between the growing end of the chain with its (X) or (XI) radical and newly approaching (X) or (XI) monomer.

## EXPERIMENTAL

## Syntheses of Vinyl Monomers

*O,O'*-dibenzoylvinylhydroquinone,<sup>6</sup> vinylhydroquinone dimethyl ether (I),<sup>5</sup> vinyl-*O,O'*-bis(1-ethoxyethyl)-hydroquinone (II),<sup>11</sup> 4-vinyl resorcinol bismethoxymethyl ether (IV),<sup>2</sup> 2-vinyl-5-methylhydroquinone dimethyl ether (V),<sup>2</sup> 2-vinyl-5-methyl-*O,O'*-bis(1-ethoxyethyl) hydroquinone (VI),<sup>2</sup> 2-vinyl-3,6-dimethylhydroquinone dimethyl ether (X),<sup>2</sup> and 2-vinyl-3,5,6-trimethylhydroquinone dimethyl ether (XI)<sup>2</sup> were synthesized by the methods presented in previous papers.

## 2-Vinylhydroquinone Di-2-pentyl Ether (III)

(III-a). Bromohydroquinone di-2-pentyl ether. A mixture of bromohydroquinone (104 g, 0.55 mol), 2-pentyl bromide (190 g, 1.25 mols), potassium hydroxide (61.6 g, 1.1 mols), 50 ml of water, and 250 ml of alcohol was heated to reflux with stirring for 24 hr. The reaction mixture was extracted with ether. The ethereal solution was washed with aqueous potassium hydroxide and then water and dried over anhydrous sodium sulfate. After removal of the solvent fractionation of residual oil gave 40 g of recovered pentyl bromide and a reddish oil; bp 120–130°C at 0.2 mm. The oily product was reduced with aqueous sodium hydrosulfite and extracted with ether. After washing of the ethereal solution with aqueous potassium hydroxide, fractionation under reduced pressure gave a slightly yellowish oil; bp 128–130°C at 0.2 mm, 36 g (20%).

ANAL. Calcd. for  $C_{16}H_{25}O_2Br$ : C 58.36%, H 7.65%. Found: C 58.26%, H 7.66%.

(III-b). 2-Hydroxyethylhydroquinone di-2-pentyl ether. To a solution of 36 g (0.12 mol) of (III-a) in 150 ml of dry ether was added 80 ml (0.13 mol) of *n*-butyllithium in hexane with stirring below 15°C, and the stirring was kept up for 1.5 more hours at 15°C. Into this solution 7.0 ml of freshly distilled ethylene oxide was added in one portion. The reaction mixture was kept standing overnight with stirring at room temperature. After washing of the reaction mixture with water and drying fractionation under reduced pressure gave a yellowish oil; bp 135–140°C at 0.2 mm 15 g (43%).

ANAL. Calcd. for  $C_{18}H_{30}O_3$ : C 73.43%, H 10.27%. Found: C 73.45%, H 10.20%.

(III). Dehydration of compound (III-b), 15 g, over potassium hydroxide heated at 270–290°C under reduced pressure (0.5 ml) gave a colorless oil, 11 g. Redistillation of the oil gave 6 g (43%) of a fraction; bp 114–118°C at 0.2 mm.

ANAL. Calcd. for  $C_{18}H_{28}O_3$ : C 78.21%, H 10.21%. Found: C 78.02%, H 10.30%.

## 2-Vinyl-6-methylhydroquinone Dimethyl Ether (VII)

(VII-a). 2-(2-hydroxyethyl)-6-methylhydroquinone dimethyl ether. To a solution of 23 g (0.1 mol) of 2-bromo-6-methylhydroquinone dimethyl

ether in 100 ml of dry ether was added *n*-butyllithium in hexane, 68 ml (0.11 mol), and the reaction mixture was kept standing with stirring at 15°C. After 2 hr 6.5 ml of freshly distilled ethylene oxide was added, and the reaction mixture was treated as in the case of (III-b). Fractionation gave a colorless oil; bp 125–135°C at 0.4 mm, 18 g (90%).

ANAL. Calcd. for  $C_{11}H_{16}O_3$ : C 67.32%, H 8.22%. Found: C 67.30%, H 8.25%.

(VII). Flashing of (VIIa), 13 g on potassium hydroxide heated at 260 to 270°C under reduced pressure (0.5 mm) gave the dehydrated product, 8 g. Redistillation gave a colorless oil; bp 102–103°C at 4 mm, 7 g (59%).

ANAL. Calcd. for  $C_{11}H_{14}O_2$ : C 74.13%, H 7.92%. Found: C 74.01%, H 8.06%.

Part of the NMR data is shown in Table I. In addition to this, signals were observed at  $\tau = 6.26, 6.33$  (methoxyl) and  $\tau = 7.72$  (methyl). No other signals were observed. This spectrum corresponds to the structure of 2-vinyl-6-methyl-hydroquinone dimethyl ether.

### 2-Vinyl-5-*t*-butylhydroquinone Dimethyl Ether (VIII)

(VIII-a). *t*-Butylhydroquinone dimethyl ether. To a mixture of *t*-butylhydroquinone (123 g, 0.74 mol) and dimethyl sulfate (227 g, 1.8 mols) in 150 ml of methanol was added, dropwise, potassium hydroxide (242 g, 4.3 mols) in 400 ml of water at 20°C. The reaction mixture was allowed to stand for 4 hr at 40–50°C with stirring. The organic layer was extracted with ether. After washing of the ethereal solution with water the solvent was distilled. Fractionation of the residual oil gave a colorless liquid; bp 96–98°C at 2 mm, 57 g (40%).

The NMR spectrum of the product in carbon tetrachloride gave signals at  $\tau$  of 8.64 (*t*-butyl), 6.40 and 6.35 (methoxyl), 3.42 (two aromatic protons), and 3.20 (one aromatic proton). No other signals were observed. This spectrum corresponds to the structure of *t*-butylhydroquinone dimethyl ether.

(VIII-b). 2-Chloromethyl-5-*t*-butylhydroquinone dimethyl ether. Hydrogen chloride gas was introduced into a mixture of *t*-butylhydroquinone dimethyl ether (58 g, 0.03 mol) and 37% formalin (36.5 g, 0.45 mol) in 50 ml of benzene at 20°C. After saturation with hydrogen chloride the reaction mixture was heated at 55–60°C for 3.5 hr with stirring. The benzene layer was separated, washed with aqueous sodium carbonate, and dried over sodium sulfate. Fractionation gave a colorless oil; bp 112–120°C at 2 mm, 57 g (78%). The oil solidified. Recrystallization from *n*-hexane gave white needles; mp 39–40°C.

The NMR spectrum of the product in carbon tetrachloride showed signals at  $\tau$  of 8.64 (*t*-butyl), 6.22 (methoxyl), 5.47 (chloromethyl), and 3.23 and 3.19 (aromatic). No other signals were observed.

(VIII). A mixture of (VIII-b) and an equimolar amount of triphenylphosphine in toluene was heated to reflux. After 4 hr the reaction mixture

was cooled. Clumps of yellow crystals separated. These were broken up, washed with toluene and ether, and dried over phosphorus pentoxide.

The product obtained (31 g) was dispersed in 200 ml of dry ether, and 15% *n*-butyllithium in hexane (39 ml) was added to the dispersion at 10°C under a nitrogen atmosphere. After 10 min trioxymethylene (7.5 g) was added with dry ether (100 ml), and the mixture was kept standing at room temperature for 2 hr more. Insoluble products were filtered off, and the ethereal solution was washed with water and dried over sodium sulfate. Removal of the solvent by distillation gave a colorless oil; bp 103–105°C at 2 mm, 8.5 g. The overall yield from (VIII-b) was 32%. The oil solidified. Recrystallization from *n*-hexane gave white needles; mp 32°C.

A part of the NMR spectrum of the product is given in Table I. Signals were observed also at  $\tau$  of 8.64 (*t*-butyl) and 6.33 and 6.29 (methoxyl). No other signals were given. This spectrum corresponds to 2-vinyl-5-*t*-butylhydroquinone-dimethyl ether.

### 2-Vinyl-5-chlorohydroquinone Dimethyl Ether (IX)

(IX-a). 2-Chloromethyl-5-chlorohydroquinone dimethyl ether. A mixture of chlorohydroquinone dimethyl ether (61 g, 0.35 mol) and 37% formalin (42 g, 0.42 mol) in 50 ml of benzene was saturated with hydrogen chloride gas at 20°C. After saturation with the gas the temperature was raised to 60°C and maintained for 7 hr with stirring and slow bubbling of the gas. The benzene layer was separated, washed, and dried over sodium sulfate. The solvent was removed by distillation, and the fractionation of the residual liquid gave a colorless oil; bp 120–130°C at 2 mm, 52 g (67%). The oil solidified. Recrystallization from *n*-hexane gave white crystalline material; mp 86–87°C.

The NMR spectrum of the product in a mixture of chloroform and carbon tetrachloride (1:1) showed signals at  $\tau$  of 6.17 and 6.14 (methoxyl), 5.42 (chloromethyl), and 3.21 and 3.06 (aromatic). No other signals were obtained.

(IX). A mixture of the product (IX-a) and an equimolar amount of triphenylphosphine in toluene was refluxed for 4 hr. On cooling, yellowish crystals were obtained. These were washed with toluene and ether and dried over phosphorus pentoxide. To a suspension of the above-mentioned product (39 g) in 400 ml of dry ether was added 15% *n*-butyllithium in hexane (51 ml) under a nitrogen atmosphere. The reaction mixture was kept standing 15 min with stirring at 10–15°C. Trioxymethylene (6 g) in 100 ml of ether was added, and stirring was continued for 3 hr more at room temperature. After filtering of the insoluble product the ethereal solution was washed with water and dried over sodium sulfate. Removal of the solvent by distillation left a colorless oil; bp 105–110°C at 2 mm. It solidified. Recrystallization from *n*-hexane gave white crystalline material; mp 55–57°C, 4 g. The overall yield was 21%.

A part of the NMR spectrum of this compound is shown in Table I. In

addition to this signals were observed at  $\tau = 6.28, 6.22$  (methoxyl). This spectrum corresponds to 2-vinyl-5-chlorohydroquinone dimethyl ether.

### Nuclear Magnetic Resonance Spectra of Vinyl Monomers

NMR spectra of the monomers were measured on a Varian Associates Model A-60 spectrometer. Carbon tetrachloride was used as solvent, and the concentration of the solution was approximately 40%. Tetramethylsilane was used as an inner standard.

### Ultraviolet Spectra of Vinyl Monomers

Ultraviolet spectra of the monomers were recorded on a Bausch and Lomb Spectronic 505 spectrometer. Methanol was used as solvent.

### Homopolymerization of Vinyl Monomers (VIII) and (IX)

The homopolymers of the monomers (VIII) and (IX) were obtained by heating the monomer in benzene at 60°C under a nitrogen atmosphere with azobisisobutyronitrile as initiator. The homopolymers were purified by repeated reprecipitation from benzene as solvent and methanol as non-solvent. Both of these polymers were soluble in aromatic hydrocarbons, acetone, and THF.

ANAL. Calcd. for  $C_{14}H_{20}O_2$  (VIII): C 76.32%, H 9.15%. Found: C 76.15%, H 8.98%.

ANAL. Calcd. for  $C_{10}H_{11}O_2Cl$  (IX): C 60.46%, H 5.58%. Found: C 60.92%, H 5.56%.

### Copolymerization of Vinyl Monomers with Styrene

The monomers were purified by either vacuum distillation or recrystallization just before use. Benzene as solvent was purified according to the usual method. Commercial  $\alpha, \alpha'$ -azobisisobutyronitrile was used as initiator. The mixtures of the monomers and styrene in different ratios (total amount, 3 g) were placed in glass polymerization tubes, and 15 mg of the initiator and 5 ml of benzene were added. The tube was sealed under nitrogen. The polymerization reaction was carried out at  $60 \pm 0.01^\circ\text{C}$  in a water bath and stopped by pouring the mixture into methanol. The polymers were collected by centrifugation. For purification the resulting polymers were dissolved in benzene and reprecipitated by methanol. After five repetitions of this procedure the polymers were freeze-dried from benzene.

The contents of the vinyl monomer units in the copolymers were calculated from the values of elemental analyses, which were carried out at Galbraith Laboratories, Inc.

We wish to acknowledge, with thanks, helpful discussion of this paper by Nobuo Nakabayashi and Gerhard Wegner and the support given this work by PHS Research Grant GM 10864, Division of Research Grants, Public Health Service.

An abstract of this paper was presented at the International Symposium on Macromolecular Chemistry, Tokyo, by Uno, September 30, 1966.

### References

1. H. G. Cassidy and K. A. Kun, *Oxidation-Reduction Polymers (Redox Polymers)*, Interscience, New York, 1965; see especially pp. 197 ff.
2. M. Hashimoto, K. Uno, and H. G. Cassidy, *J. Polymer Sci. A-1*, **5**, 993 (1967).
3. R. E. Moser, "Spectral and Redox Properties of Oligomeric Hydroquinones," Dissertation, Yale University, 1965.
4. R. E. Moser and H. G. Cassidy, *J. Org. Chem.*, **30**, 3336 (1965).
5. H. Kamogawa and H. G. Cassidy, *J. Polymer Sci. A*, **2**, 2409 (1964).
6. H. Kamogawa and H. G. Cassidy, *J. Polymer Sci. A*, **1**, 1971 (1963).
7. M. Fineman and S. D. Ross, *J. Polymer Sci.*, **5**, 259 (1950).
8. E. S. Gould, *Mechanism and Structure in Organic Chemistry*, Henry Holt, New York, 1959; cf. Chap. 7.
9. C. Walling, E. R. Briggs, K. B. Wolfstirn, and F. R. Mayo, *J. Am. Chem. Soc.*, **70**, 1537 (1948).
10. R. W. Taft, Jr., in *Steric Effects in Organic Chemistry*, Melvin S. Newman, Ed., Wiley, New York, 1956, (a) Chap. 13, (b) p. 619.
11. R. E. Moser, H. Kamogawa, H. Hartmann, and H. G. Cassidy, *J. Polymer Sci. A*, **2**, 2401 (1964).

Received September 22, 1966

Revised February 23, 1968

## Optically Active Imidazole-Containing Polymers\*

C. G. OVERBERGER† and IWHAN CHO,  
*Department of Chemistry, Institute of Polymer  
Research, Polytechnic Institute of Brooklyn,  
Brooklyn, New York 11201*

### Synopsis

In order to investigate the stereospecificity of enzyme-catalyzed reactions, an optically active copolymer of 4(5)-vinylimidazole and 2,5(*S*)-dimethyl-1-hepten-3-one was synthesized, and its effects on the solvolytic rates, in ethanol-water, of the *p*-nitrophenyl and 4-carboxy-2-nitrophenyl esters of 3(*R*)- and 3(*S*)-methylpentanoic acid and of the commercially available *N*-carbobenzoxy-(*R*)- and (*S*)-phenylalanine *p*-nitrophenyl esters were investigated. The optically active comonomer was prepared by thermal decomposition of solid (+)-1-piperidino-2,5(*S*)-dimethylheptan-3-one hydrochloride, which was obtained from the reaction of 2(*S*)-methylbutyllithium with 3-piperidino-2-methylpropionitrile. The 3(*R*)-methylpentanoic acid was prepared in 92% optical purity from *L*-alloisoleucine via diazotization in concentrated hydrobromic acid and subsequent reductive debromination with zinc amalgam in dilute hydrochloric acid. In the optically active copolymer-catalyzed solvolyses of the optically active esters performed at pH values of 6-8 no significant differences between the solvolytic rates of (*R*) and (*S*) isomers of substrates were observed. Poly-*L*-histidine was also employed as a catalyst for the solvolyses of these substrates. At pH 6.0 in ethanol-water the latter catalyst also failed to exhibit specificity towards (*R*) and (*S*) substrates.

### INTRODUCTION

Most of the naturally occurring enzymes exhibit a characteristic stereospecificity as well as structural specificity in their catalytic actions toward their various substrates. The specific activity of an enzyme toward one enantiomer of a substrate is often utilized to resolve a racemic mixture.<sup>1</sup>  $\alpha$ -Chymotrypsin,<sup>2</sup> a hydrolytic enzyme, which has been studied extensively and is known to contain imidazole(s) at its active site, is remarkable in its ability to discriminate between two enantiomers of certain substrates.<sup>3</sup>

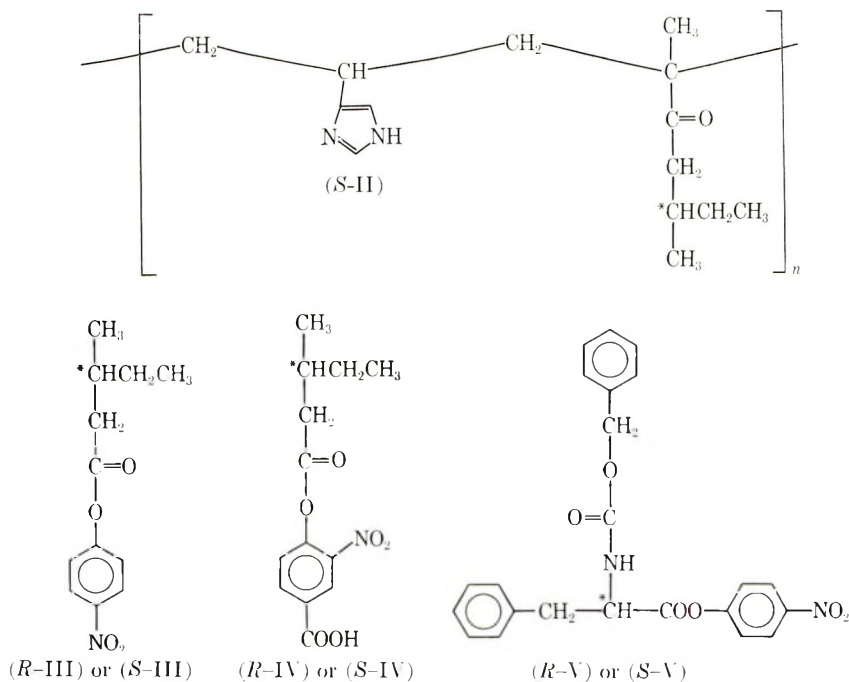
In recent years many synthetic polymers<sup>4</sup> that contain both charged groups and catalytically active functions have been investigated to elucidate enzyme catalysis. Although these synthetic polymers have simpler structural features than those of naturally occurring enzymes, these investi-

\* This paper comprises a portion of the dissertation submitted by I. Cho in partial fulfillment of the requirements for the degree of Doctor of Philosophy in the Graduate School of the Polytechnic Institute of Brooklyn, 1967.

† Present Address: Department of Chemistry, The University of Michigan, Ann Arbor, Michigan 48104

gations<sup>4</sup> have yielded considerable information on the mechanism of enzyme action. Because the homopolymer and copolymers of 4(5)-vinylimidazole (I) had been utilized successfully to elucidate aspects of esterolytic enzyme action,<sup>5</sup> the behavior of optically active polymers with pendent imidazole groups toward asymmetric substrates was of considerable interest.

We have synthesized an optically active copolymer (*S*-II) of (I) and investigated its effects on the solvolytic rates of optically active substrates in ethanol-water. [*S*-II signifies optically active (II), whose asymmetric carbon(s) possess an absolute configuration (*S*); "II" refers to racemic (II).] The substrate esters employed for the investigation were the neutral enantiomeric substrates *p*-nitrophenyl-3(*R*)- and -3(*S*)-methylpentanoate, (*R*-III) and (*S*-III), respectively, the anionic, enantiomeric substrates 4-[3(*R*)- and 4-[3(*S*)-methylpentanoyloxy]-3-nitrobenzoic acid, (*R*-IV) and (*S*-IV), respectively, and the commercially available *N*-carbobenzoxy-(*R*)- and -(*S*)-phenylalanine *p*-nitrophenyl esters, or (*R*-V) and (*S*-V), respectively.



Poly-L-histidine (*S*-VI), a peptide that has an asymmetric center close to the catalytically active imidazole group (the name poly-L-histidine is used here as a common name without regard to the configuration of the  $\alpha$  carbon in histidine), is known to exist in a helical form in water of pH above 5.<sup>6,7</sup> It was also of interest to use to investigate the effects of (*S*-VI) on the solvolytic rates of optically active esters.

## RESULTS AND DISCUSSION

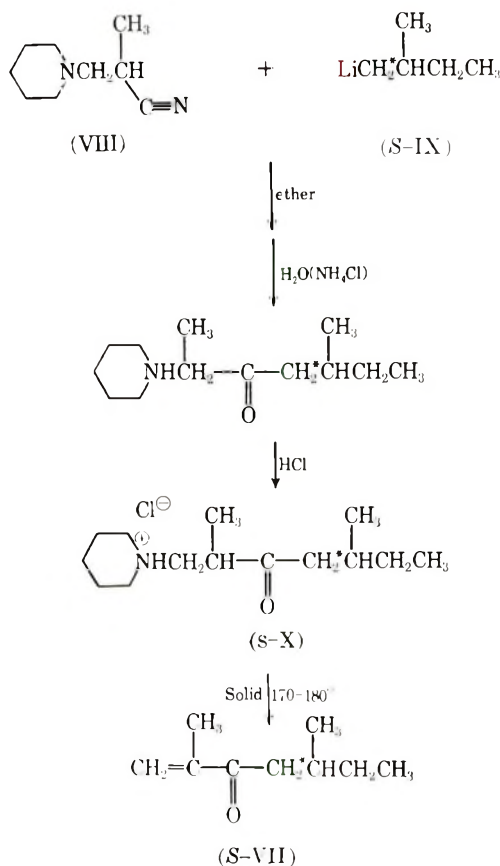
## Synthesis of Polymer

There is a significant number of optically active addition monomers that are known or can be synthesized. Among these are optically active alkenes,<sup>8-10</sup> optically active aryl<sup>11,12</sup> and alkyl<sup>13,14</sup> vinyl ethers, optically active acrylates and methacrylates,<sup>15,16</sup> optically active acrylamides and methacrylamides,<sup>17-19</sup> and other optically active monomers that can be polymerized or copolymerized.<sup>20</sup> However, those monomers which possess any hydrolyzable groups, such as esters and amides, are not to be used for copolymerization with (I), because the ester and amide groups will be readily hydrolyzed by catalytically active, neighboring imidazole groups. The optically active alkenes would not be expected to copolymerize with (I). Optically active styrene-type monomers<sup>21,22</sup> may copolymerize with (I) but the resulting copolymers would, most likely, be insoluble in water or alcohol-water mixtures. Since optically active vinyl ethers could be prepared readily and should not interact with the imidazole group, they were considered possible monomers to be used for the copolymerization with (I). Attempts to copolymerize *sec*-butyl vinyl ether with (I) were made by utilizing various initiation methods (racemic compound was prepared by mercuric chloride-catalyzed *trans*-etherification<sup>23</sup> of various commercially available, high-boiling vinyl ethers with *sec*-butyl alcohol). However, all attempts yielded only the homopolymer of (I). This result indicated that for a successful copolymerization with (I) the comonomer should have an electron-withdrawing substituent on the vinyl group; hence, vinyl ketones were chosen for investigation. A preliminary examination of the copolymerizability of a vinyl ketone with (I) with the use of the commercially available 1-penten-3-one indicated that a vinyl ketone was indeed a good choice. Since an isopropenyl group ( $\text{CH}_2=\text{C}(\text{CH}_3)-$ ) is more sterically hindered than a vinyl group for polymerization,<sup>24,25</sup> an isopropenyl ketone was considered to be more advantageous for the copolymerization. The optically active isopropenyl ketone 2,5(*S*)-dimethyl-1-hepten-3-one (*S*-VII) was chosen, and it was expected that this monomer would be extremely resistant to homopolymerization.

Among attempted syntheses of (*S*-VII) the synthetic route that involves a  $\beta$ -amino ketone hydrochloride as precursor to the unsaturated ketone was found to be most satisfactory.

Addition of carbanions to aminonitriles has been reported previously by Hauser and Humpfle<sup>26</sup>, Blicke and Tsao,<sup>27</sup> Pohland and Sullivan,<sup>28</sup> and Chauvière et al.<sup>29</sup> In most cases Grignard reagents were used as the carbanion source. It was reported<sup>29</sup> that the yield of product varied significantly, depending upon the structures of the carbanion and aminonitrile. This effect was also observed in the present investigation when it was found that, although 3-methylbutylmagnesium bromide reacted with 2-methyl-3-piperidinopropionitrile (VIII), 2-methylbutylmagnesium bromide failed to react. In order to facilitate the reaction, the more reactive

carbanion derived from 2-methylbutyllithium was employed. The latter was prepared from 2-methylbutyl bromide in anhydrous ether by utilizing a lithium-copper couple according to the procedure of Gilman et al.,<sup>30</sup> and it was found to be effective when reacted with (VIII).



The commercially available 2(*S*)-methylbutyl alcohol was brominated with phosphorus tribromide according to Brauns's procedure<sup>31</sup> and subsequently converted to 2(*S*)-methylbutyllithium (*S*-IX).<sup>32, 33</sup> The (*S*-IX) then reacted with (VIII) to give (+)-1-piperidino-2,5(*S*)-dimethylheptan-3-one hydrochloride (*S*-X) in 16% yield (we believe that the salt isolated and purified is probably one diastereomer; we do not know the configuration of the other asymmetric carbon, C-2), based on the bromide, and in 35% yield, based on the nitrile. A disadvantage of this synthesis is that a 1 mol excess of the alkyl lithium per mole of aminonitrile is required, because the alkyl lithium forms a 1:1 complex with the amino group before addition to the nitrile group.<sup>27</sup>

Although the amino ketone salts were reported to have melting points,<sup>34</sup> it was found that the  $\beta$ -amino ketone hydrochloride did not melt but decomposed, giving an amine hydrochloride and an unsaturated ketone.

The amino ketone hydrochloride (*S*-X) decomposed in the solid state at 170–180°C under reduced pressure, giving piperidine hydrochloride and (*S*-VII) in good yield. Crude (*S*-VII) containing about 8% of a single impurity, which appeared to be a saturated ketone, was purified by vapor phase chromatography (Aerograph Autoprep 700, SE-30 column) at 155°C.

Pure (*S*-VII) had a boiling point of 73°C (21 mm),  $n_D^{25} = 1.4368$ , and  $[\alpha]_D^{25} = +11.21^\circ$  (methanol). The infrared spectrum exhibited a strong carbonyl absorption band at 1675  $\text{cm}^{-1}$  and vinyl absorptions at 1630 and 930  $\text{cm}^{-1}$ . The ultraviolet spectrum showed absorptions at 220  $\text{m}\mu$  ( $\epsilon_{\text{max}} = 7800$ ) and at 320  $\text{m}\mu$  ( $\epsilon_{\text{max}} \approx 200$ ) in methanol. The NMR spectrum in carbon tetrachloride possessed peaks at 5.86 (1 H, singlet; C-1 hydrogen *trans* to carbonyl), 5.64 (1 H, singlet with fine splitting; C-1 hydrogen *cis* to carbonyl), 2.5 (2 H, multiplet; C-4 hydrogens), and 1.80 (3 H, singlet with fine splittings; C-2 methyl hydrogens) ppm downfield from tetramethyl silane as internal standard (for the complete spectrum and assignment of the peaks see the thesis of Iwhan Cho). The multiplet centered at 2.5 ppm was analyzed on the basis of the three-spin system analyses of Fraenkel and Dix<sup>35</sup> and Snyder.<sup>36</sup>

The attempted radical-initiated homopolymerization of (*S*-VII) with azobisisobutyronitrile (AIBN) failed, indicating that the introduction of a methyl group at the 2 position increases the steric hindrance sufficiently to prevent this monomer from polymerizing (*vide supra*). No further attempts were made to obtain the homopolymer of (*S*-VII) by other means. However, it was found that (*S*-VII) copolymerizes readily with (I) under free-radical (AIBN) polymerization conditions, indicating that the copolymerization is not only electronically favorable but also sterically favorable. A copolymerization monomer feed of ratio of (*S*-VII) to (I) of 1.0:3.5 yielded a copolymer, (*S*-II), with a composition of 1.0:0.96. These results indicated that (*S*-II) has a high degree of alternation.

Optically active copolymer (*S*-II) was a fluffy, white powder. It was soluble in alcohol and insoluble in water and in ether, and it swelled in acetone. The infrared spectrum exhibited carbonyl absorption at 1695  $\text{cm}^{-1}$ , and the spectrum was similar to a superposition of the infrared spectra of poly-4(5)-vinylimidazole and the homopolymer of (*S*-VII). [A sample of homopolymer of (*S*-VII) was obtained when the monomer in an NMR tube containing carbon tetrachloride and a trace of tetramethylsilane was left standing for a few months; the polymer was obtained as a white powder when reprecipitated from chloroform into methanol; the infrared spectrum had a strong carbonyl absorption band at 1700  $\text{cm}^{-1}$ .] The copolymer (*S*-II) had  $[\alpha]_D^{24} = +8.25 \pm 0.04^\circ$  (methanol) and  $[\eta]^{26} = 0.14 \pm 0.02$  dl/g (methanol).

Since the copolymer (*S*-II) appears capable of forming intramolecular hydrogen bonds between imidazole groups and neighboring carbonyl groups, an attempt was made to detect any evidence of hydrogen bonding. However, a close examination of the carbonyl stretching band in the infrared

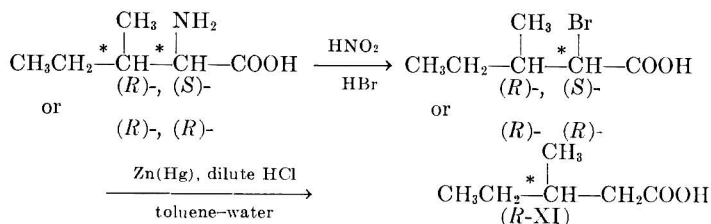
spectrum of (*S*-II) did not indicate any hydrogen-bond formation.<sup>37</sup> The possibility of intramolecular nucleophilic attack of the carbonyl groups by neighboring imidazole groups was considered, but no evidence of such interaction was observed under the conditions employed in the present investigation.

### Syntheses of Substrates

The (*S*) form of *p*-nitrophenyl 3-methylpentanoate, (*S*-III), was readily obtained from the commercially available 2(*S*)-methylbutyl alcohol. The alcohol was converted to the corresponding bromide,<sup>31</sup> from which 3(*S*)-methylpentanoic acid<sup>33</sup> (*S*-XI) was obtained. The acid was converted to the acid chloride, which was reacted following Spassow's procedure<sup>38</sup> to give *p*-nitrophenyl ester (*S*-III).

The (*R*) form of 3-methylpentanoic acid, (*R*-XI), was difficult to obtain because 2(*R*)-methylbutyl alcohol is not a naturally occurring compound. All attempts to resolve racemic 3-methylpentanoic acid failed. Attempts to prepare 2(*R*)-methylbutyric acid, which could subsequently be converted to 2(*R*)-methylbutyl alcohol, also failed, because the brucine resolution of racemic 2-methylbutyric acid, according to Schütz and Markwald's procedure,<sup>39</sup> gave the optically active acid in low optical purity. However, we found that (*R*-XI) could be prepared successfully from either L-alloisoleucine or D-isoleucine via diazotization and subsequent reductive debromination (an account of reductive dehalogenation of  $\alpha$ -halo acids will be published elsewhere).

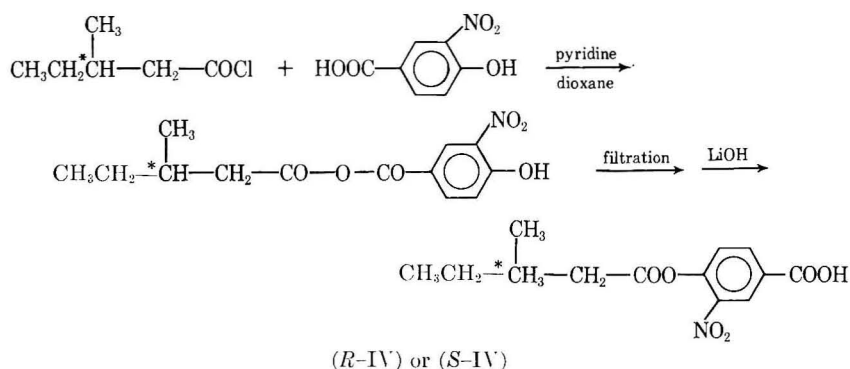
Commercially available isoleucine is a mixture of four isomers. According to the present synthesis, both L-alloisoleucine and D-isoleucine would give the desired (*R*-XI). However, the procedure of Greenstein et al.<sup>40</sup> for the separation and resolution of isoleucine could be best utilized to obtain



L-alloisoleucine. From the L-alloisoleucine of  $[\alpha]_{\text{D}}^{25} = +4.0^\circ$  (4.5*N* hydrochloric acid) (*S*-XI) was obtained in 92% optical purity.<sup>33</sup> At present it is not certain during which step the partial racemization (4%) occurred. (*R*-XI) was then converted to *p*-nitrophenyl ester (*R*-III) by the same procedure as that employed for the preparation of (*S*-III).

The negatively charged substrate 4-acetoxy-3-nitrobenzoic acid had been prepared previously from 3-hydroxy-2-nitrobenzoic acid by being treated with excess acetic anhydride in the presence of sodium hydroxide.<sup>5</sup> However, the acid anhydride method was not a feasible procedure when a limited amount of optically active acid was available. In the present

investigation the desired substrates (*R*-IV) and (*S*-IV) were prepared by alkaline rearrangement of 3-methylpentanoic 4-hydroxy-3-nitrobenzoic anhydride, which was obtained by reacting 3-methylpentanoyl chloride with 4-hydroxy-3-nitrobenzoic acid in dioxane in the presence of pyridine. The formation of the acid anhydride was confirmed by isolating and characterizing it. The choice of lithium hydroxide as the base was governed by its solubility in dioxane.



### Catalytic Effects of Optically Active Imidazole-Containing Polymers

All kinetic investigations of the solvolyses of optically active substrates catalyzed by optically active copolymer (*S*-II) were performed in buffered 80% ethanol–water mixtures at an ionic strength  $\mu$  of 0.02. Although the solvolytic rates would be greater in solvent mixtures containing a larger proportion of water, the copolymer precipitated when the solvent mixture contained more than 25% water.

In Table I are listed the measured first-order rate constants ( $k_{\text{meas}}$ ) for

TABLE I  
First-Order Measured Rate Constants for the Solvolyses<sup>a</sup> of Optically Active Substrates in the Presence of Optically Active Copolymer (*S*-II) in 80% Ethanol–Water at 26°C,  $\mu = 0.02$

Substrates	pH	$k_{\text{meas}} (\times 10^6)^b \text{ min}^{-1}$		
		( <i>R</i> )	$\pm$	( <i>S</i> )
<i>p</i> -Nitrophenyl 3-methylpentanoate, ( <i>R</i> -III) and ( <i>S</i> -III)	8.0	5.9	6.4	7.2
4-(3-Methylpentanoyloxy)-nitrobenzoic acid, ( <i>R</i> -IV) and ( <i>S</i> -IV)	6.3	22	—	23
	7.3	18	—	23
<i>N</i> -Carbobenzoxy-phenylalanine <i>p</i> -nitrophenyl esters, ( <i>R</i> -V) and ( <i>S</i> -V)	7.2	92	80	78
	8.0	200	180	210

<sup>a</sup> Catalyst concentration,  $2.5 \times 10^{-4}M$  (in imidazole); substrate concentration,  $3-5 \times 10^{-5}M$ .

<sup>b</sup> Blank rates were about half of the measured rates.

the solvolyses of optically active substrates in the presence of (*S*-II).

Particular attention was given to substrates (*R*-IV) and (*S*-IV) because an anionic substrate would be attracted to the active site more tightly than

TABLE II

First-Order Measured Rate Constants for the Solvolyses<sup>a</sup> of Optically Active Substrates in the Presence of Poly-L-histidine in Buffered Ethanol-Water at pH 6.0, 26°C,  $\mu = 0.1$ .

Substrates	Solvents, % ethanol	$k_{\text{meas}} (\times 10^3), \text{min}^{-1}$		
		( <i>R</i> )	<i>dl</i>	( <i>S</i> )
4-(3-Methylpentanoyloxy)-3-nitrobenzoic acid	10	0.88	—	1.1
<i>N</i> -Carbobenzoxyphenylalanine <i>p</i> -nitrophenyl esters	30 <sup>b</sup>	5.7	6.8	6.8

<sup>a</sup> Catalyst concentration,  $4.7 \times 10^{-3}M$  (in imidazole); substrate concentration,  $1-60 \times 10^{-5}M$ .

<sup>b</sup> The increase in alcohol content was due to the solubility of substrates.

a neutral substrate because of the ionic interaction between substrate molecules and imidazolium ions.<sup>5</sup> The choice of substrates (*R*-V) and (*S*-V) was based on the expectation that a substrate with large substituents attached to the asymmetric center would facilitate the stereoselectivity of polymer catalyst.

Although there are some differences between the solvolytic rates of two enantiomeric substrates (Table I), they are well within the range of experimental uncertainty and allow no conclusion to be drawn concerning any positive catalytic selectivity by polymer (*S*-II). These results may indicate that the asymmetric center of the polymer was too far from the catalytically active imidazole groups.

The solvolyses of the optically active substrates were repeated in the presence of poly-L-histidine (*S*-VI) under the modified conditions employed by Katchalski and his co-workers<sup>41</sup> in their investigation of hydrolytic catalysis by (*S*-VI). Although the chemistry of (*S*-VI) has not been thoroughly investigated, the peptide has at least two evident stereochemical features. First, the asymmetric center is closer to the imidazole group than is that in copolymer (*S*-II). Second, (*S*-VI) can exist in helical form in a certain pH range.<sup>6,7</sup> In Table II are listed the first-order measured rate constants for the solvolyses of the optically active substrates and, as may be seen from the kinetic data, (*S*-VI) also did not exhibit any significant specificity toward the enantiomeric substrates employed.

Although it is possible that the structures of the substrates employed in the present investigation do not favor the observation of any specificity, it is also conceivable that the polymers employed under the conditions of this study were not appropriate models and/or that the control of higher-order structure of a polymer catalyst is necessary to allow any specificity.

## EXPERIMENTAL

In the following all melting and boiling points are uncorrected. Elemental analyses were performed by A. Bernhardt, Mikroanalytisches Lab. in Max-Planck-Institut für Kohlenforschung, 433 Mülheim, Germany.

Infrared spectra were determined on a Perkin-Elmer Model 521 or Model 137 Infracord as neat liquids, Nujol mulls, or potassium bromide pellets. Ultraviolet spectra were determined on a Perkin-Elmer Model 202 recording spectrophotometer. NMR spectra were determined on either a Varian A-60 or HR-60 spectrometer with tetramethylsilane as an internal standard in solution. Optical rotations were measured on a Rudolph Model 80 Polarimeter.

**4(5)-Vinylimidazole (I).** 4(5)-Vinylimidazole was prepared by the procedure of Overberger and Vorchheimer.<sup>42</sup> Purification of this monomer was best accomplished by sublimation at 60–75°C under vacuum ( $10^{-4}$  mm). This monomer could be also purified by recrystallizing from water, to give colorless cubes; mp 83.5°C.

**3-Piperidino-2-methylpropionitrile.** This material was prepared in 80% yield by the method of Pines and Marechal.<sup>43</sup>

**2(S)-Methylbutyl Bromide.** According to the procedure of Brauns,<sup>31</sup> 2(S)-methylbutyl alcohol ( $\alpha_D^{25} -9.19^\circ$ , neat, 2 dm, Aldrich Chemical Co.) was converted, in 65% yield, to 2(S)-methylbutyl bromide,  $\alpha_D^{25} +9.50^\circ$ , neat, 2 dm. The bromide was dried by distilling over calcium hydride under reduced pressure, the bath temperature maintained below 80°C. No change in rotation was observed after the drying process.

**(+)-1-Piperidino-2,5(S)-dimethylheptan-3-one Hydrochloride (S-IX).** A 500 ml, four-necked flask was fitted with a thermometer, a mechanical stirrer, and a separatory funnel, and was connected to a distillation unit. The entire apparatus was flame-dried and kept under a positive argon pressure.

In the flask was placed 2.5 g (0.36 mol) of lithium metal pieces alloyed with copper dust by being pounded in a mortar. Anhydrous ether (250 ml), which had refluxed overnight over lithium aluminum hydride, was distilled directly into the flask. Dry 2(S)-methylbutyl bromide (19 g, 0.125 mol) was then added slowly and dropwise with vigorous stirring from a separatory funnel to the reaction flask. The bromide was added at such a rate that the reaction temperature was maintained at about  $-10^\circ\text{C}$  with a Dry Ice bath. As the reaction started, the solution became slightly cloudy, and bright spots appeared on the surfaces of the lithium metal pieces. The addition of bromide required about 2 hr, after which stirring was continued for an additional 30 min. The reaction mixture was then brought to room temperature and stirred for an additional 30 min; this was followed by settling of the unreacted lithium metal pieces to the bottom of the flask.

The ether solution of 2(S)-methylbutyllithium was taken out through a serum cap by a 50 ml hypodermic syringe and injected into a dry ether solution (150 ml) of 3-piperidino-2-methylpropionitrile (7.5 g, 0.05 mol) with stirring at  $0^\circ\text{C}$  under a dry nitrogen atmosphere. About 30 min were required to transfer all of the lithium reagent to the nitrile solution. The reaction mixture was allowed to stand for 1 hr more with stirring on an ice-water bath.

The reaction mixture was hydrolyzed by 300 ml of a cold, ammonium chloride-saturated water solution, and the resulting products were stirred overnight. The ether layer was then separated and dried over anhydrous magnesium sulfate. By passing dry hydrogen chloride through the dry ether solution the product aminoketone was precipitated as a hydrochloride salt. The entire mixture was evaporated to dryness by means of a rotatory evaporator. About 100 ml of fresh, anhydrous ether was then added and again evaporated. This process was repeated a few more times. Hot benzene extraction of the resulting solid residue gave the desired amino ketone hydrochloride (*S*-IX) in 16% yield, based on the bromide used, and in 35% yield, based on the amino nitrile used. Further recrystallization of the salt from benzene afforded (*S*-IX) as colorless leaflets; mp 140°C (decomp.). The infrared spectrum exhibited a group of bands between 2700 and 2400  $\text{cm}^{-1}$  and carbonyl absorption at 1700  $\text{cm}^{-1}$ ;  $[\alpha]_{\text{D}}^{25} = +8.62^\circ$  ( $c = 14.4$ , methanol).

ANAL. Calcd. for  $\text{C}_{14}\text{H}_{21}\text{ONCl}$  (%): C 64.22, H 10.77, N 5.33, Cl 13.55. Found (%): (64.99, H 10.88, N 5.31, Cl 13.42).

**2,5(*S*)-Dimethyl-1-hepten-3-one (*S*-VII).** In a 50 ml distilling flask fitted with a microdistillation head was placed 4 g of (*S*-IX). With the system maintained under reduced pressure (30 mm), an oil bath preheated at 175°C was applied to heat the flask. The hydrochloride salt started to decompose immediately, and the unsaturated ketone distilled over. The receiver was cooled with an ice-water bath. The decomposition was completed in 15–20 min, and 2 g of distillate was obtained. This crude product contained a small amount of water and about 8% of a single impurity, which appeared to be a saturated ketone exhibiting strong carbonyl absorption at 1710  $\text{cm}^{-1}$  in its infrared spectrum. From the crude product was separated pure (*S*-VII) by vapor phase chromatography (Aerograph Autoprep 700, 3/8 in.  $\times$  20 ft SE-30 column) at 155°C. Under these conditions the retention time of (*S*-VII) was 22 min.

Pure (*S*-VII) had a characteristic odor, bp 73°C (21 mm),  $n_{\text{D}}^{25} = 1.4368$ ,  $[\alpha]_{\text{D}}^{25} = +11.2^\circ$  ( $c = 4.05$ , methanol),  $\lambda_{\text{max}}^{\text{MeOH}} = 220 \text{ m}\mu$  ( $\epsilon = 7800$ ),  $\lambda_{\text{max}}^{\text{MeOH}} = 320 \text{ m}\mu$  ( $\epsilon \approx 200$ ). The infrared spectrum has a strong carbonyl absorption at 1675  $\text{cm}^{-1}$  and vinyl absorptions at 1630 and 930  $\text{cm}^{-1}$ . The NMR spectrum in carbon tetrachloride possessed peaks at 5.86 (1 H, singlet; C-1 hydrogen *trans* to carbonyl), 5.64 (1 H, singlet with fine splitting; C-1 hydrogen *cis* to carbonyl), 2.5 (2 H, multiplet; C-4 hydrogens) and 1.80 (3 H, singlet with fine splittings; C-2 methyl hydrogens) ppm downfield from tetramethylsilane and internal standard.

ANAL. Calcd. for  $\text{C}_9\text{H}_{16}\text{O}$  (%): C 77.09, H 11.5. Found (%): C 76.62, H 11.33.

**Copolymerization of 2,5(*S*)-Dimethyl-1-hepten-3-one with 4(5)-Vinylimidazole (I).** A solution of 1.15 g (0.0082 mol) of (*S*-VII), 0.217 g (0.0023 mol) of (I), and 10 mg of AIBN in 7 ml of thiophene-free benzene was placed in a polymerization tube. After degassing of the solution

the tube was sealed and placed in a methanol vapor bath for a 24 hr period. During this period the copolymer precipitated.

The precipitated copolymer was separated by filtration and reprecipitated from methanol into acetone and from methanol into anhydrous ether. Fluffy, white copolymer was obtained (0.15 g).

The copolymer (*S*-II) softened at about 200°C and had rotations  $[\alpha]_D^{24} = +8.24 \pm 0.04^\circ$ ,  $[\alpha]_{550}^{24} = +9.47 \pm 0.04^\circ$ , and  $[\alpha]_{510}^{24} = +10.11 \pm 0.04^\circ$  ( $c = 4.85$ , methanol). The infrared spectrum exhibited a distinctive carbonyl absorption band at  $1695\text{ cm}^{-1}$ ;  $[\eta]^{26} = 0.14 \pm 0.02$  (methanol).

ANAL. Found (%): C 65.79, H 8.93, N 12.26. The copolymer composition calculated from the nitrogen content was 1 part imidazole to 0.958 part ketone.

**3(*S*)-Methylpentanoic Acid (*S*-XI).** The procedure of Gilman and Kirby<sup>44</sup> was utilized. A Grignard reagent was prepared from 5 g (0.033 mol) of 2(*S*)-methylbutyl bromide ( $\alpha_D^{25} = +9.50^\circ$ , neat, 2 dm) and 1.0 g (0.042 mol) of magnesium turnings in anhydrous ether. After passing of dry carbon dioxide through the Grignard reagent the reaction mixture was hydrolyzed by dilute sulfuric acid. The ether layer was separated and washed with 20% sodium hydroxide solution, which extracted the acid. The acid was then regenerated by acidifying the extract with concentrated hydrochloric acid. The acid was extracted with ether and dried over anhydrous magnesium sulfate. Distillation of the ether solution afforded 3.0 g (79% yield) of (*S*-XI); bp 92°C (12 mm),  $[\alpha]_D^{25} = +8.98$  ( $c = 7.07$ , *n*-hexane), and  $\alpha_D^{25} = +8.58^\circ$  (neat, 1 dm). This rotation corresponds to 97% optical purity on the basis of the data of Lardicci and Conti.<sup>33</sup>

***p*-Nitrophenyl-2(*S*)-methylpentanoate (*S*-III).** By Spassow's procedure<sup>38</sup> (*S*-III) was obtained in 80% yield from 3(*S*)-methylpentanoyl chloride. Pure (*S*-III) was a pale liquid, bp 110°C (0.01 mm),  $n_D^{27} = 1.5161$ ,  $[\alpha]_D^{25} = +7.64^\circ$  ( $c = 11.3$ , *n*-hexane). The infrared spectrum exhibited carbonyl absorption at  $1760\text{ cm}^{-1}$ , phenyl absorptions at 1610 and  $1595\text{ cm}^{-1}$ , and nitro group absorptions at 1520 and  $1270\text{ cm}^{-1}$ .

ANAL. Calcd. for  $\text{C}_{12}\text{H}_{15}\text{NO}_4$  (%): C 60.75, H 6.37, N 5.90. Found (%): C 60.67, H 6.29, N 6.10.

**L-Alloisoleucine.** L-Alloisoleucine was obtained in 70% yield from commercially available isoleucine mixture (Mann Research Lab., Inc., New York) by Greenstein's procedure;<sup>40</sup>  $[\alpha]_D^{25} = +40.0^\circ$  ( $c = 1.70$ , 4.5*N* hydrochloric acid); (lit.,<sup>40</sup>  $[\alpha]_D^{25} = +40.5^\circ$  ( $c = 1.0$ , 5*N* hydrochloric acid)).

**Diazotization of L-Alloisoleucine.** A solution of 13 g (0.10 mol) of L-alloisoleucine, ( $[\alpha]_D^{25} = +40.0^\circ$ ) in 75 ml of 48% hydrobromic acid was cooled to 0°C in an ice-water bath. To this solution was added dropwise a solution of 13 g (0.19 mol) of sodium nitrite in 20 ml of water, the reaction temperature maintained below 10°C. After completion of addition, the reaction mixture was allowed to stand with stirring, until the temperature

of the solution returned to 0°C. The ice-water bath was then removed, and the mixture was allowed to stand overnight at room temperature. The product was extracted with ether and dried over anhydrous magnesium sulfate. Distillation of the ether solution gave 8.5 g (50% yield) of 2(*S*)-bromo-3(*R*)-methylpentanoic acid; bp 90°C (0.15 mm). The bromo acid exhibited carbonyl absorption at 1710 cm<sup>-1</sup> in its infrared spectrum and a doublet (*J* = 8.0 cps) centered at 4.10 ppm due to  $\alpha$ -proton in its NMR spectrum determined in carbon tetrachloride.

**3(*R*)-Methylpentanoic Acid (*R*-XI).** To a solution of 1.5 g of mercuric chloride in 50 ml of water containing several drops of concentrated hydrochloric acid was added 15 g (0.23 mol) of zinc dust. When amalgamation was complete, the remaining solution was decanted, and the zinc amalgam was washed a few times with deionized water.

To the amalgam was added 75 ml of dilute hydrochloric acid (50:50) and a solution of 8.5 g (0.055 mol) of 2(*S*)-bromo-3(*R*)-methylpentanoic acid in 50 ml of toluene. The reaction mixture was refluxed vigorously overnight. The toluene layer was then separated and dried over anhydrous magnesium sulfate. Distillation of the toluene solution gave, in almost quantitative yield, (*R*-XI),  $\alpha_D^{25} = -7.50^\circ$  (neat, 1 dm). This rotation corresponds to 92% optical purity.<sup>33</sup>

***p*-Nitrophenyl 3(*R*)-Methylpentanoate (*R*-III).** The 3(*R*)-methylpentanoic acid was converted to (*R*-III) by the same procedure as that employed for the preparation of (*S*-III). (*R*-III) obtained showed  $[\alpha]_D^{25} = -7.11^\circ$  (*c* = 5.71, *n*-hexane).

ANAL. Calcd. for C<sub>12</sub>H<sub>15</sub>NO<sub>4</sub> (%): C 60.75, H 6.37, N 5.90. Found (%): C 60.63, H 6.42, N 6.23.

**4-3(*S*)- and 3(*R*)-Methylpentanoyloxy-3-nitrobenzoic Acid, (*R*-IV) and (*S*-IV).** To a solution of 1.5 g (0.0082 mol) of 4-hydroxy-3-nitrobenzoic acid and 1.0 g (0.013 mol) of pyridine in 25 ml of dry dioxane was added slowly and with stirring 1.5 g (0.1 mol) of 3(*R*)- or 3(*S*)-methylpentanoyl chloride. The temperature of reaction was maintained below 10°C with an ice-water bath. The reaction mixture was then filtered, to remove precipitated pyridine hydrochloride. In order to confirm the formation of anhydride, a small amount of filtrate was evaporated on a glass plate. The resulting crystals exhibited the typical doublet (1810 and 1710 cm<sup>-1</sup>) characteristic of an anhydride in its infrared spectrum. To the filtrate was added 2.0 g (0.083 mol) of lithium hydroxide, and the mixture was heated to reflux for 5 min. After being cooled to room temperature the reaction mixture was diluted with 30 ml of anhydrous ether. The ether-dioxane solution was washed with dilute hydrochloric acid until the ether layer became acidic. The ether solution gave a crude, solid product, which was subsequently recrystallized to give in 20% yield (*R*-IV) or (*S*-IV) as colorless plates; mp 98–99°C,  $[\alpha]_D^{25} = -1.3^\circ$  (*c* = 4.4, methanol) for (*R*-IV) and  $[\alpha]_D^{25} = +1.4^\circ$  (*c* = 2.8, methanol) for (*S*-IV). The infrared spectrum possessed bands at 1780 cm<sup>-1</sup> due to ester carbonyl absorption and at 1340 cm<sup>-1</sup> due to nitro group absorption.

ANAL. Calcd. for  $C_{13}H_{15}NO_6$  (%): C 55.51, H 5.38, N 4.98. Found (%): for (*R*-IV) C 55.41, H 5.33, N 5.12. Found (%): for (*S*-IV): C 55.21, H 5.28, N 5.14.

### Kinetic Measurements

In the case of the optically active copolymer (*S*-II) all solvolytic rates were measured in 80% (v/v) ethanol–water buffered with 0.02*M* tris-(hydroxymethyl)aminomethane (Tris) and hydrochloric acid with sufficient potassium chloride to adjust the ionic strength to 0.02. Below pH 6.5 sodium acetate–acetic acid was used as the buffer.

In the case of (*S*-VI), poly-L-histidine (Mann Research Lab., Inc.), catalyst solutions ( $4.7 \times 10^{-3}M$  in imidazole) were prepared in 10 and 30% ethanol–water buffered with 0.1*M* Tris and hydrochloric acid and sufficient potassium chloride to adjust the ionic strength to 0.1. (*S*-VI) was at first dissolved in a solvent mixture of desired ethanol content at pH 2, and then the solution was diluted with the solvent, which contained the desired amount of alcohol, and was buffered at the desired pH. It was found that (*S*-VI) stayed in the solution long enough for the kinetic measurements under the conditions employed.

A substrate solution ( $10^{-3}M$  to  $10^{-4}M$ ) was prepared by dissolving a certain amount of substrate in the appropriate solvent mixture.

For the kinetic measurement 2.8 ml of buffered catalyst solution was mixed with 0.2 ml of substrate solution in a 3 ml quartz cell. After thorough mixing the cell was placed in a Beckman spectrophotometer (Model DU) thermostatted at 26°C. Solvolytic rates were followed by measuring the absorbance ( $OD_t$ ) of *p*-nitrophenol as a function of time *t*. Blank rates were measured in exactly the same manner but without the polymer catalysts. The infinity values ( $OD_{inf}$ ) were obtained by measuring the absorbance after a sufficiently long period of time had elapsed. For the slow reactions the kinetic solutions were transferred into sealed ampules and placed in a methanol bath (65°C) for an adequate period of time (at least five half-lives). The solutions were then transferred into the cells, and the absorbances were measured. Extreme care was taken to maintain identical conditions for the solvolyses of different substrate isomers.

The recorded kinetic data were treated as first-order kinetics by plotting  $OD_{inf} - OD_t$  versus time *t* on semilog section papers. The measured rate constants  $k_{meas}$  were obtained graphically by utilizing the linear portions of the plots.

Support of this work by the Research Laboratory, United States Army, Edgewood Arsenal is gratefully acknowledged.

### References

1. J. P. Greenstein, *Advan. Protein Chem.*, **9**, 121 (1954).
2. C. Niemann, *Science*, **143**, 1287 (1964), and references cited therein.
3. For example, S. G. Cohen and S. Y. Winstein, *J. Am. Chem. Soc.*, **86**, 5326 (1964).
4. For example, R. L. Letsinger and T. J. Savereide, *J. Am. Chem. Soc.*, 3122 (1962).
5. C. G. Overberger, T. St. Pierre, N. Vorchheimer, J. Lee, and S. Yaroslavsky, *J. Am. Chem. Soc.*, **87**, 296 (1965) and the subsequent papers on the subject.

6. K. S. Norland, G. D. Fasman, E. Katchalski, and E. R. Blout, *Biopolymers*, **1**, 277 (1963).
7. S. Beychok, M. N. Pflumm, and J. E. Lehmann, *J. Am. Chem. Soc.*, **87**, 3990 (1965).
8. P. Pino and G. P. Lorenzi, *J. Am. Chem. Soc.*, **82**, 4745 (1960).
9. W. J. Baily and E. T. Yates, *J. Org. Chem.*, **25**, 1800 (1960).
10. S. Murahashi and H. Yuki, *Bull. Chem. Soc. Japan*, **34**, 1673 (1961).
11. G. J. Schmitt and C. Schuerch, *J. Polymer Sci.*, **45**, 313 (1960).
12. G. Natta and M. Farina, *Makromol. Chem.*, **43**, 68 (1961).
13. P. Pino, G. P. Lorenzi, and S. Previetera, *Atti Accad. Nazl. Lincei, Mem. Classe Sci. Fis. Mat. Nat. Sez. II*, **29**, 562 (1960).
14. M. Goodman and Y.-L. Fan, *J. Am. Chem. Soc.*, **86**, 4922 (1964).
15. N. Beredjik and C. Schuerch, *J. Am. Chem. Soc.*, **78**, 2646 (1961); *ibid.*, **80**, 1933 (1958).
16. L. Arcus and D. W. West, *Chem. Ind. (London)*, **1958**, 230.
17. G. Manecke and G. Gunzel, *Makromol. Chem.*, **51**, 199 (1962).
18. R. C. Schulz, P. Elzer, and W. Kern, *Makromol. Chem.*, **42**, 197 (1961).
19. R. C. Schulz and H. Hartmann, *Makromol. Chem.*, **65**, 106 (1963).
20. For a recent review see M. Goodman, A. Abe, and Y.-L. Fan, *Macromol. Rev.*, **1**, 1 (1967).
21. C. S. Marvel and C. G. Overberger, *J. Am. Chem. Soc.*, **68**, 2106 (1946).
22. C. G. Overberger and L. C. Palmer, *J. Am. Chem. Soc.*, **78**, 666 (1956).
23. R. L. Adelman, *J. Am. Chem. Soc.*, **77**, 1669 (1955).
24. P. R. Thomas, G. J. Tyler, T. E. Edwards, A. T. Radcliffe, and R. C. P. Cubbon, *Polymer*, **5**, 525 (1964).
25. E. M. McMahon, J. N. Roper, Jr., W. P. Utermohlen, Jr., R. H. Hask, R. C. Harris, and J. H. Brant, *J. Am. Chem. Soc.*, **70**, 2971 (1948).
26. C. R. Hauser and W. J. Humpfflett, *J. Org. Chem.*, **15**, 359 (1950).
27. F. F. Blicke and E.-P. Tsao, *J. Am. Chem. Soc.*, **75**, 5587 (1953).
28. A. Pohland and H. R. Sullivan, *J. Am. Chem. Soc.*, **77**, 2817 (1955).
29. G. Chauvière, M. B. Tehoubar, and Z. Welvart, *Bull. Soc. Chim. France*, **1963**, 1428.
30. H. Gilman, J. A. Beel, C. G. Beel, C. G. Brennen, M. W. Bullock, G. E. Dunn, and L. S. Miller, *J. Am. Chem. Soc.*, **71**, 1499 (1949).
31. D. H. Brauns, *J. Res. Natl. Bur. Std. A.*, **18**, 315 (1937).
32. G. Natta and M. Farina, *Chim. Ind. (Milan)*, **42**, 1362 (1961).
33. L. Lardicci and L. Conti, *Ann. Chim. (Rome)*, **51**, 823 (1961).
34. A. W. Ruddy and J. S. Buckley, Jr., *J. Am. Chem. Soc.*, **72**, 718 (1950).
35. G. Fraenkel and D. T. Dix, *J. Am. Chem. Soc.*, **88**, 979 (1966).
36. E. Snyder, *J. Am. Chem. Soc.*, **88**, 1155 (1966).
37. K. Nakanishi, *Infrared Absorption Spectroscopy*, Holden-Day, San Francisco, 1964, p. 42.
38. A. Spassow, *Ber.*, **75**, 779 (1942).
39. O. Schütz and W. Markwald, *Ber.*, **29**, 52 (1896).
40. J. P. Greenstein, M. S. Birnbaum, and L. Levintow, *Biochem. Prepn.*, **3**, 84 (1943).
41. E. Katchalski, G. D. Fasman, E. Simons, E. R. Blout, F. R. N. Gurd, and W. L. Kolthun, *Arch. Biochem. Biophys.*, **88**, 361 (1960).
42. C. G. Overberger and N. Vorchheimer, *J. Am. Chem. Soc.*, **85**, 951 (1963).
43. H. Pines and J. Marechal, *J. Am. Chem. Soc.*, **77**, 2815 (1955).
44. H. Gilman and R. H. Kirby, *Org. Syn.*, Coll. Vol. I, Wiley, New York, 1941, p. 361.

Received February 29, 1968

## Hydrazine-Based Polyimides and Model Compounds

R. A. DINE-HART, *Materials Department, Royal Aircraft Establishment, Farnborough, Hampshire, England*

### Synopsis

The reaction of hydrazine hydrate with aromatic anhydrides may give either *N*-amino imides or cyclohydrazides. The conditions that favor the formation of *N*-aminoimides, in which the imide contains respectively a 5- and 6-membered ring, are discussed. These compounds may be reacted with aromatic anhydrides to give *N*-*N*-linked imides. The properties of a number of model compounds and polymers are described, and it is shown that those compounds which have alternating 5- and 6-membered imide rings give the maximum oxidative stability in air at 400°C.

### INTRODUCTION

A previous article<sup>1</sup> described the synthesis of *N*-*N*-linked polyimides and model compounds (see Table I) by the reaction of aromatic *N*-aminoimides and aromatic anhydrides of suitable functionality. The preparation and properties of these polymers and model compounds are now described in greater detail, of particular importance being the factors that determine the ease with which the key *N*-aminoimides may be synthesized.

### DISCUSSION

#### Synthesis Routes to the *N*-Aminoimides

Either *N*-aminoimides or cyclohydrazides may be obtained by condensation of hydrazine hydrate with aromatic anhydrides. The relative stability of these two structural isomers is determined by the interplay of ring strain and conjugation effects. As shown by Drew and Hatt,<sup>2</sup> both (II) and (III) may be obtained from phthalic anhydride via the intermediate (I), but high temperature or extended reaction time leads to the formation of the more stable 6-membered ring cyclohydrazide, i.e.,

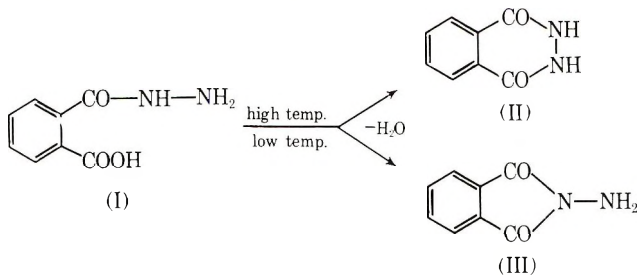
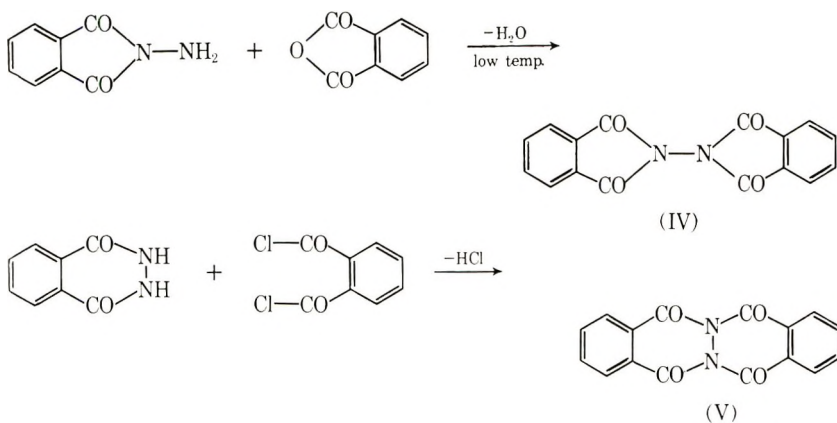


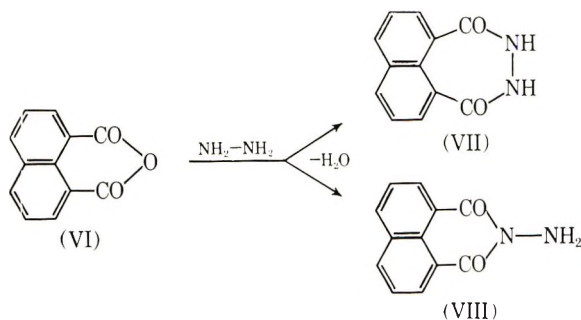
TABLE I  
 Model Compounds and Polymers

No.	Structure	M.p., °C	Prepara- tion
IV		311-313	Drew and Hatt <sup>2</sup>
V		350-360	Drew and Hatt <sup>2</sup>
IX		320	Bistrzycki and Risi <sup>1</sup>
X		330	Bistrzycki and Risi <sup>1</sup>
XIII		490-500	expt. 4
XIV		530-540	expt. 5
XII		none	expt. 6
XVI-A		none	expt. 7
XVI-B		none	expt. 7
XVII		none	black, glassy solid by melt polymerization at 250-400 °C

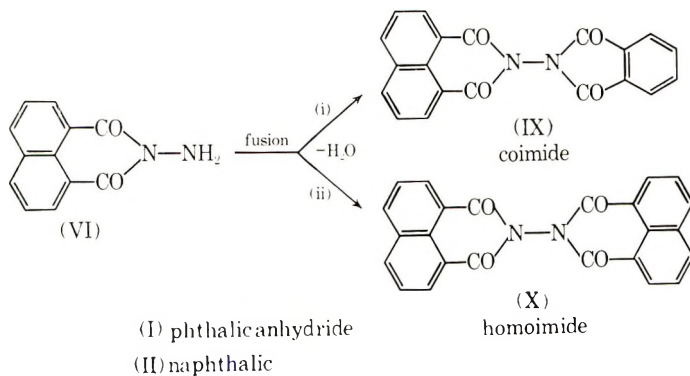
These compounds will react further to give the simple model compounds shown in Table I.



With naphthalene 1,8-dicarboxylic acid dianhydride the conditions under which the less stable 7-membered ring cyclohydrazide (VII) may be prepared are poorly established,<sup>3,4</sup> whereas the *N*-aminoimide (VIII) has been known since 1911.<sup>5</sup>



Compound (VIII) may further react with phthalic or naphthalic anhydride to give the coimide and homoimide model compounds.



Because of their stability it was relatively easy to prepare the mono- and difunctional naphthalimide amines and to use them for the synthesis of *N-N*-linked imides. It was more difficult to prepare the corresponding phthalimide and pyromellitimide compounds. Loncrini *et al.*<sup>6</sup> observed that benzoylation of the amino function stabilized the imide isomer against rearrangement and in the present work it was verified that acetylation produced the same effect. By preparing the intermediate from pyromellitic dianhydride corresponding to (I) at low temperature, by simultaneously acetylating and cyclizing, and by subsequent deacetylation of the *N*-amino group it was possible to isolate the compound (XV) in 50% yield.

### Synthesis Routes to the Polyimides

The diamines were of low solubility and reactivity and this affected the preparation of the polyimides. The copolyimides were the most easily obtained, since the stable but unreactive *N*-aminonaphthalimides could be

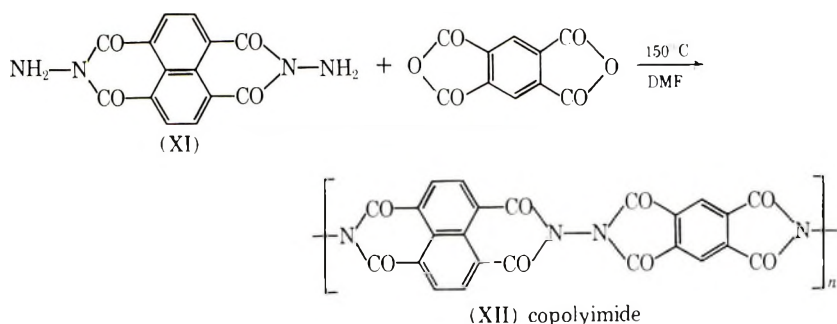
TABLE II  
Oxidative Stability at 400°C in Air<sup>a</sup>

Sample	Test conditions	Heating period, hr	Avg. rate of wt. loss, % hr <sup>-1</sup>
Model compound (XIII)	Dry air. Moist air, RH (25°C) 60-70%	30	0.60
		50	0.96
Model compound (XIV)	Dry air. Moist air, RH (25°C) 60-70%	30	0.37
		50	0.90
Polymer (XII)	Dry air. Moist air, RH (25°C) 60-70%	30	0.05
		70	0.25
Polymer (XVI)	Dry air. Moist air, RH (25°C) 60-70%	30	0.97
		50	1.20
Controls:			
Polyimide powder from PMDA and DDM <sup>b</sup>	Dry air. Moist air, RH (25°C) 60-70%	30	0.37
		50	1.00
Polyimide powder from PMDA and DAPE <sup>b</sup>	Dry air. Moist air, RH (25°C) 60-70%	60	0.35
		30	1.30
Polymer (XVII)	Moist air, RH (25°C) 60-70%	30	2.50

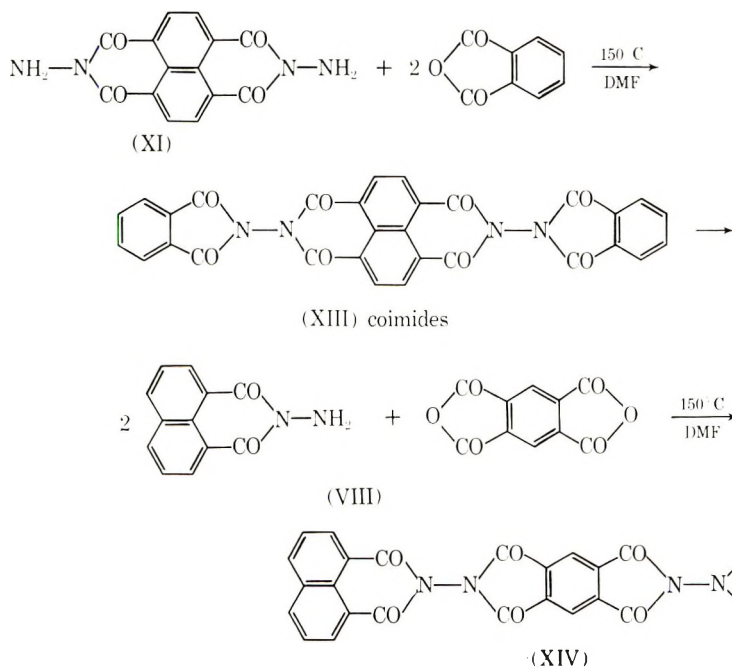
<sup>a</sup> Determinations of oxidative stability were made by continuous methods on a Stanton Mass-flow Thermobalance and by discontinuous methods with glass crucibles enclosed in heated aluminum blocks.

<sup>b</sup> PMDA, pyromellitic dianhydride; DDM, 4,4'-diaminodiphenylmethane; DAPE, 4,4'-diaminodiphenylether.

condensed at high temperature, in the usual solvents, with the more soluble and reactive 5-membered-ring anhydrides. The need to use hot solvents precluded the isolation of a soluble polyamic acid intermediate and resulted in the precipitation of polyimide (XII), which was probably of low molecular weight (experiment 6).

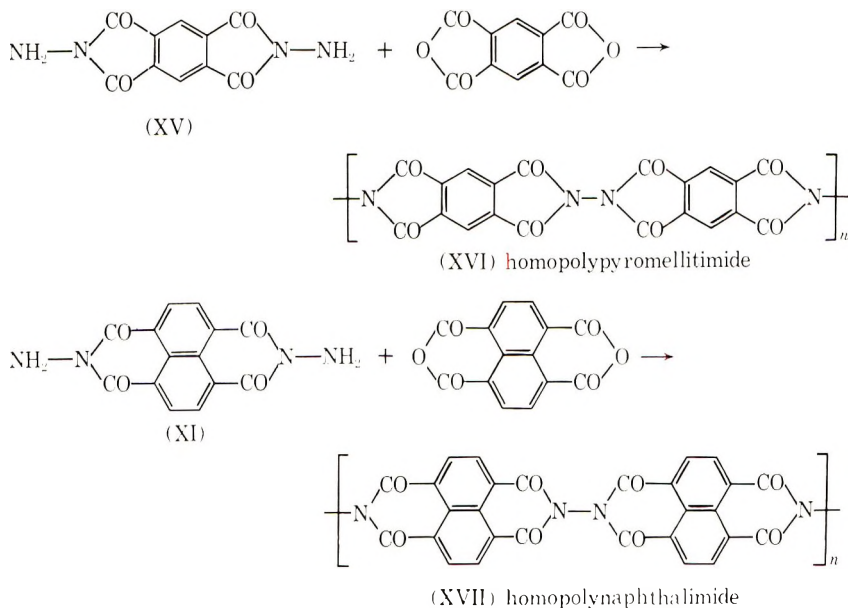


This polymer was intractable and only slightly soluble in concentrated sulfuric acid. It was very thermally stable (Table II), but attempts at fabrication by high-temperature sintering techniques were not successful. The brittleness of the samples may have arisen either from innate structural effects or from a low molecular weight of the polymer. The thermal stability of the two coimide model compounds (XIII) and (XIV), made by the reaction shown below, was only slightly less than that of the polymer (experiments 4 and 5).



These materials did not darken or char during oxidative degradation at 400°C and, unlike some aromatic polyimides, gave infrared spectra that remained sharp and distinctive. This may indicate that these compounds oxidize unit by unit rather than by reactions involving rearrangement and "coking" processes.

With the two possible homopolyimides (XVI) and (XVII) there was some doubt about the structure of the products (the structures shown below are provisional).



The compound (XVI), a polyamic acid of low viscosity, was obtained in a reaction of the diamine and dianhydride in solution at room temperature, this being chemically cyclized to precipitate the polyimide. The polymerization route was chosen to favor formation of the (XVI-A) rather than the (XVI-B) structure (see Table I), but the infrared spectrum, was inconclusive (see Table III). In particular, the imide carbonyl doublet<sup>7</sup> was missing, there being only one strong band at  $1750\text{ cm}^{-1}$ ; neither were any of the remaining bands particularly "imide-like." Hence the possibility of rearrangement to structure (XVI-B) cannot be excluded. This polymer was also intractable but was less thermally stable than (XII); see Table II.

Attempts to prepare the homopolynaphthalimide (XVII) in solution failed because of the low reactivity and solubility of the starting material. By fusion of the reagents between  $250$  and  $400^\circ\text{C}$  a brittle, black, glassy solid of inferior thermal stability was obtained.

### Mode of Thermal Degradation

The thermal degradation data in Table II show a significant effect of water vapor on what is primarily oxidative degradation. Since completing this work it has been found that atmospheric moisture can have a considerable effect on the oxidative degradation of many polyimides; these results will be presented later.

TABLE III  
Important Infrared Absorption Bands<sup>a</sup>

<i>N</i> -aminoimides	Bands, <sup>b</sup> cm <sup>-1</sup>				
	—NH <sub>2</sub> stretch	C=O stretch	—NH <sub>2</sub> band	Imide low-freq. band	
<i>N</i> -aminonaphthalimide	3300 W, 3200 W	1700 M, 1660 S	1610? M	775 S	
<i>N,N'</i> -diaminonaphthalimide	3300 W, 3250 W	1690 M, 1630 S	1550 M	760 S	
<i>N,N'</i> -diaminopyromellitimide	3300 W, 3250 W	1780 W, 1720 S	1600 W	720 M	

Bands divided into convenient groups <sup>b</sup>				
<i>N-N</i> -linked imides	Group I (C=O str.)	Group II	Group III	Group IV
Model compound (XIII)	1750 S	1310 S	1120 M	885 M
	1710 S	1250 S	1080 M	765 M
		1190 M	990 M	755 M
				705 M
Model compound (XIV)	1760 S	1315 S	1115 M	900 M
	1730 S	1240 S		845 M
	1700 S	1180 M		780 M
				720 M
Polymer (XII)	1750 S	1310 S	1100 M	840 M
	1730 S	1240 S	985 W	810 W
	1700 S	1200 M, broad doublet		760 M
				745 M
Polymer (XVI)	1750 S	1360 W	1080 W	710 M
		1270 M		835 M
				708 M

<sup>a</sup> A consistent band of medium strength at 1580–1590 cm<sup>-1</sup> is shown by compounds containing the naphthalene nucleus.

<sup>b</sup> S, strong; M, medium; W, weak.

The lack of any appreciable change in the polymer and model compound residues during the oxidative degradation has already been described. Further evidence of the breakdown mechanism was obtained from examination of the light-colored sublimates formed during degradation in air. Infrared examination showed these to be predominantly mixed imides. This suggested that degradation occurred mainly at the N—N bond and was followed by hydrogen abstraction, giving the simple imides.

## EXPERIMENTAL

### Preparation of the *N*-Aminoimides

***N*-Aminonaphthalimide (VIII).** Naphthalene-1,8-dicarboxylic acid anhydride (2.0 g) was dissolved in pyridine (25 ml) at 80°C, and excess hydrazine hydrate (0.7 g) was added slowly. A brilliant amber coloration

resulted. The temperature was raised to 100°C for 1 hr. On cooling to 0°C a mass of prismatic yellow needles was obtained. These were filtered off, washed with ether, and dried at 80°C; yield 1.5 g.

The infrared spectrum showed that this product contained complexed naphthalic anhydride. It was necessary to recrystallize three times from glacial acetic acid before the anhydride content was removed. This material gave a sharp melting point of 267–268°C, whereas the literature values are 262–263°C, perhaps because the complex was present in the earlier samples. A white, powdery hydrochloride was formed by reaction with concentrated hydrochloric acid. Acetylation of the amino function in hot acetic anhydride–glacial acetic acid gave water-white platelets of melting point 264–267°C (lit. 260–261°C). These derivatives produced the changes that would be expected from the infrared spectrum of a primary amino compound.

***N,N'*-Diaminonaphthalene-1,4,5,8-tetracarboxydi-imide (XI).** To naphthalene-1,4,5,8-tetracarboxylic acid dianhydride (4.0 g) was added an excess of hydrazine hydrate (2.0 g) in acetone (40 ml). There was an exothermic reaction accompanied by the formation of a black solid. The solution was filtered, and the residue was washed with acetone and air-dried. The black coloration was observed to lighten slowly to a medium-brown tint. The product was heated at 150°C under vacuum for 2 hr to ensure complete cyclization; yield 4.2 g, mp 440–450°C.

ANAL. Calcd.: C 56.7, H 2.7, N 18.9, O 21.7. Found: C 56.8, H 2.9, N 13.8, O 26.3.

The product (1.0 g) was vigorously heated in a test tube to give 0.6 g of an orange colored crystalline sublimate (identified as the naphthalenediimide) and 0.3 g of carbonaceous residue.

**Preparation of *N,N'*-Diamino Pyromellitimide (XV).** Pyromellitic dianhydride (5.0 g) was partially dissolved in an acetone–acetic anhydride mixture (40:10 ml); excess hydrazine hydrate (3.0 g) was dissolved in acetone (15 ml) and stirred into this mixture to give complete solution. An amber coloration was observed, but the temperature did not rise above 30°C. After 30 min, pyridine (10 ml) was added to give a rapid “clouding” and more gradual formation of a granular yellow precipitate. This was allowed to stand for several hours and then was filtered off, washed with ether, and dried at 60°C; yield 6.0 g, mp (decomp.) 330–340°C. To this was added concentrated hydrochloric acid (5 ml) to give a thin paste, which was allowed to stand for 48 hr. Water (150 ml) was added, and the solid was filtered off and washed with very dilute ammonia until the washings were just alkaline. The light-orange product was dried over P<sub>2</sub>O<sub>5</sub>; yield 3.0 g. This compound slowly reverted to the cyclohydrazide on standing at room temperature over a period of weeks. On being heated its conversion was very rapid between 100 and 200°C.

ANAL. Calcd.: C 48.8, H 2.4, N 22.8, O 26.0. Found: C 47.4, H 3.0, N 22.1, O 27.5.

### Preparation of the Model Compounds and Polymers

**Model Compound (XIII).** *N,N'*-diaminonaphthalene-1,4,5,8-tetracarboxydiimide (1.0 g) and phthalic anhydride (1.0 g) were refluxed for 2 hr in a mixture of *N*-dimethylformamide (50 ml) and pyridine (5 ml); a partial precipitation (completed by cooling) of pink prismatic needles occurred; yield 1.7 g, mp 490–500°C (decomp.).

ANAL. Calcd.: C 64.7, H 2.2, N 10.1, O 23.0. Found: C 64.7, H 2.0, N 9.9, O 24.3.

**Model Compound (XIV).** *N*-aminonaphthalimide (2.0 g) and pyromellitic dianhydride (1.0 g) were refluxed for 2 hr in *N*-dimethylformamide (80 ml) and pyridine (5 ml) to give a fine, white precipitate. This was filtered from the cold solution and washed with acetone; yield 2.6 g, mp 530–540°C (decomp.).

ANAL. Calcd.: C 67.3, H 2.3, N 9.2, O 21.1. Found: C 65.2, H 2.1, N 8.4, O 25.6.

**Polymer (XII).** *N,N'*-diaminonaphthalene-1,4,5,8-tetracarboxydiimide (1.86 g) and pyromellitic dianhydride (1.0 g) were refluxed in *N*-methylpyrrolidone (100 ml) for 4 hr. Slow dissolution occurred and gave a dark-amber solution (which gelled on cooling) with a simultaneous gradual precipitation of polyimide as a grey-brown powder. This was filtered off and washed with acetone; yield 2.1 g.

ANAL. Calcd.: C 60.3, H 1.3, N 11.7, O 26.7. Found: C 58.5, H 1.8, N 11.1, O 27.6.

**Polymer (XVI), First Method.** *N,N'*-diaminopyromellitimide (1.00 g) and pyromellitic dianhydride (0.92 g) reacted overnight in cold, stirred, *N*-dimethylformamide (50 ml). The diamine dissolved slowly to give a pale-yellow solution with a small amount of suspended solid. This was filtered off, and an acetic anhydride-pyridine mixture (50:50, 5 ml) was added to the solution to give a gradual precipitation of cyclized polymer. After separation this light-yellow solid was washed with acetone and dried at 200°C for 0.5 hr. The yield was low, 0.85 g, and the infrared spectrum showed that there were probably anhydride endgroups present.

**Polymer (XVI), Second Method.** The initial addition reaction was as described above but, instead of chemically cyclizing, the polymer was isolated by pouring the yellow solution into a petri dish and evaporating off the DMF at 100°C. This gave a residual gummy polymer which on heating to 200°C for 1 hr formed a brittle, opaque, buff colored mass. The infrared spectrum was the same as that of the polymer obtained previously but was free from extraneous anhydride bands. It was considered that formation of the polymer intermediate stabilized the *N,N'*-diaminopyromellitimide against rearrangement in a manner analogous to that encountered with the benzoyl and acetyl derivatives.

### References

1. R. A. Dine-Hart and W. W. Wright, *Chem. Ind. (London)*, **1967**, 1565.
2. H. D. K. Drew and H. H. Hatt, *J. Chem. Soc.*, **1937**, 16.
3. E. S. Vassermann and G. P. Miklukhin, *J. Gen. Chem. USSR*, **10**, 202 (1940); through *Chem. Abstr.*, **34**, 7179 (1940).
4. A. Bistrzycki and J. Risi, *Helv. Chem. Acta*, **8**, 810 (1925); through *Chem. Abstr.*, **20**, 1075 (1926).
5. A. Ostrogovich and M. Mihailescu, *Gazz. Chem. Ital.*, **41**, 757 (1911); through *Chem. Abstr.*, **6**, 995 (1912).
6. D. F. Lonerini, W. L. Walton, and R. B. Hughes, *J. Polymer Sci. A-1*, **4**, 440 (1966).
7. L. J. Bellamy and R. L. Williams, *Z. Electrochem.*, **64**, 563 (1960).

Received February 5, 1968

Revised March 7, 1967

## The Structure and Transport Properties of Poly(methacrylic Acid) in Aqueous Solution

E. E. KERN\* and D. K. ANDERSON,  
*Department of Chemical Engineering,  
Michigan State University, East Lansing, Michigan 48823*

### Synopsis

Diffusion and anisotropic electrical conductivity measurements have been used to investigate the structure of poly(methacrylic acid) in aqueous solution at various degrees of neutralization. Both kinds of measurement indicate that the polyion chain opens from a coiled to an extended configuration as the chain is neutralized. In addition it was found that, at low concentrations, the opening of the chain is a two-step process, whereas at higher concentrations the mechanism involves a single step.

### INTRODUCTION

The transport properties of linear polyelectrolyte solutions have been studied by a number of investigators over the past several years.<sup>1-7</sup> These studies have been valuable as a means of determining the structure of the polyion in solution. Of particular interest has been the effect of degree of ionization on the structure, because the molecule tends to be coiled in the neutral state and extended to a linear structure when ionized. However, there is some question about the mechanism by which the chain uncoils. In this work partially ionized poly(methacrylic acid) in solution is investigated with the aim of understanding better the structure of the molecule and the effect of the structure on the transport properties.

The degree of ionization,  $\alpha$ , of poly(acrylic acid) can be controlled by partial neutralization with sodium hydroxide. The acid groups ionize only slightly, whereas sodium is strongly ionized. At 0-50% neutralization the degree of ionization can be taken as approximately equal to the degree of neutralization.<sup>2</sup> Expansion (uncoiling) of the molecular chain occurs because of the strong repulsive forces among the negative charges along the ionized chain. These results are assumed in this work to be applicable to poly(methacrylic acid) (PMA).

Katchalsky and Lifson<sup>5</sup> calculated the electrostatic free energy of a solution of rodlike, ionized molecules. Calculated osmotic coefficients were practically independent of molecular weight and polyelectrolyte concentration and were determined only by the degree of ionization. The calculated osmotic coefficients were close to the experimental osmotic coefficients

\* Present address: Monsanto Company, Springfield, Massachusetts 01129.

determined by Kern<sup>6</sup> at high degrees of ionization and dilute concentrations. These theoretical studies indicate that the shape of the macromolecular ion (polyion) is between that of a coiled chain and a rodlike structure, depending upon the degree of ionization and the concentration of the polyelectrolyte solution.

Light-scattering data by Oth and Doty<sup>7</sup> indicate that the expansion of the polyion is about sevenfold when the degree of neutralization ( $\alpha$ ) of poly(methacrylic acid) (molecular weight, 84000) was increased from 0 to 70%. This expansion, according to Oth and Doty, is approximately one-half the contour length of the polyion. Kedem and Katchalsky's diffusion data<sup>4</sup> show that the polyion is completely extended at 70% neutralization.

More recently Mandel et al.<sup>8,9</sup> discussed the transition from the coiled (*a*) to the extended (*b*) state. Their potentiometric and spectroscopic measurements confirm that PMA in aqueous solution changes from the *a* to the *b* state in the region of  $\alpha$  from 0 to 0.4 and that there are approximately equal amounts of the two states at  $\alpha = 0.17$ . However, their potentiometric data indicate that at  $\alpha = 0.1$  the molecules are nearly all in the coiled state, while the spectroscopic measurements indicate that 25–30% are uncoiled. The authors argue that the coiled form is stabilized by van der Waals interactions between the methyl groups rather than hydrogen bonding. Liquori et al.,<sup>10</sup> on the other hand, conclude that hydrophobic forces at low ionization hold the chain in a tightly bound configuration. As ionization proceeds, the chain cooperatively opens up in order to allow internal COOH groups to be solvated.

Kedem and Katchalsky<sup>4</sup> derived an equation for the diffusion of polyelectrolytes as a function of the hydrodynamic resistance, the number of counterions, and the osmotic pressure coefficient:

$$D = kT/\rho\nu[\phi + \partial\phi/(\partial \ln n)] \quad (1)$$

where  $D$  = diffusion coefficient,  $\rho$  = hydrodynamic resistance,  $\nu$  = number of ionized groups,  $\phi$  = osmotic coefficient,  $n$  = moles of solute per milliliter,  $k$  = Boltzman constant, and  $T$  = absolute temperature, °K.

From this equation one can see that  $D$  is inversely proportional to the size of the polyion due to the hydrodynamic resistance and directly proportional to the number of ionized groups. Because of the greater mobility of the counterions a Nernst potential is developed, which effectively increases the diffusion coefficient of the polyelectrolyte as the degree of neutralization is increased. Thus, diffusion measurements can be used to study both the size and the degree of ionization of the polyion.

An independent means of determining the size and shape of the polyion is by the measurement of the electrical anisotropy effect with a Couette apparatus, described by several workers in the field of colloidal science.<sup>11–13</sup> The measurement of the electrical anisotropy effect allows estimation of the rotational diffusion constant, which is related approximately to the length of the charged particle<sup>14</sup> by the equation

$$L(\text{cm}) \simeq (8kT/\pi\eta_0 D_r)^{1/3} \quad (2)$$

where  $L$  = length,  $\eta_0$  = viscosity of the solvent, and  $D_r$  = rotational diffusion constant.

The rotational diffusion constant and, in turn, the length of the polyion can be determined by measuring the relative change of electrical conductivity in the direction of flow as a function of velocity gradient in a Couette apparatus. The procedure for making this determination was outlined by Götz.<sup>12</sup>

In this work the size and shape of the polyion of poly(methacrylic acid) was studied as a function of the degree of neutralization and concentration by the measurement of the diffusion coefficients and the electrical anisotropy effect of poly(methacrylic acid) in aqueous solution.

### EXPERIMENTAL

The diffusion coefficients were determined with a Mach-Zehnder diffusimeter.<sup>15,16</sup> The diffusimeter measures the refractive index of the solutions in a glass-windowed diffusion cell with an optical interferometer. The instrument was patterned after a similar diffusimeter described by Caldwell et al.<sup>17</sup> The experimental diffusivities were obtained by measuring the mutual diffusion of two solutions of different concentrations. The measured value was taken to be that of a solution with a concentration equal to the average of the two solutions. The instrument has proved to be accurate to within 0.5% for sucrose-water solutions.<sup>18</sup>

The electrical anisotropy effect of polyelectrolyte solutions was measured with a Couette type of apparatus, which was constructed according to the description given by Heckman.<sup>13</sup> The apparatus consists of two concentric cylinders with a narrow, annular gap between them. The outside cylinder can be rotated at various speeds to produce a uniform velocity gradient in the solution between the cylinders.

The electrical conductivity of the solutions in the direction of flow was measured by using two electrodes imbedded in the surface of the inner

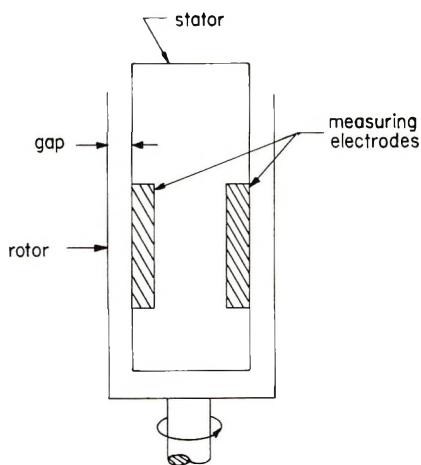


Fig. 1. Schematic of Couette apparatus used for anisotropic conductivity measurements.

cylinder (Fig. 1). Both cylinders are covered with nonconductive material. Conductivity measurements were made at 25°C with an Industrial Instrument, Inc. conductivity bridge operating at 1000 Hz.

Apparent viscosities were measured at 25.0°C with an Ostwald-Fenske type of viscometer. The efflux times were long enough to eliminate kinetic-energy corrections.

The poly(methacrylic acid) was synthesized from the monomer, methacrylic acid, by a free-radical addition type of polymerization. The monomer, purchased from Eastman Chemicals, was first distilled under a vacuum, to remove the inhibitor, and then polymerized in a water-methanol solution with 0.5% benzoyl peroxide as the free-radical initiator. The polymer was dissolved in methanol and precipitated with ether to remove the monomer and catalyst. This procedure was repeated several times to ensure the complete removal of monomer and catalyst.

The poly(methacrylic acid) was then redissolved in methanol and fractionally precipitated by the gradual addition of ether to give different molecular weights. The fractionation procedure used was essentially that proposed by Flory.<sup>19</sup> The fractions were dried in a vacuum at 110°C for 48 hr and then ground to a fine powder.

The molecular weights were determined by viscosity measurements of polymer solutions in 2*N* sodium hydroxide according to the procedure outlined by Katchalsky and Eisenberg.<sup>20</sup>

### Results and Conclusions

Figures 2 and 3 are plots of diffusivity  $D$  versus degree of neutralization for poly(methacrylic acid) for different concentrations and molecular weights. The initial increase in  $D$  is readily explained by the increase in the number of counterions, which exert a strong drag effect on the coiled polyions. At 0–10% neutralization the molecules are hypercoiled, and their hydrodynamic resistance  $\rho$  is relatively small. At 10–25% the macromolecules open to an extended configuration, so that  $\rho$  increases rather abruptly, resulting in a decrease in  $D$ . At a concentration of 0.0320 monomols/l (Fig. 2) only one depression in  $D$  is observed, whereas at a lower concentration, 0.0213 monomols/l (Fig. 3), two depressions in  $D$  are observed. This suggests that there is a two-step process involved in the uncoiling of the polyion at lower concentrations.

The end-to-end length of the polyion was estimated from the rotational diffusion data [eq. (2)] by measurement of the electrical anisotropy effect of the PMA solutions. Götz<sup>12</sup> showed that the length of a charged particle in solution is related to the relative change in conductivity [ $K_R = (K - K_0)/K_0$ ] of the solution in an orienting shear field. The details of the derivation of the equations involved are lengthy and will not be reproduced here, since they are available elsewhere.<sup>11,12</sup> In effect,  $K_R$  is measured as a function of shear rate over the range from random orientation to nearly complete orientation. A rotational diffusion constant can be determined from the data. In principle, the data should be taken at (or extrapolated

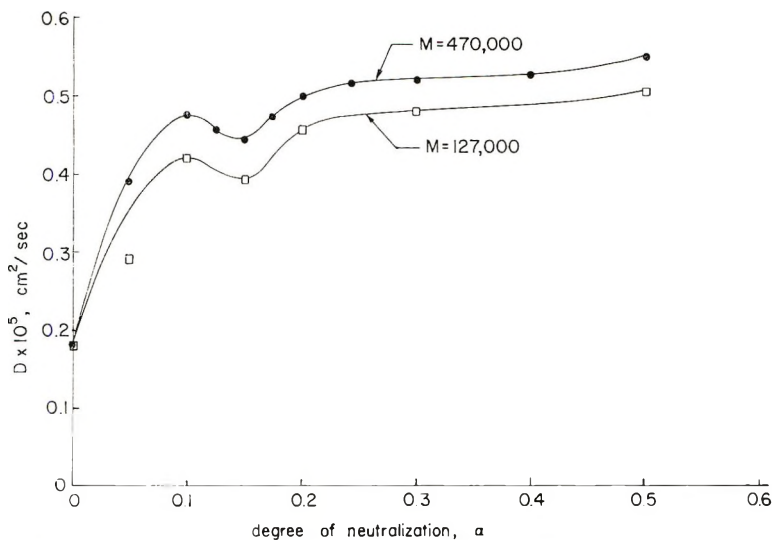


Fig. 2. Diffusion of poly(methacrylic acid) in water as a function of degree of neutralization. Interdiffusion of 5.0 and 0.5 g/l solutions.  $M$ , molecular weight.

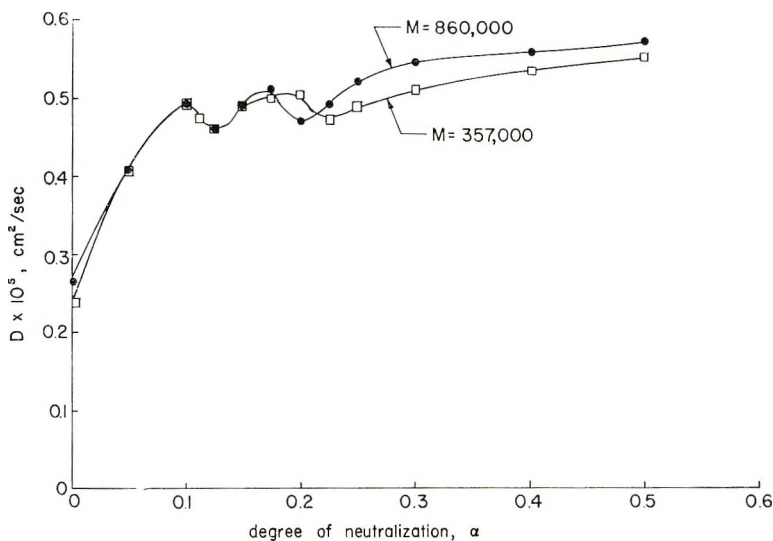


Fig. 3. Diffusion of poly(methacrylic acid) in water as a function of degree of neutralization. Interdiffusion of 3.0 and 0.3 g/l solutions.  $M$ , molecular weight.

to) infinite dilution. This was not possible in these studies, since concentration was one of the variables of interest. However, the highest concentration used was 0.0291 monomols/l, and it is assumed that the measurements at least give a good qualitative, if not quantitative, measure of the rotational diffusion coefficient and chain length.

Figure 4 is a typical set of plots of the relative change of conductivity as a function of angular velocity (RPM) at different degrees of neutraliza-

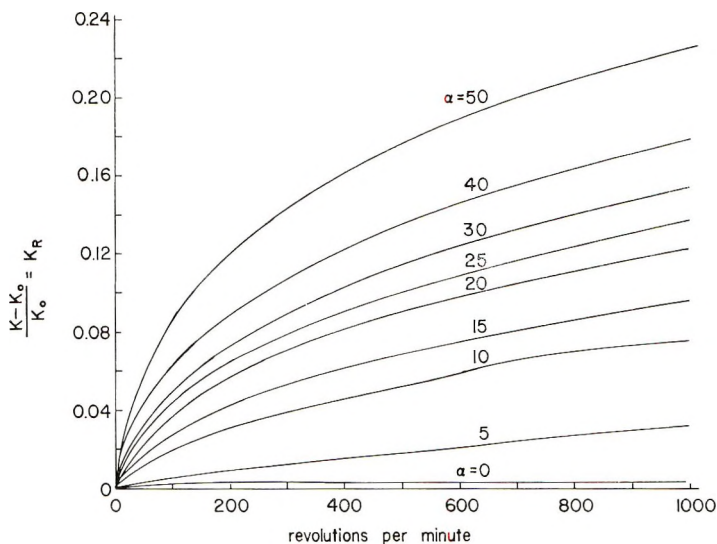


Fig. 4. Relative change in conductivity versus RPM for PMA at 0.0058 monomoles/l.  $K_0$ , conductance;  $\alpha$ , degree of neutralization;  $K_0$ , conductance at zero RPM.

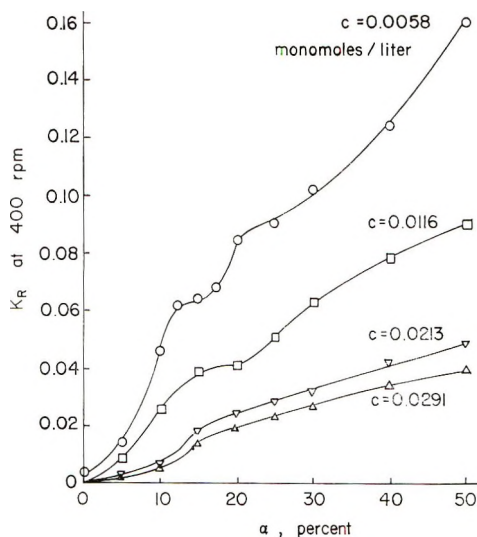


Fig. 5. Relative conductivity at fixed shear rate ( $4530 \text{ sec}^{-1}$ ) as a function of degree of neutralization for PMA solutions. Molecular weight = 206000.

tion (for the apparatus used the inner and outer radii were 5.42 and 5.47 cm, respectively, and thus the velocity gradient, in  $\text{cm}^{-1}$ , is  $11.33 \times \text{RPM}$ ).  $K_R$  should increase with degree of orientation and with the length of the polyon. Since the orientation is caused by the shear rate in the apparatus, at constant angular velocity changes in  $K_R$  with degree of neutralization are a result of changing polyon extension. The longer the polyon is, the

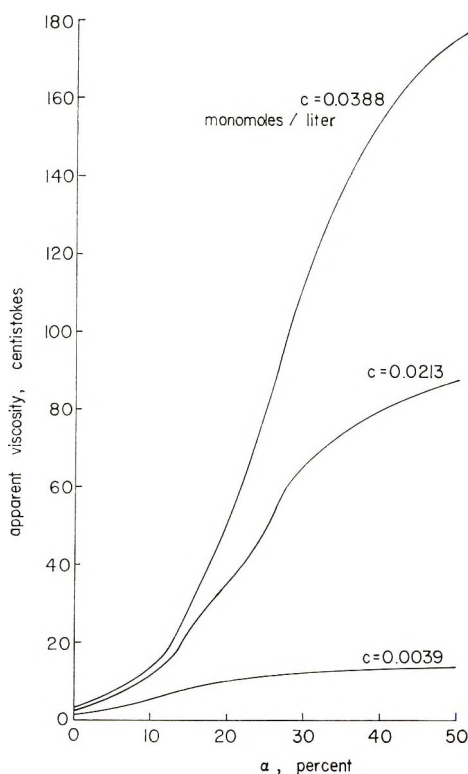


Fig. 6. Apparent viscosity as a function of degree of neutralization for PMA solutions. Molecular weight 860000.

more completely oriented will it be in the shear field. Thus, by plotting  $K_R$  versus  $\alpha$  at fixed RPM (see Fig. 5) one can determine qualitatively how the length of the polyion is changing.

At the lower concentration ( $C = 0.0058$  monomols/l) there are two distinct and sudden increases in molecular extension, and at the higher concentrations the opening of the chain is more gradual, the greatest effect occurring in the range of  $\alpha$  between 10 and 20%. This is in agreement with the diffusion measurements.

Thus, the data from the electrical anisotropy measurements verify that the depressions in the diffusion curves are due to the rapid increase of the size of the polyion and indicate that a two-step process is involved in the opening and uncoiling of the polyion at low concentrations.

Figure 6 gives the apparent viscosity of the PMA solutions at three different concentrations. These plots show an irregular change in viscosity in the range of  $\alpha$  between 10 and 25%, presumably because of the effects mentioned above.

A possible explanation of the data presented in this paper is that the first abrupt increase in the size of the polyion is due to the breaking of hydrogen bonds, resulting in an expansion of the coiled polyion, and that

TABLE I  
Polyion Size of Poly(methacrylic Acid) and Rotational  
Diffusion Constants of Poly(methacrylic Acid) Solutions<sup>a</sup>

$\alpha$ , %	Concn., monomols/l	$D_r$ , sec <sup>-1</sup>	Estd. extension, Å
50	0.0058	38.3	6000
50	0.0116	76.5	5180
50	0.0213	191	3830
50	0.0291	383	3040
10	0.0058	3800	1410

<sup>a</sup> Fully extended length, 6500 Å.

the second abrupt increase in size is due to an uncoiling of the polyion, in which the polyion approaches a rod-like structure.

Table I gives the approximate size, in angstroms, of the polyion with its corresponding rotational diffusion constant. The fully extended length of the polyion is 6500 Å. From these data it appears that the polyion is nearly completely extended at low concentrations and high degrees of neutralization.

This work was supported by a grant from the Petroleum Research Fund, administered by the American Chemical Society. Grateful acknowledgment is hereby made to the donors of the fund.

### References

1. H. Vink, *Makromol. Chem.*, **67**, 105 (1963).
2. J. R. Huizenga, P. F. Grieger, and F. T. Wall, *J. Am. Chem. Soc.*, **72**, 4228 (1950).
3. F. E. Harris and S. A. Rice, *J. Polymer Sci.*, **15**, 151 (1955).
4. O. Kedem and A. Katchalsky, *J. Polymer Sci.*, **15**, 321 (1955).
5. A. Katchalsky and S. Lifson, *J. Polymer Sci.*, **13**, 43 (1954).
6. W. Kern, *Z. Physik. Chem.*, **A181**, 249 (1938).
7. A. Oth and P. Doty, *J. Phys. Chem.*, **56**, 43 (1952).
8. M. Mandel, J. C. Leyte, and M. G. Stadhouders, *J. Phys. Chem.*, **71**, 603 (1967).
9. M. Mandel and M. G. Stadhouders, *J. Makromol. Chem.*, **80**, 141 (1964).
10. A. M. Liquori, G. Barone, V. Crescenzi, F. Quadrioglio, and V. Vitagliano, *J. Macromol. Chem.*, **1**(2), 291 (1966).
11. G. Schwarz, *Z. Physik*, **145**, 563 (1956).
12. K. G. Götz, *J. Colloid Sci.*, **20**, 289 (1965).
13. K. Heckman, *Z. Physik. Chem. (Frankfurt)*, **9**, 318 (1956).
14. W. Kuhn, *Z. Physik. Chem. (Leipzig)*, **A161**, 1 (1932).
15. L. Mach, *Sitzber. Wiener Akad.*, **101**, 5 (1892).
16. L. Zehnder, *Z. Instrumentenk.*, **11**, 275 (1891).
17. C. S. Caldwell, J. R. Hall, and A. L. Babb, *Rev. Sci. Instr.*, **28**, 816 (1957).
18. D. L. Bidlack, Ph.D. Thesis, Michigan State University (1964).
19. P. J. Flory, *J. Am. Chem. Soc.*, **65**, 375 (1943).
20. A. Katchalsky and H. Eisenberg, *J. Polymer Sci.*, **6**, 145 (1951).

Received January 9, 1968

Revised March 11, 1968

## Reaction of Chlorine-Containing Polymers with Living Polymers

YUJI MINOURA, *Research Institute for Atomic Energy, Osaka City University, Osaka*, and HISASHI HIRONAKA, TOSHIYUKI KASABO, and YUKIO UENO, *Kyowa Rubber Industry Company, Ltd., Osaka, Japan*

### Synopsis

A graft polymer was prepared by means of the coupling reaction of chlorinated ethylene-propylene terpolymer with living polystyrene, obtained with a sodium-naphthalene complex as initiator, under various conditions; the grafting efficiency and the percentage of grafting are discussed. Poly(chloroprene), chlorinated butyl rubber, poly(vinyl chloride), poly(epichlorohydrin), and epichlorohydrin-ethylene oxide copolymer were also used as chlorine-containing polymers. The grafting efficiencies were found to be in the following order: chlorinated butyl rubber > poly(epichlorohydrin) > epichlorohydrin-ethylene oxide copolymer > chlorinated ethylene-propylene terpolymer > poly(chloroprene) > poly(vinyl chloride). A graft polymer was obtained from the reaction between chlorinated ethylene-propylene terpolymer and living poly(isoprene), with butyllithium in benzene. The undesirable metal-halogen interchange reaction was considerable.

### INTRODUCTION

It is now well known<sup>1-4</sup> that the carbanionic endgroups in living polymers obtained by anionic polymerization react with a number of functional groups, such as ester groups and the halogens of alkyl halides. It has been shown<sup>5,6</sup> that a living polymer having a narrow molecular weight distribution can be prepared under carefully controlled conditions. Thus a graft polymer having branches of constant chain length can be obtained from the reaction of polymers containing ester groups or halogens with a living polymer.

Finaz et al.<sup>7</sup> and Gallot et al.<sup>8</sup> obtained graft polymers from the reactions of poly(methyl methacrylate) and poly(vinyl chloride) with living polystyrene, prepared with phenylisopropyl potassium. Alteares and his co-workers<sup>9</sup> obtained comb and star types of branched polymers from the reactions of chloromethylated polystyrene, 1,2,4-tri- and 1,2,4,5-tetrachloromethyl benzene with living polystyrene, prepared with butyllithium. Minoura and Shiina<sup>10</sup> obtained a graft polymer from the reaction of PVC with living PSt, prepared with BuLi. These workers characterized the graft polymers, which are useful as model substances for the study of polymer properties. However, no details have been published on the coupling

reaction of chlorine-containing polymers with living polymers. Hence in the present study the chlorinated ethylene-propylene terpolymer (Cl-EPDM) was made to react with living polystyrene (PSt), prepared with a sodium-naphthalene complex ( $C_{10}H_8Na$ ) as initiator, under various conditions, and the grafting efficiency and the percentage of grafting were considered.

The grafting efficiency at a constant living PSt concentration increased with increase in the concentration of Cl-EPDM and approached a constant value (37–39%) when the ratio of the chlorine in the polymer to the sodium in the initiator was unity. When the concentrations of Cl-EPDM and living PSt were constant, the per cent grafting increased with increase in the degree of polymerization of the living PSt.

Poly(chloroprene) (PCR), chlorinated butyl rubber (Cl-IIR), polyvinyl chloride (PVC), poly(epichlorohydrin) (PECH), and epichlorohydrin-ethylene oxide copolymer (ECH-EO) also were used as chlorine-containing polymers, and living poly(isoprene) was used as a living polymer.

## EXPERIMENTAL

### Materials

Cl-EPDM (chlorine content 34.5 wt-%), PCR (Neoprene AD), Cl-IIR (chlorine content, 1.2 wt-%), PVC (degree of polymerization 1050), PECH (molecular weight  $5 \times 10^5$ , chlorine content 38.0 wt-%), and ECH-EO (molecular weight  $2.8 \times 10^6$ , chlorine content 26.0 wt-%) were obtained commercially. They were purified by reprecipitation and dried *in vacuo* before use.

Tetrahydrofuran (THF), benzene, styrene, isoprene, and the other reagents were purified and dried by the usual methods. Commercial BuLi solution in *n*-heptane was used.

### Coupling Reaction Procedure

$C_{10}H_8Na$  in THF solution was prepared in a 100 ml reaction flask under nitrogen. Styrene monomer was added dropwise to this solution through a syringe and polymerized at 30°C for 4 hr. The monomer conversion was 100%. To this reddish, living PSt solution in THF, was added, under a stream of nitrogen, a degassed Cl-EPDM solution in THF. The coupling reaction was carried out at 30°C for 5 hr and then the contents were poured into a large quantity of methanol. The precipitated polymers were filtered, washed, dried *in vacuo*, and weighed. The polymer mixture was extracted with boiling acetone, and free polystyrene was removed. The amount of grafted styrene was determined from the increase in the weight of the insoluble portion in boiling acetone.

The grafting efficiency and percentage grafting were calculated from the following equation:

$$\begin{aligned}\text{Graft. eff. (\%)} &= (\text{wt. St grafted} \times 100)/(\text{wt. tot. PSt yield}) \\ \text{grafting (\%)} &= (\text{wt. St grafted} \times 100)/(\text{wt. Cl-EPDM used})\end{aligned}$$

PCR, Cl-IIR, PVC, PECH, and ECH-EO reacted with living PSt in a similar manner. The free PSt was extracted with a mixture of acetone and methanol (7:1 volume ratio) from the PCR system and with ethyl ether from the PECH and ECH-EO systems.

### Infrared Spectra

The infrared absorption spectra of thin films cast on rock-salt plates were obtained with a Perkin-Elmer 337 Grating Infrared spectrophotometer.

### Intrinsic Viscosity

The intrinsic viscosities  $[\eta]$  of benzene solutions of the polymers were obtained with a Ubbelohde viscometer at 30°C. The degree of polymerization,  $\bar{P}_n$ , of the free PSt was calculated from the following relationship given by Johnson and Tobolsky:<sup>11</sup>

$$\bar{P}_n = 1770 [\eta]_{\text{St}}^{1.4}$$

## RESULTS AND DISCUSSION

### Reaction of Cl-EPDM with Living PSt Obtained with a Sodium-Naphthalene Complex

**Separation of Graft Polymer.** The reaction product after Cl-EPDM (3.64 g/l) had reacted with living PSt ( $[\text{St}] = 0.79 \text{ mol/l}$ ,  $\text{C}_{10}\text{H}_8\text{Na} = 7.91 \times 10^{-3} \text{ mol/l}$ ) in THF at 30°C for 5 hr was extracted repeatedly with boiling acetone, until the extract did not become cloudy when methanol was added. It was confirmed by elemental analysis and the infrared absorption spectrum (Fig. 1b) that the portion soluble in acetone was free PSt. On the other hand, the infrared spectrum of the portion insoluble in acetone (Fig. 1c) showed both the bands of PSt and the band of the methyl group from the Cl-EPDM at  $2950 \text{ cm}^{-1}$ . Furthermore, the elemental analysis indicated that this insoluble portion consisted of Cl-EPDM-PSt graft polymer and free Cl-EPDM.

When a mixture of Cl-EPDM and homopolystyrene was extracted by a similar method, the homopolystyrene was completely removed by the acetone and the Cl-EPDM used was obtained as the insoluble part. When EPDM, instead of Cl-EPDM, reacted with living PSt, this extraction method yielded no grafted polymer.

In Figure 1 the infrared spectra of Cl-EPDM, PSt, and the graft copolymer are shown.

The spectrum of Cl-EPDM (Fig. 1a) showed the absorptions of the methylene group at  $2926$  and  $1475 \text{ cm}^{-1}$  and of the methyl group at  $2950$  and  $1385 \text{ cm}^{-1}$ . The spectrum of the residue (Fig. 1c) showed both the absorption bands of PSt (Fig. 1b) and the band at  $2950 \text{ cm}^{-1}$  assigned to the methyl group of Cl-EPDM. Therefore the residue was confirmed to consist of the graft copolymer and Cl-EPDM.

**Influence of Cl-EPDM Concentration.** Cl-EPDM at various concentrations (1.82, 3.64, 9.09, and 16.36 g/l) reacted with living PSt (0.79

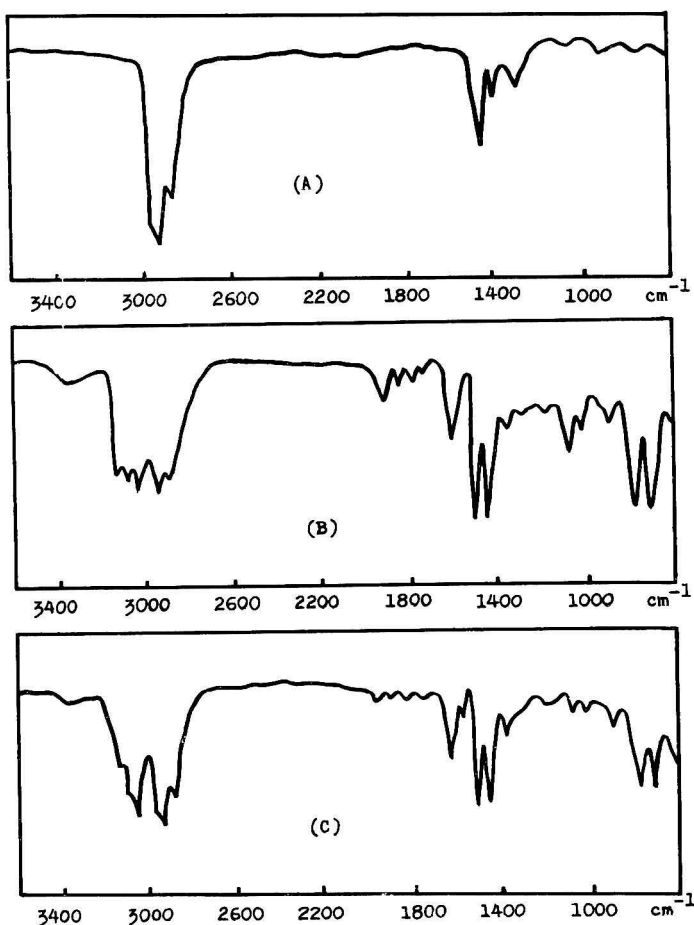


Fig. 1. Infrared spectra of polymers, in THF at 30°C for 5 hr: (a) Cl-EPDM; (b) free PSt; (c) graft polymer. Concentrations:  $C_{10}H_8Na$ ,  $7.91 \times 10^{-2}$  mol/l; St, 0.79 mol/l; Cl-EPDM, 3.64 g/l.

mol/l of styrene was polymerized with  $7.91 \times 10^{-2}$  mol/l of  $C_{10}H_8Na$ ) in THF at 30°C. for 0.5, 1, 2, 3, 5, and 10 hr. The relationship between the grafted styrene content and reaction time is shown in Figure 2.

The grafting efficiency and the percentage of grafting increased with increase in the reaction time and attained constant values at all the Cl-EPDM concentrations after 3 hr. Therefore, in order to find the effect of the Cl-EPDM concentration both on the grafted styrene content and on the grafting efficiency, the values for 5 hr were compared with each other. The results are shown in Figure 3.

The grafted styrene content and the grafting efficiency increased with increase in the Cl-EPDM concentration, and they approached an equilibrium value (grafting efficiency 37–39%) when the ratio of chlorine to the sodium in the initiator was unity. The reaction system, however, was still red after reacting for 5 hr, except in the case of the highest Cl-

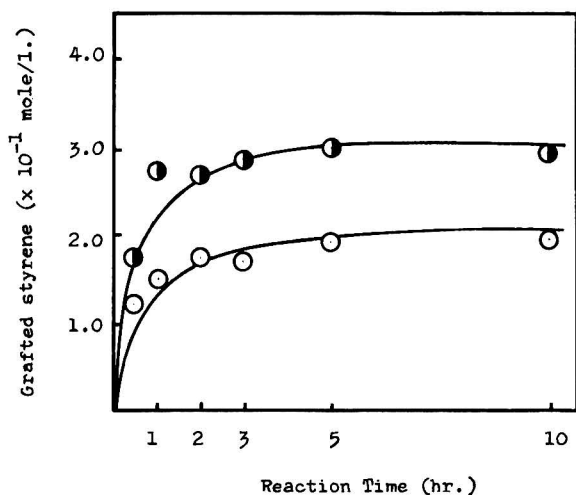


Fig. 2. Relationship between grafted styrene content and reaction time, in THF at 30°C for (O) Cl-EPDM, 1.82 g/l; (●) Cl-EPDM, 9.09 g/l. Concentrations:  $C_{10}H_8Na$ ,  $7.91 \times 10^{-2}$  mol/l; St, 0.79 mol/l;  $[St]/[Na] = 10.14$ .

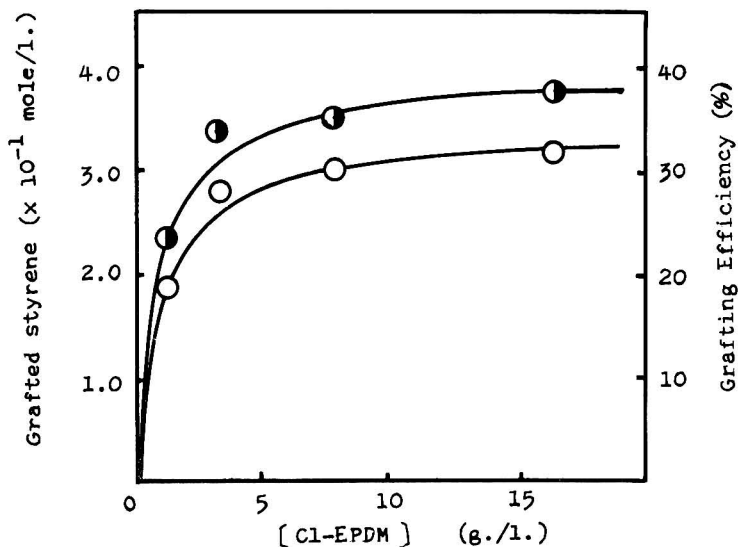


Fig. 3. Effect of CL-EPDM concentration on (O) grafted styrene content and on (●) grafting efficiency, in THF at 30°C for 5 hr. Concentrations:  $C_{10}H_8Na$ ,  $7.91 \times 10^{-2}$  mol/l; St, 0.79 mol/l,  $[St]/[Na]$ , 10.14.

EPDM concentration, which indicated the presence of styryl anion. Gel formation occurred during the reaction, and insoluble graft polymers were obtained.

**Effect of  $\bar{P}_n$  of Living PSt.** Living PSt having various  $\bar{P}_n$ 's reacted with Cl-EPDM at constant concentrations of both. The effects of the  $\bar{P}_n$  of the living PSt on the grafted styrene content and the grafting efficiency are shown in Figure 4.

The grafted styrene content and per cent grafting increased with increase in the  $\bar{P}_n$  of the living PSt. It may be considered that the grafting efficiency is independent of the  $\bar{P}_n$  of the living PSt and is constant. However, it decreased with increase in the  $\bar{P}_n$  of the living PSt, as shown in Figure 4.

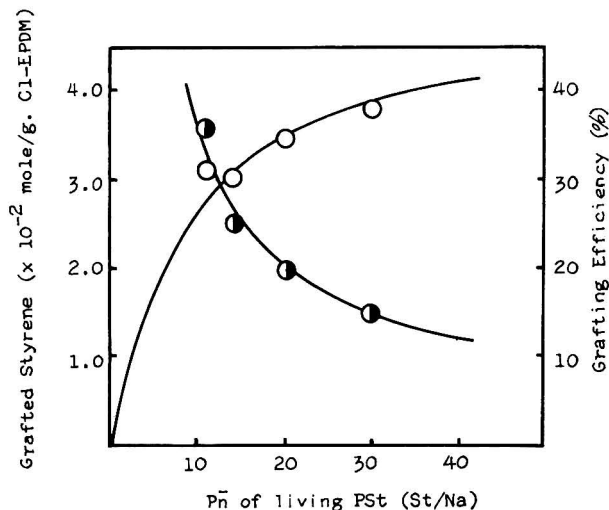


Fig. 4. Effect of  $\bar{P}_n$  of living PSt on (O) grafted styrene content and on (●) grafting efficiency, in THF at 30°C for 5 hr. Concentrations:  $C_{10}H_8Na$ ,  $7.91 \times 10^{-2}$  mol/l; Cl-EPDM, 9.09 g/l;  $[Cl]/[Na]$ , 1.12.

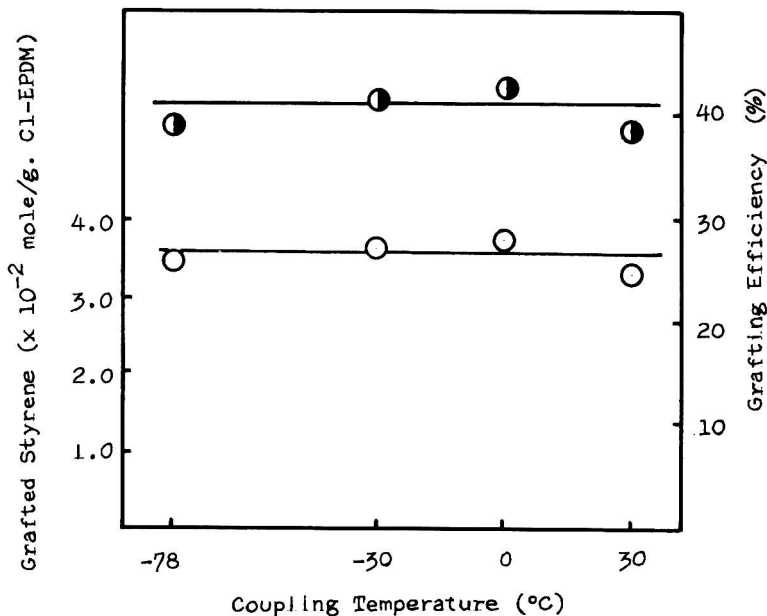


Fig. 5. Effect of coupling temperature on (O) grafted styrene content and on (●) grafting efficiency, in THF for 5 hr. Concentrations:  $C_{10}H_8Na$ ,  $7.91 \times 10^{-2}$  mol/l; St, 0.79 mol/l;  $[St]/[Na]$ , 10.14; Cl-EPDM, 9.09 g/l;  $[Cl]/[Na]$ , 1.12.

Although this reason is not clear, it seemed reasonable to assume that the decrease in grafting efficiency resulted from a restriction of molecular motion and diffusion that may be attributable to the increase in viscosity, since the viscosity of the reaction system increased outstandingly with increase in the  $\bar{P}_n$  of the living PSt. The graft polymers obtained were insoluble in THF and benzene.

**Effect of Coupling Temperature.** The coupling reactions were carried out at  $-78$ ,  $-30$ ,  $0$ , and  $30^\circ\text{C}$  at constant concentrations of Cl-EPDM and living PSt. The effects of the coupling temperature on the grafted styrene content and grafting efficiency are shown in Figure 5.

The coupling temperature was found to have very little effect on the grafted styrene content and the grafting efficiency within the range of this experiment. The graft polymers obtained were insoluble in THF and benzene.

### Reaction of Cl-EPDM with Living PSt Obtained with BuLi

It has been found by Szwarc and his co-workers<sup>12</sup> that living PSt obtained with  $\text{C}_{10}\text{H}_8\text{Na}$  is bifunctional. Thus, it may be considered that gel formation results from crosslinking with the bifunctional living PSt. In this study, to avoid crosslinking, monofunctional living PSt was made to react with Cl-EPDM of various concentrations at  $30^\circ\text{C}$  for 5 hr in THF. The results are shown in Figure 6.

The grafted styrene content and the grafting efficiency increased with increase in the Cl-EPDM concentration, and the maximum grafting efficiency was about 65%, higher than that in the case of the living PSt obtained with  $\text{C}_{10}\text{H}_8\text{Na}$ . The graft polymers, however, were insoluble in THF and benzene.

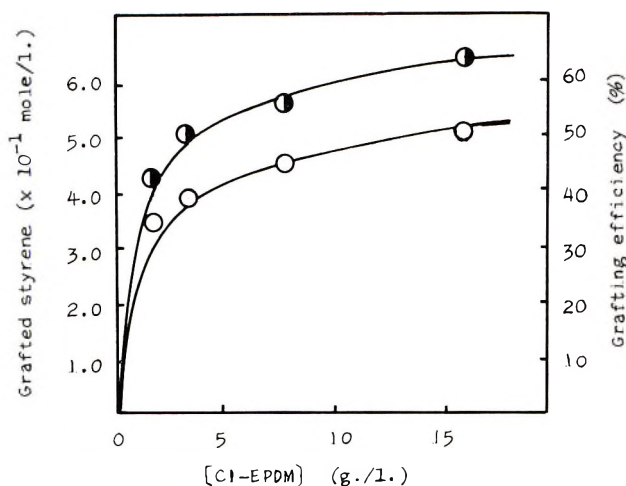


Fig. 6. Effect of Cl-EPDM concentration on (O) grafted styrene content and on (●) grafting efficiency in reaction of Cl-EPDM with living PSt obtained with BuLi, in THF at  $30^\circ\text{C}$  for 5 hr. Concentrations: BuLi,  $7.47 \times 10^{-2}$  mol/l; St, 0.79 mol/l;  $[\text{St}]/[\text{BuLi}]$ , 10.62.

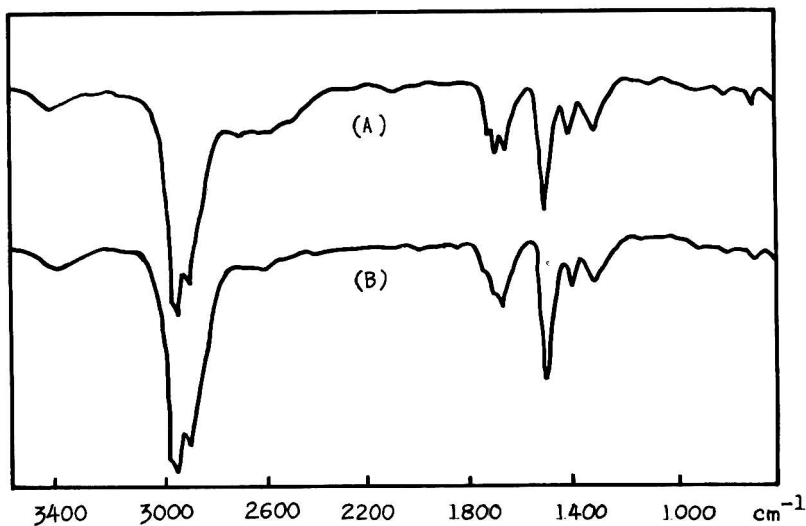
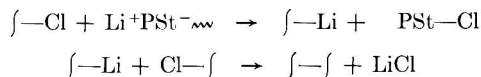


Fig. 7. Infrared spectra of carbonated Cl-EPDM polymer, in THF at 30°C for 5 hr, after reaction (a) with  $C_{10}H_8Na$  (concentrations:  $C_{10}H_8Na$ ,  $1.06 \times 10^{-1}$  mol/l; Cl-EPDM, 7.5 g/l;  $[Cl]/[Na]$ , 0.68) and (b) with BuLi (concentrations: BuLi,  $1.87 \times 10^{-2}$  mol/l; Cl-EPDM, 3.6 g/l;  $[Cl]/[Na]$ , 1.89).

It may be considered that the gel formation results from the metal-halogen interchange reaction followed by reaction of the metal-containing polymer with another Cl-EPDM:



#### Carbonation of Mixture of Cl-EPDM and $C_{10}H_8Na$

The carbonation reaction is the most useful method of identifying organoalkali compounds. This method was applied to a mixture of Cl-EPDM and  $C_{10}H_8Na$  in THF to confirm that the C—Na bond was introduced into the Cl-EPDM by the interchange reaction.

A reaction mixture of Cl-EPDM and  $C_{10}H_8Na$  (or BuLi) in THF was poured into a slurry of THF and solid carbon dioxide, and the insoluble polymer was obtained by the usual treatment. The infrared spectrum of this polymer showed absorptions due to the carbonyl group at 1710, 1680, and 1650  $\text{cm}^{-1}$  and to the OH group at about 3400  $\text{cm}^{-1}$  (Fig. 7).

It may be concluded from these results that gel formation is due to crosslinking not only by the bifunctional living PSt but also through the metal-halogen interchange reaction.

#### Reaction of Other Chlorine-Containing Polymers with Living PSt

Chlorine-containing polymers other than Cl-EPDM reacted with living PSt obtained with  $C_{10}H_8Na$  in THF. The polymers used in this experiment were PCR, Cl-IIR, PVC, PECH, and ECH-EO.

TABLE I  
Intrinsic Viscosities of Graft Polymers for Cl-IIR<sup>a</sup>

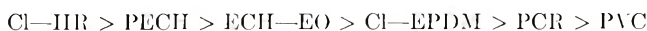
Expt. no.	Cl-IIR, g	Graft, eff., %	Grafting, %	$[\eta]$ of graft polymer <sup>b</sup>
I-1-1	0.1	18.77	85.3	0.655
I-1-2	0.15	19.47	59.0	0.747
I-1-3	0.2	19.82	45.1	0.758
I-1-4	1.2	60.79	23.0	1.209

<sup>a</sup> Reaction conditions:  $[C_{10}H_8Na] = 0.43 \times 10^{-1}$  mol,  $[St] = 4.36 \times 10^{-3}$  mol,  $St/Na = 101.4$ , in 50 ml of THF at 30°C for 5 hr.

<sup>b</sup> Intrinsic viscosity of Cl-IIR used and free polystyrene were 0.591 and 0.216 ( $\bar{P}_n = 207.2$ ), respectively.

An  $8.73 \times 10^{-3}$  mol amount of styrene was polymerized with  $0.43 \times 10^{-3}$  mol of  $C_{10}H_8Na$  in 30 ml of THF. The chlorine-containing polymer dissolved in 20 ml of THF and reacted with the living PSt; the amounts were 0.02, 0.05, 0.2, and 0.5 g for PCR, PECH, and ECH-EO, and 0.02, 0.025, 0.05, 0.5, and 2.5 g for PVC. The reaction conditions for Cl-IIR are given in Table I.

The grafted styrene contents and the grafting efficiencies increased with increase in the concentrations of the chlorine-containing polymers, as in the case of Cl-EPDM, and the grafting efficiencies became constant at about 27, 61, 25, 50, and 42% for PCR, Cl-IIR, PVC, PECH, and ECH-EO, respectively, when the amounts of the chlorine-containing polymer were 0.02, 1.2, 0.25, 0.2, and 0.2 g for PCR, Cl-IIR, PVC, PECH, and ECH-EO, respectively. Thus, the grafting efficiencies were in the following order:



Soluble graft polymers were obtained only with Cl-IIR and with low concentrations of PVC, PECH, and ECH-EO. The intrinsic viscosities  $[\eta]$  of the graft polymers of Cl-IIR are shown in Table I.

The infrared spectra of the graft polymers are shown in Figure 8. These spectra showed bands of both the backbone polymers and the grafted PSt; that is, the infrared spectrum of the PSt-grafted PCR in Figure 8a showed both the bands due to PSt at 3060, 3020, 2850, 1900, 1495, 1455, and 700  $cm^{-1}$  and the bands due to PCR at 1475 ( $-CH_2-$ ) and 680 (C-Cl)  $cm^{-1}$ . The infrared spectra of the graft polymers other than the PSt-grafted PCR similarly showed the bands due to Cl-IIR at 2940  $cm^{-1}$  ( $-CH_3$ ) and 1475  $cm^{-1}$  for the PSt-grafted Cl-IIR (Fig. 8b), the bands due to PVC at 1200, 635 (C-Cl), and 615 (C-Cl)  $cm^{-1}$  for the PSt-grafted PVC (Fig. 8c), and the band due to the ether bond at 1150-1090  $cm^{-1}$  for the PSt-grafted PECH (Fig. 8d) and ECH-EO (Fig. 8e), together with the bands of the PSt.

It has been found that dehydrochlorination, in addition to the coupling of organic groups, occurs especially during the reaction of secondary or tertiary

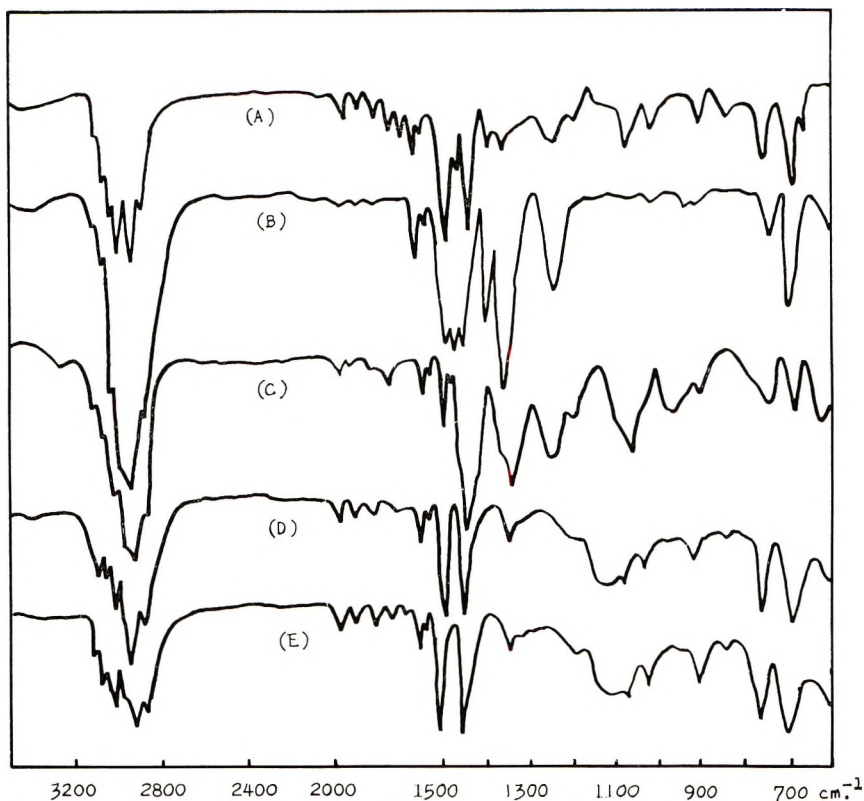


Fig. 8. Infrared spectra of Pst-grafted polymers for (a) PCR, (b) Cl-IIR, (c) PVC, (d) PECH, and (e) ECH-EO.

alkyl halides with an alkyl lithium compound, and it has been shown by Minoura and Shiina<sup>10</sup> that various reactions such as dehydrochlorination, metal-halogen interchange, and crosslinking occur during the reaction of PVC with BuLi or  $C_{10}H_8Na$ . Furthermore, the infrared spectra of the carbonation products of Cl-IIR, ECH-EO, and PECH mixtures with  $C_{10}H_8Na$  in THF showed absorptions due to the carbonyl group at 1750–1720  $cm^{-1}$  and to the hydroxyl group at about 3400  $cm^{-1}$ .

It may be concluded from the results that gel formation is due to crosslinking not only by the bifunctional living PSt but also through metal-halogen interchange, and that these undesirable reactions can be avoided by decreasing the concentration of the chlorine-containing polymer.

#### Reaction of Chlorine-Containing Polymers with Living Poly(isoprene)

The reaction of living poly(isoprene) (PIS), instead of living PSt, with chlorine-containing polymers was carried out by a similar method. In the presence of nitrogen  $3.0 \times 10^{-2}$  mol of isoprene was polymerized with  $1.1 \times 10^{-3}$  mol of  $C_{10}H_8Na$  in 30 ml of THF in a 100 ml reaction flask. The living PIS reacted with solutions of chlorine-containing polymers (0.5 g)

in 20 ml of THF at 30 and 50°C for 5 hr. Cl-EPDM, Cl-IIR, PECH, and ECH-EO were used as the chlorine-containing polymers. The free PIS was extracted with ethyl ether, and the weight of the fraction insoluble in ethyl ether did not increase for any of the chlorine-containing polymers; that is, no grafted polymers were obtained. A  $0.9 \times 10^{-2}$  mol amount of isoprene was polymerized with  $1.03 \times 10^{-3}$  mol of BuLi in 30 ml of benzene, and the living PIS reacted with 0.5 g of Cl-EPDM dissolved in 20 ml of benzene at 30°C for 5 hr. After extraction with ethyl ether the infrared spectrum of the extracted residue showed absorptions due to the C=C in PIR at 1650 and about 900  $\text{cm}^{-1}$ .

These results indicate that the fraction insoluble in ethyl ether contained PIS-grafted Cl-EPDM. The grafting efficiency and the per cent grafting, calculated from the increase in weight of the extracted residue, were 18.41 and 56.90%, respectively. The graft polymer was insoluble in THF and benzene.

It is known<sup>13-15</sup> that the PIS obtained in THF with  $\text{C}_{10}\text{H}_8\text{Na}$  as initiator is a mixture of the 1,2 and 3,4 structures and that the PIS obtained in benzene with BuLi as initiator consists almost entirely of the 1,4 structure. Therefore, it was concluded that in the coupling reaction the reactivities of the carbanionic endgroups of the living PIS having the 1,4 structure were higher than those of the living PIS having the 1,2 and 3,4 structures.

### References

1. H. Sehreiber, *Makromol. Chem.*, **36**, 86 (1959).
2. P. Rempp and M. H. Loucheux, *Bull. Soc. Chim. France*, **1958**, 1497.
3. M. H. Loucheux, G. Meyer, and R. Rempp, *Compt. Rend.*, **252**, 2552 (1961).
4. S. P. S. Yen, paper presented at the 145th Meeting of the American Chemical Society, New York, September 1963; *Polymer Preprints*, **4**, 332 (1963).
5. R. Waack, A. Rembaum, J. D. Coombes, and M. Szwarc, *J. Am. Chem. Soc.*, **79**, 2026 (1957).
6. W. B. Brown and M. Szwarc, *Trans. Faraday Soc.*, **54**, 416 (1958).
7. G. Finaz, Y. Gallot, P. Rempp, and J. Parrod, *J. Polymer Sci.*, **58**, 1363 (1963).
8. Y. Gallot, P. Rempp, and J. Parrod, *J. Polymer Sci. B*, **1**, 329 (1963).
9. T. Alteares, Jr., D. P. Wyman, V. R. Allen, and K. Meyersen, *J. Polymer Sci. A*, **3**, 4131 (1965).
10. Y. Minoura and K. Shiina, *J. Polymer Sci. A-1*, **4**, 1069 (1966).
11. D. H. Johnson and A. V. Tobolsky, *J. Am. Chem. Soc.*, **74**, 938 (1952).
12. M. Szwarc, M. Levy, and R. Milkovich, *J. Am. Chem. Soc.*, **78**, 2656 (1956).
13. H. Morita and A. V. Tobolsky, *J. Am. Chem. Soc.*, **79**, 5853 (1957).
14. A. V. Tobolsky and C. E. Rogers, *J. Polymer Sci.*, **38**, 205 (1959).
15. A. V. Tobolsky and C. E. Rogers, *J. Polymer Sci.*, **40**, 73 (1959).

Received January 30, 1968

Revised March 13, 1968

## Wide Line and Pulsed NMR Studies of Carboxyl-Terminated Polybutadiene Polymers and Binders

A. S. TOMPA, R. D. BAREFOOT, and E. PRICE, *Naval Ordnance Station Naval Ordnance Research, Indian Head, Maryland 20640*

### Synopsis

Nuclear magnetic resonance relaxation and line width studies were performed on two carboxyl-terminated polybutadiene polymers and their corresponding binders at temperatures from  $-170$  to  $25^{\circ}\text{C}$ . It was observed that the line widths of the binders increased as the functionality of the corresponding liquid polymers increased. In addition, glass transition temperatures and activation energies obtained from line width measurements were determined. From pulse measurements the magnitude of the relaxation time  $T_1$  and the temperature at which  $T_1$  is a minimum were determined for a polymer and its corresponding binder. These empirical quantities for the carboxyl-terminated polybutadiene polymers were lower than those of the corresponding binders because of less restraints in the internal motions of the polymer chain.

### INTRODUCTION

The physical properties of polymers depend to a large extent upon the molecular motions of the individual polymer chains. The molecular motions in turn are dependent upon the polymer structure, polymer composition, and temperature. Wide line and pulsed nuclear magnetic resonance (NMR) studies have provided useful information on the molecular motions and relaxation properties of polymers.<sup>1-5</sup> Line width measurements as a function of temperature have been used to determine transition temperatures and activation energies for the motional (main chain and side chain) processes involved.<sup>2</sup>

The nuclear spin system experiences two relaxation processes, which are sensitive to molecular motion. One is the spin-lattice relaxation, characterized by a time constant  $T_1$ . This is the process that produces thermal equilibrium between the nuclear spin system and the environment (lattice). The other process is the spin-spin relaxation, characterized by  $T_2$ , which is a measure of the width of the resonance absorption due to interactions with neighboring magnetic dipoles. Slichter and Davis<sup>6</sup> found  $T_1$  to depend on the *cis-trans* content in polybutadiene. Takeda et al.<sup>7</sup> determined glass transition temperatures in *cis*- and *trans*-polybutadiene from line width measurements at  $-95$  and  $-69^{\circ}\text{C}$ , respectively.

In this paper we have initiated a systematic study to characterize two similar polymers and their corresponding binders (in the present studies

“binder” refers to an unfilled but cured elastomeric organic matrix) by nuclear magnetic resonance techniques. Line widths and pulse measurements as a function of temperature for two carboxyl-terminated polybutadiene polymers (CTPB-A and CTPB-B) and their binders were determined. The binders were binder A, CTPB-A with tris-[1-(2-methyl)-aziridinyl] phosphine oxide (MAPO) and binder B, CTPB-B with MAPO. The data are interpreted in terms of differences in functionalities of the polymers, crosslinking in the binders, and glass transition temperatures in the polymers and binders.

## EXPERIMENTAL

### Materials

Two binders were prepared by curing carboxyl-terminated polybutadiene (CTPB-A and CTPB-B) with tris-[1-(2-methyl)aziridinyl] phosphine oxide (MAPO) at 150°F for 72 hr. The carboxyl contents for CTPB-A and CTPB-B were 1.26 and 1.21%, respectively. The functionalities of CTPB-A and CTPB-B were 2.42 and 2.14, respectively.<sup>8</sup> “Functionality” is defined as the number of reactive groups per molecule; the carboxyl content is in units of weight per cent per gram of sample; a higher carboxyl content implies a lower number-average molecular weight but is not necessarily related to functionality. Binder A (CTPB-A with MAPO) cured faster than binder B (CTPB-B with MAPO). The unsaturation distribution in CTPB-A and CTPB-B was determined by infrared spectroscopy.<sup>9</sup> The values for CTPB-A and CTPB-B were within 2% of each other and were in the range of 42% *trans*, 23% vinyl, and 35% *cis*. The unsaturation distribution for binders A and B was not determined. However, if some *cis-trans* isomerization occurred during the curing process, we have no reason to believe that the change would not be the same for the two binders.

### Experimental Method

The nuclear magnetic resonance experiments were performed at the National Bureau of Standards on instruments designed and built by Dr. Thomas C. Farrar. Line shape measurements were performed with a regenerative spectrometer operating at 29.5 and 40.0 MHz. Line width measurements were obtained from room temperature to  $-170^{\circ}$ . The proton spin-lattice relaxation time  $T_1$  was measured on CTPB-B and binder B from room temperature to  $-80^{\circ}\text{C}$ . These measurements of  $T_1$  were made with a spin-echo apparatus at 19.0 MHz. The  $T_1$  values were measured by the 180–90° pulse method of Carr and Purcell.<sup>10</sup>

Differential thermal analysis curves were run on a du Pont Model 900 at a heating rate of 5–10°/min and at a  $\Delta T$  scale of 0.2°/in. with glass beads as the reference sample. Dynamic tensile modulus measurements were performed on an instrument described in the literature.<sup>11</sup>

## DISCUSSION

## Line Widths and Transition Temperatures

The line widths  $\delta H$ , measured in Gauss as the separation between the points of maximum and minimum slope of the derivative resonance absorption curves, were plotted against the temperature for the CTPB polymers and their binders. Typical curves are shown in Figures 1 and 2 for CTPB-A and binder A. As the temperature is lowered, the line width increases, because the internal motion (reorientation) of the polymer chain decreases. In the neighborhood of the glass transition temperature  $T_g$  there is a marked broadening of the resonance line, which is associated with main-chain motion. The glass transition temperatures obtained from the inflection points of  $\delta H$ - $T$  curves are listed in Table I. Glass transition temperatures

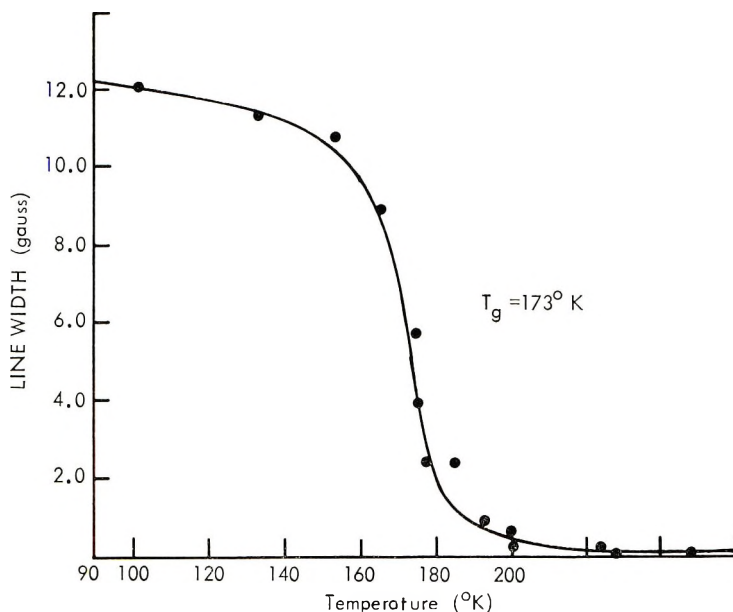


Fig. 1. Temperature dependence of NMR line width for CTPB-A.

were also determined by differential thermal analysis (DTA), as shown in Figure 3. NMR data show that  $T_g$  comes at a lower temperature for polymers than for binders, because there are more restraints on the internal motion in the crosslinked binders. Differences in the  $T_g$ 's of the polymers and binders themselves are minor. DTA data do not distinguish between the  $T_g$ 's of the polymers and binders. There is good agreement in the  $T_g$ 's of the binders by NMR and DTA, but not in the  $T_g$ 's of the polymers. However, it is evident from the curves that NMR measurements are more sensitive to changes occurring in the polymers at  $T_g$  than are DTA measurements, in which changes in the specific heat results only in a shift in the base line of the curve.

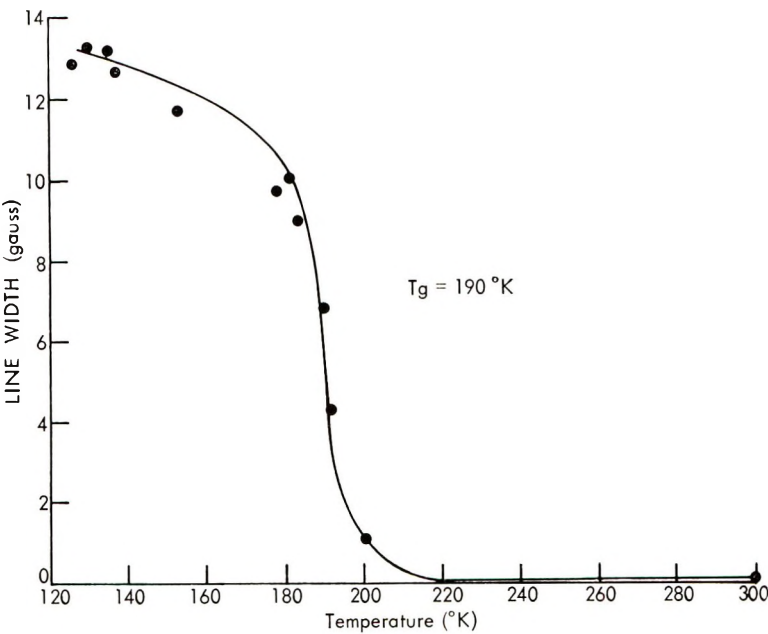


Fig. 2. Temperature dependence of NMR line width for binder A.

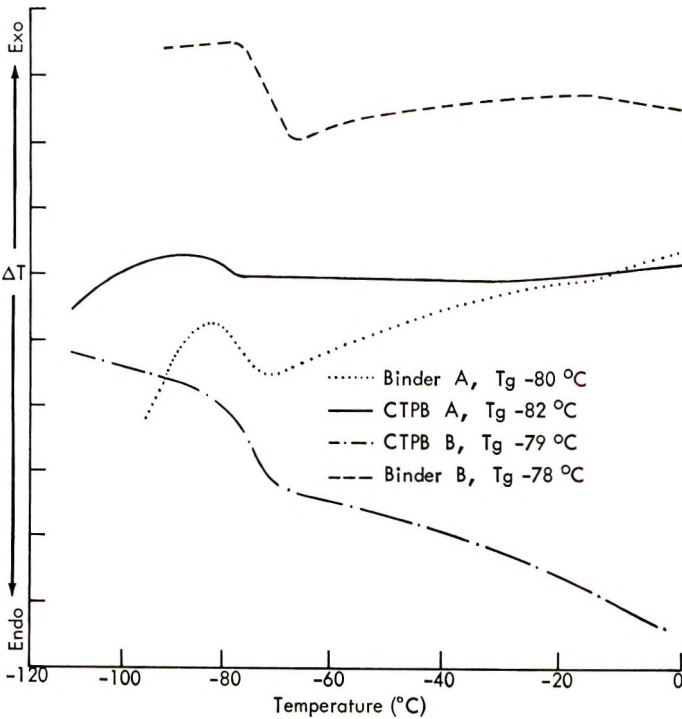


Fig. 3. DTA curves for glass transition of CTPB polymers and binders.

TABLE I  
Glass Transition Temperatures from Nuclear Magnetic Resonance and Differential Thermal Analysis Measurements of CTPB Polymers and Binders

	$T_g, ^\circ\text{C}$	
	NMR	DTA
CTPB-A	-100	-82
CTPB-B	-95	-79
Binder A	-83	-80
Binder B	-82	-78

Figure 4, a plot of dynamic tensile modulus versus temperature (room to  $-45^\circ\text{C}$ ), indicates that a transition occurs at about  $-32^\circ\text{C}$ , which may be due to a secondary amorphous transition involving some main-chain seg-

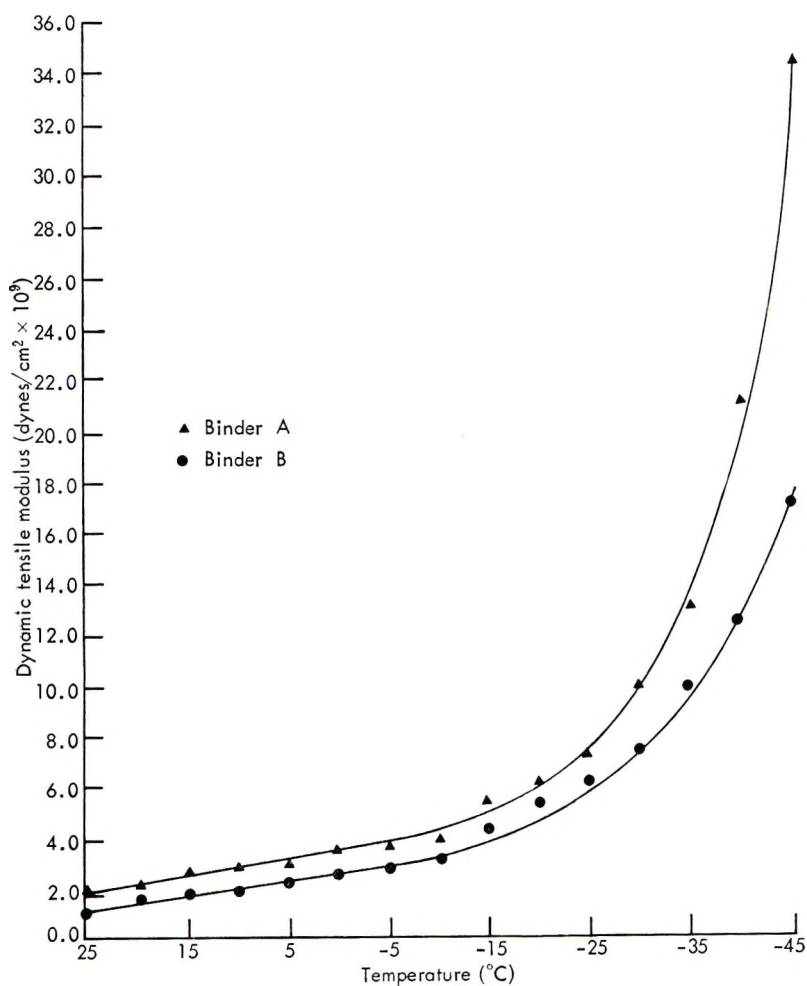


Fig. 4. Temperature dependence of dynamic tensile modulus of CTPB binders.

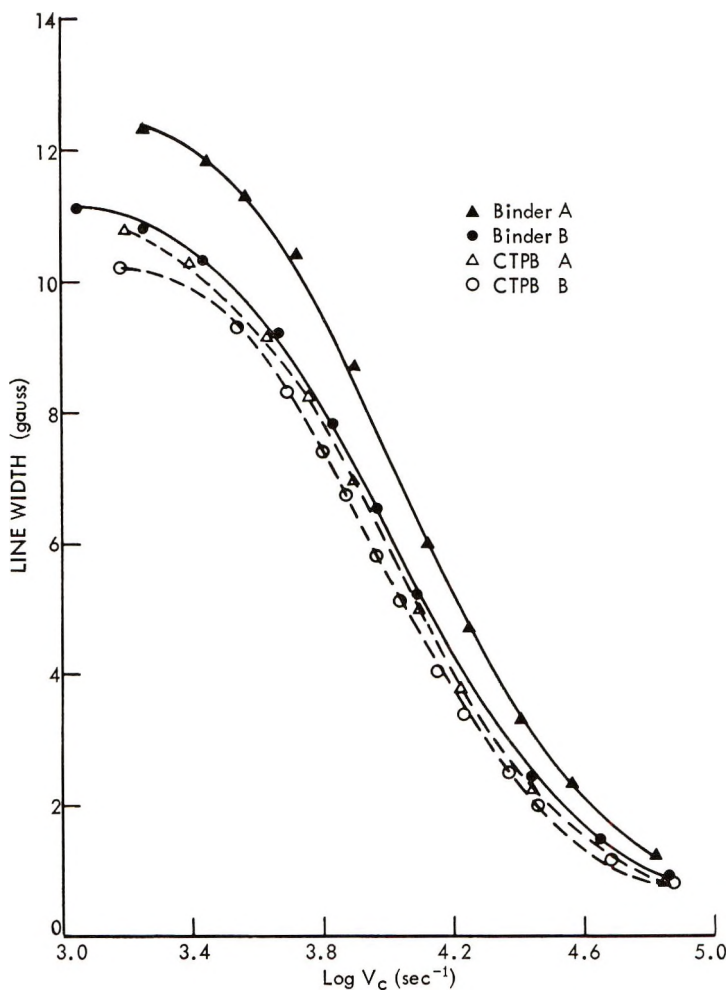


Fig. 5. Plot of NMR line width versus correlation frequency for CTPB polymers and binders.

mental motion. These transitions show up more clearly in mechanical than in NMR measurements, because they occur at much lower frequencies, namely 1–1000 Hz, as compared to  $10^3$ – $10^4$  Hz for NMR. Thus, NMR and dynamic-mechanical methods are supplementary in providing information about internal segmental motion in polymers.

Figure 5 is a plot of line width versus correlation frequency (i.e. frequency of rotation of the polymer chain). As the line width narrows, the frequency of reorientation increases. The line width increases in the order CTPB-B, CTPB-A, binder B, and binder A. The increase in linewidth implies that there are more restraints on polymer motion. Binder A has a higher cross-link density than binder B, because CTPB-A has a higher functionality than CTPB-B. As the crosslinking increases, the potential barrier for internal

rotation about carbon-carbon single bonds increases, and consequently there are more interactions between neighboring magnetic dipoles; this results in a broader line.

### Activation Energies

The theory of Bloembergen et al.,<sup>12</sup> relating line width and correlation frequency, which characterize the motion responsible for a particular line narrowing, has been modified by Gutowsky and Pake<sup>13</sup> and Kubo and Tomita.<sup>14</sup> The modified expression is

$$2\pi V_c = \alpha\gamma\delta H / \tan [(\pi/2)(\delta H^2 - B^2)/C^2 - B^2] \quad (1)$$

where  $V_c$  is the correlation frequency for the motion narrowing the line,  $\delta H$  is the line width in the transition region,  $B$  is the line width at a temperature higher than the transition region, and  $C$  is the rigid lattice line width. In the present study  $B$  was 0.04 G at room temperature, and  $C$  was 13.1 and 11.6 G for binders A and B, respectively, at  $-145^\circ\text{C}$  and 11.5 and 10.9 G for CTPB-A and CTPB-B, respectively, at  $-170^\circ\text{C}$ . The constant  $\alpha$  is  $(8 \ln 2)^{-1}$  and  $\gamma$  is the gyromagnetic ratio ( $2.675 \times 10^4 \text{ G}^{-1} \text{ sec}^{-1}$ ). Assuming the Arrhenius expression  $V_c = V_0 \exp \{-E_a/RT\}$ , the activation energy  $E_a$  of the motions of the polymer chain may be calculated. Figure 6 is a typical plot of  $\log V_c$  versus  $1/T$  for a CTPB polymer and binder. The activation energies obtained for CTPB polymers and binders were of the order of 6–8 kcal/mol and 13–15 kcal/mol, respectively. The activation energies have an uncertainty of  $\pm 10\%$ , because one of the as-

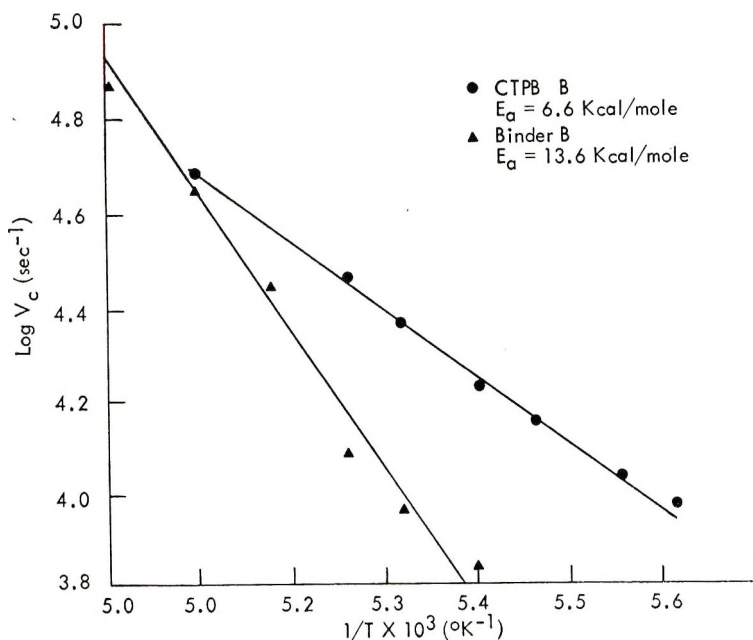


Fig. 6. Plot of correlation frequency versus  $1/T$  for CTPB-B polymer and binder B.

sumptions in the derivation of the equation is that the motion involved occurs with a single correlation frequency in the transition region rather than with a broad distribution of such frequencies, as is actually the case in polymeric systems. It is difficult to interpret these activation energies in terms of specific motions in the polymer, and these values therefore represent an average process of the motions existing in the polymer.

### Spin-Lattice Relaxation Times

Bloembergen et al.<sup>12</sup> showed that the spin-lattice relaxation time  $T_1$  is most effective (i.e., the relaxation time is shortest) when the lattice frequency is comparable to the resonant frequency of the nuclei. Thus, the presence of a  $T_1$  minimum identifies a predominant frequency, which may be taken to characterize the molecular motion of the nuclei at the corresponding temperature.<sup>6</sup> Figure 7 shows a plot of the temperature dependence of the spin-lattice relaxation for a liquid polymer (B) and a cross-linked binder (B). The correlation frequency  $V_c$  of the nuclei at the temperature of the  $T_1$  minimum is  $3.0 \times 10^7 \text{ sec}^{-1}$ , which is 1.6 times the resonance frequency (19.0 MHz). Three observations are evident: (1) the

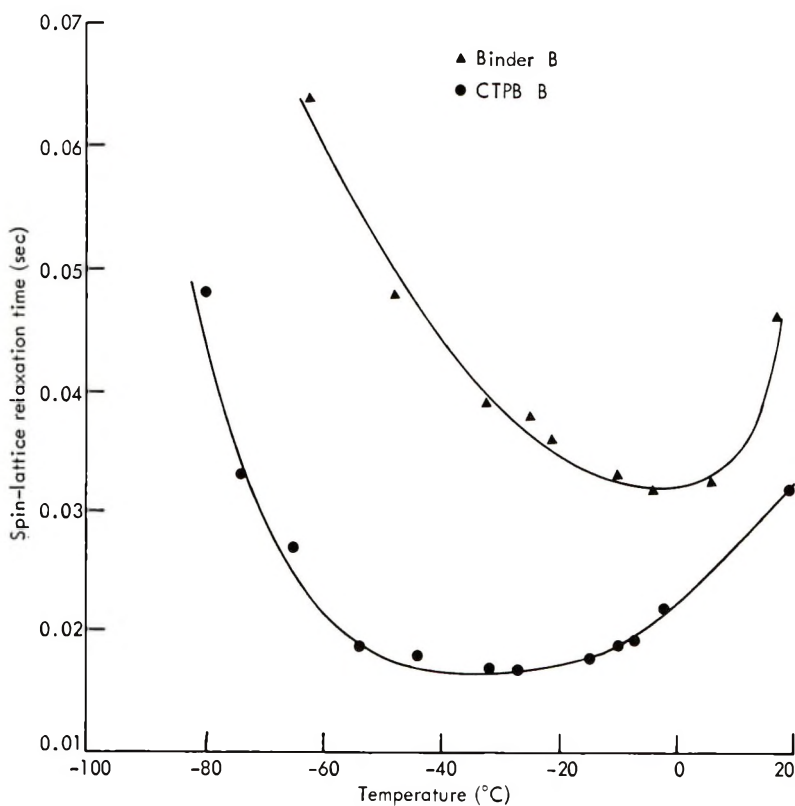


Fig. 7. Temperature dependence of spin-lattice relaxation time for CTPB polymer and binder.

$T_1$  minimum occurs at a higher temperature for the binder (about 0°C) than for the polymer (about -30°C), (2) the polymer has a lower  $T_1$  minimum (0.017 sec) than the binder (0.032 sec), and (3) the broad  $T_1$  minimum indicates that there exists a wide distribution of correlation times for polymer segmental motions. These observations may be explained on the basis of greater constraints on segmental motion in the binder because of the existence of a crosslinked network, which reduces the chain's mobility. Consequently, the temperature of the  $T_1$  minimum increases, and the efficiency of spin-lattice relaxation decreases; this results in a longer time for the relaxation process to take place. Slichter and Davis<sup>6</sup> found that the temperature for  $T_1$  minimum increased from *cis*- to *cis-trans*- to *trans*-polybutadiene, which parallels the increase in degree of crystallinity and, hence, the decrease in chain mobility in these polymers. They found that a 53% increase in *trans* content increased the temperature of the  $T_1$  minimum by 10°C. Therefore, we believe that in the present study, if some *cis-trans* isomerization did occur during cure, the resulting increase in *trans* content would be small and have a negligible effect on the shift of the temperature at the  $T_1$  minimum.

## CONCLUSION

Wide line and pulsed nuclear magnetic resonance measurements provide a powerful technique for studying chain motion and relaxation processes in polymers and binders. An increase in functionality of CTPB polymers gives rise to an increase in crosslink density of the corresponding binders. This results in an increase in line width, which can be used to characterize two similar binders. We observed that  $T_g$  and  $E_a$  from line width measurements and the magnitude of the  $T_1$  minimum and the temperature at the  $T_1$  minimum from pulse measurements of CTPB polymers were lower than those of the corresponding binders; this was attributed to less restraints in the internal motion of the polymer chains. The determination of glass transition temperatures by NMR was found to be more sensitive than that by DTA.

We are grateful to Drs. Thomas Farrar and Ronald Dehl for the use of their instrument and for many helpful discussions. We would like to thank Dr. George Wilmot for discussions, Dr. Joseph Crisler for DTA curves, and Mr. Marbury Bryan for DTM curves.

This program was supported by the Standards Laboratory Program of the Naval Ordnance Systems Command.

## References

1. J. G. Powles, *Polymer*, **1**, 219 (1960).
2. W. P. Slichter, *Forsch. Hochpolymer-Forsch.*, **1**, 35 (1958).
3. Y. Slonim, *Russ. Chem. Rev.*, **31**, 308 (1962).
4. J. A. Sauer and A. E. Woodward, *Rev. Mod. Phys.*, **35**, 3103 (1964).
5. A. E. Woodward, *SPE Trans.*, **2**, 1 (1962).
6. W. P. Slichter and D. D. Davis, *J. Appl. Phys.*, **35**, 3103 (1964).
7. M. Takeda, K. Tanaka, and R. Nagao, *J. Polymer Sci.*, **57**, 517 (1962).
8. R. A. Strecker and A. S. Tompa, *J. Polymer Sci. A-1*, **6**, 1233 (1968).

9. R. S. Silas, J. Yates, and V. Thornton, *Anal. Chem.*, **31**, 529 (1959).
10. H. Y. Carr and E. M. Purcell, *Phys. Rev.*, **94**, 630 (1954).
11. O. C. Hansen, T. F. Fabry, L. Macken, and O. J. Sweeting, *J. Polymer Sci. A*, **1**, 1585 (1963).
12. N. Bloembergen, E. M. Purcell, and R. V. Pound, *Phys. Rev.*, **73**, 679 (1948).
13. H. S. Gutowsky and G. E. Pake, *J. Chem. Phys.*, **18**, 162 (1950).
14. R. Kubo and K. Tomita, *J. Phys. Soc. Japan*, **9**, 888 (1954).

Received February 14, 1968

Revised March 11, 1968

## Molecular Weight Distributions in Polymerizing Systems with Different Coexisting Active Centers

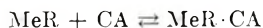
S. E. BRESLER, B. L. ERUSSALIMSKY  
and I. V. KULEVSKAYA,

*Institute of High Molecular Weight Compounds,  
Leningrad, U.S.S.R.*

### Synopsis

Polymerization of acrylonitrile initiated by organomagnesium compounds  $\text{Bu}_2\text{Mg}$  or  $\text{BuMgCl}$  leads to almost monodisperse polymers. The molecular weight distribution (MWD) of these polymers is so narrow that it cannot be measured by means of the ultracentrifuge. It remains narrow till high conversions. On the other hand, initiation by complex  $\text{Bu}_3\text{Mg}\cdot\text{I}$  leads to polymers with a broad MWD. From kinetic measurements we know that this reaction is free of chain termination and chain transfer. Also the initiation of chains is practically immediate. The reason for broad MWD in this particular case is the coexistence of different growing centers of polymerization. The propagation constants for these centers are obviously different. If these different active centers can periodically undergo transition from one type into the other the MWD of resulting polymer chains will broaden. A very simple semiquantitative theory for this phenomenon was developed. It shows that the fewer exchanges between the coexisting centers that occur during the reaction time, the broader will be the MWD of the polymer chains. Hence it was concluded that the broadest MWD of products must be found at low conversions. With an increase of reaction time and conversion the MWD becomes more narrow. This peculiar prediction was corroborated by experiment.

It is well known that in many cases of ionic polymerization characterized by the absence of chain termination practically monodisperse polymers are formed. Deviations from this rule are caused by several factors, namely, relatively low initiation rate, chain-transfer reactions, or by heterogeneity of the system. Another factor that must be taken into account is the non-equivalency of coexisting active centers taking part in polymerization. As an example of such systems we can mention the anionic polymerization initiated by organometallic compounds ( $\text{MeR}$ ) in the presence of complexing agents (CA) under conditions of reversible equilibrium:



As will be shown, different types of active centers can coexist, even in the absence of complexing agents. A quantitative approach to such systems was proposed by Hostalka et al.<sup>1</sup> In this paper we will describe and discuss experimental data illustrating the connection between the character of the molecular weight distribution (MWD) of the polymer and the nature of

the initiating agent. All results are concerned with polyacrylonitrile obtained by anionic polymerization under the action of organomagnesium compounds and their complexes.

### Experimental Results

The investigation of acrylonitrile (AN) polymerization initiated by different organomagnesium compounds with or without complexing agents led to the conclusion that these processes were free of termination reactions.<sup>2</sup> On the other hand, the MWD of polymers obtained by the use of initiators of the above type was found to be dependent on the nature of the catalyst. An extremely narrow MWD for polymers formed at  $-75^{\circ}\text{C}$ . in the system AN-BuMgCl-toluene has been noted recently.<sup>3</sup> As was shown for a polymer obtained at rather high conversion (23%), the width of its MWD lay in the range of errors of the ultracentrifugation; the dispersion of molecular weights was lower than 5% (Fig. 1). The MWD of

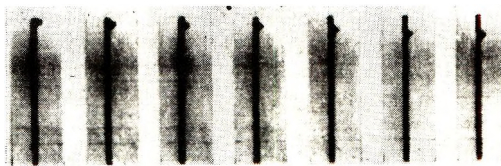


Fig. 1. Sedimentation diagram of PAN obtained under the action of BuMgCl in toluene at  $-75^{\circ}\text{C}$ . Concentrations of catalysts and monomer 0.005 and 2.5 mole/l., respectively; conversion 23%;  $[\eta] = 2.39$ . Conditions of sedimentation: solution 0.01% in dimethylformamide, acceleration  $2.35 \times 10^5 g$ .

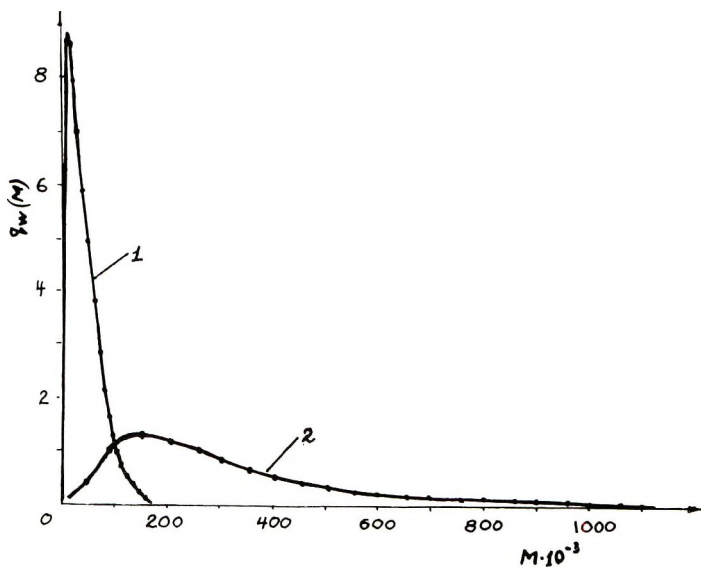


Fig. 2. MWD of PAN obtained under the action of Bu<sub>3</sub>MgI at  $-75^{\circ}\text{C}$ . in toluene: (1) 5.7% conversion; (2) 28% conversion. Concentration of catalyst and monomer 0.01 and 1.5 mole/l., respectively.

polyacrylonitrile (PAN) obtained under analogous conditions under the action of  $\text{Bu}_2\text{Mg}$  has a similar shape. In contrast,  $\text{Bu}_3\text{Mg}_2\text{I}$  leads to PAN with a much broader MWD. The peculiarity of this reaction is that the

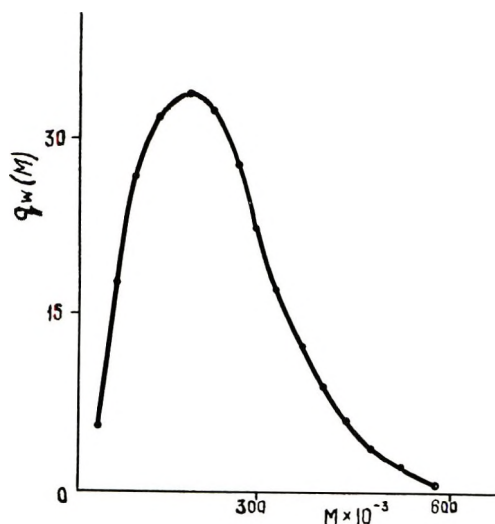


Fig. 3. MWD of PAN obtained under the action of  $\text{BuMgCl}$  in toluene in the presence of DFA at  $-75^\circ\text{C}$ .  $[\text{DMF}]/[\text{Mg}]$  ratio = 1; other conditions same as Figure 1.

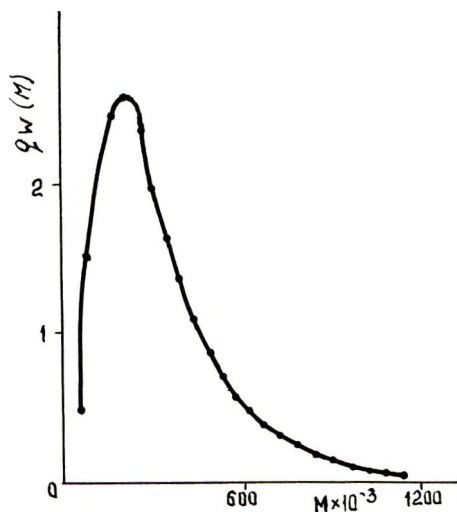
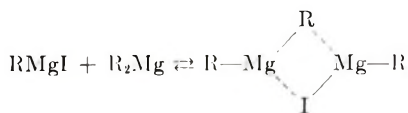


Fig. 4. MWD of PAN obtained under the action of  $\text{BuMgCl}$  in toluene in the presence of DSO at  $-75^\circ\text{C}$ .  $[\text{DMSO}]/[\text{Mg}] = 5$ ; other conditions same as for Figure 1.

lower the conversion, the broader the MWD (Fig. 2). The kinetics of polymerization initiated by  $\text{Bu}_3\text{Mg}_2\text{I}$  are practically the same as in the cases of  $\text{BuMgCl}$  and  $\text{Bu}_2\text{Mg}$ . Therefore the different character of MWD found for the corresponding polymers must be related to the specificity of the

initiator. In this case there exists the possibility of an equilibrium of the type



The nonequivalence of the R groups in the catalyst and consequently in the growing active centers must lead to different values of propagation constant  $k_p$  for different Mg—C bonds. The variations of state of each growing chain (i.e., variations of  $k_p$ ) during polymerization cause the formation of a polymer with broad MWD.

We have studied also two systems of the type AN—RMgX—CA—toluene including dimethylformamide (DMF) and dimethyl sulfoxide (DMSO) as complexing agents. These experiments were briefly described previously,<sup>2,4</sup> but the data concerning the MWD of polymers were not mentioned. The presence of catalytic amounts of DFA or DMSO results in polymers with a broad MWD even when the organomagnesium compound BuMgCl was used as initiator (Figs. 3 and 4). As mentioned above, in the absence of complexing agents BuMgCl leads to a monodisperse polymer. Kinetic data for the systems with DMF and DMSO do not support the idea of chain termination or slow initiation rate. Hence the formation of polymers with broad MWD can be interpreted by the assumption of the coexistence of different active centers. In the case of complexing agents the following scheme may be used:



As will be shown, the presence of nonequivalent active centers in a polymerizing system can result in the formation of polymers with broad MWD. We will consider the simple case when only two types of active centers coexist.

### Analysis of MWD

We will consider the MWD for the case when at time zero two types of active centers coexist:  $N_1$  centers of the first and  $N_2$  of the second kind. We will assume that no transfer or termination reactions take place. The propagation rate constant for the first kind of centers is  $k_1$ , for the second  $k_2$ . If all centers would grow independently we should obtain a mixture of two monodisperse polymers with molecular weights  $M_1 = k_1 M_0 t$  and  $M_2 = k_2 M_0 t$ , where  $M_0$  is the molecular weight of the monomer and  $t$  is the reaction time. If there exists a continuous transition from one kind of center to the other, we will obtain a polymer with an average molecular weight

$$\bar{M} = \frac{M_1 + \alpha M_2}{1 + \alpha} = \frac{M_0 t (k_1 + \alpha k_2)}{1 + \alpha}$$

where  $\alpha = N_2/N_1$  is the equilibrium constant. If the exchange between the polymerization centers occurs very often, the resulting polymer will have a narrow MWD. If this exchange is a rare event and takes place only few times during polymerization, the MWD will broaden and fill up the whole range between  $M_1$  and  $M_2$ .

We will designate by  $\tau$  the average lifetime of a polymerization center in the first state between acts of transition. Therefore the average lifetime in the second state will be  $\alpha\tau$ . We will assume that  $\alpha < 1$ ; then the MWD function  $dN/dM$  can be found by a simple argument.

As already stated, we would get an infinitely narrow distribution if the exchange between the centers would proceed infinitely often. The molecular weight of this monodisperse polymer would be  $\bar{M}$ . If the exchange does not take place at all we will obtain the greatest variation in molecular weights

$$\delta = \bar{M} - M_2 = \frac{M_1 + \alpha M_2}{1 + \alpha} - M_2 = \frac{M_1 - M_2}{1 + \alpha}$$

If the exchange between the centers proceeds, on the average,  $n$  times during the polymerization, there will be on the average molecules which underwent growth  $n$  times in the first and  $n$  times in the second state. But there will be in the statistical ensemble chains which will stay  $n + 1$  interval in the first state and  $n - 1$  in the second, and correspondingly  $n + k$  and  $n - k$ .

The statistical distribution of chains between both different states of growth will correspond to Bernoulli's distribution of two alternative events, having the probabilities  $\alpha$  and  $1 - \alpha$ . The distribution, as well known, will be

$$W(n, k) = \frac{n!}{k!(n - k)!} \alpha^k (1 - \alpha)^{n - k}$$

This formula is precise, but for the sake of qualitative argument we approximate it by a Gaussian function, which in our particular case is a poor approximation.

After elementary transformations we get for the MWD a Gaussian distribution

$$dN/d\Delta M = (1/\sqrt{2\pi\xi^2})e^{-\Delta M^2/2\xi^2}$$

where  $\Delta M = M - \bar{M}$ . The dispersion of the distribution is approximately

$$\xi^2 = \overline{\Delta M^2} = \delta^2/n$$

where

$$dN/d\Delta M = (1/\sqrt{2\pi\delta^2/n})e^{-\Delta M^2/(2\delta^2/n)}$$

The average number of transitions is then

$$n = t/[\tau(1 + \alpha)]$$

Of course we can use a Gaussian function if the distribution is not too broad, i.e., the number of exchanges is not too small. In our case  $\bar{M}_w/\bar{M}_n$  is in the range 1.3–1.5. This gives

$$\bar{M}_w/\bar{M}_n = 1 + \overline{\Delta M^2}/\bar{M}^2 = 1 + (\delta^2/n)/\bar{M}^2 = 1.3\text{--}1.5$$

Actually we do not know the constants  $k_1$ ,  $k_2$ ,  $\alpha$ . Therefore we cannot calculate  $n$ . It is obvious, nonetheless, that  $n$  is of the order of a few units. Therefore the use of Gaussian distribution is not precise. It gives a simple qualitative outlook for the general picture, and we can use the precise Bernoulli function when needed.

An important consequence of the theory is the prediction that MWD must be broad at low times  $t$  or low conversions and becomes narrow if the time  $t$  increases very much. We have shown that this prediction is in agreement with experimental data (Fig. 2). It is a very specific statement. In all other cases of polymerization the MWD has a tendency to broaden when the reaction proceeds, which is just the opposite of the results observed.

### Summary

Polymerization of acrylonitrile (AN) initiated by  $\text{Bu}_3\text{Mg}_2\text{I}$  leads to polymers with broad MWD in contrast to the polymer obtained in the presence of  $\text{Bu}_2\text{Mg}$  or  $\text{BuMgCl}$ , which are characterized by extremely narrow distributions. It was shown that in this particular case different coexisting centers are initiating polymerization. A simple theoretical approach showed that the broadness of the MWD depends on the number of transitions between these active centers. Hence the MWD at low times and conversions must be the broadest. This prediction is in good agreement with the experimental results.

The able assistance of V. Shadrin is acknowledged.

### References

1. H. Hostalka, R. Figini, and G. V. Schulz, *Makromol. Chem.*, **71**, 198 (1964).
2. B. Erussalimsky, I. Kulevskaya, and V. Mazurek, paper presented at International Symposium on Macromolecules, Prague, 1965, Preprints, p. 126; *J. Polymer Sci.*, **16**, 1355 (1967).
3. I. Kulevskaya, B. Erussalimsky, and V. Mazurek, *Vysokomolekul. Soedin.*, **8**, 876 (1966).
4. B. Erussalimsky and I. Kulevskaya, *Vysokomolekul. Soedin.*, **7**, 2180 (1965).

Received July 25, 1966

## Investigation of the Change in the Fine Structure of *Valonia* Cellulose upon Wet Heating and Mercerization

SABURO OKAJIMA and AKIRA KAI, *Faculty of Technology,  
Tokyo Metropolitan University, Setagaya-ku, Tokyo, Japan*

### Synopsis

A *Valonia* cellulose (NV), a cellulose II derived from NV by mercerization (MV), and a cast cellulose II film (F) were deuterated repeatedly (wetting-drying cycle) in vapor phase at 25°C; the integrated deuteration time amounts to  $5 \times 10^5$  min. A region C, which cannot be attacked by the exchange reaction, exists in NV and MV, amounting to 80 and 18% in the respective samples. In the case of F, it could not be determined exactly due to the too large scattering of the data. On heating in liquid D<sub>2</sub>O for 5 or 10 min., OD groups develop within C above 190 and 170°C in NV and MV, respectively. Above 190°C the exchange is larger in NV than in MV. These OD groups within the pre-existing crystallites begin to disappear after treating with NaOH solution at the concentration at which cellulose begins to be converted to alkali cellulose I. The resistant OD groups developed within the amorphous and intermediate regions are rehydrogenated by the more dilute alkaline solutions.

### INTRODUCTION

Deuteration of cellulose fibers has been studied by many authors since 1934.<sup>1</sup> According to these studies,<sup>2</sup> deuteration is rapid at first but it soon slows down. This phenomenon has led to the application of deuteration to the quantitative determination of crystallinity, or, precisely speaking, accessibility. Mann and Marrinan<sup>3</sup> found that when a deuterated cellulose was dried, a part of the OD groups remains without being converted back to OH groups by rehydrogenation at room temperature, and they defined the remaining OD groups as resistant OD, or R-OD. Since then, such development of R-OD has been used for studying the change in the fine structure of cellulose<sup>4,5</sup> and poly(vinyl alcohol),<sup>6,7</sup> resulting in various treatments which may introduce so-called crystallization, provided that the deuteration and the rehydrogenation attack only the amorphous region but not the crystallites.

One of the present authors<sup>8</sup> has found that the crystalline region of regenerated cellulose can be deuterated readily at high temperatures. Jeffries,<sup>9</sup> Sepall and Mason,<sup>10</sup> and Wadehra and Manley<sup>11</sup> also reported that crystalline OH groups could be deuterated or tritiated gradually when deuteration or tritiation was continued for a very long time at room temper-

ature or also when a short time exchange reaction at room temperature was repeated many times.

Thus, it is not always correct to say that the entire amount of the R-OD developed equals the increment of crystallinity, especially when the treatment is carried out at high temperatures.<sup>12</sup>

In the present paper the authors distinguished the resistant OD within the pre-existing crystallites from that developed in the noncrystalline region and followed the change in the fine structure of *Valonia* cellulose during heat treatment in the presence of water.

## EXPERIMENTAL METHOD

### Sample

A sample of *Valonia macrophysa* of Japanese origin was used after purification<sup>13</sup> (NV). Then, part of it was converted to cellulose II by mercerizing (rolled with a fine mesh stainless steel gauge) with a 25% NaOH aqueous solution for about three months at 15°C (MV). The extremely high resistance of *Valonia* cellulose to mercerization has been reported already.<sup>13</sup>

A cellulose film regenerated from acetyl cellulose (F) was also used for the purpose of comparison with the above two samples. The method of preparation has been described in detail previously.<sup>12</sup>

### Deuteration

Film of NV, MV, and F, a few microns thick, whether the samples had sustained heat treatment or not, was mounted to a small glass ring, which was placed into an exactly fitting glass cell C (Fig. 1). Two glass or  $\text{CaF}_2$  windows were secured tightly to this cell with epoxy resin and the cell connected to a vacuum line at A and E. The air was pumped out first

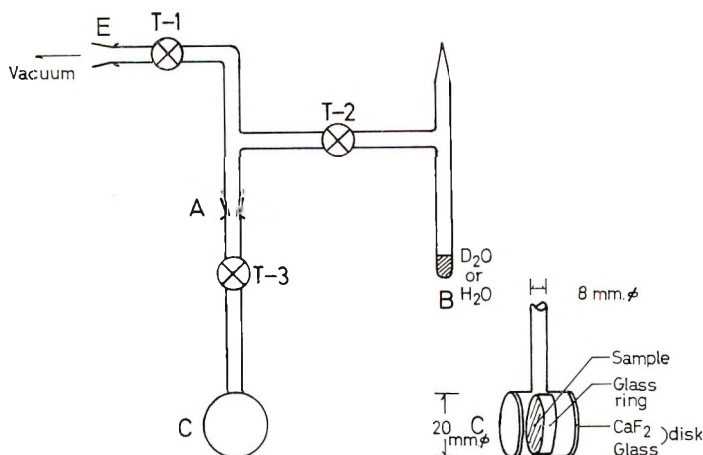


Fig. 1. Apparatus used for deuteration or rehydrogenation.

through the taps T-1 and T-2, with T-3 closed, until a small quantity of 99.7 mole-%  $D_2O$  which had been placed in B was frozen. Then the specimen was vacuum-dried ( $10^{-3}$  mm Hg, room temperature, 4 hr) by closing T-2 and opening T-1 and T-3.

Deuteration was conducted by closing T-1 and opening T-2 and T-3, causing  $D_2O$  vapor to come in contact with the specimen through T-2 and T-3. During the deuteration, the apparatus shown in Figure 1 was detached from the vacuum line at E and placed in an air thermostat controlled at  $25^\circ C$ . After deuteration was carried out for a programmed time, the specimen was vacuum-dried as before and the cell C was detached at A after closing T-3. The OD groups thus developed were determined by means of infrared spectrography.

The cell was attached to the line at A and E, and the operation described above was repeated again and again; the increase in OD groups was followed against the integrated time of deuteration  $t$ .

### Rehydrogenation

The specimens, which had been heat-treated with liquid  $D_2O$  as described below were rehydrogenated with  $H_2O$  vapor at  $25^\circ C$  repeatedly by using the same method as the vapor-phase deuteration, but with  $H_2O$  placed in the B portion of the apparatus instead of  $D_2O$ .

The deuteration or rehydrogenation was carried out repeatedly on the same specimen in order to minimize error.

### Determination of the Degrees of Deuteration and Rehydrogenation

The degree of deuteration or rehydrogenation was represented by the fraction of OH or OD groups relative to the total number of OH groups in the original untreated state. The determination of the amount of OD or OH groups was carried out by an infrared spectrographic method with the use of an EPI-II apparatus, double-beam type, constructed by Hitachi Ltd.

Mann and Marrinan's method was used for MV and F, while in the case of NV the residual OH fraction was evaluated from the residual absorbency of the OH band at  $3350\text{ cm}^{-1}$ , standardized by dividing by the absorbency of the CH band at near  $2900\text{ cm}^{-1}$ , relative to that of the original specimen. The amount of OD groups was given by 100 minus the per cent residual OH groups in %.

### Heat Treatment with Liquid $H_2O$ or $D_2O$

A specimen was heat-treated in a small autoclave with liquid  $H_2O$  or  $D_2O$  at  $170$ – $210^\circ C$ . for 5 or 10 min as already described previously.<sup>12</sup>

## RESULTS

### Deuteration at Room Temperature

Figure 2 indicates the change in the OH amount versus the logarithmic integrated time  $t$  during the vapor-phase deuteration of NV, MV, and F at

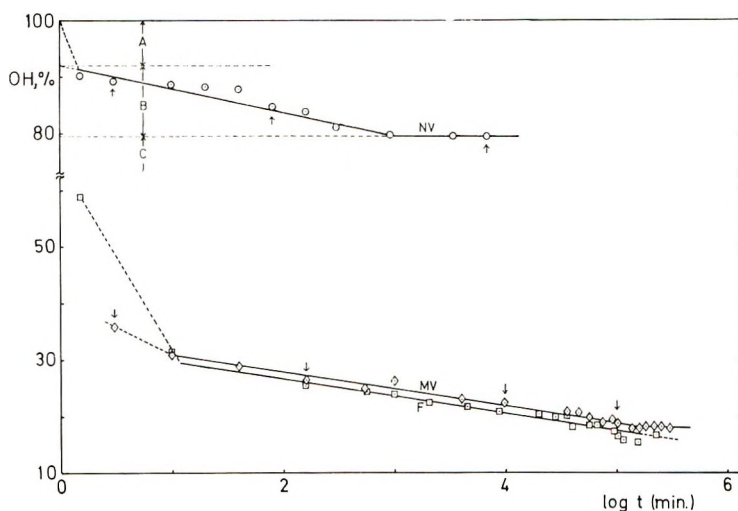


Fig. 2. Relation between the OH content and the integrated time  $t$ . (NV) *Valonia* cellulose; (MV) mercerized *Valonia* cellulose; (F) cast cellulose II film.

25°C. The deuteration of NV slows down after a rapid exchange reaction for 1–2 min, continues linearly until about  $10^3$  min and then terminates completely. From this process, NV can be divided into three regions. A, B, and C. The lateral order becomes higher from A to C, and A, B, and C correspond roughly to amorphous, intermediate, and crystalline regions, respectively. According to this definition, the crystalline region is completely resistant to the vapor-phase deuteration at room temperature.

The B fraction can be estimated by extrapolating the OH versus  $\log t$  line to  $\log t = 0$ . A is then  $100 - (B + C)$  %. In this evaluation it is assumed that the B region begins to be exchanged at  $t = 1$  min. This assumption is more or less arbitrary, so the separation of the regions A and B is less definite than that of B and C. The results obtained are summarized in Table I.

The deuteration process of MV or F resembles that of NV, except that the A fraction is extremely large and the C fraction very small in MV or F. In the case of F, the line denoting the B region is parallel and close to that denoting the B region of MV. This phenomenon suggests the very interesting fact that NV, having an extremely high crystalline and extraordinary stable texture, changes on mercerization to a less stable and less crystalline

TABLE I  
Fine Structures of *Valonia* Cellulose and Regenerated Cellulose Film

Sample	A, %	B, %	C, %
NV	8	12	80
MV	66	16	18
F	67	>16	<17

TABLE II  
Change in the Fine Structure of NV on Heat Treatment with Liquid D<sub>2</sub>O

Treating conditions		OD, %	(R-OD) <sub>1t</sub> , %	R-OD <sub>t</sub> , %	(R-OD) <sub>10t</sub> , %	$\frac{(R-OD)_i}{(R-OD)}$	A, %	B, %	C, %
Temp., °C	Time, min								
Control	—	20	—	—	—	—	8	12	80
170	5	20	0	5.5	5.5	0	6	8.5	85.5
170	10	20	0	18.5	18.5	0	—	1.5	98.5
190	5	21	1	18.5	17.5	0.054	—	2.5	97.5
190	10	24	4	21.4	17.4	0.19	0	2.6	97.4
210	10	30	10	25.7	15.7	0.39	0	4.3	95.7

texture akin to that of cast film, although it does not undergo dissolution. However, the exchange reaction of F seems to be still in progress, and the experimental error is too large to permit a conclusion regarding whether or not the C region exists in F. In the case of MV, the C region appears clearly, although it is only 18%.

The previously determined accessibility value for regenerated cellulose obtained by deuteration for 1–4 hr is about 70%, which accords numerically well with our A, plus a part of B for  $t = 1\text{--}4$  hr. However, adoption of 1–4 hr for  $t$  in the ordinary accessibility measurement seems to us to be arbitrary from the results shown above. The measurement is better obtained by plotting the per cent OH versus  $\log t$  and dividing the result into A, B, and C. But in this case, a part of the B must be considered to be crystalline from the viewpoint of x-ray data, although it is defined as intermediate here. This view agrees with the conclusion of Spedding and Warwick.<sup>14</sup> This contradiction is associated with the suggestion<sup>15</sup> that water can penetrate into the cellulose II crystal, although it does not penetrate into the cellulose I crystal. Therefore, it is considered that a distribution of order exists also in cellulose II crystals, in which the B region is the region of comparatively lower order while the C region is that of higher order. The former is likely of more or less paracrystalline nature.

There may be some contention that C is the cellulose I crystal remaining unmercerized because *Valonia* cellulose resists mercerization. But this is refuted by an infrared spectrograph of C which shows it to be typical of the cellulose II type, as indicated in Figure 8; then the B region of NV must be of different texture from that of MV or F. This point is further discussed below.

In the case of NV, there is no doubt concerning the deuteration time for accessibility measurement because the exchange reaction ceases after a comparatively short deuteration. Lang and Mason<sup>5</sup> reported 27% for the accessibility of their *Valonia* cellulose; this value is larger than that in Table II, but agrees rather well with the value (15–16%) obtained by Dechant<sup>16</sup> for a bacterial cellulose.

### Change in the Fine Structure of NV by Heat Treatment

Even when NV is deuterated with liquid phase D<sub>2</sub>O at 170°C for 5 or 10 min, the ultimate OD content does not increase above 20% (the value of A + B of the original sample), but it increases gradually when the deuteration temperature is elevated above 190°C (Table II). These OD groups in excess of 20% are considered to exist in the C region. So this is designated by (R-OD)<sub>i</sub> in Table II, which is 1–10% of the total OH, depending on the condition of treatment.

When the NV deuterated at high temperature is rehydrogenated at 25°C, OD decreases with increasing  $t$ , just as OH in the deuteration process, but some fraction of OD remains unhydrogenated (Fig. 3); this is the resistant OD, R-OD, which increases also with the temperature and time of deuteration.

This R-OD is composed of  $(R-OD)_i$  and  $(R-OD)_o$ , the latter being resistant OD developed outside the pre-existing crystallites, i.e., within the A and B regions, but predominantly in B. This  $(R-OD)_o$  is the very inaccessible part, newly developed during the heat treatment, which contributes to the improvement of the swelling property of rayon.<sup>17</sup>

The amount of A and B obtained from Figure 3 is listed in Table II. A decreases in amount more rapidly than does B, while C increases to  $80 + (R-OD)_o$ .

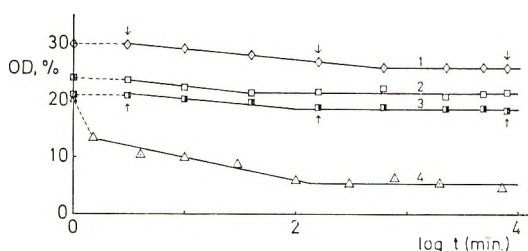


Fig. 3. Rehydrogenation of NV deuterated at high temperature. (1) deuteration at 210°C, 10 min; (2) 190°C, 10 min; (3) 190°C, 5 min; (4) 170°C, 5 min. The relation for 170°C, 10 min coincides closely with (3) and is omitted from the figure.

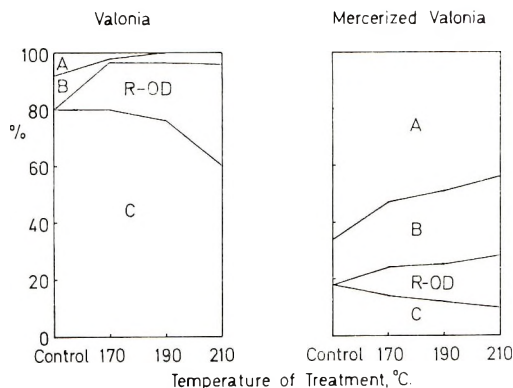


Fig. 4. Change in the A, B, and C fractions and the resistant OD distribution after the deuteration at high temperature.

These changes in the fine structure are more clearly shown in Figure 4; the resistant OD develops more readily in the intermediate region than in the crystallites, possibly because the crystalline region is most highly ordered and most strongly hydrogen bonded. The  $(R-OD)_o$  can be observed after the 170°C treatment, however,  $(R-OD)_i$  is not yet detectable.

As to the B region, the slope of the rehydrogenation line is less steep compared with the deuteration line, especially when the temperature of treatment is elevated above 190°C, so the B region must change in order as well as in amount.

### Change in the Fine Structure of MV by Heat Treatment

When MV which has been treated with liquid  $\text{H}_2\text{O}$  at  $170\text{--}190^\circ\text{C}$  for 5 or 10 min is deuterated with  $\text{D}_2\text{O}$  vapor at  $25^\circ\text{C}$ , OH is exchanged (Fig. 5), and A, B, and C can be evaluated in a similar way as in Table II. The results are shown in Table III.

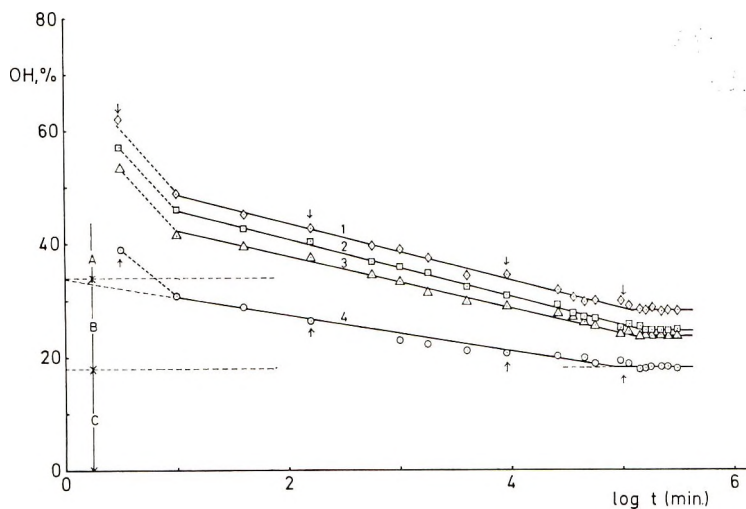


Fig. 5. Change in OH content during the vapor-phase deuteration of the MV treated at high temperature ( $\text{H}_2\text{O}$  liquid, 5 min): (1)  $210^\circ\text{C}$ ; (2)  $190^\circ\text{C}$ ; (3)  $170^\circ\text{C}$ .

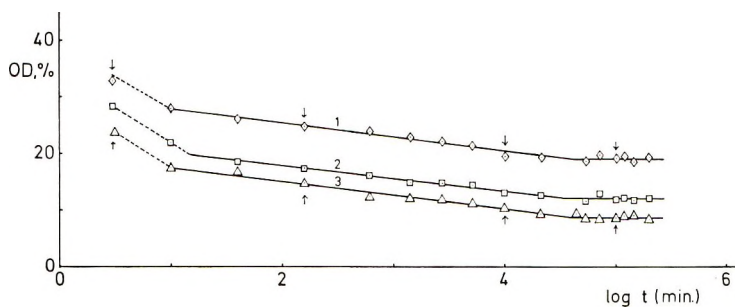


Fig. 6. Rehydrogenation of the MV deuterated at high temperature for 5 min: (1)  $210^\circ\text{C}$ ; (2)  $190^\circ\text{C}$ ; (3)  $170^\circ\text{C}$ .

It can be seen that OH resisting deuteration, so-called resistant OH, R-OH, develops and increases as the heating condition becomes severe. Of course the newly developed R-OH is generated outside the pre-existing crystallites. Hence, R-OH in excess of the C amount of the untreated sample is to be defined by  $(\text{R-OH})_o$ .

This  $(\text{R-OH})_o$  is smaller than the R-OD when the sample is heated with liquid  $\text{D}_2\text{O}$  under the same conditions (Fig. 6), because the latter is composed of  $(\text{R-OD})_i$  and  $(\text{R-OD})_o$ , and the  $(\text{R-OD})_o$  must be equal in amount

TABLE III  
Change in the Fine Structure of MV on Treatment with Liquid H<sub>2</sub>O

Treating conditions		Time, min	R-OH, %	R-OD, %	(R-OH) <sub>m</sub> , %	(R-OD) <sub>s</sub> , %	(R-OD) <sub>liq</sub> , %	$\frac{(\text{R-OD})_i}{(\text{R-OD})_{\text{liq}}}$	A, %	B, %	C, %
Temp., °C											
Control	—	—	18	18	—	—	—	—	66.5	15.5	18
170	5	5	24	8.5	6.0	2.5	14	0.18	53	23	24
190	5	5	24.5	12	6.5	5.5	16.5	0.33	49	26.5	24.5
210	5	5	28	19	10	9	24	0.38	46	26	28

to  $(\text{R-OH})_o$ . Therefore  $(\text{R-OD})_i$  can be obtained by subtracting  $(\text{R-OH})_o$  from  $\text{R-OD}$ . These results are shown in Figure 4 in comparison with those for NV. The trends of both samples are similar, but  $(\text{R-OD})_i$  is larger and  $(\text{R-OD})_o$  is smaller in MV than in NV.

### Change in the Infrared Spectra Features of the OH and OD Bands during Deuteration and Rehydrogenation

Some examples of the OH and OD bands of typical specimens for the above deuteration and rehydrogenations are shown in Figures 7*a*–7*c* and 8*a*–8*d*. The number between a pair of OH and OD bands denotes the deuteration or rehydrogenation time  $t$  of that specimen, which is indicated by an arrow on the corresponding degree of exchange versus  $\log t$  plot in Figure 2, 3, 5, or 6.

Figure 7*a* shows the change during the vapor-phase deuteration at room temperature of NV, according to which the OH and OD bands are crystalline and amorphous types, respectively, and the types are not affected by the degree of exchange. Under these conditions the C region is not exchanged, so the B region of NV seems not to contain any regularly ordered texture from the viewpoint of the infrared spectra. The barely detectable effect of the degree of exchange upon the OH band is due to the very small quantity of B compared with C.

When NV is deuterated with liquid  $\text{D}_2\text{O}$  at  $170^\circ\text{C}$  for 10 min, however, the OD band indicates slightly crystalline feature, i.e., two peaks of different hydrogen-bonding strengths<sup>18–21</sup> are resolved (Fig. 7*b*,  $t = 0$ ), although the degree of exchange is equal to that of the specimen of  $t = 5400$  min in Figure 7*a*. This is because the order of the A and B regions of the untreated NV has been improved by the wet heating at  $170^\circ\text{C}$ . This trend is more marked when the deuteration is carried out at  $210^\circ\text{C}$  for 10 min (Fig. 7*c*,  $t = 0$ ). This is due to the additional effect of deuteration of a part of the OH in the pre-existing C region, in addition to the further improvement of order by the wet heating at higher temperature. This is in accordance with the less steep slope of the rehydrogenation curve of the sample which has been deuterated at  $210^\circ\text{C}$  compared to that of the untreated sample or the one deuterated at  $170^\circ\text{C}$  for 5 min. (Fig. 3).

Even though these specimens deuterated at high temperature are rehydrogenated; the features of the OH and OD bands change very slightly, because only a small fraction of the OH groups can be rehydrogenated and most of the OD groups remain as  $\text{R-OD}$ . It is noteworthy that the OH spectra of the C region (Fig. 7*a*,  $t = 5400$  min; Figs. 7*b* and 7*c*,  $t = 0$ ) become more sharply resolvable as the deuteration temperature is elevated, because of the improvement of the order of the C region.

In the case of MV, the vapor-phase deuteration brings about comparatively marked changes in the infrared spectrum of the residual OH, i.e., a well-known diffuse band at  $t = 0$  separates into four small bands assigned to the intra- and intermolecular hydrogen-bonding OH stretchings of different strengths and their resolution becomes sharper with increase in  $t$  and at the

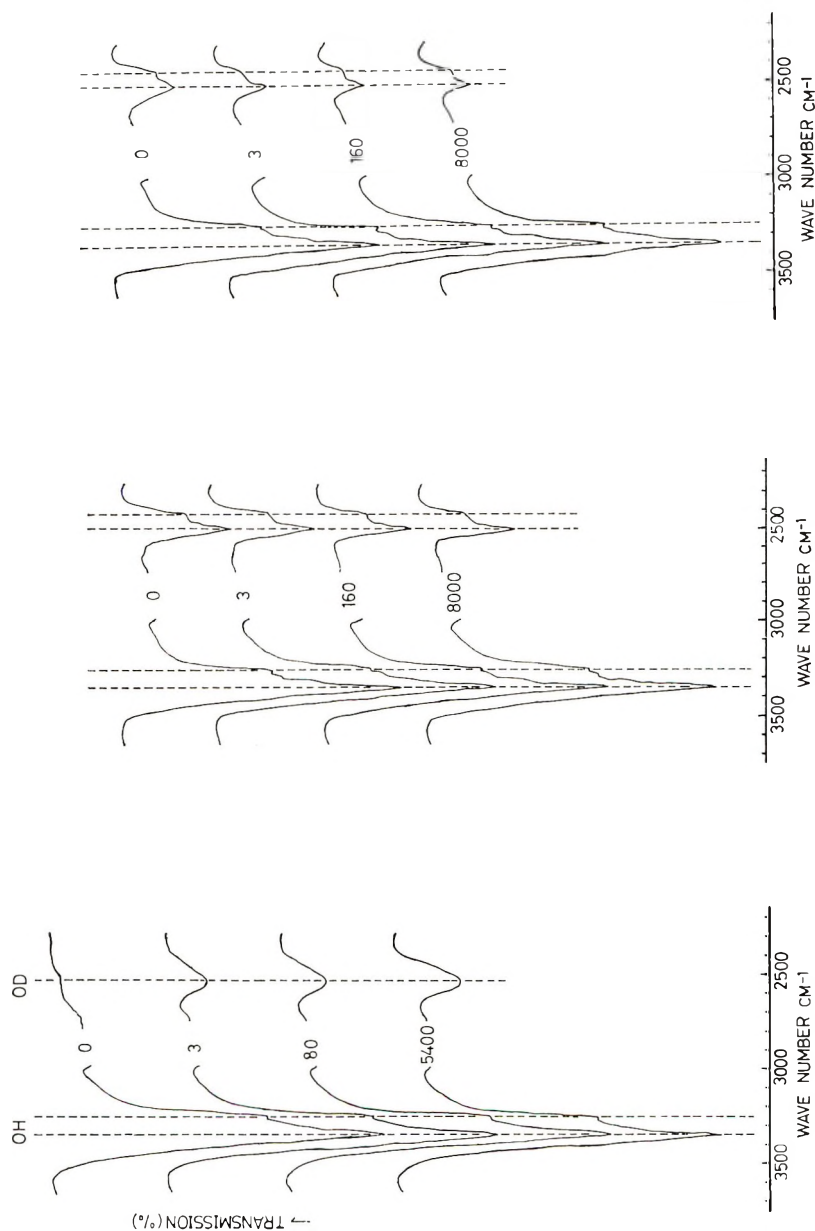
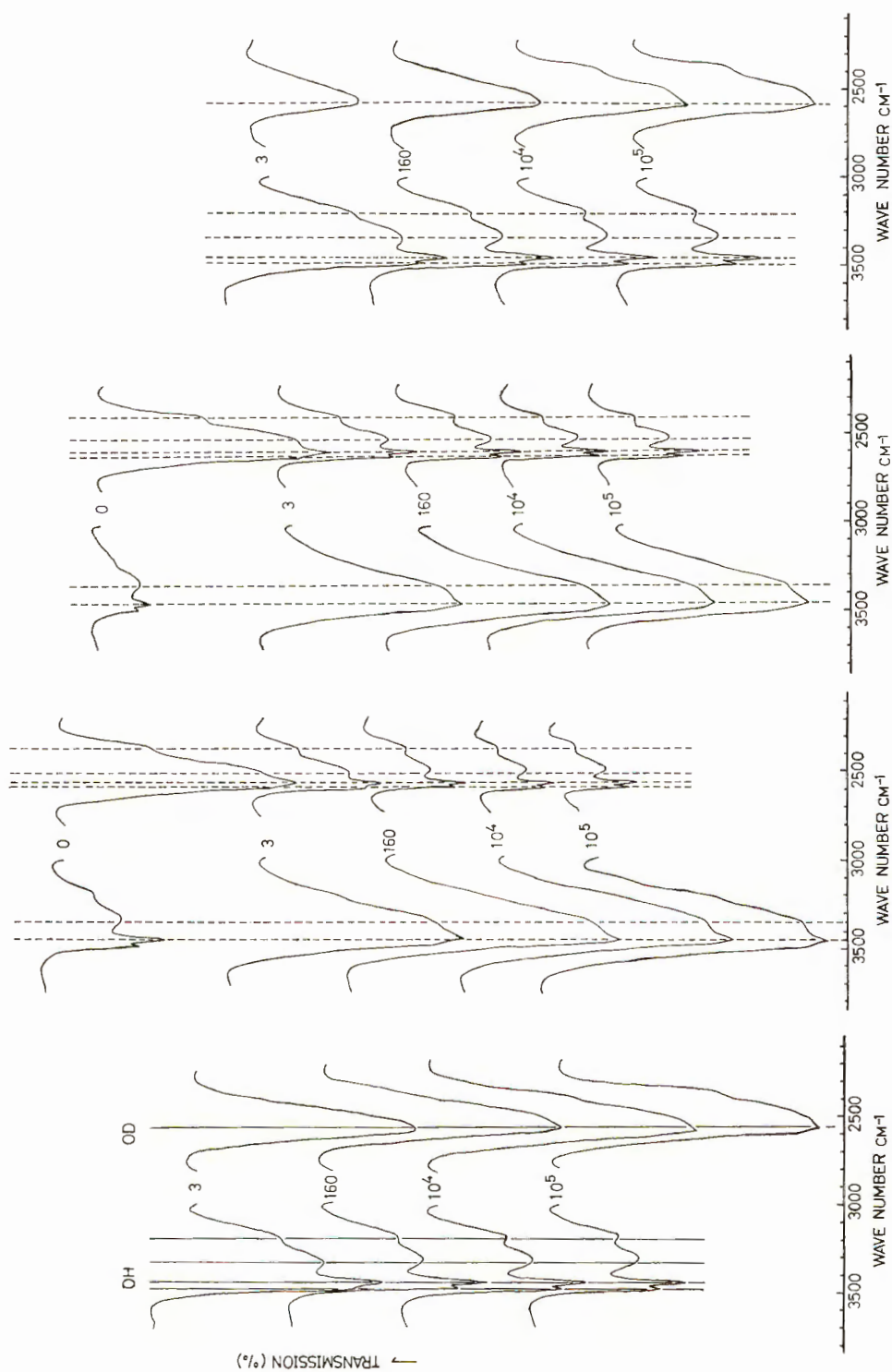


Fig. 7. Infrared spectra of (a) NV deuterated for various times with vapor phase  $D_2O$  at  $25^\circ C$ , where the number between a pair of OH and OD bands indicates the value of  $t$  in minutes; (b) NV deuterated with liquid  $D_2O$  at  $170^\circ C$  for 10 min, followed by the rehydrogenation for 0, 3, 160, and 8000 min; (c) NV deuterated with liquid  $D_2O$  at  $210^\circ C$  for 10 min, followed by rehydrogenation for 0, 3, 160, and 8000 min.



same time, very interestingly, the two intermolecular bands<sup>18,19,22</sup> (3100–3400  $\text{cm}^{-1}$ ) shift slightly toward low frequency, as indicated in Figure 8a.

The OD band too is at first diffuse, but as the B is deuterated progressively the band begins to show two shoulders. This is an indication of the paracrystalline nature of B as described already. When the deuteration is carried out at 170 or 210°C, an increased fraction of C is also deuterated and, hence, the OD band sharpens gradually and indicates two shoulders in the range of 2300–2500  $\text{cm}^{-1}$ , corresponding to the intermolecular OD stretchings (Fig. 8a,  $t = 10^5$  min; Figs. 8b and 8c,  $t = 0$ ).

The fine structure of the OD band becomes progressively sharper as the successive rehydrogenation proceeds and the intermolecular OD bands also shift gradually toward low frequency. These changes are in good correspondence to those of the OH bands observed in Figure 8a.

Such phenomena suggest that the C of NV is highly crystalline with a sharp distribution of lateral order. But when it is converted into MV, the order lowers and its distribution broadens considerably, even within the C region. Therefore the exchange reaction proceeds more readily in the less ordered region, and the strength of the intermolecular hydrogen-bonding of the residual OH or OD increases gradually.

Figure 8d shows the infrared spectra of deuterated MV which has been heated with liquid  $\text{H}_2\text{O}$  at 210°C for 5 min (Fig. 5, curve 1). The change in feature of the OH or OD after various degrees of vapor-phase deuteration is exactly like that shown in Figure 8a, although the degree of deuteration is considerably smaller in Figure 8d than in Figure 8a at equal value of  $t$ . This is illustrated by the improvement of lateral order of the B region resulting from the wet heating.

## DISCUSSION

According to the literature, a section of a microfibril of *Valonia* cellulose is about  $200 \times 100 \text{ \AA}$ <sup>23,24</sup> and thicker than that of ramie, cotton, or wood pulp. If the *Valonia* cell wall is composed of these microfibrils and the A region corresponds to the outwardly protruding OH groups of the cellulose molecules composing the surface layer of each microfibril, the amount of these OH groups can be estimated from the above dimension of the microfibril and lattice spacing of cellulose I to be 7% of the total OH groups. This is in good coincidence with the observed value of 8% in Table II.

If the residual OH of the surface layer molecules, as well as the outwardly protruding OH groups from the secondary layer molecules, contribute to the B region, the amount of B must be 14%, which is nearly equal to the

---

Fig. 8. Infrared spectra of MV deuterated: (a) with vapor-phase  $\text{D}_2\text{O}$  at 25°C for 3, 160,  $10^3$ , and  $10^5$  min; (b) deuterated with liquid  $\text{D}_2\text{O}$  at 170°C for 5 min, followed by rehydrogenation for 0, 3, 160,  $10^3$ , and  $10^5$  min; (c) deuterated with liquid  $\text{D}_2\text{O}$  at 210°C for 5 min, followed by rehydrogenation for 0, 3, 160,  $10^3$ , and  $10^5$  min; (d) heated with liquid  $\text{H}_2\text{O}$  at 210°C for 5 min, followed by deuteration for 3, 160,  $10^3$ , and  $10^5$  min.

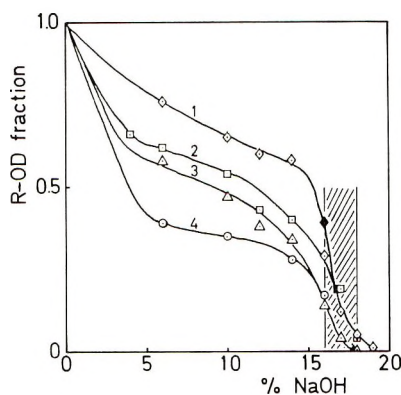


Fig. 9. Change in R-OD in the NV deuterated at high temperature after treating with NaOH solution of various concentrations at 20°C.: (1) deuteration (10 min) at 210°C; (2) 190°C; (3) 170°C; (4) 150°C. Solid points are the calculated values of  $(R-OD)_i/(R-OD)$ . The hatched portion is the lowest range of NaOH concentration necessary for mercerization of NV.

observed value, 12%. The remaining OH groups belong to the C region.

The  $(R-OD)_o$  of the NV generated during the heat treatment amounts ultimately to 16–18% of the entire amount of OH, i.e., 80–90% of the OH belonging to A and B. It is considered, therefore, that a microfibril of NV is a crystalline string whose surface layer is composed of more or less disordered molecules. Thus, the deuteration of OH at room temperature can occur only on the surface (A region) and between the first (surface) and the second layer molecules (B region) of each microfibril. The heat treatment not only improves the order of the surface layer but also rebuilds more intense hydrogen bridges between the first and second layers, resulting in the conversion of a larger part of A and B into C. But the following observation shows that this newly generated C is still less ordered than the previously existing crystallites.

As is readily expected, resistant OD can be rehydrogenated progressively when a deuterated cellulose is swollen by a caustic alkaline solution of increasing concentration. In the case of deuterated NV, a 17–19% NaOH solution is necessary to rehydrogenate all of the R-OD as shown in Figure 9. Figure 9 indicates that the residual fraction of R-OD of a deuterated NV is a function of NaOH concentration. When it is considered that mercerization of cotton or ramie can be completed by 11–16% of NaOH solution at 20°C, the order of this last trace of R-OD (i.e., the specimen treated at 210°C) is surprisingly high, because it is contained within the crystalline phase of the *Valonia* cellulose having an extraordinary high resistance to mercerization.<sup>13</sup> The crystalline phase of NV is so stable that the heat-treated NV cannot be mercerized considerably by solutions less than 16% NaOH. So the R-OD disappearing on treatment with NaOH solutions less than 16% can be called  $(R-OD)_o$  and that still remaining can be called  $(R-OD)_i$ . The ratios of  $(R-OD)_i$  to  $(R-OD)$  of the treated NV at 170, 190, and 210°C

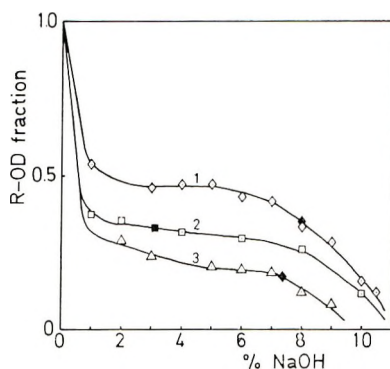


Fig. 10. Change in R-OD in MV deuterated at high temperature after treating with NaOH solution of various concentrations at 20°C.: (1) deuteration temperature (5 min) 210°C; (2) 190°C; (3) 170°C. Solid points are the calculated values of  $(R-OD)_i / (R-OD)_{liq}$ . The hatched portion is the lowest range of NaOH concentration necessary for conversion of cellulose II into alkali cellulose I.

are calculated to be 0, 0.19, and 0.39, respectively, as shown in Table II. When these values are plotted on the corresponding curves in Figure 9, they fall within an NaOH concentration range of 15.5–17%. This is in very good accordance with the results. So the heat treatment is considered to have little effect on the crystalline phase of NV, i.e., it does not accelerate growth of crystallites in size or number. It probably contributes only to the packing of the A and B regions. This is reasonable from the texture of *Valonia* cellulose discussed above.

Figure 10 shows the effect of similar treatment of MV, where the fractional R-OD on each curve is expressed in relation to the OD remaining after immersion of the corresponding sample in water at 25°C for 3 hr. The latter value is not equal to the R-OD defined in this paper, so it is designated  $(R-OD)_{liq}$ . According to the preliminary tests,  $(R-OD)_{liq}$  is nearly equal to the residual OD after 6 hr rehydrogenation with  $H_2O$  vapor, as shown in Table IV.

TABLE IV  
Comparison Between the Rates of Exchange Reactions  
in the Liquid and Vapor Phases ( $H_2O$  or  $D_2O$ )

	OH, %			OD, %		
	Ex- change 120 min	Ex- change 240 min	Ex- change 360 min	Ex- change 180 min	Ex- change 300 min	Ex- change 747 min
Liquid phase	32.4	29.8	28.5	7.6	—	—
Vapor phase	37.0	32.2	30.7	—	8.0	7.8

When the  $(R-OD)_{liq}$  is obtained by interpolation in Figure 6 and the ratio of  $(R-OD)_i$  to  $(R-OD)_{liq}$  is plotted on the corresponding curve, the

solid points, except for one, fall within a range of NaOH concentration of 7–8%. This exception cannot be explained at present; it may be due to error. Taking into consideration the fact<sup>25</sup> that cellulose II begins to be converted to alkali cellulose I in nearly the same NaOH concentration range as cellulose I (ordinary cellulosic material) does, the above alkaline concentration (7–8%) corresponds to the starting range of conversion from cellulose II to alkali cellulose I. This is an evidence for the existence of (R-OD)<sub>i</sub> in the preexisting crystallites of cellulose II, similarly as in cellulose I.

Finally, we will touch on the mechanism of deuteration, which has not yet been illustrated clearly. The OH of the A region is considered to be deuterated directly by exchanging with diffused D<sub>2</sub>O molecules, but for the B and C regions it is not clear. The observed relation between the amount of OD (OH) and the logarithmic integrated time  $t$  argues against a predominant role of the diffusion of D<sub>2</sub>O (H<sub>2</sub>O) molecules in the B region. If cellulose film is dried completely before the  $n$ th deuteration (rehydrogenation) it cannot be shown that a change in OD (OH) is observed immediately after the beginning of the  $n$ th operation. The  $n$ th deuteration (rehydrogenation) would not begin until the D<sub>2</sub>O (H<sub>2</sub>O) molecules diffused from the surface and reached the front of the deuterated (rehydrogenated) layer and a long time would elapse. Such diffusion does not, however, actually occur, and therefore the successive exchange between cellulose OD and cellulose OH may be more probable. In order to discuss this concept more definitely further evidence is necessary, especially with regard to the last stage of desorption of water, which must be studied in greater detail. Irrespective of these mechanisms, the rate of deuteration or rehydrogenation is a function of order, i.e., the intensity of the cohesive force, the hydrogen bonding, of the region.

The authors wish to thank Mr. K. Takahashi for help in a part of the work on sample F. The expenses of this research were defrayed by a Scientific Research Encouragement Grant from the Ministry of Education, to which thanks are also due.

## References

1. K. F. Bonhoeffer, *Z. Elektrochem.*, **40**, 469 (1934).
2. J. V. Frilette, J. Haule, and H. Mark, *J. Amer. Chem. Soc.*, **70**, 1107 (1948).
3. J. Mann and H. J. Marrinan, *Trans. Faraday Soc.*, **52**, 481, 487, 492 (1956).
4. H. Sobue and S. Fukuhara, *Kogyo Kagaku Zasshi*, **63**, 520, 1059 (1960).
5. A. R. Lang and S. G. Mason, *Can. J. Chem.*, **38**, 373 (1960).
6. N. Takahashi, K. Onozato, and S. Okajima, *Nippon Kagaku Zasshi*, **78**, 767 (1957).
7. N. Takahashi, S. Okajima, and K. Onozato, *Kogyo Kagaku Zasshi*, **60**, 1193 (1957).
8. S. Okajima and K. Inoue, *J. Polym. Sci. B*, **1**, 513 (1963).
9. R. Jeffries, *Polymer*, **4**, 375 (1963).
10. O. Sepall and S. G. Mason, *Can. J. Chem.*, **39**, 1934, 1944 (1961).
11. J. L. Wadehra and R. St. John Manley, *J. Appl. Polym. Sci.*, **9**, 3499 (1965).
12. S. Okajima and K. Inoue, *J. Polym. Sci. A*, **2**, 461 (1964).
13. S. Okajima and A. Kai, *J. Appl. Polym. Sci.*, **11**, 289 (1967).

14. H. Spedding and J. O. Warwick, *J. Polym. Sci. A*, **2**, 3933 (1964).
15. P. H. Hermans, *Physics and Chemistry of Cellulose Fibers*, Elsevier, New York, 1949.
16. J. Dechant, *Faserforsch. u. Textiltechn.*, **18**, 239 (1967).
17. S. Okajima, K. Inoue, M. Yazawa, and Y. Kuwazuka, *Textile Res. J.*, **32**, 843 (1962).
18. M. Tsuboi, *J. Polym. Sci.*, **25**, 159 (1957).
19. J. Mann and H. J. Marrinan, *J. Polym. Sci.*, **32**, 357 (1958).
20. C. Y. Liang and R. H. Marchessault, *J. Polym. Sci.*, **37**, 385 (1959).
21. A. J. Pennings, W. Prins, R. D. Hale, and B. G. Rånby, *J. Appl. Polym. Sci.*, **5**, 676 (1961).
22. R. Jeffries, *Polymer*, **4**, 375 (1963).
23. R. D. Preston, *Discussions Faraday Soc.*, **11**, 165 (1951).
24. R. St. John Manley, *Nature*, **204**, 1155 (1964).
25. W. Schramek, *Kolloid-Beih.*, **40**, 87 (1934); **42**, 306 (1935).

Received January 5, 1968

Revised February 26, 1968

# Molecular Structure of Synthetic Rubber.

## I. Light-Scattering Properties of Styrene-Butadiene Copolymers\*

WILLIAM S. BAHARY and LEWIS BSHARAH,†  
*Texas-U. S. Chemical Company, TEXUS Research Center,  
 Parsippany, New Jersey*

### Synopsis

The discrepancy between the values reported for the weight-average molecular weight and molecular weight distribution of cold-type styrene-butadiene rubber is examined. The results obtained indicate that aggregation of the rubber due to hydrogen bonding or cluster formation is not a contributing factor to the high weight-average molecular weights obtained. The very broad molecular weight distributions, the  $\bar{M}_w/\bar{M}_n$  of the order of 10-20, are attributable to the presence of a few per cent of very high molecular weight fraction microgel in samples polymerized to moderate conversions. This microgel has been removed to various degrees by several methods: (1) mastication, (2) treatment with  $\text{CaSO}_4$ , (3) ultracentrifugation, and (4) ultrafiltration. The nature of this microgel is examined in terms of its light-scattering property, intrinsic viscosity, and concentrated solution viscosity. The weight-average molecular weight obtained by light scattering on these samples after removal of microgel are lower by as much as an order of magnitude. The operational definition of the weight-average molecular weight,  $\bar{M}'_w$ , is therefore introduced, corresponding to the one obtained after removal of the microgel. It is suggested that the actual and the operational weight-average molecular weights be used in conjunction in the characterization of these copolymers.

### INTRODUCTION

A discrepancy exists in the literature concerning the weight-average molecular weight and the molecular weight distribution of cold-type styrene-butadiene rubber (SBR). Booth and Beason<sup>1</sup> report a value of 280000 for the weight-average molecular weight and 3.45 for the breadth of the molecular weight distribution,  $\bar{M}_w/\bar{M}_n$ , in good agreement with the values calculated from their kinetic distribution curves. On the other hand, Cooper and co-workers<sup>2</sup> report values in the range of 800000 to 1.7 million with  $\bar{M}_w/\bar{M}_n$  in the range of 7-14 obtained from osmometry and light scattering. These same authors get a value of 2.3-2.5 for  $\bar{M}_w/\bar{M}_n$  using their fractionation data. Experiments performed in our laboratory confirm the variable results obtained by Cooper, and there is good reason to believe

\* Presented at the 147th American Chemical Society Meeting, Philadelphia, Pennsylvania, April 1964.

† Present address: Petrolite Corp., St. Louis, Mo.

that the observed discrepancies are due to the presence of a small fraction of highly branched high molecular weight polymer, or microgel. It is therefore of practical and theoretical interest to determine the nature of the microgel observed in cold-type SBR and to throw some light on the true molecular weight distribution of these types of polymers. To this end, these studies have been undertaken.

## EXPERIMENTAL

### Light Scattering

Light-scattering experiments were performed with the Brice-Phoenix Universal light-scattering photometer at a wavelength of 546 m $\mu$ . The calibration constants for the instrument were checked with a sample of Cornell Standard Polystyrene (Styron 60); turbidity, observed,  $1.15 \times 10^{-3} \text{ cm}^{-1}$ ; expected  $1.18 \times 10^{-3} \text{ cm}^{-1}$  at wavelength of 546 m $\mu$ . The weight-average molecular weight of another sample of Cornell Standard Polystyrene was found to be  $5.4 \times 10^5$ ; expected,  $5.05 \times 10^5$  which is within the 10% experimental accuracy expected in light scattering. The molecular weights were determined by the method of Zimm plots<sup>3</sup> and a program was written to perform most of the calculations on a 1620 IBM computer. The solutions were successively filtered through 1.2, 0.3, and 0.22  $\mu$  pore size Millipore filters under pressure and then were filtered directly into the cell by use of a syringe with 0.45  $\mu$  pore size Millipore filter and filter holder unless specified otherwise. Schleicher & Schuell type O-coarse filters were used with those polar solvents which affected the Millipore filters. The standard solvent chosen for most of this work was carbon tetrachloride on account of its low scatter and the relatively high value of the refraction index differential for SBR,  $dn/dc = 0.995 \text{ ml/g}$  at  $\lambda = 546 \text{ m}\mu$ . No antioxidant in addition to that in the sample was added, after preliminary experiments showed that the copolymer was adequately protected if the sample was dissolved overnight and the experiments run the next day. The corrections for depolarization and fluorescence were found to be a few per cent and were not applied.

### Osmometry

A high-speed Mechrolab osmometer, Model 501, was used to determine the number-average molecular weight. A 1% solution of a sample in toluene was precipitated from four times its volume of methanol, dried in a vacuum oven at room temperature, redissolved in toluene, and run the same day. The membrane employed was number 300 gel cellophane. The operation of the instrument was checked with a sample of polystyrene 705 obtained from the National Bureau of Standards:  $\bar{M}_n$  (observed), = 160000;  $\bar{M}_n$  (expected) = 170000.

### Viscometry

Ubbelohde viscometers were employed with toluene at  $30 \pm 0.01^\circ\text{C}$ . The intrinsic viscosities were calculated by use of the usual extrapolation

methods. Concentrated solution viscosities were determined at 25°C with a Brookfield viscometer, Model RVF. Solvent corrections were applied in all cases.

### Mastication and Ultracentrifugation

Mastication was done on an 8-in. standard two-roll mill at room temperature. About 50-g samples were passed ten times through the mill at the openings described below without allowing the sample to band on the rollers. The mill masticated samples were analyzed at once, and no sample was employed if it had aged more than 24 hr after plasticization due to the crosslinking tendency of the rubber. Ultracentrifugation was performed on the Beckman Model L preparative ultracentrifuge using 0.5% SBR solutions in carbon tetrachloride at 60000*g* for 3 hr at room temperature, and the top fractions were withdrawn for analysis. Since this was the maximum safe speed recommended, further experiments at higher rates of rotation were not attempted.

### CaSO<sub>4</sub> Treatment

The CaSO<sub>4</sub> treatment consisted in shaking a 0.5% solution of the SBR in CCl<sub>4</sub> with 1 g of the anhydrous reagent-grade powdered salt since treatment with greater amounts did not further decrease the weight average molecular weight.

### Materials and Solvents

Reagent grade solvents were used without further purification, except for the dioxane which was stored over sodium wire for a minimum of one week and distilled in the presence of metallic sodium immediately before use. The samples employed were fresh commercial samples of SBR prepared by Texas-U. S. Chemical Company. Samples 102 and 110 were cold SBR type 1502,<sup>4a</sup> emulsion polymerized at 5°C; sample 115 was a standard hot 50°C emulsion polymer,<sup>4b</sup> and sample 116 was a hot polymer obtained by blending low and high conversion lattices. Some pertinent properties of the samples examined are given in Table I.

TABLE I

Sample	ETA, %	[ $\eta$ ], dl/g
102	8.7	2.20
110	6.4	2.00
115	5.3	1.99
116	5.8	2.11

The per cent ETA in column 2 of Table I is based on the rubber-extractable material in a 70/30 ethanol-toluene azeotrope and consists primarily of the rosin acids and antioxidant in the samples. None of the samples contained any gel. Both in intrinsic viscosity and light-scattering

experiments the concentration was determined by taking the dry weight of the solution and correcting for the per cent ETA. Most of the experiments were performed on the cold-type samples 102 and 110, and samples 115 and 116 were used to confirm some of the results.

## RESULTS

The first problem examined in running light-scattering experiments on SBR was compositional heterogeneity.<sup>5</sup> Several authors,<sup>6,7</sup> including Benoit and co-workers,<sup>8,9</sup> have shown the variations in the apparent weight-average molecular weight of copolymers arising from compositional heterogeneities. However, in the case of the samples of this study analysis of fractionated SBR showed only a 2% variation in styrene content. This change is within experimental error so that this source of difficulty was ruled out.

The variability in the light-scattering properties of SBR due to filtration is exemplified in Table II, where the weight-average molecular weight and  $z$ -average root-mean-square end-to-end distance of the polymer,  $(\overline{r_z^2})^{1/2}$ , are shown to drop rapidly with decreasing pore size.

TABLE II  
Effect of Pore Size of Filter on  $\overline{M}_w$  of SBR Sample 102

Pore size, $\mu$	Residue, %	$\overline{M}_w \times 10^{-5}$	$(\overline{r_z^2})^{1/2}$ , Å
3.00	0.0	32.0	5300
1.20	4.3	13.0	3030
0.45	6.2	7.1	820

The per cent residue in the second column of Table I is the incremental amount of high molecular weight polymer retained on the filter. A typical Zimm plot for the case where a 3- $\mu$  pore size filter was employed is given in Figure 1. The variability in  $\overline{M}_w$  with the pore size of the filter employed, the high scattering at low angles, and the change in the interaction constant  $A_2$  with angle of observation indicate the presence of microgel in the samples of cold SBR studied.

The nature of the microgel was examined by light-scattering experiments performed in polar solvents, dioxane and pentanone, and also on acetylated rubber. These experiments did not show any significant drop in  $\overline{M}_w$ , indicating that the microgel is not a loose aggregate of partially oxidized hydrogen bonded molecules.<sup>10</sup> Further determinations at elevated temperatures did not show a drop in  $\overline{M}_w$ , so cluster formation in these samples was ruled out.<sup>11</sup>

The effect on the weight-average molecular weight of heating and aging a solution of sample 110 in dioxane is shown in Figure 2. The solutions were heated to 70°C for 2 hr in the early part of the experiment to accelerate the degradation although the scattering experiments were performed at

room temperatures. The drop in  $\bar{M}_w$  from 600 000 to 90 000 indicates the polymer as well as the microgel is degraded by the free radicals generated in the dioxane solution, whereas no such drop in the weight-average molecular weight is observed when 0.2% tris(nonyl phenyl) phosphite antioxidant (Polygard) is added to the dioxane.

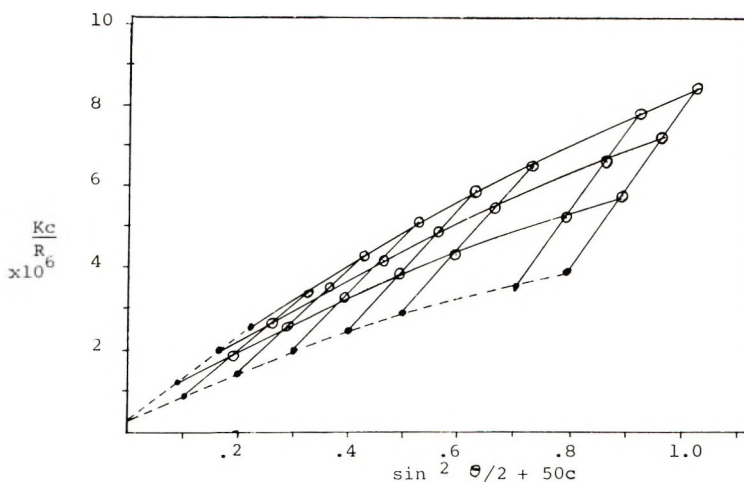


Fig. 1. Zimm plot of SBR sample 102.

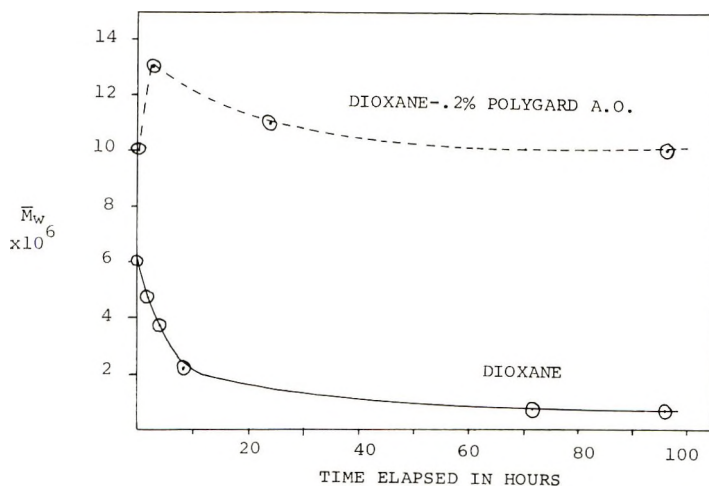


Fig. 2. Effect on  $\bar{M}_w$  of aging SBR sample 102 in dioxane solutions.

Since microgel is not a loose aggregate but copolymer which is degradable in dioxane under conditions which degrade the bulk of the rubber molecules as well, it is concluded that the microgel is polymer crosslinked by primary bonds. If microgel particles are formed by molecular entanglements, these entanglements are not resolvable in dilute solution at elevated temperatures.

In Table III the effect of cold mastication at various roller openings on both the light-scattering properties and intrinsic viscosity is shown. It is readily observed that the weight-average molecular weight and the  $z$ -average root-mean-square end-to-end distance drop drastically with the reduction of the roller opening, whereas the intrinsic viscosity is moderately reduced. At a roller opening of 0.012 in., a drop in  $\bar{M}_w$  of 52% shows a corresponding drop of 8% in intrinsic viscosity. The number-average molecular weight is not significantly affected by the above mill treatment; the  $\bar{M}_n$  before mastication was 85000 and after mastication, 92000; the change of plus 8% is within experimental error. These figures indicate that the microgel is very sensitive, whereas the bulk of the polymer is relatively insensitive to the shearing forces of the mill. Furthermore, the milled, in contrast to the unmilled samples, did not clog the 0.22  $\mu$  pore size Millipore filters and filtered much more rapidly, attesting to the breakdown of microgel by milling. That the microgel is compact and approaches a spherical shape is evidenced by its small contribution to intrinsic viscosity as compared to its molecular weight.

TABLE III  
Effect of Mastication on  $\bar{M}_w$  and  $[\eta]$  of SBR Sample 110

Roller opening, in.	$\bar{M}_w \times 10^{-5}$	$(r_z^2)^{1/2}$ , Å	$A_2 \times 10^4$	$[\eta]$ , dl/g
Unmasticated (control)	8.22	2540	7.5	2.00
0.025	4.33	1700	8.2	1.88
0.012	3.87	1240	8.3	1.85
Closed	2.82	1160	9.5	1.53

Another interesting property of the microgel is its capacity for entanglement notwithstanding its compactness. In Table IV the effect of milling on the intrinsic viscosity, 10% concentrated solution viscosity, and the weight-average molecular weight of three samples of SBR is shown. The mastication was done with a roller opening of 0.012 in. It is observed that the intrinsic viscosity drop upon milling is less than 10% in all cases whereas the reduction in solution viscosity is many times more depending on the

TABLE IV  
Effect of Mill Mastication on the Intrinsic Viscosity, Solution Viscosity and  $\bar{M}_w$  of SBR

Sample No.	$[\eta]$ , dl/g		10% solution viscosity		$\bar{M}_w \times 10^{-5}$	
	Unmilled	Milled	Unmilled	Milled	Unmilled	Milled
110	2.00	1.85	731	407	8.22	3.4
115	1.99	1.86	1127	452	$\infty$	9.5
116	2.11	2.04	5822	741	$\infty$	34.5

solution viscosity of the unmilled sample. The high solution viscosity and large decrease upon milling reflects the high concentration of microgel in sample 116.

The weight-average molecular weights for unmilled samples 115 and 116 could not be determined since the Zimm plots extrapolated to zero or a negative number. The smallest pore size through which these samples could be filtered was  $5.0\ \mu$  in contrast to the  $0.22\ \mu$  for the masticated samples. The Zimm plot for milled and unmilled sample 116 is shown in Figure 3. The explanation for the anomalous Zimm plot for unmilled sample 116 may be that the size of the microgel particles is too large to be adequately handled by this technique. Calculations by Peebles<sup>12</sup> indicate that light

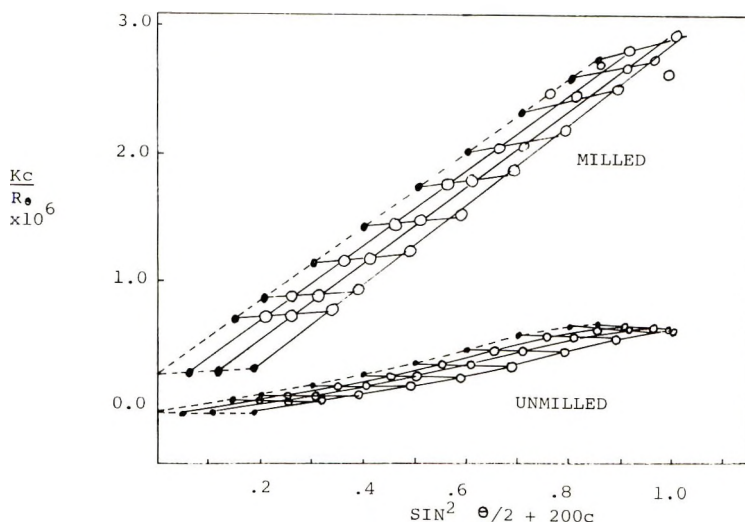


Fig. 3. Zimm plots of unmilled and milled SBR sample 116.

scattering is valid for polydisperse coils of less than  $3000\ \text{\AA}$   $z$ -average end-to-end distance. For dimensions much greater than this, the apparent molecular weight approaches rapidly to infinity. In order to perform reliable light-scattering experiments on microgel containing samples, it is therefore necessary to remove this component.

Some other methods have been employed to remove the microgel to various degrees, namely, ultracentrifugation<sup>13</sup> and treatment with anhydrous  $\text{CaSO}_4$ .<sup>14</sup> The results obtained with the various techniques are compared in Table V. All the samples were filtered in identical manner and the control experiment is included for comparison.

In experiment 4 of Table V, the roller mill opening chosen was  $0.012\ \text{in.}$  since the evidence suggested that the microgel is degraded whereas the bulk of the polymer is relatively intact. Also included in Table V is the result obtained when the sample was masticated and subsequently treated with  $\text{CaSO}_4$ . Experiment 6 is a duplicate of experiment 5 performed to show

the reproducibility of the method. It should be noted that light-scattering experiments and intrinsic viscosity determinations on samples one month after being milled showed a 54% increase in  $\bar{M}_w$ , whereas the intrinsic viscosity went up by only a few per cent. This behavior is due to the regeneration of gel by crosslinking reactions about fragments of the original microgel.

TABLE V  
Comparison of Methods Employed to Remove Microgel  
(Sample 110)

Expt. no.	Treatment	$\bar{M}_w$ $\times 10^{-5}$	$(\bar{r}_z^2)^{1/2}$ , Å	$A_2 \times 10^4$	$\bar{r}_z^2/\bar{M}_w$	$[\eta]$ , dl/g
1	Control	8.20	2540	7.5	7.9	2.00
2	Ultracentrif- ugation	7.41	2240	6.4	6.8	
3	Treatment with CaSO <sub>4</sub>	5.10	1700	9.0	5.7	2.01
4	Milling ( $\Delta = 0.012$ in.)	3.90	1450	8.3	5.4	1.85
5	Milling and treatment with CaSO <sub>4</sub>	3.40	1240	8.1	4.5	
6	Milling and treatment with CaSO <sub>4</sub>	3.50	1360	11.0	5.3	1.85

## DISCUSSION

The microgel in the above samples may arise from two sources: (1) crosslinking and long-chain branching reactions in latex particles during polymerization, and (2) post-polymerization crosslinking of the rubber molecules due to reaction with oxygen. The size of the microgel particles and the fact that fresh samples were employed suggest that most of the microgel of concern here is formed during polymerization, despite the fact that the conversion level was about 55% in the cold SBR samples 102 and 110. The reaction leading to microgel formation is free-radical attack on dead copolymer chain in the emulsion.<sup>15</sup> The size of microgel is limited during polymerization by the dimension of the latex particle.

The weight-average molecular weight of the microgel in sample 102 can be estimated from the data in Table II, showing that removal of 6.2% of the rubber dropped  $\bar{M}_w$  from  $32 \times 10^5$  to  $7.1 \times 10^5$ . On this basis,  $\bar{M}_w$  of the microgel is in the order of 41 million. This is in good agreement with the value of approximately 40 million given by Cooper and co-workers.<sup>14</sup>

It should be realized that SBR has a continuous range of molecular weights from very low molecular weight polymer to very high molecular weight microgel. There is therefore no clear-cut technique for removing microgel, and the several techniques compared in Table V are arbitrary. In Table V is observed that ultracentrifugation, treatment with CaSO<sub>4</sub>,

and mastication remove the microgel to variable degrees in that order and that the molecular weight and z-average root-mean-square end-to-end distance drop accordingly. It is to be noted that after satisfactory removal of microgel, the values for the coil size are no longer larger than the pore size of the filter employed. Furthermore, the values for the second virial coefficient  $A_2$ , given in Tables III and V, increase as the microgel is removed. The depressing effect of the microgel on the second virial coefficient is also observed by other authors.<sup>14</sup> In the sixth column of Table V the values for  $\overline{r_z^2}/\overline{M}_w$  are recorded. This ratio is independent of molecular weight for a monodisperse polymer in the critical consolute mixture.<sup>16</sup> The large drop, about 40%, observed in these samples is further evidence for polydispersity.

Of several techniques described for removing microgel prior to light scattering experiments, the method of milling and subsequent treatment with  $\text{CaSO}_4$  is reproducible, and has the advantage of producing a more homogeneous sample. The normal Zimm plot obtained after removal of microgel by this type of treatment is shown in Figure 3. The  $\text{CaSO}_4$  treatment is included since it has been found that the  $\text{CaSO}_4$  acts as a filter aid in the removal of microgel in SBR.

Since microgel is a structural component of the SBR and imparts some desirable properties,<sup>15</sup> it cannot be justifiably ignored. To this end, it is suggested that two weight-average molecular weights be used,  $\overline{M}_w$  and  $\overline{M}_w'$ .  $\overline{M}_w$  is defined as the weight-average molecular weight of the total rubber, whereas  $\overline{M}_w'$  is the weight-average molecular weight obtained after removal of the few per cent microgel.  $\overline{M}_w'$  is the operational weight-average molecular weight. Then it is seen that the molecular weight distribution of SBR may be very broad, depending on the microgel concentration. For sample 110, with a number-average molecular weight of 88000 obtained from osmometry, the breadth of the molecular weight distribution  $\overline{M}_w/\overline{M}_n$  is 9.3, whereas the operational breadth  $\overline{M}_w'/\overline{M}_n$  is 3.9. It is suggested that the actual and operational values for the weight-average molecular weight and molecular weight distribution be used in conjunction in the characterization of these copolymers.

## References

1. C. Booth and L. R. Beason, *J. Polym. Sci.*, **42**, 93 (1960).
2. W. Cooper, G. Vaughan, D. E. Eaves, and R. W. Madden, *J. Polym. Sci.*, **50**, 159 (1961).
3. B. H. Zimm, *J. Chem. Phys.*, **16**, 1093, 1099 (1961).
4. M. Morton, *Introduction to Rubber Technology*, Reinhold, New York, 1959, (a) p. 260; (b) p. 276 (cold rubber), p. 270 (hot rubber).
5. R. Trembley, M. Rinfret, and R. Rivest, *J. Chem. Phys.*, **20**, 523 (1952).
6. W. H. Stockmayer, L. D. Moore, Jr., M. Fixman, and B. N. Epstein, *J. Polym. Sci.*, **16**, 517 (1955).
7. S. Krause, *J. Phys. Chem.*, **65**, 1618 (1961).
8. W. Bushuk and H. Benoit, *Comp. Rend.*, **246**, 3167 (1958).

9. H. Benoit and P. Rempp, paper presented at American Chemical Society Rubber Division Meeting, Montreal, Canada, May 1967.
10. Q. Trementozzi, P. Doty, and R. F. Steiner, *J. Amer. Chem. Soc.*, **74**, 2070 (1952).
11. P. Doty, H. Wagner, and S. Singer, *J. Phys. Chem.*, **51**, 32 (1947).
12. L. H. Peebles, *J. Amer. Chem. Soc.*, **80**, 5603 (1958).
13. L. T. Muus and F. Billmeyer, Jr., *J. Amer. Chem. Soc.*, **79**, 5079 (1957).
14. W. Cooper, G. Vaughan, and J. Yardley, *J. Polym. Sci.*, **59**, 241 (1962).
15. W. O. Baker, *Rubber Chem. Technol.*, **22**, 935 (1959).
16. K. A. Stacey, *Light Scattering in Physical Chemistry*, Butterworths, London, 1956, p. 125.

Received March 4, 1968

## Thermal Degradation of Nadic Methyl Anhydride-Crosslinked Novolac Epoxy Resin\*

ELI S. FREEMAN and AARON J. BECKER, *Illinois Institute of Technology Research Institute, Chicago, Illinois 60616*

### Synopsis

The physicochemical high-temperature reactions of a nadic methyl anhydride-cross-linked novolac epoxy resin were investigated by means of differential thermal analysis, thermogravimetric analysis, and by other analytical procedures. The thermogravimetric study revealed that decomposition involving weight loss occurred in two stages. Chemical analysis showed that the major gaseous products formed during weight loss were 2-methylcyclopentadiene, carbon dioxide, and carbon monoxide. The formation of a fine mist of solid particles was observed during the second stage of degradation. Changing various experimental parameters affected the degradation processes. The kinetics of degradation were also investigated. The method of Freeman and Carroll was used to find that a zero-order rate law was followed at the beginning of both first and second stages of reaction. The activation energy associated with the major portion of the first stage of weight loss was 15 kcal/mole. There was good agreement between the observed reaction rates and the reaction rates calculated from a theoretical model which depended on desorption as the rate-controlling step. The activation energy for the beginning of the second stage of weight loss was 24 kcal/mole. By using DTA, the heat of exothermal reaction during this latter phase of decomposition was evaluated as 65 cal/g.

### INTRODUCTION

Differential thermal analysis and thermogravimetric analysis have been used to study the thermal degradation of polymers.<sup>1-3</sup> The nonisothermal method for the treatment of kinetic data obtained from TGA traces developed by Freeman and Carroll<sup>4</sup> is a rapid method of deriving orders of reaction and activation energies.

Other workers have studied the pyrolytic decomposition products of polymers by various analytical methods available to the chemist.<sup>5</sup>

Anderson<sup>6</sup> has studied the thermal decomposition of epoxide polymers containing nadic methyl anhydride, but could recognize and account for only one of the products of degradation, namely, carbon dioxide.

The present study has taken the kinetic and thermodynamic properties of a polymer and correlated the data with analytical data by using methods available to the polymer scientist.

\* Presented in part at the 153rd National Meeting, American Chemical Society, Miami Beach, Florida, April 9-14, 1967.

## EXPERIMENTAL

### Material

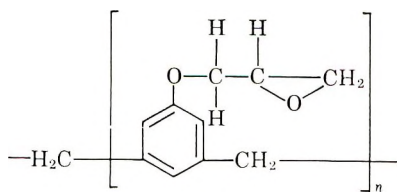
The polymer, provided by the Ames Research Center, NASA, was a phenolic epoxide, crosslinked through nadic methyl anhydride. Table I summarizes its preparation and composition. The polymer was pulverized and the powder sieved for studies on the effect of particle dimensions. It was then stored in a vacuum desiccator.

TABLE I  
Polymer Composition and Preparation

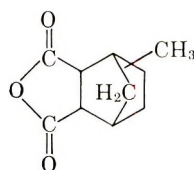
Parameter	Polymer lot No.		
	1A	1B	1C
Composition, parts by weight			
DEN 438	100	100	100
NMA	75	85	95
DMP 30	1.5	1.5	1.5
Cure temperature, °F			
Step 1	105	105	105
Step 2	200	200	200
Cure time, hr			
Step 1	4	4	4
Step 2	16	16	16

Several pieces of the polymer were specially machined into specific geometric configurations by NASA. These samples were spheres 0.8 cm in diameter, cylinders 1.0 cm in diameter  $\times$  0.25 cm high, and rhombohedral solids 1.0 cm high  $\times$  0.025 cm wide  $\times$  0.025 cm long.

DEN 438 was obtained from Dow Chemical Company, Freeport, Texas; nadic methyl anhydride from Allied Chemical Company, National Aniline Division; DMP 30 from Rohm and Haas, Philadelphia; and 2-methyl-cyclopentadiene dimer from Aldrich Chemical Company.



DEN 438  
 $n = 1.6$



NMA

### Apparatus and Procedures

**Differential Thermal Analysis (DTA).** The DTA experiments were carried out with the apparatus pictured in Figure 1. A Y-tube diverted a stream of gas into each sample vessel when gas flows were desired. Flow

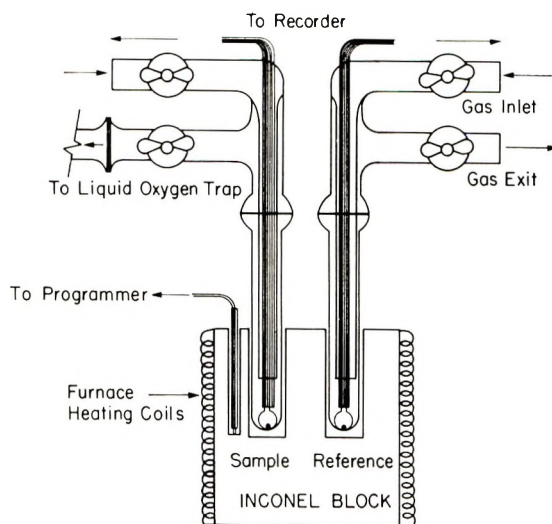


Fig. 1. DTA system.

rates were adjusted with a precalibrated flowmeter and a needle valve connected directly to the gas tank.

The output of the DTA apparatus was fed into a Moseley 7030A  $x-y$  recorder. Reference temperature was plotted on the  $x$  axis of the DTA curves. Reference temperatures were also recorded independently on a Moseley model 680 strip-chart recorder to insure linear heating rates. The DTA experiments were generally carried out up to  $650^{\circ}\text{C}$  and in some cases as high as  $900^{\circ}\text{C}$ .

The effect of different particle sizes in the DTA experiments were observed by performing experiments on both fine and coarse fractions of sieved pulverized polymer and by using the bulk polymer samples previously described.

Aging experiments were performed with closely sieved powdered polymer, screen fraction 80/100. The samples were heated to the desired temperatures in the DTA apparatus and rapidly removed from the test tube block.

Quantitative enthalpic analyses were obtained by using the differential thermal analysis curve of carbon under an oxygen atmosphere. The area under the exotherm corresponding to the oxidation of carbon served as a standard for comparisons with the polymer. The weight of carbon which remained at the conclusion of the exotherm was obtained. The heat of reaction of this amount of carbon oxidizing to a calculated number of moles of carbon dioxide formed during the reaction was equated to the area under the DTA curve. Estimates of the heats of reaction were based on a comparison of the exothermal DTA area of the polymer with the exothermal area of the carbon curve.

**Thermogravimetric Analysis (TGA).** The TGA experiments, exclusive of those performed under vacuum, were made with a Chevenard thermo-

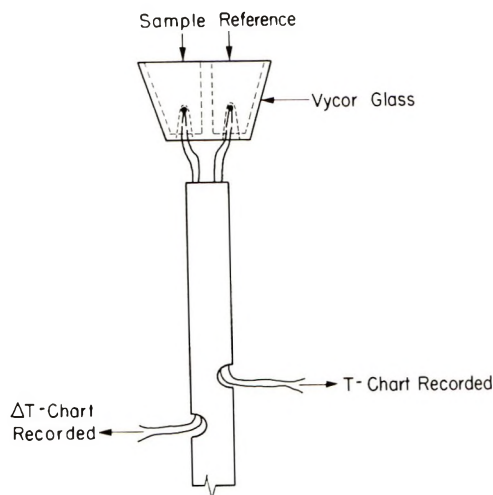


Fig. 2. Simultaneous TGA-DTA. Method of mounting sample in divided crucible in Chevenard thermobalance.

balance, modified for electronic recording; the sample vessels used were No. 00000 Coors crucibles obtained from Fisher Scientific Company. The programmer was identical to the one used in the DTA experiments.

Placement of the sample temperature thermocouple at a point touching the bottom of the sample vessel insured accurate readout of temperature.

Sample vessels containing 100 mg of polymer were mounted on the stem of the Chevenard thermobalance. The stem consisted of a four-hole ceramic insulator and a thermocouple placed through two of the four holes. A Chromel ring was mounted on top by making use of the other two holes. The bottom end of the thermocouple was brought through the ceramic and connected to coiled 0.001-in. thermocouple wire to safeguard against interference in the balance movement.

The hollow tube provided in the interior of the Chevenard furnace permitted direct introduction of the desired atmosphere. The pen deflection caused by the thermocouple input was electrically adjusted so that 100°C was equilibrated to either 1 or 2 in. of pen deflection.

From the thermogravimetric curves, a series of values of the rate of weight loss  $dw/dt$ ,  $W_r$  (the total weight change at completion of reaction minus the change in weight at temperature  $T$ ) and absolute temperature  $T$  under a variety of experimental conditions, were obtained and used for the kinetic evaluations.

Vacuum TGA experiments were performed with the Cahn electrobalance adapted for use in conjunction with the R. L. Stone Company DTA equipment.

**Simultaneous DTA-TGA.** Part of the DTA-TGA apparatus is pictured in Figure 2. One half of the crucible contained the sample and the other half the aluminum oxide reference material.

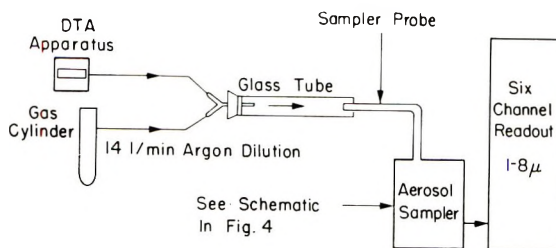


Fig. 3. Fine-particle thermal analysis system.

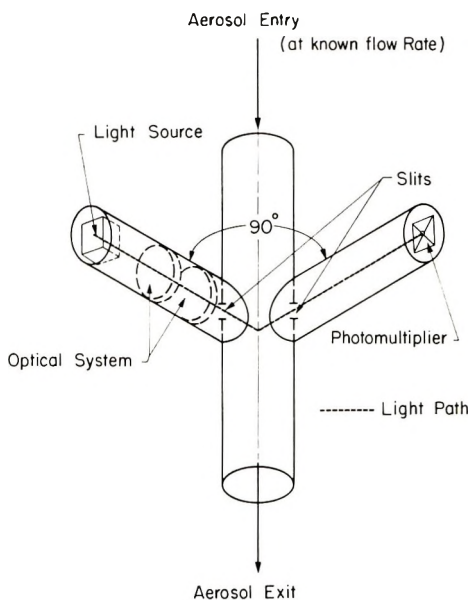


Fig. 4. Aerosol sampler.

The Bristol two-pen recorder in combination with a time switch was connected to the induction coil attached to the moment arm of the Chevenard balance via a demodulator. This permitted weight changes to be recorded by one pen and both differential temperature and sample temperature to be recorded by the second pen via the time switch and a properly adjusted resistance.

**Fine-Particle Thermal Analysis (FPTA).** A portable DTA unit was used as a plug-in module for analysis of the effluent gas stream containing particulate smoke. All the modules discussed under DTA apparatus were placed on a cart that was moved adjacent to a fine-particle analyzer. The photocell at the exit of the light-scattering system was connected directly to a six-channel counting system, which gave automatic readout on all six channels. Each channel represented a particle-size range and gave a numerical readout of the number of particles in each size range in a 19-sec time interval.

The analyses of the fine particles moving into the gaseous flow system during decomposition were obtained under DTA conditions. Particle-size analysis was made over 10°C intervals from 180 to 540°C by placing the gas exit tube from the DTA apparatus directly into the particle analyzer. Figures 3 and 4 are schematic diagrams illustrating the equipment used for FPTA.

**Analytical Procedures.** Analysis of the reaction products was facilitated by dividing the decomposition products into three categories: (1) effluent gases and particles visible by mass spectrometry or FPTA, (2) liquid and solid residues soluble in one of several common solvents, and (3) insoluble char and solid polymer.

Category 1 was analyzed in detail. A liquid oxygen trap was placed around the U-tube to collect the gaseous product. O-ring joints provided gas-tight seals. After the gaseous samples were trapped (each sample was trapped over 20°C intervals beginning at 240°C), the vessels were attached to the inlet system of a Bendix time-of-flight mass spectrometer.

Acetone was found to be the best solvent for category 2. The solutions were analyzed in a Hitachi mass spectrometer. They were also injected into a gas chromatograph, and the substituents identified. The Hitachi-Perkin-Elmer mass spectrometer was used in later experiments for also analyzing gaseous samples. This was done by placing some powdered material in the sampling system and heating it at 10°C/min to 325°C. When heating began, analyses were made in 20°C intervals.

Mass-spectral analyses of DEN 438, nadic methyl anhydride, and 2-methylcyclopentadiene were made by this technique also. Gaseous decomposition products for all these materials were identified over the temperature range of 25–325°C in the furnace-enclosed sampling system of the Hitachi mass spectrometer.

Infrared analyses were performed on a Perkin-Elmer Infracord. Spectra were first obtained on unheated samples and then in 20°C intervals from 240 to 440°C.

The x-ray studies were made on the powders in aluminum sample holders. A North American Philips x-ray instrument was used.

## RESULTS

The initial experiments showed that the method of sample pulverization did not effect the DTA or TGA curves of the polymer; mass spectral analysis supported the conclusion that the polymer remained unchanged as the result of exposure to Dry Ice, liquid nitrogen, or atmospheric conditions during pulverization.

Seven experimental parameters were tested for their effect on the high temperature physicochemical reactions of the polymer. Concurrently, the effect of variation in the quantity of nadic methyl anhydride used in the curing process was also investigated. All of these results were compared to the standardized experiment.

### Standard Experiments

The DTA curves shown in Figure 5 indicate that the first major DTA band is an endotherm which has a peak at 300°C. During this endotherm the sample was observed to become tacky, and a light brown condensate formed on the cooler parts of the test tube. At 320°C an exothermal peak began to form and proceeded to a maximum at 365°C. During the latter portion of the exotherm, a mist of fine particles emanated from the decomposing polymer. The figure also contains curves which show the effect of varying the quantity of NMA on the DTA spectrum. As the amount of NMA was increased, the exothermal peak flattened.

TGA curves in Figure 6 show the difference between the thermal decomposition behavior of the polymer as a function of the amount of NMA used in the cure procedure. As the amount of nadic methyl anhydride was increased from 75 to 95 parts by weight, the initial decomposition tempera-

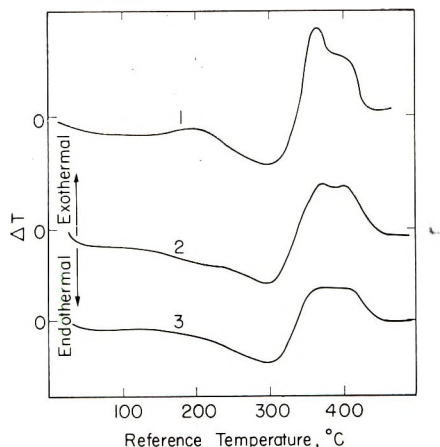


Fig. 5. DTA of polymers 1A, 1B, and 1C (100 mg): (1) polymer 1A; (2) polymer 1B; (3) polymer 1C. Argon flow, 300 ml/min; heating rate, 10°C/min.

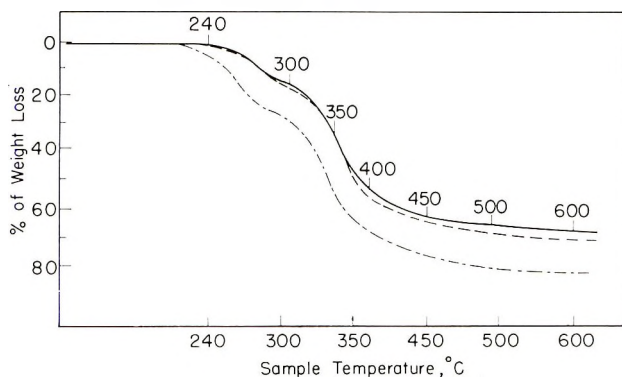


Fig. 6. TGA of (---) polymer 1A, (—) polymer 1B, and (- - -) polymer 1C; 100 mg of each sample was used. Argon flow, 300 ml/min; heating rate, 10°C/min.

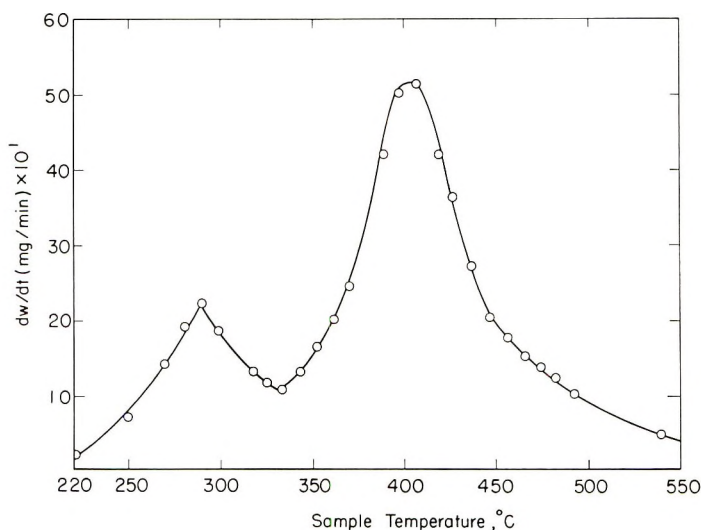


Fig. 7. Derivative TGA curve of polymer (100 mg). Argon flow, 300 ml/min; heating rate, 10°C/min.

ture decreased. The value for the residual yield of the polymer containing 95 parts by weight NMA was 20%, whereas the yield for the polymers containing 85 and 75 parts by weight NMA was 32%. It should be noted that these values were for samples heated up to 600°C. Other residual yield values referred to may apply to experiments carried out to different temperatures and so cannot be directly compared with these values.

A comparison of the DTA and derivative TGA (Fig. 7) curves for polymers 1A indicated that the DTA endotherm corresponds to the first weight loss region in the TGA experiment. The second weight loss region occurred during the exotherm appearing in the DTA curve. This exotherm contained at least two reaction zones and the weight loss region could be expected to be complex.

Complete kinetic analysis includes some knowledge of the nature of the products of reaction and degradation. Below 200°C, trace quantities of toluene and water were observed. By means of parallel experiments on the polymer and nadic methyl anhydride, it was determined that the principal gaseous product during the first weight loss region was 2-methylcyclopentadiene. At the beginning of the second weight loss region, CO<sub>2</sub> and CO predominated as the major effluent gases.

Infrared spectra corroborated the observation that the polymer decarboxylated at the beginning of the second weight loss region. From these spectral studies it was also found that the DEN 438 segment of the polymer was stable up to approximately 400°C.

The fine particulate smoke observed during most of the second weight loss region consisted of DEN 438 fragments. Analysis of the size and quantity of the particles was made and these results are listed in Table II.

TABLE II  
Fine-Particle Analysis<sup>a</sup>

Temperature, °C	Particle count in each range					
	1.0-1.41 $\mu$	1.41-2.8 $\mu$	2.8-4.2 $\mu$	4.2-5.6 $\mu$	5.6-7.0 $\mu$	7.0-8.4 $\mu$
340	81	1	0	1	0	0
350	441	1	0	1	0	0
360	3731	5	0	0	0	0
370	4000	4116	4	0	0	0
380	3498	3582	1981	9	0	0
390	345	1102	1299	131	0	0
400	38	307	231	231	12	0
410	46	130	341	210	12	0
420	30	68	225	177	23	0
430	13	39	145	138	28	0
444	9	39	102	111	15	0
450	28	58	171	124	19	0
460	19	62	158	153	11	0
470	25	73	195	135	6	0
480	53	152	304	100	4	0
490	79	266	501	171	6	0
500	212	563	905	116	0	0
510	745	1888	1689	64	0	0
520	1432	3212	2197	45	0	0
530	2739	4300	2175	7	0	0
540	3534	3812	1719	5	0	0
550	4338	3422	1247	6	0	0
560	3857	3060	861	0	0	0

<sup>a</sup> This technique measured particles from 1 to 8.4  $\mu$ .

These particles were slightly soluble in acetone, and analysis of the solution by mass spectrometry indicated that several tropilium ion derivatives were present. Gas chromatographic analysis indicated that *o*- and *p*-cresol were substituents of the particles. Evidence strongly indicated that they were derived from the DEN 438. Lack of evidence for the existence of NMA in the residue, indicated it was no longer present in any measurable amounts.

The x-ray patterns indicated the polymer and residual char, were amorphous.

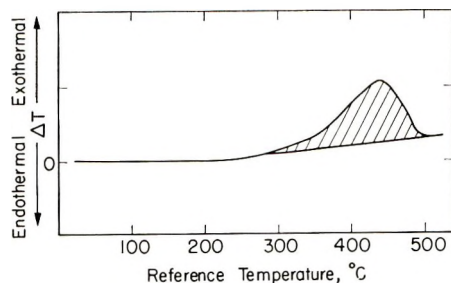


Fig. 8. DTA of Nuchar carbon. Oxygen flow, 150 ml/min; heating rate, 10°C/min.

Figure 8 is a DTA curve of carbon heated in oxygen. The area under the peak was taken as a standard in obtaining the heat associated with the exothermal decomposition of the polymer. The heat of reaction was estimated to be 65 cal/g.

### Effect of Heating Rate

Figure 9 shows the DTA experiments in which the heating rate for the polymer was varied.

The shift in the low-temperature exotherm at the high heating rate was undoubtedly due to passage through this reaction zone at a relatively fast rate as compared to the reaction rate. As a result of the increased extent of the first exotherm at 340°C in the DTA curve obtained at 10°C/min, the second exothermal band shifted to lower temperatures in the 4°C/min curve.

Another series of experiments was undertaken to determine the effect of very fast heating rates on the DTA curve of the polymer 1A. Figure 10 shows the results. The heating rate was varied from 900°C/min to 2000°C/min. The technique involved preheating the DTA furnace block to 900°C. A drill press stand was used to plunge the sample and reference into the block. The sample vessels were Vycor tubes about 2 in. long and 9 mm in diameter. The linear heating rate ranged from 125 to 500°C. The exothermal peaks shifted significantly upward from those of the slower heating rate experiments. This is due to the reaction rate effect as well as thermal conductivity factors, which should play a role at these very high heating rates. It was also observed in the TGA experiments that as the

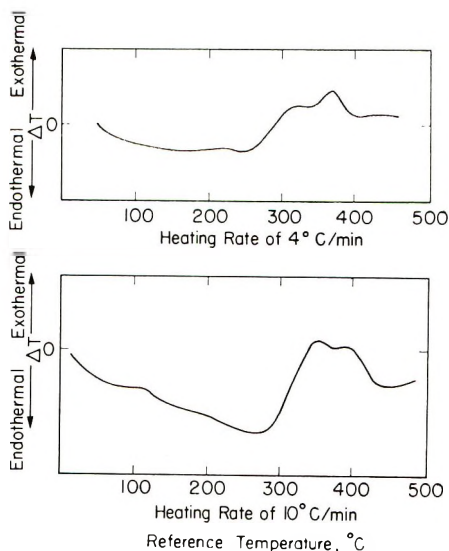


Fig. 9. Effect of heating rate on DTA curve of polymer 1A: (a) heating rate 4°C/min; (b) heating rate 10°C/min. Argon flow, 300 ml/min.

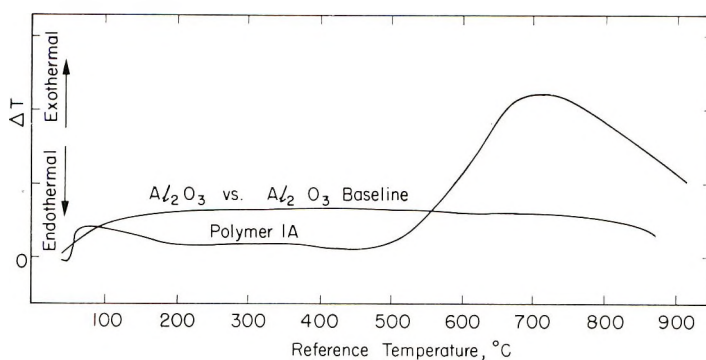


Fig. 10. Effect of heating rate on DTA of polymer 1A (100 mg). Argon flow, 300 ml/min; heating rate, 900–2000°C/min.

heating rate was reduced the degradation curves were shifted to lower temperatures.

### Aging Studies

Principal concern in the investigation of aging is the effect of further polymerization on the thermal stability of the resulting material.

Figures 11 and 12 show the results of a series of experiments in which the DTA run was stopped after each endothermal or exothermal change. The sample was cooled, and thermoanalysis was conducted on the aged samples. Upon repeating the DTA and TGA experiments, the various regions of reaction were systematically eliminated as a result of aging. This is of importance because it shows that each of these reactions produces a product and that the reaction of the product at higher temperatures is then responsible for the subsequent exothermal peak. It appears that there were three reactions associated with the various thermal changes.

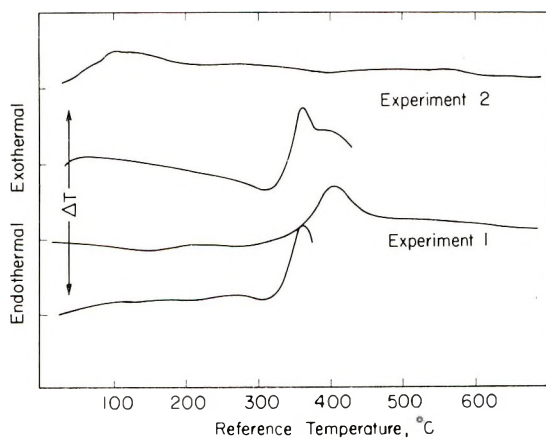


Fig. 11. DTA of polymer 1A showing aging effect (sample weight 100 mg): (1) sample heated to 390°C; (2) sample heated to 420°C. Argon flow, 300 ml/min; heating rate, 10°C/min.

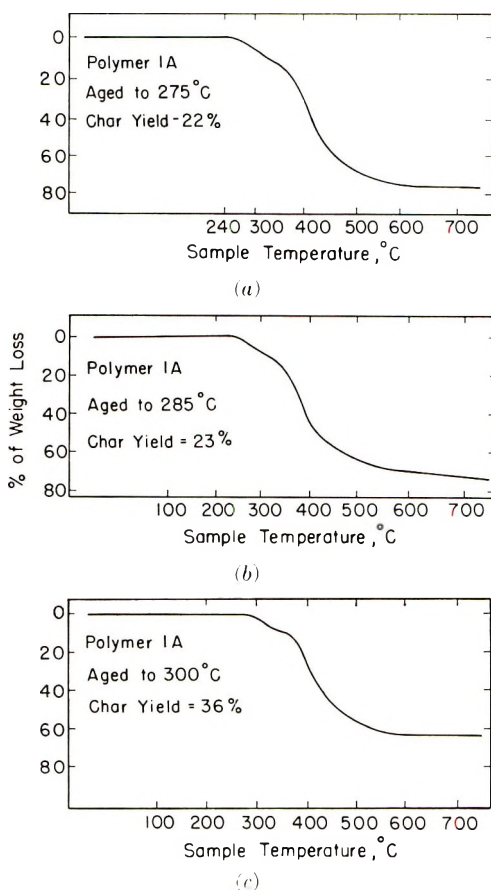


Fig. 12. TGA curves of polymer 1A aged to various temperatures: (a) 275°C, char yield, 22%; (b) 285°C, char yield 23%; (c) 300°C, char yield 36%. Argon flow, 300 ml/min; heating rate, 10°C/min; sample weight, 200 mg.

The TGA experiments on the polymer preheated to 285 or 300°C showed that the samples lost weight at higher temperatures and residual char increased as compared with the unaged material. The material preheated at 275°C did not seem to have a significantly different char yield from the original material. In this case the samples were heated to 750°C.

#### Effect of Particle Size

There was a definite trend toward the minimization of the first stage of reaction and the increase of the temperature range of the final stage of weight loss as the particle size was increased. This can be expected for a surface-controlled reaction, if the rate of reaction is proportional to the surface area. Figure 13 shows this effect.

Three samples of bulk polymer formed into spherical, cylindrical and prismoid shapes were also studied. There were two purposes for this work: (1) to determine whether the ratio of surface to volume or mass is related

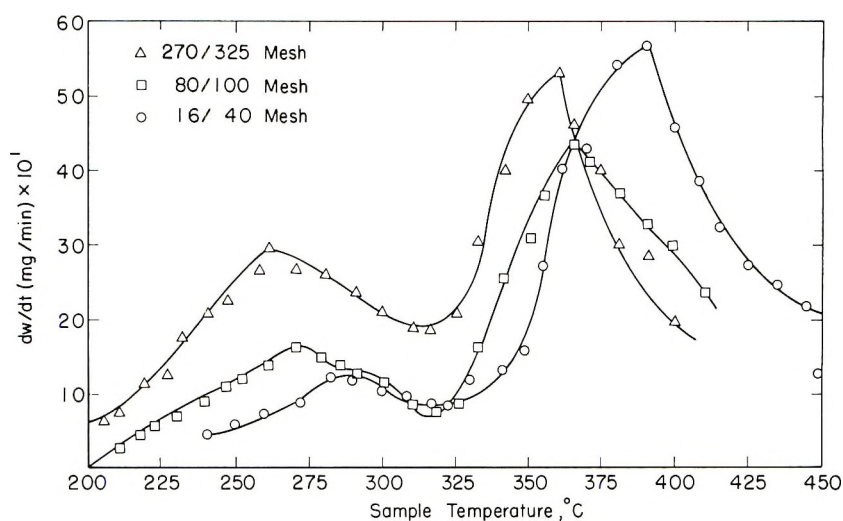


Fig. 13. Derivative TGA curve showing effect of particle size for polymer 1A: ( $\Delta$ ) 270/325 mesh; ( $\square$ ) 80/100 mesh; ( $\circ$ ) 16/40 mesh. Argon flow, 300 ml/min; heating rate,  $10^{\circ}\text{C}/\text{min}$ ; sample weight, 100 mg.

to the rate of decomposition, and (2) to determine the effect of very large particles on reaction rate. Figure 14 shows the TGA curves, and Table III summarizes the results. The first reaction observed in the powders was absent and the temperature of the second stage of decomposition was significantly increased. It appears that primary products of reaction may have undergone further reaction during diffusion through the polymer particles. This follows the general trend seen for the screened powdered samples.

TABLE III  
Effect of Particle Shape on Decomposition

	Sphere	Disk	Prism
Reaction, %	4.5	4.5	4.5
Rate of reaction, mg/min (at 4.5% reaction)	255.0	56.0	14.5
Surface area, $\text{cm}^2$	2.00	2.36	1.13
Volume, $\text{cm}^3$	0.2678	0.1960	0.0625
Weight, mg	336.8	242.8	74.2
Residual char, %	16	33	33
Initial temperature of decomposition, $^{\circ}\text{C}$	415	280	335
Density, $\text{g}/\text{cm}^3$	1.25	1.24	1.25
$A/W$ (surface area/weight)	5.9	9.7	15.3
Rate of reaction, $/\text{cm}^2 \text{ min}$ (at 4.5% reaction)	127.5	23.8	12.9
Fraction decomposed/min	0.74	0.23	0.20

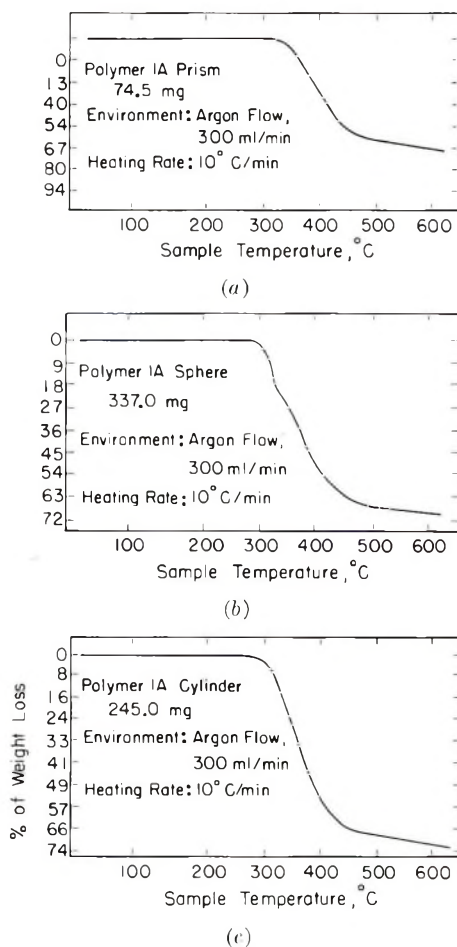


Fig. 14. TGA curve showing effects of different shapes of polymer solids on thermal stability of polymer IA: (a) prism (74.5 mg); (b) cylinder (245.0 mg); (c) sphere (337.0 mg). Argon flow, 300 ml/min; heating rate, 10°C/min.

The per cent char residue was least for the spheres. The shapes of the decomposition curves were quite different for the variously shaped polymers. The most pronounced difference was that of the spheres, which initially decomposed quite slowly, then decomposed rapidly. The decomposition curves of the other shapes did not show the sharp transition from low to high temperatures. The cylinders and prisms exhibited similar overall decomposition characteristics in contrast to the spherical shape. The data on the bulk particles show that the initial rate of reaction per unit surface area is considerably higher for the sphere than for the other shapes. The rate of reaction appears to be more closely related to the ratio of mass to surface area than to any of the other parameters in Table III. This behavior may be explained in terms of heat transfer. The heat losses from a sphere due to its lower surface to mass ratio would be the slowest of all of the samples. Since the reaction is exothermal, one may expect a

rapid heat build-up after an initially slow reaction. This general decomposition behavior was observed and was in contrast to the powder where the reaction rate increases with an increase in specific surface.

### Effect of Flow Rate

At argon flow rates of 300 and 600 ml/min the difference between the curves was rather small. In general, the initial stage of decomposition was not markedly affected by changing the flow rate from 100 to 600 ml/min. However, the rate of weight loss during the second region of the TGA curve increased significantly as the flow rate was increased.

### Effect of Gaseous Atmosphere

Identical experiments were performed on samples of polymers with all conditions as described under the standard experiment, except that the gas flow was replaced with static air. From 240 to 350°C the weight loss in both experiments followed the same decay curve. During the remainder of the run, the rates of weight loss were considerably different in each temperature range for the two experiments. At 350°C the rate of weight loss in air accelerated.

At 390°C an inflection point appeared in the air curve, while no such point appeared in the argon curve. However, in the interval of 460 and 500°C the argon curve showed a decided increase in rate of weight loss. In contrast, the air curve showed a point of inflection at 450°C toward a decrease in rate of weight loss, with a constant change in slope thereafter until total weight loss had taken place.

With the samples in a flow of oxygen, the rates of reaction of the polymer were significantly accelerated. Reaction rate was markedly increased at higher temperatures. The endotherm, which appeared in the air curve at 240°C, occurred at 220°C in oxygen. The height and the area of the exothermal band were significantly increased. The temperatures of the maxima, however, were the same in oxygen, air, and argon.

In oxygen, the exotherm beginning at 200°C represented a preignition process, which led to self-propagative ignition of the polymer at 240°C. Several successive explosions occurred at 400°C, and heating was terminated. Examination of the sample tube revealed the absence of any residue. The polymer mixed with 50% alumina did not ignite, as did the polymer alone.

The decomposition characteristics of the polymer did not appear to be significantly affected in an atmosphere of carbon dioxide or of 2-methylcyclopentadiene, which formed during the initial stages of decomposition. The carrier gas used for the pentadiene was argon.

### Effect of Sample Mass

There were no significant differences between the results in which 100 mg and 200 mg were used, indicating mass had no effect on behavior under these experimental conditions.

### Effect of Added Solid Surfaces

Upon addition of alumina to the powdered polymer, no significant change occurred in the DTA spectrum. In oxygen, however, addition of alumina prevented ignition of the polymer.

### Kinetics of Thermal Decomposition

Figures 15 and 16 show the Freeman-Carroll plots of the polymer heated in a flow of argon of 300 ml/min at 10°C/min. These plots are based on the equation:

$$\Delta \ln (dw/dt) = (-E^*/R) \Delta(1/T) - x \Delta \ln W_r$$

where  $dw/dt$  is the rate of weight loss or gain,  $E^*$  is the activation energy,  $T$  is absolute temperature,  $x$  is the order of reaction, and  $W_r$  is the total weight change at completion of reaction minus the change in weight at any given time.

A plot of  $\Delta \log (dw/dt)$  versus  $\Delta \log W_r$  at constant  $\Delta 1/T$  yields a straight line whose slope is  $x$  and whose  $y$  intercept is  $-E^*/2.3R$ .

Since the TGA curves exhibited two principal areas of weight loss, Freeman-Carroll plots were made to encompass each of the corresponding

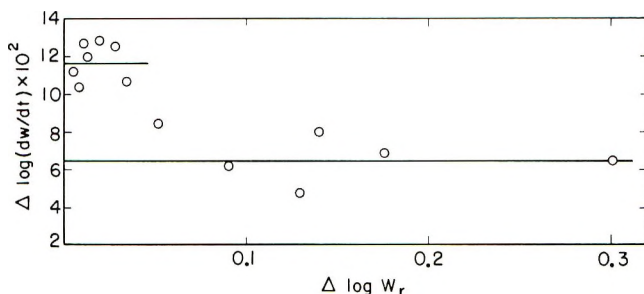


Fig. 15. Freeman and Carroll plot of first stage of decomposition of polymer 1A. Data obtained from the standard TGA experiment:  $\Delta(1/T) = 1 \times 10^5$ .

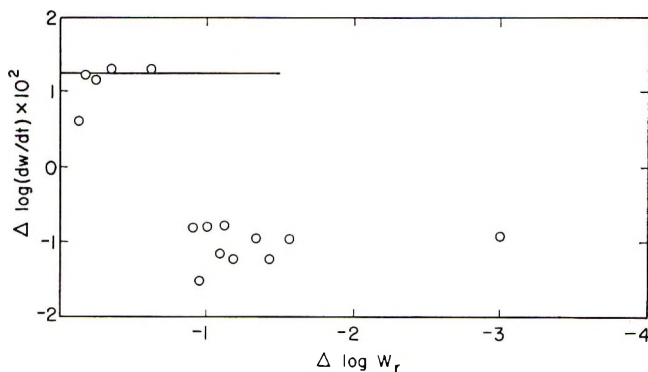


Fig. 16. Freeman and Carroll plot of the second stage of weight loss data obtained from the standard TGA experiment.  $\Delta(1/T) = 2.5 \times 10^5$ .

TABLE IV  
Kinetics of Reaction; Stage 1<sup>a</sup>

Sample	Branch 1				Branch 2			
	Temperature range, °C	Extent of reaction, %	$E^*$ , kcal/mole	Order	Temperature range, °C	Extent of reaction, %	$E^*$ , kcal/mole	Order
Polymer 1A	220-250	15	25 <sup>b</sup>	0	250-305	85	16 <sup>b</sup>	0
Polymer 1A, aged	230-255		22 <sup>c</sup>	0	255-320		15 <sup>c</sup>	0
			25 <sup>b</sup>	0			13 <sup>b</sup>	0
Polymer 1B	230-258		28 <sup>c</sup>	0			14 <sup>c</sup>	0
Polymer 1C	200-225		26 <sup>c</sup>	0	255-315		15 <sup>c</sup>	0
			23 <sup>c</sup>	0	255-305		13 <sup>c</sup>	0

<sup>a</sup> Experimental conditions: heating rate, 10°C/min; flow rates, 300 ml/min argon.<sup>b</sup> Freeman and Carroll plot.<sup>c</sup> Zero-order plot.

temperature regions in the TGA curves separately. The first area of weight loss was resolved into two zero-order branches. Table IV and V summarize the results. The second zero-order segment covered 80% of the weight loss in the first stage of degradation.

TABLE V  
Kinetics of Reaction;<sup>a</sup> Stage 2

Sample	Temperature range, °C	Extent of reaction, %	$E^*$ , kcal/mole <sup>b</sup>	Order
Polymer 1A	305-700	25	27	0
Polymer 1A, aged	325-660		23	0
Polymer 1B	315-715		23	0
Polymer 1C	310-675		26	0

<sup>a</sup> Experimental conditions: heating rate, 10°C/min; flow rate, 300 ml/min argon.

<sup>b</sup> Zero-order plot.

The above results were confirmed by the zero-order plots of  $\log dw/dt$  versus  $1/T$  shown in Figure 17. Figure 17 shows that the data may be represented by two linear branches for all of the samples on which the

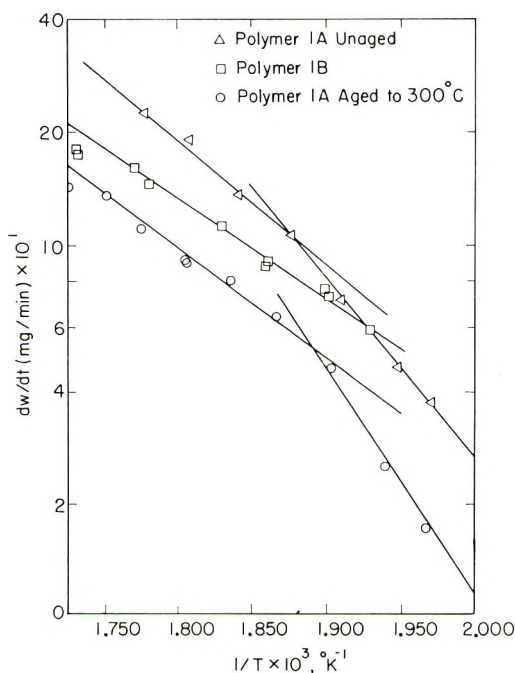


Fig. 17. Zero-order plots of the first stage of decomposition under standard conditions.

Freeman-Carroll plots were used. The activation energies were obtained from the slopes of these curves and agreed with the Freeman-Carroll treatment.

Table VI compares the kinetic data obtained from experiments conducted at heating rates of 5 and 10°C/min, and also shows the activation energies for polymer 1C were somewhat lower than were those for polymers 1A and 1B.

TABLE VI  
Effect of Heating Rate on Kinetic Parameters for Polymer 1A in Argon Flow of 300 ml/min

Heating rate, °C/min	Temperature range, °C	Extent of reaction, %	$E^*$ , kcal/mole	Order of reaction
10	220-250	15	22	0
5	218-235	15	27	0
10	250-305	85	15	0
5	235-285	85	13	0
10	305-700	10	27	0
5	285-620	10	30	0

The effect of particle size on the rate parameters of decomposition of the polymer are summarized in Table VII. It was clear from the kinetic plots that the activation energy for the first zone of decomposition increased as the particle size increased.

On the other hand, the activation energy appeared to be relatively constant with particle size during the second stage of decomposition but, because of the scatter of points, was somewhat less certain. The positions of the curves, which represent the early part of the second region of decomposition, however, indicate that the rate constants for reaction were inversely proportional to the particle size.

Figure 18 shows the zero-order temperature dependency plot for the decomposition of polymer 1A heated at 5°C/min at a reduced pressure of  $10^{-2}$  mm/Hg. The activation energy was calculated to be 20 kcal/mole.

TABLE VII  
Effect of Particle Size on Kinetic Parameters for Polymer 1A in 300 ml/min Argon Flow at a Heating Rate of 10°C/min

Mesh	Temperature range, °C	$E^*$ , kcal/mole	Order of reaction
16/40	250-280	20.4	0
16/40	285-310	21	0
80/100	250-280	13.3	0
80/100	285-310	18	0
270/325	250-280	12.4	0
270/325	285-310	21	0

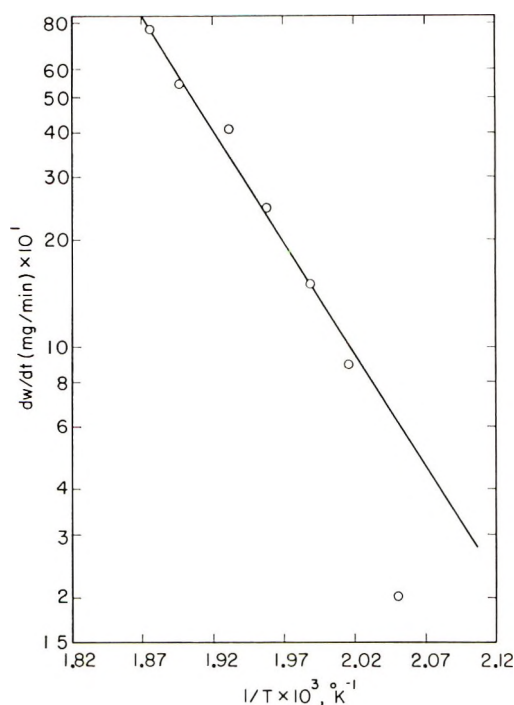


Fig. 18. Zero-order plot of the first stage of decomposition of polymer 1A. Decomposition carried out under vacuum. Heating rate  $10^\circ\text{C}/\text{min}$ ; sample weight, 10 mg.

A series of isothermal experiments was carried out for the purpose of confirming the kinetic results obtained from the TGA curves. These experiments were made over the temperature range of  $230$ – $270^\circ\text{C}$  in argon at a flow rate of  $300\text{ ml}/\text{min}$ . The isothermal data indicated zero-order kinetics with an average activation energy of  $15\text{ kcal}/\text{mole}$ .

It appears the optimum crosslinking reaction occurs with 85 parts by weight of nadic methyl anhydride and 100 parts of the epoxide DEN 438. However, the polymer which contained 75 parts of nadic methyl anhydride was only slightly less stable than polymer 1B.

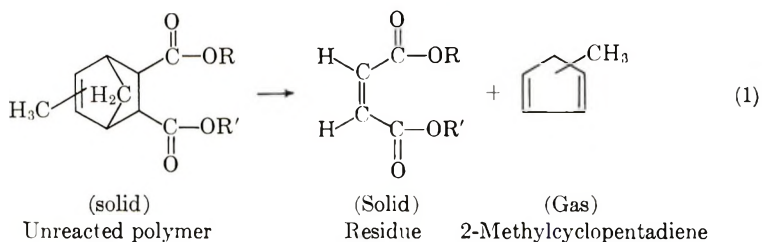
The effect of heating rate is probably a result of heating at a relatively fast rate compared to the rate of reaction; this causes the reactions to occur (1) principally at higher than normal temperature and (2) over a shorter period of time. The result is a high exotherm, as was observed.

The flow rate of argon had little effect on the initial stage of decomposition but had a distinct effect of increasing the rate of weight loss during the second stage of decomposition, apparently due to the rapid transport of the fine particulate product observed.

By comparing the DTA curve with the weight loss curves, it was clear that the endotherm with its peak at  $300^\circ\text{C}$  corresponded to the initial stage of weight loss and the subsequent exotherms were associated with the second and final stage of weight loss.

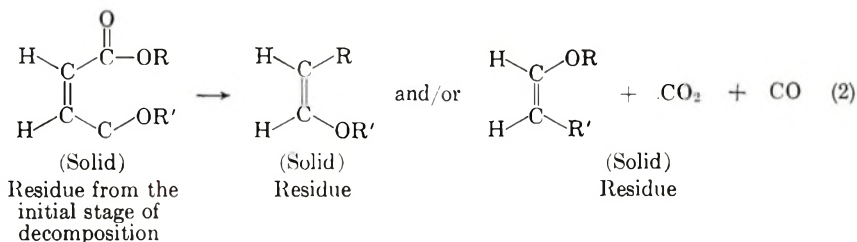
Chemical analysis and aging experiments indicated that the reactions were consecutive, rather than simultaneous, thus simplifying interpretation of the kinetic results.

Based on analytical results, it appeared that the initial decomposition reaction that was associated with the endotherm at 300°C and corresponded to the initial region of weight loss can be expressed as shown in eq. (1).



Bond rupture takes place as indicated in eq. (1). It can be expected that the reaction is endothermal, as was found to be the case from the DTA curves. The heat of reaction was estimated from bond energy considerations and was calculated to be 57 kcal/mole and the diester was assumed to be the major portion of the original polymer, although infrared analysis showed evidence for the presence of some monoester.

The reaction for the initial phase of the second stage of weight loss occurred from approximately 260–382°C and was found to be as shown in eq. (2).



This reaction corresponded primarily to the initial exotherm beginning at 320°C. As the amount of gaseous products sharply decreased, fragments formed the major product of decomposition. Other products, such as *m*- and *p*-cresol and propane derivatives, were found to be present in the residue upon extraction with solvents and subsequent analysis. If the fragmentation reaction is endothermal, this may account for the endothermal dip in the exotherm. The part of the exotherm at 400°C can be accounted for by polymerization reactions of the residue as the polymer is heated from 365°C to complete reaction over 450°C.

Formation of the fine particle fragments may account in part for the effect of flow rate on the second stage of weight loss, so pronounced during the middle to latter part of the second zone of weight loss. This appeared to be independent of the gas used, and may have been due to the blowing of these fine particles by the gas stream from the remainder of the sample.

The activation energy for the initial stage of weight loss was  $15 \pm 3$  kcal/mole at  $250^\circ\text{C}$  and higher. This reaction appears to be a reverse Diels-Alder reaction. Berson<sup>7</sup> has done extensive work on the kinetics of the Diels-Alder reaction between maleic anhydride and cyclopentadiene and has found the activation energy to be 12.4 kcal/mole. His calculations predict that the reverse Diels-Alder reaction of these two compounds should give an activation energy of approximately 30–34 kcal/mole. It should be noted that the activation energy during the initial branch of the first stage of decomposition was 25 kcal/mole and is not far from the value for the ideal system studied by Berson. A zero-order process can also be expected for the reverse Diels-Alder reaction, if the rate-controlling decomposition reaction occurs on the surface of the particles. If the rate-controlling reaction is occurring on the surface of the particles and is dependent upon the number of surface reaction sites, it should be possible to derive a theoretical treatment that would account for the observed rates of reaction based on the absolute rate theory. The basic equation to consider is:

$$v = C_a (kT/h)(f^*/f)e^{-E^*/RT}$$

where  $v$  is the rate of reaction,  $k$  is Boltzmann's constant,  $h$  is Planck's constant,  $E^*$  is the activation energy,  $T$  is the absolute temperature,  $f$  is the partition function,  $f^*$  is the partition function for the activated state, and  $C_a$  is the concentration of molecules absorbed on the surface.

For the case of surface desorption, this equation reduced to:

$$v = C_a (kT/h)e^{-E^*/T}$$

where  $kT/h = 10^{13} \text{ sec}^{-1}$ ,  $C_a = 10^{12} \text{ molecules/cm}^2$ ,  $E^* = 25 \text{ kcal/mole}$ ,  $T = 513^\circ\text{K}$ .

Based on the total surface area of  $100 \text{ cm}^2$  for 100 mg of sample, the calculated rate of decomposition is  $10^{14} \text{ molecules/sec-cm}^2$ . The observed rate of reaction at the same temperature is  $10^{12} \text{ molecules/sec-cm}^2$ .

## CONCLUSION

The polymer studied underwent four reactions. The first two involved the formation of the gaseous products 2-methyl-cyclopentadiene, carbon dioxide, and carbon monoxide.

The third region consisted of fragmentation of the DEN 43S segment of the polymer and could be observed in the formation of a white smoke.

Further polymerization-decomposition took place during the fourth region, resulting in little evolution of gas. Three of the four reactions appeared to overlap in time, thus accounting for imperfect correlation of DTA, TGA, and analytical data. However, the first reaction was well characterized in the three reaction zones and yielded the proposed reaction mechanism.

The authors wish to thank Dr. John Parker and Ernest Winkler of the Ames Research Center, NASA, Moffett Field, California for their helpful discussions and advice during this program. The authors also thank Dr. Robert Scholz for conducting the mass spectrometric analysis.

This work was supported by NASA Ames under Contract No. NAS7-343.

### References

1. D. A. Anderson and E. S. Freeman, *J. Appl. Polymer Sci.*, **1**, 192 (1959).
2. D. A. Anderson and E. S. Freeman, *Anal. Chem.*, **31**, 1697 (1959).
3. W. W. Wendlandt and G. R. Warton, *Anal. Chem.*, **34**, 1098 (1962).
4. E. S. Freeman and B. Carroll, *J. Phys. Chem.*, **62**, 393 (1958).
5. G. P. Shulman and H. W. Lochte, *J. Appl. Polym. Sci.*, **10**, 619 (1966).
6. H. C. Anderson, *J. Appl. Polymer Sci.*, **6**, 484 (1962).
7. J. A. Berson and W. A. Mueller, *J. Amer. Chem. Soc.*, **83**, 4940 (1961).

Received September 19, 1967

Revised February 2, 1968

## Emulsion Polymerization. V. Lowest Theoretical Limits of the Ratio $k_t/k_p$

J. L. GARDON, *Rohm and Haas Company, Spring House, Pennsylvania*  
19477

### Synopsis

It is assumed that the propagating polymeric radicals have no diffusive mobility in the very highly viscous medium within latex particles. Chain growth takes place on a lattice when the polymeric radical reacts with a monomer present on a lattice site adjacent to that occupied by the reactive chain end. For termination, two radical chain ends must be positioned on adjacent lattice sites at the same instant. The  $k_t/k_p$  ratios calculated with this model are either similar to or somewhat lower than the values determined in emulsion polymerization experiments. A minimum value of  $k_t/k_p$  can be calculated with the aid of the rate equation of Part III by assuming that only "living" polymer is produced during emulsion polymerization. This value of  $k_t/k_p$  is significantly lower than that calculated by the lattice model. Since the value corresponding to the lattice model gives the slowest practically achievable termination rate, it is concluded from these calculations that emulsion polymerization cannot be carried out under conditions in which chain termination is completely suppressed.

In emulsion polymerization the sole loci of polymerization are the monomer-swollen latex particles. During the so-called interval II, the monomer volume fraction  $\phi_m$  in the particles and the particle number  $N$  are constant and the conversion-time relationship is described by the following equations, as shown in Parts III<sup>1</sup> and IV<sup>2</sup>:

$$P = At^2 + Bt \quad (1)$$

$$A = 0.102 (k_p^{1.94}/k_t^{0.94})(d_m/d_p N_A)[\phi_m^{1.94}/(1 - \phi_m)^{0.94}]R \quad (2)$$

$$B = 0.5 (k_p/N_A)(d_m/d_p)\phi_m N \quad (3)$$

Here  $P$  is the volume of polymer,  $t$  is time,  $k_p$  and  $k_t$  are the respective rate constants of propagation and of termination,  $R$  is the rate of radical production in the aqueous phase,  $d_m$  and  $d_p$  are the monomer and polymer densities, and  $N_A$  is the Avogadro number.

Application of these equations to experimental data<sup>2</sup> and independent measurements<sup>2</sup> indicate that in interval II the ratio  $k_t/k_p$  is of the order of 10-100, by several orders of magnitude lower than in homogeneous polymerization at low conversion. The reason for this is that termination rate is diffusion-controlled. The particles contain 50-75% monomers and polymers of  $10^6$ - $10^7$  molecular weight. The viscosity in the particles is therefore high, and a diffusion controlled process must be slow.

For latexes of small particle size,  $P = Bt$  is the conversion-time relationship at low initiation rates,<sup>2</sup> as predicted by Smith and Ewart.<sup>3</sup> However, for latexes of very large particle size and at high initiation rates, the equation  $P = At^2$  describes the data with adequate accuracy. These observations are consistent with eqs. (1), (2), and (3). If  $k_t$  is very small,  $At^2 \gg Bt$ , and  $P = At^2$  would also hold in this case.

The Smith-Ewart case is valid for infinitely fast termination. In this paper the opposite case is examined, and a lowest theoretical limit of  $k_t$  is established. At this lowest theoretical limit the hypothetical conversion-time relationship is:

$$P = A_{\max} t^2 \quad (4)$$

Part I<sup>3</sup> shows that the conversion rate can be related to the average number of radicals per particle  $Q$ :

$$dP/dt = 2BQ \quad (5)$$

At very slow termination, a large fraction of all radicals survive in the particles. When  $k_t$  is smaller than a hypothetical limit (not necessarily equal to zero), all radicals survive. The average rate of entry of radicals into the particles is  $R/N$ , thus at time  $t$  in the absence of termination the following equations hold:

$$Q = (R/N) t = (1/2B) (dP/dt) \quad (6)$$

$$P = (BR/N) t^2 \quad (7)$$

$$A_{\max} = BR/N \quad (8)$$

If  $A_{\max}$  is set equal to  $A$  of eq. (2) and eqs. (3) and (8) are used, the following lowest theoretical limit for  $k_t/k_p$  is obtained:

$$(k_t/k_p)_{\min} = 0.185 \phi_m / (1 - \phi_m) \quad (9)$$

It is desirable to obtain some mechanistic interpretation for the existence of  $(k_t/k_p)_{\min}$  and to determine whether it is possible to obtain only "living" polymers during emulsion polymerization in such a way that no termination takes place throughout the reaction. In the very viscous polymerization medium, the polymer molecules and the bulk of the polymeric radicals can be assumed to be immobile. Only the chain ends of the radicals move, not by diffusion, but by growing.

The time  $t_1$ , the average interval between the addition of two monomers to a single chain, is needed for the calculations. It follows from eqs. (3) and (5) that the rate of volume increase of polymer in a single particle containing  $q$  radicals is  $(k_p/N_A)(d_m/d_p)\phi_m q$ . If  $V_m$  is the volume of a monomer unit, the following relationship holds:

$$V_m/t_1 = (k_p/N_A)(d_m/d_p)\phi_m q \quad (10)$$

The latex particle is assumed to be a lattice, and a chain propagates if its end moves from one lattice site to another. Such movement is obtained

when a monomer on a site adjacent to a radical chain end becomes converted and thus becomes the new chain end. If two chain ends are positioned at the same instant on two adjacent lattice sites, they cross-terminate.

If a radical chain end is at site A of Figure 1, none of sites B can contain a radical, otherwise the radical at A would have terminated. When a monomer adds to the radical, the chain end is displaced to one of the B sites. This event takes place in time  $t_1$ . If a radical is located on any of the C sites which neighbor the B site where the chain end is now located, termination will take place. Thus the probability  $p_1$  that termination takes place in time  $t_1$  can be calculated.

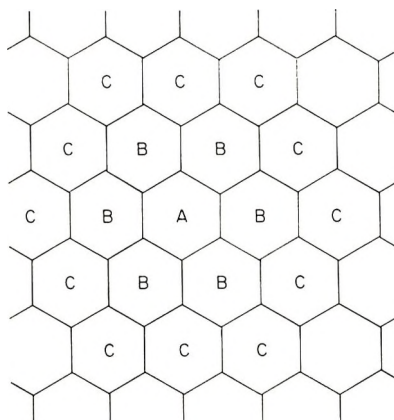


Fig. 1. Lattice model for termination rate.

A new parameter, the second-neighbor coordination number  $\sigma$ , is defined. If a radical chain end moves from the original site to a neighboring site,  $\sigma$  is the number of sites which neighbor the new location of the chain end but do not include the original site or any site adjacent to the original site. In terms of Figure 1,  $\sigma$  is the number of C neighbors of any B site. In the two-dimensional hexagonal lattice of Figure 1,  $\sigma$  is 3. In a close-packed three-dimensional hexagonal lattice,  $\sigma$  is 8.

The volume of the particle is  $V$ , and the volume of a lattice site is assumed to be  $V_m$ . The total number of sites is  $V/V_m$ .

The number of chain ends with which a given radical can terminate is  $q - 1$ . The probability that a given site is occupied by any of these chain-ends is  $(q - 1)$  divided by the total number of sites, or  $(q - 1)(V_m/V)$ . The number of sites which could be occupied by a radical, so that the original radical can terminate with it while moving from site A to a site B, is  $\sigma$ . Thus the probability that a chain will terminate in time  $t_1$  is:

$$p_1 = \sigma(q - 1)(V_m/V) \quad (11)$$

Let  $dp$  be the probability that a given chain terminates in  $dt$ .

$$dp/dt = p_1/t_1 \quad (12)$$

Substitution from eqs. (10) and (11) gives:

$$dp/dt = (k_p/N_A) (d_m/d_p V) \phi_m \sigma q(q-1) \quad (13)$$

Each termination event reduces the number of radicals in a particle by 2. The rate of radical entry into the particles is  $R/N$ . The number of radicals within particles is therefore given by the eq. (14):

$$dq/dt = R/N - 2dp/dt \quad (14)$$

Correspondingly, the following relationship was used to derive the conversion-time relationship of eqs. (1), (2), and (3) [cf. eq. (25) of Part III<sup>1</sup>]:

$$dq/dt = R/N - (k_t/VN_A)q(q-1) \quad (15)$$

This equation is phenomenologically equivalent to combined eqs. (13) and (14). For mathematical equivalence, the following relationship must hold:

$$(k_t/k_p)_L = 2\sigma(d_m/d_p)\phi_m \quad (16)$$

Here the subscript L indicates the lattice treatment. It is reasonable to associate  $(k_t/k_p)_L$  with the slowest possible termination rate and to compare it to  $(k_t/k_p)_{\min}$  of eq. (9).

Table I shows that  $(k_t/k_p)_L$  calculated with  $\sigma = 8$  (for a closely packed, hexagonal lattice) is always significantly larger than  $(k_t/k_p)_{\min}$  (that corresponds to absence of termination). It is concluded that some termination between chains must take place even in an extremely viscous medium of polymerization. Table II shows  $k_t/k_p$  ratios calculated from experimental values of  $A$ ,  $B$ ,  $N$ ,  $R$ , and  $\phi_m$  by eqs. (1)–(3). These values are either of the same order as or higher than the lowest possible value calculated from

TABLE I  
Values of  $k_t/k_p$

$\phi_m$	$(k_t/k_p)_{\min}$ , by eq. (9)	$(k_t/k_p)_L$ , by eq. (16) for $\sigma = 8$ , $d_p/d_m = 1.3$
0.1	0.021	1.23
0.25	0.062	3.08
0.5	0.185	6.15
0.75	0.555	9.25

TABLE II

Monomer	$\phi_m$	Range of $k_t/k_p$ from experimental values reported in Part IV <sup>2</sup>
Methyl methacrylate	0.73	29–115
Styrene	0.6	15–150
Butyl methacrylate	0.65	4–88

the lattice model. Evidently, these experimentally determined  $k_t/k_p$  ratios are consistent with the values to be expected for a very viscous reaction medium.

### References

1. J. L. Gardon, *J. Polym. Sci. A-1*, **6**, 665 (1968).
2. J. L. Gardon, *J. Polym. Sci. A-1*, **6**, 687 (1968).
3. J. L. Gardon, *J. Polym. Sci. A-1*, **6**, 623 (1968).

Received December 28, 1967

## Emulsion Polymerization. VI. Concentration of Monomers in Latex Particles

J. L. GARDON, *Rohm and Haas Company,  
Spring House, Pennsylvania 19477*

### Synopsis

Nonpolymerizing latex particles surrounded by an aqueous phase saturated with monomer absorb only a finite amount of monomer, even if the monomer is a good solvent for the polymer, because the surface energy of each particle increases on swelling. At equilibrium the change in surface energy and the free energy of mixing exactly balance. Equations based on this thermodynamic principle predict with good accuracy the saturation swelling of crosslinked and uncrosslinked latex particles and the partitioning of monomer between the aqueous phase and latex particles at partial saturation. The available experimental data on swelling of latex polymers with monomers are reviewed. Earlier papers assumed that during emulsion polymerization the monomer concentration in the latex particles is independent of conversion as long as monomer droplets are present. This assumption is shown to be a justifiable approximation. The thermodynamics of the swelling of latex particles with a blend of two monomers is presented. The calculations indicate that copolymerization in emulsion should define reactivity ratios differing from those of homogeneous copolymerization by not more than 40% if the solubility of the comonomers in water is low. The reactivity ratio scheme is strictly applicable to emulsion copolymerization if the solvent properties of the two comonomers are identical.

In the first four papers of this series (Parts I-IV<sup>1-4</sup>), it was assumed that the sole locus of chain propagation during emulsion polymerization is in the latex particles swollen by monomer. The purpose of the present paper is to review the theoretical considerations and experimental facts related to the swelling of the latex particles by monomers.

### THERMODYNAMIC THEORY

#### Saturation Swelling of Uncrosslinked Latex Particles

The monomer is assumed to have limited solubility in water. Such a monomer (or other suitable solvent) is added to a dead, nonpolymerizing latex so that the aqueous phase should become saturated with monomer. Even if the monomer is a good solvent for the polymer and is miscible with the polymer at any ratio in bulk, only a limited amount of monomer is absorbed by the latex particles because the surface energy increase on swelling partially compensates for the free energy of mixing. It is assumed that water does not dissolve in the latex particles or in the pure monomer.

This monomer is in excess to that needed to saturate the latex particles and water. Experiments in this laboratory proved that no polymer is dissolved in this excess monomer. Since the three phases are in equilibrium, the chemical potential of the monomer in the particles has to be the same as that of the pure monomer.

Morton et al.<sup>5</sup> calculated the chemical potential change due to the increase in interfacial free energy caused by the increase of surface area on swelling. An alternate starting point for the derivation is the classical Gibbs-Thomson equation<sup>6</sup> which gives the difference between chemical potentials of a material in a sphere of finite radius  $r$  and in a sphere of infinite radius:

$$\Delta\mu_s = \mu(r) - \mu(\infty) = 2V_m\gamma/r \quad (1)$$

Here  $\Delta\mu_s$  is the surface term of the chemical potential,  $V_m$  is the molar volume of the monomer,  $\gamma$  is the interfacial free energy (for liquid-liquid systems equal to the interfacial tension), and  $r$  is the particle radius. It is convenient to express  $r$  in terms of the radius of the unswollen particle  $r_0$ ,

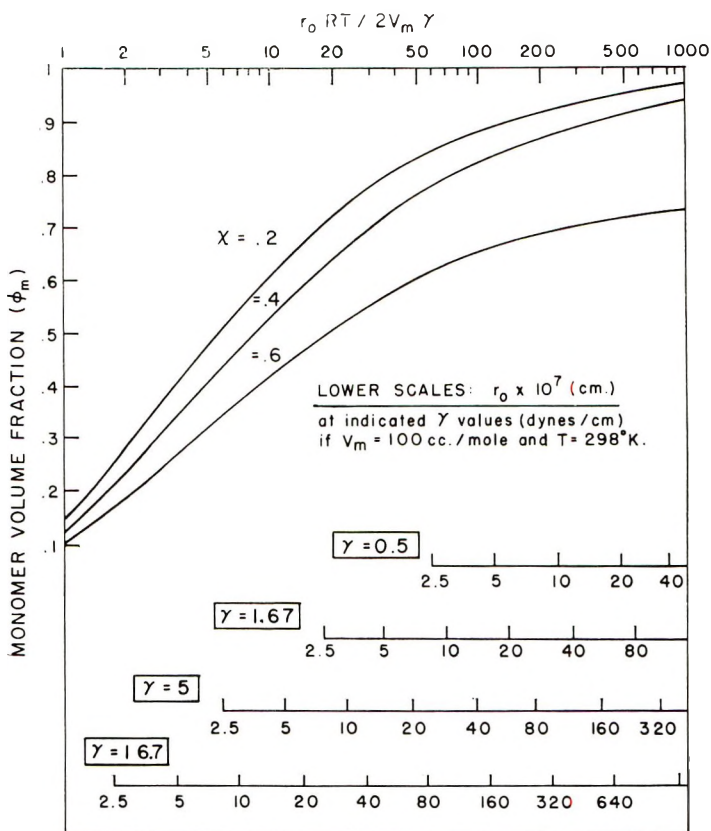


Fig. 1. Saturation swelling of uncrosslinked latex particles with monomers as described by Morton et al.<sup>5</sup> [eqs. (2) and (4)].

the volume swelling ratio  $H_v$ , the monomer volume fraction in the particles  $\phi_m$ , or polymer volume fraction  $\phi_p$ :

$$(r/r_0)^3 = H_v = 1/(1 - \phi_m) = 1/\phi_p \quad (2)$$

When a low molecular weight solvent (or monomer) is mixed with a very high molecular weight polymer, its chemical potential is reduced by  $\Delta\mu_M$  given in the Flory-Huggins theory:<sup>7</sup>

$$\Delta\mu_M/RT = \ln(1 - \phi_p) + \phi_p + \chi\phi_p^2 \quad (3)$$

Here  $R$  is the gas constant,  $T$  is temperature, and  $\chi$  is an interaction constant.

At equilibrium with pure monomer the sum of  $\Delta\mu_M$  and  $\Delta\mu_S$  is zero. Combination of eqs. (1), (2), and (3) gives the Morton, Kaizerman, and Altier equation:

$$-H_v - H_v^2 \ln(1 - 1/H_v) = \chi + (2V_m \gamma/RT)(H_v^{5/3}/r_0) \quad (4)$$

The  $\phi_m$  values calculated by this equation are shown in Figure 1.

### Partial Swelling of Uncrosslinked Latex Particles

If not enough monomer is added to the latex to saturate it, there is no pure monomer phase present. In the vapor phase in equilibrium with the latex the monomer vapor pressure is  $p$ , lower than the vapor pressure of the pure monomer,  $p_0$ . The chemical potential of the monomer in the latex particles is:

$$\Delta\mu = RT \ln(p/p_0) = \Delta\mu_M + \Delta\mu_S$$

Under these conditions the swelling of latex particles is described by eq. (5):

$$H_v^2 [\ln(p/p_0) - \ln(1 - 1/H_v)] - H_v = \chi + (2V_m \gamma/RT r_0) H_v^{5/3} \quad (5)$$

Typical results calculated according to eq. (5) are shown in Figure 2. A similar equation was also derived by Vanzo et al.,<sup>8</sup> but these authors failed to distinguish between the radii of swollen and unswollen particles.

### Saturation Swelling of Crosslinked Latex Particles

If a difunctional comonomer is used at polymerization, the latex particles become crosslinked. On swelling, the crosslinked network strains and stores elastic energy, which limits the swelling in a manner similar to the restriction due to surface energy.

The contribution of the elastic energy to the chemical potential difference between pure solvent (monomer) and swelling solvent,  $\Delta\mu_E$ , is given by the Flory-Rehner<sup>7,9</sup> theory. The equation shown below is valid only for densely crosslinked polymers of high molecular weight.

$$\Delta\mu_E = (V_m d_p/M_c)(\phi_p^{1/3} - \phi_p/2)RT$$

Here  $d_p$  is the polymer density and  $M_c$  is the molecular weight between crosslinks. At saturation swelling the sum of  $\Delta\mu_M$ ,  $\Delta\mu_S$ , and  $\Delta\mu_F$  is zero. The resulting equation is:

$$-H_v^2 \ln \left( 1 - \frac{1}{H_v} \right) - H_v - \left( \frac{V_m d_p}{M_c} \right) \left( H_v^{5/3} - \frac{H_v}{2} \right) = \chi + \left( \frac{2V_m \gamma}{RT} \right) \left( \frac{H_v^{5/3}}{r_0} \right) \quad (6)$$

### Swelling of Latex Particles by a Blend of Two Monomers

Krigbaum and Carpenter<sup>10</sup> considered the swelling of insoluble cross-linked polymer networks by binary solvent mixtures in bulk. By equating the chemical potentials of solvents 1 and 2 in the ternary polymer-containing phase and in the binary polymer-free phase, they calculated the value of a composition ratio  $K$ , defined in terms of the volume fractions of solvents 1 and 2 in the ternary phase,  $\phi_1$  and  $\phi_2$ , and in the binary phase,  $v_1$  and  $v_2$ .

$$K = (\phi_1/\phi_2)/(v_1/v_2) \quad (7)$$

Their theory also contains the parameter  $\phi_p$ , the polymer volume fraction in the ternary phase. The dependence of  $\phi_p$  on solvent composition is not defined.

The intrinsic parameters of the system are Flory-Huggins constants for solvent-solvent (1-2) and solvent-polymer (1- $p$  and 2- $p$ ) interactions and the ratio

$$j = (\text{molar volume of 1})/(\text{molar volume of 2}) \quad (8)$$

The Krigbaum-Carpenter equation is:

$$-\ln K = (1 - j) \ln (\phi_2/v_2) + 2\chi_{12}(\phi_2 - v_2) + (\chi_{12} + \chi_{1p} - j\chi_{2p})\phi_p \quad (9)$$

The derivation of this equation contains no term which limits it to bulk swelling of crosslinked polymers. It is applicable to any system in which a ternary phase of a polymer and two solvents is in equilibrium with a binary phase of two solvents. The mechanism, by which the swelling is limited, is not implicit to the theory; the limitation of swelling is expressed by the parameter  $\phi_p$ . It follows that eq. (9) is also applicable to latex swelling. If water does not dissolve in the monomer phase and thereby does not change the chemical potential of the components there, it cannot influence the applicability of the theory because at equilibrium the activity of each monomer in the two organic phases and in the aqueous phase is the same. However, a careful distinction has to be made in that  $v_1$  and  $v_2$  are the volume fractions in the binary monomer phase if the theory is to be applied to latex swelling.

The following relationships hold by definition:

$$\begin{aligned} v_1 &= 1 - v_2 \\ \phi_1 &= 1 - \phi_p - \phi_2 \\ K &= (1 - v_2)\phi_2/v_2(1 - \phi_p - \phi_2) \end{aligned}$$

To obtain an explicit relationship between  $\phi_2$ , the dependent, and  $v_2$ , and independent variable, eq. (9) is rearranged:

$$\ln \phi_2^j / (1 - \phi_p - \phi_2) - 2\chi_{12}\phi_2 = \ln v_2^j / (1 - v_2) - 2\chi_{12}v_2 + J \quad (10)$$

$$J = (\chi_{12} + \chi_{1p} - j\chi_{2p})\phi_p \quad (11)$$

Equation (10) contains four parameters:  $j$ ,  $\phi_p$ ,  $\chi_{12}$ , and  $J$ . The new parameter  $J$  contains all five parameters characteristic of the system. Once the dependence of  $\phi_2$  upon  $v_2$  is defined, the composition ratio  $K$  can also be calculated as a function of  $v_2$  and any parameter.

Some theoretical results are shown in Figure 3. The values of the five parameters are chosen to conform with the range found in experiments. These curves will be discussed at the end of this paper and in the context of copolymerization.

## EXPERIMENTAL METHODS

### Static Centrifugation

Excess monomer is stirred into a radical-free latex, the mixture is subsequently centrifuged, the supernatant monomer is removed, and the monomer content of the latex is determined. In this laboratory it was found convenient to do these determinations at various latex concentrations. If  $X$  is the weight fraction of polymer in the monomer-free latex,  $G$  is the weight of monomer-saturated sample which contains  $P$  weight of polymer,  $y$  is the saturation weight fraction of monomer in water, and  $H_w$  is the weight swell ratio, the following relationship holds:\*

$$G/P = H_w + (1 + y)[(1/X) - 1] \quad (12)$$

Table I shows that the determined value of  $H_w$  is indeed independent of  $X$  and that  $y$  obtained from latex swelling data agrees well with independent values. Other authors determined swelling after centrifugation by volumetry or spectrophotometry. The advantage of the present procedure is that experimental errors due to monomer polymerization, emulsion inversion and monomer emulsification can be easily detected. Furthermore, the results are corrected for the solubility of monomer in water.

It should be noted that the value of  $H_w$  is related to  $H_v$ , the volume swell ratio, to the weight fraction of polymer and monomer,  $\Omega_p$  and  $\Omega_m$ , and to polymer and monomer density,  $d_p$  and  $d_m$ , by the following equations:

$$H_w = (H_v - 1)(d_m/d_p) + 1 = 1/\Omega_p = 1/(1 - \Omega_m) \quad (13)$$

To convert  $H_w$  to  $H_v$ , the density values can be taken from Table III of Part II.

\* A monomer saturated latex sample of gross weight  $G$  contains  $(P/X - P)$  weight of water. The weight of monomer dissolved in water is  $y(P/X - P)$ , and the weight of monomer absorbed in latex particles is  $(H_w - 1)P$ . Consideration of material balance leads to eq. (12).

TABLE I  
Illustration of Experimental Results Obtained by the Static Centrifugation  
Method of This Laboratory<sup>a</sup>

Polymer	100X	G/P	H <sub>w</sub>
Poly(methyl methacrylate) <sup>b</sup>	14.31	9.419	3.34
	12.09	10.682	3.41
	9.11	13.409	3.29
	6.05	19.109	3.32
Poly(ethyl acrylate) <sup>c</sup>	15.174	9.793	4.15
	10.069	13.134	4.11
	5.067	23.100	4.18
Poly( <i>n</i> -butyl acrylate) <sup>d</sup>	15.40	8.642	3.13
	12.15	10.441	3.18
	9.05	13.212	3.11
	6.42	17.763	3.13
Poly( <i>n</i> -butyl methacrylate) <sup>e</sup>	16.22	7.800	2.61
	12.17	9.976	2.72
	8.11	14.153	2.76
	4.06	26.413	2.66
Poly(methyl acrylate) <sup>f</sup>	11.9	11.59	3.82
	8.2	15.78	4.02
	4.46	26.43	3.94

<sup>a</sup> All polymers were prepared isothermally at 40/60 monomer/polymer ratio; 1% sodium lauryl sulfate (SLS) and 0.35% K<sub>2</sub>S<sub>2</sub>O<sub>8</sub> were used for the first four polymers; for poly(methyl acrylate) 0.5% SLS and 0.1% K<sub>2</sub>S<sub>2</sub>O<sub>8</sub> were used; the temperature was 40°C. for the first three and 60°C. for the last two polymers. The particle radii were determined by soap titration. The swelling measurements were made at room temperature. The values of *G*, *P*, and *X* were experimentally determined; *y* was calculated from the least-squares fit to eq. (12), and *H<sub>w</sub>* was calculated with the aid of this *y* value. The values of *y<sub>lit</sub>* are the independently determined monomer solubilities in water.<sup>11</sup>

<sup>b</sup> *r*<sub>0</sub> = 0.119 μ; *y* = 0.015; *y<sub>lit</sub>* = 0.016.

<sup>c</sup> *r*<sub>0</sub> = 0.085 μ; *y* = 0.010; *y<sub>lit</sub>* = 0.015.

<sup>d</sup> *r*<sub>0</sub> = 0.036 μ; *y* = 0.004.

<sup>e</sup> *r*<sub>0</sub> = 0.051 μ; *y* = 0.0053.

<sup>f</sup> *r*<sub>0</sub> = 0.052 μ; *y* = 0.050; *y<sub>lit</sub>* = 0.052.

### Static Vapor Pressure Method

Increasing amounts of monomer are added to a radical-free latex. Below saturation the vapor pressure increases with monomer concentration, above saturation the vapor pressure stays constant. Although the endpoint is difficult to determine precisely, this method is most convenient to use at nonambient conditions and for studying latex swelling below the saturation level.

### Disappearance of Monomer Droplets During Polymerization

The transition between intervals II and III occurs at this point, at a fractional conversion equal to  $\Omega_p = 1/H_w$ . One can either determine visually the disappearance of monomer droplets or one can note the drop in vapor pressure; during intervals I and II the vapor pressure over the system is constant.

### Maximum in the Conversion Rate–Time Curve of Emulsion Polymerization

In interval II the rate, given by the slope of the conversion–time curve, is either constant or increases with time. The rate is proportional to the  $\phi_m Q$  product, where  $Q$  is the average number of radicals per particle. At a fractional conversion larger than  $\Omega_p$ , the value of  $\phi_m$  can no longer correspond to saturation swelling and must therefore decrease with increasing time. If the decrease in  $\phi_m$  is not compensated by an undue increase in  $Q$ , the overall conversion rate reaches a maximum at a fractional conversion equal to the saturation value of  $\Omega_p$ . In other words, there is an inversion in the conversion–time curve at  $\Omega_p$  fractional conversion as shown in Figure 1 of Part IV for styrene and *n*-butyl methacrylate. The calculation of  $\Omega_p$  from this inversion point is justified only for monomers which do not show a marked gel effect in interval III. For example, Figure 1 of Part IV shows that, for methyl methacrylate, the inversion point in the conversion–time curve is at a fractional conversion higher than that corresponding to  $\Omega_p$ .

## RESULTS AND DISCUSSION

### Review of Data Obtained with Homopolymer Latexes Saturated with Their Own Monomers

According to eq. (4), the swelling of a given latex by a given monomer depends on such experimental variables such as the particle size, the interfacial tension between particle and water,  $\gamma$ , and the temperature. The swell ratio increases with increasing temperature and particle size, and with decreasing  $\gamma$ . Though one would expect  $\gamma$  to depend mainly on soap concentration, other factors may also influence it. Polar chain ends at the particle–water interface reduce  $\gamma$ , and salts present in water tend to increase it.<sup>12</sup> Even at the same polymer, monomer, soap level, particle radius, and temperature, the equilibrium swelling of the latex may depend upon the conditions of its synthesis. For convenience, the synthesis conditions are disregarded here. Tables II–IV show the weight swell ratio values as functions of particle size, soap, and temperature of measurement.

It should be emphasized that, in most of the cited papers, the monomer concentration of latexes was considered to be of secondary importance. The experimental methods were often described inadequately, and no attempt was made to verify results by using different methods or by comparing them with results of previous literature. The monomer concentration in the particles was given in a variety of units, such as monomer/polymer ratio or moles of monomer per liter of swollen polymer. In Tables II–IV all results are converted to  $H_w$ . The reported radius values refer to the unswollen latex. The radius values of this laboratory are those obtained by soap titration.

TABLE II  
Saturation Swelling of Miscellaneous Latexes by Their Own Monomers

Monomer	$r_0 \times 10^6$ , cm.	Soap		Exptl. method <sup>a</sup>	Temperature, °C.	$H_w$	Ref. <sup>b</sup>
		% on polymer	Type				
Chloroprene	7-9	2	K laurate	M	40	2.7	13
Vinylidene chloride	2	6-12	K laurate	S	Room	1.2	14
Vinyl chloride	?		Amphoseife	M, S	50	1.49	15
	?	?		D	?	1.3	16
Isoprene	2-3	5	ORR	C	Room	1.85	17
Butadiene	?	10	SF Flake	D	50	1.91	18
	?	0.6	SF Flake	D	50	1.66	18
	5-7	5	ORR	S	Room	1.85	19
Vinyl acetate	15	2	Pluronic F 68	C	Room	7.6	20
	5	7	Pluronic F 68	C	Room	5.6	20
	13	None		C	40	8.4 <sup>c</sup>	21
	?	?		S	30	1.7	8
	?	?		S	60	3.1	8
Vinyl caproate	8	10	Na lauryl sulfate	C	Room	7.8	22
Methyl acrylate	8	10	Na lauryl sulfate	D	25	6.8	22
	5.2	0.5	Na lauryl sulfate	C	25	3.9	TW

Ethyl acrylate	?	10	Na lauryl sulfate	M	25	5.9	23
	?	10	Na lauryl sulfate	D	25	5.9	23
	8.5	1	Na lauryl sulfate	C	Room	4.15	TW
<i>n</i> -Butyl acrylate	10	0.56	Triton X-202	C	Room	3.75	TW
	3.6	1	Na lauryl sulfate	C	Room	2.75	TW
<i>n</i> -Butyl methacrylate	5.1	1	Na lauryl sulfate	C	Room	2.69	TW
	3.0	1	Na lauryl sulfate	C	Room	2.52	TW
	3.0	1	Na lauryl sulfate	M	45	2.20	TW
Isobutyl methacrylate	3.2	1	Na lauryl sulfate	C	Room	2.67	TW
	3.2	1	Na lauryl sulfate	M	45	2.0	TW
Methylstyrene	3-20	4-20	Amphoseife	M	35-56	1.7-2.4	24
	3-4	6-8	Na lauryl sulfate	M, C	30-40	4-6	25
	3-4	6-8	Na lauryl sulfate	M, C	50-70	2-5	25
Dimethylstyrene	2	4-20	Amphoseife	M	45	2	24

<sup>a</sup> Experimental methods: C = static centrifugation; S = static vapor pressure; D = disappearance of monomer droplets; M = maximum in conversion rate.

<sup>b</sup> TW stands for this work.

<sup>c</sup> The vinyl acetate swell ratio of 8.4 was obtained by extrapolating partial swelling data to saturation swelling.

TABLE III  
 Saturation Swelling of Polystyrene Latexes by Styrene

$r_0 \times 10^6$ , cm.	Soap		Experi- mental method <sup>a</sup>	Temper- ature, °C.	$H_w$	Ref.
	% on polymer	Type				
2	1	Na lauryl sulfate	C	Room	2.35	TW
4	?		C	Room	2.52	25
?	?		D	?	2.00	16
5-9	8-9	Na lauryl sulfate	C	Room	2.1-2.7	22, 23
			M	25	2.2	
			D	25	2.2	
4-6	1-5	ORR	C	Room	2.25	17
~5	3	K laurate	C	40	2.57	27
	3	K laurate	C	50	2.51	
	3	K laurate	C	70	2.1	
3	2	Aerosol MA	C	Room	2.2	28
9			C	Room	3.0	
4.5	5.7	Na lauryl sulfate	C, D <sup>b</sup>	30.5	2.08	25
4.4	5.7	"		40.5	2.22	
4.6	6.0	"		51	2.64	
3.8	8.5	"		50.2	3.27	
4.6	7.4	"		50.2	3.27	
3.1	8.9	"		70.9	2.58	
~4	8.5	Amphoseife	M	35	2.30	24, 29
				40	2.35	
				45	2.47	
				50	2.11	
				56	2.47	
?	?		S	30	1.82	8
?	?		S	60	2.20	8
1.35		K laurate <sup>c</sup>	C	Room	2.81 <sup>b</sup>	5
4.0		K laurate	C	Room	3.92 <sup>b</sup>	5
8.65		K laurate	C	Room	5.60 <sup>b</sup>	5

<sup>a</sup> See Table II.<sup>b</sup> Static centrifugation and monomer drop disappearance gave results in excellent agreement.<sup>c</sup> After synthesis was complete, K laurate was post-added to the level of the critical micelle concentration in the aqueous phase. These swelling results define  $\chi = 0.43$  and  $\gamma = 4.5$  dyne/cm. in terms of eq. (4).

The following points are of interest in connection with the data of Tables II-IV.

(a) Static methods (either centrifugation or vapor pressure, C or S) and kinetic methods (either monomer drop disappearance or, at fast termination rates, maximum in conversion rate, D or M) give similar swell ratios for all monomers where such comparisons can be made (styrene; methylstyrene; butadiene; methyl and ethyl acrylate; methyl, *n*-butyl, and isobutyl methacrylate). During polymerization the particles must be swollen to an extent corresponding to static equilibrium at conversion values near the point where the monomer droplets disappear. It is also

TABLE IV  
Saturation Swelling of Poly(methyl Methacrylate) Latexes by Methyl Methacrylate

$r_0$ $\times 10^6$ , cm.	Soap		Experi- mental method <sup>a</sup>	Temper- ature, °C.	$H_w$	Ref.
	% on polymer	Type				
4-6	4.7	Amphoseife	C	Room	3.68	13
4	4.7	Amphoseife	M	45	3.5	13
11-14	10	Na lauryl sulfate	C	Room	3.5-4.1	24
	10	Na lauryl sulfate	D	25	3.8	24
22	0.2	Tergitol 7	D	60	3.3	22
5	0.2	Tergitol 7	D	60	2.4	22
14	1	Na lauryl sulfate	D	40	3.4	TW
11.9	1	Na lauryl sulfate	C	Room	3.29 <sup>b</sup>	TW
3.6	6	Na lauryl sulfate	C	Room	2.29 <sup>b</sup>	TW
11.9	—		C	Room	3.52 <sup>c</sup>	TW
4.6	—		C	Room	3.11 <sup>c</sup>	TW
2.3	—		C	Room	2.96 <sup>c</sup>	TW

<sup>a</sup> See Table II.

<sup>b</sup> These results define  $\chi = 0.58$  and  $\gamma = 4.90$  dyne/cm. by eq. (4).

<sup>c</sup> These results define  $\chi = 0.585 \pm 0.005$  and  $\gamma = 1.6 \pm 0.20$  dyne/cm. by eq. (4).

TABLE V  
Interfacial Tensions Between Pure Monomer and Water Phases<sup>a</sup>

Monomer	Interfacial tension, dyne/cm.		Latex characteristics		
			Radius 10 <sup>6</sup> , cm.	Weight swell ratio $H_w$	Monomer solubility in water, g./l. <sup>b</sup>
	To pure water	To latex			
Styrene	38.4	34.0	4.0	2.35	0.07
Isobutyl methacrylate	—	21.4	3.2	2.67	5.0
<i>n</i> -Butyl methacrylate	—	18.5	5.1	2.59	4.0
<i>n</i> -Butyl acrylate	—	13.3	3.6	2.75	10.0
Methyl methacrylate	13.5	11.0	11.9	3.29	15.9
Ethyl acrylate	—	5.9	8.5	4.15	15.1

<sup>a</sup> All latexes used in the measurements were saturated with their own monomer and contained 10% solids based on water and 1% sodium lauryl sulfate based on polymer. The interfacial tensions were determined by the ring method at room temperature.

<sup>b</sup> Data of Bovey,<sup>32</sup> Rohm & Haas,<sup>11</sup> and Table II.

reasonable to suppose that the monomer concentration in the particles would be close to the equilibrium value at much lower conversions. Consequently, the hypothesis advanced by Harkins<sup>30</sup> that the monomer concentration in the particles during polymerization is adjusted by a steady state of monomer absorption into and monomer consumption inside the particles is not tenable.

(b) The best investigated monomers are styrene and methyl methacrylate (Tables III and IV), and the reported swell ratios vary in a relatively narrow range, 2-3 for styrene and 3-4 for methyl methacrylate,

despite the great variation in the particle size, the soap quality, the soap level, and the experimental temperature, because the effects of these variables are partially self-compensating. For example, higher soap levels reduce the interfacial tension and, coincidentally, also reduce the particle size at synthesis. This justifies the assignment of typical  $\phi_m$  values to monomers in Table III of Part II.

(c) Among the monomers which are known to be good solvents for their polymers in bulk, the ones with better solubility in water, such as vinyl acetate, methyl methacrylate, ethyl and methyl acrylate, swell their latex polymers to a greater extent than the poorly water-soluble styrene, methylstyrene, butyl acrylate and methacrylate, butadiene, and isoprene.

TABLE VI  
Saturation Swelling of Styrene and Ethyl Acrylate  
Homopolymer and Copolymer Latexes with These Monomers<sup>a</sup>

Composition (St/EA), wt.-%		$r_0 \times 10^6$ , cm.	Weight swell ratio $H_w$
Polymer	Swelling monomer		
56/44	100/0	6.0	2.73
	80/20		2.73
	56/44		3.02
	20/80		3.31
	0/100		3.43
100/0	100/0	4.0	2.35
	0/100		2.63
0/100	100/0	8.5	2.46
	0/100		4.15

<sup>a</sup> The latexes contained 1% sodium lauryl sulfate on polymer. The static centrifugation method was used to determine swelling. After the exact swell ratios were determined, monomer mixtures were added to the 56 St/44 EA copolymer latex samples containing 10% polymer solids so that  $2/3$  of the monomer should saturate the latex phase and  $1/3$  should be in excess. The excess monomer was separated by centrifugation and was analyzed by gas-liquid chromatography. The composition of this monomer phase was identical to the applied monomer composition indicating that neither of the monomers swells the latex preferentially. The value of  $K$ , defined in eq. (7), was therefore unity.

One reason for this may be that the monomer dissolved in water causes a reduction in the interfacial tension between the aqueous and organic phases. A correlation between the interfacial tension, the monomer solubility in water, and  $H_w$  is shown in Table V. An illustration of the surface tension effect is also shown in Table VI. The monomers ethyl acrylate and styrene have about the same solubility parameters<sup>31</sup> and hence the same solvent power. Nevertheless, ethyl acrylate is a more powerful swelling agent than styrene for poly(ethyl acrylate) or polystyrene homopolymers and styrene-ethyl acrylate copolymer because the interfacial tension between it and water is lower.

### Experimental Tests for the Thermodynamic Theory

Figure 2 shows that the experimental results and the theoretical predictions for partial latex saturations are very similar. The theoretical predictions fit very well the data for poly(methyl methacrylate), but less closely the data for polystyrene. It is of interest that below saturation (as in the interval III of emulsion polymerization), the partitioning of the monomer between the latex particles and the aqueous phase adjusts itself so that the aqueous phase is closer to saturation than the latex particles.

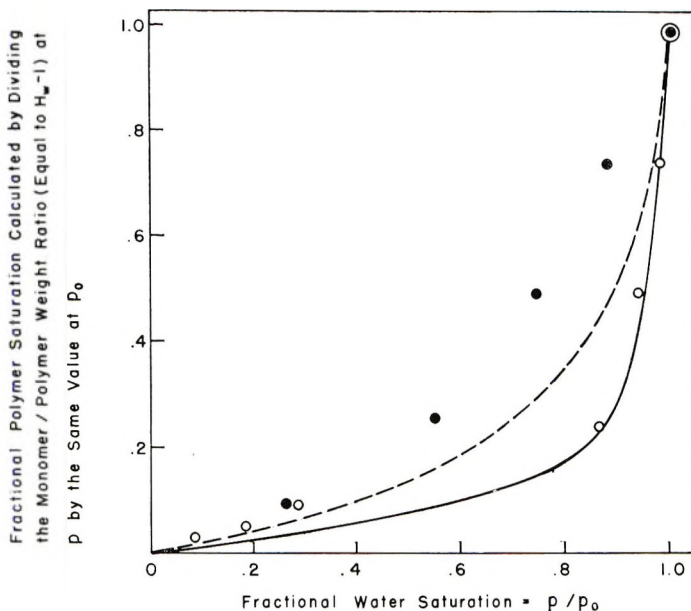


Fig. 2. Swelling of latex particles at partial saturation: (●) polystyrene/styrene,  $r_0 = 0.02 \mu$ , saturation swell weight ratio = 2.35, 1% Na lauryl sulfate on polymer; (---) theory by eq. (5) for this polystyrene latex with assumed  $\chi = 0.35$  and  $\gamma = 35$  dyne/cm.; (○) poly(methyl methacrylate),  $r_0 = 0.119 \mu$ , saturation swell ratio = 3.29, 1% Na lauryl sulfate on polymer; (—) theory by eq. (5) for this MMA latex with assumed  $\chi = 0.55$  and  $\gamma = 11.0$  dyne/cm. The assumed  $\chi$  and  $\gamma$  values exactly satisfy the swelling data obtained at saturation. The value of  $p/p_0$  is the actual vapor pressure divided by the saturation value. This ratio is equal to fractional water saturation because Henry's Law was shown to hold for latex-free water. For obtaining  $p/p_0$ , the vapor in equilibrium with the latex samples was analyzed by gas-liquid chromatography. The value of  $p/p_0$  is the ratio of peak heights corresponding to the monomer at partial and at complete saturation.

Table VII shows that the swelling of crosslinked latex particles gives very plausible values of crosslinking efficiency when treated in terms of eq. (6). The crosslinking efficiencies calculated from latex swelling data agree within experimental error with those calculated from swelling results obtained in a homogeneous medium.

From what is known about polymer-solvent interactions,<sup>33</sup> the value of  $\chi$  should be about 0.2–0.6 for most practical systems. The value of  $\gamma$  may range from 1 to 30 dyne/cm. The radii of latexes for which swelling data are available range from 2 to  $14 \times 10^{-6}$  cm. If the monomer molar volume is about 100, the swell ratios at room temperature should be in the 1.6–20 range when calculated by the theory of Morton et al. [eq. (4)].

TABLE VII  
Swelling of Crosslinked Copolymers of Butyl Acrylate and Butylene Diacrylate<sup>a</sup>

BDA in polymer, %	$r_0 \times 10^5$ , cm.	Latex swelling with butyl acrylate monomer <sup>b</sup>		Bulk swelling with pyridine <sup>c</sup>	
		$H_v$	Cross- linking efficiency, % <sup>d</sup>	$H_v$	Cross- linking effi- ciency, % <sup>d</sup>
0	1	4.43	—	—	—
0.1	1.38	4.21	100	12.8	100
0.25	1.38	3.98	51	10.0	88
0.5	1.32	3.79	43	8.6	62
1	1.32	3.56	58	6.4	55
5	1.43	2.49	36	3.1	52

<sup>a</sup> All latex samples contain 0.56% Triton X-202 based on polymer.

<sup>b</sup> Latex swelling with butyl acrylate was determined by static centrifugation. To interpret these data, 100% crosslinking efficiency was assumed for 0.1% butylene diacrylate (BDA) in the polymer. The combined data of 0 and 0.1% BDA define, in terms of eq. (6),  $\chi = 0.565$  and  $\gamma = 3.25$  dyne/cm. For latexes containing more than 0.1% BDA, the  $M_c$  values were calculated with the aid of these fixed  $\chi$  and  $\gamma$  values.

<sup>c</sup> "Bulk swelling" in pyridine was carried out by adding pyridine to the latex, and subsequently distilling out the water. For all crosslinked polymers a dispersion of swollen particles was thus obtained. The swelling of particles was estimated with the aid of the Einstein law from the viscosity of the pyridine dispersion. In calculating  $M_c$  values, it was assumed that  $\gamma$  between the particles (swollen with pyridine) and pyridine is zero. Assuming 100% crosslinking efficiency, the swelling data of the polymer with 0.1% BDA defines  $\chi = 0.39$ . This value was used in calculating the other  $M_c$  values.

<sup>d</sup> The reported crosslinking efficiency is the amount of difunctionally reacted BDA, calculated from the  $M_c$  values, divided by the total BDA content.

With the exception of the data for vinylidene chloride and vinyl chloride, for which  $\chi$  could be much greater than 0.6, all available swell ratios summarized in Tables II–IV are in the range 1.6–9, well within the theoretical predictions.

The available  $\chi$  and  $\gamma$  values of Table VIII calculated according to the theory from latex swelling data are plausible. Exact comparison with independently determined values is at present not possible, because  $\chi$  depends on concentration and molecular weight when it is determined from thermodynamic properties of solutions, and because the true value of  $\gamma$  at particle-water interfaces cannot be directly determined.

TABLE VIII  
Flory-Huggins Constants and Interfacial Tensions Calculated from Latex Swelling Experiments

Series	Polymer	Swelling agent	Temperature, °C.	$\chi$	$\gamma$ , dyne/cm.	Reference
A <sup>a</sup>	Polystyrene	Styrene	~25	0.43	4.5	5
		Toluene	~25	0.48	3.5	5
		Cyclohexanone	~25	0.53	2.1	
B <sup>b</sup>	Poly(methyl methacrylate)	Methyl methacrylate	~25	0.58	4.9	TW
			~25	0.55	1.6	TW
			~25	0.35	35	TW
	Polystyrene	Styrene	30	0.30	31.2	8
		Styrene	60	0.26	12.4	8
		Methyl methacrylate	~25	0.55	11.0	TW
C <sup>c</sup>	Poly(methyl methacrylate) Poly(vinyl acetate)	Vinyl acetate	30	0.33	3.0	8
		Vinyl acetate	60	0.28	3.2	8
		Styrene	60	0.42	5.3	8
		Vinyl caproate	60	0.52	34.2	8
		Vinyl caproate	60	0.10	9.5	8
	Poly(vinyl caproate) Poly(butyl acrylate) crosslinked with butylene diacrylate	Butyl acrylate	~25	0.565	3.25	TW

<sup>a</sup>  $\gamma$  was assumed to be constant for various latexes having different  $r_0$  values. Saturation values of  $H_v$  were established [cf. eq. (4)].

<sup>b</sup>  $H_v$  of the same latex was determined at different partial saturations [cf. eq. (5)].

<sup>c</sup>  $H_v$  values of uncrosslinked and slightly crosslinked latexes were compared. The  $M_c$  was calculated from chemical composition [cf. eq. (6)].

Styrene and toluene are similar solvents and should give similar  $\chi$  values with polystyrene. The  $\chi$  values obtained with toluene solutions of polystyrene vary between 0.3 and 0.44<sup>34-36</sup> and are in the same range as the corresponding values in Table VIII. The  $\chi$  values of poly(methyl methacrylate) in Table VIII seem too high. Since this polymer dissolves in its monomer in bulk,  $\chi \leq 0.5$  is expected.<sup>31</sup> It is possible that water dissolved in monomer raised the  $\chi$  value by reducing the solvent power of the monomer.

Morton et al.<sup>5</sup> post-added soap to their polystyrene latex samples. In their swelling experiments the potassium laurate was at the critical micelle formation concentration and the monomer/latex interfacial tension was 14 dyne/cm., as determined by the De Nouy ring method. This value of  $\gamma$  was higher than that calculated by eq. (4) and shown in Table VIII because the ring method is not accurate when applied to soap solutions. The soap molecules adsorb into the interface rather slowly. When the interfacial film is suddenly ruptured in a ring measurement, the equilibrium conditions are not established. Roe and Brass<sup>37</sup> measured 4 dyne/cm. interfacial tension between toluene and aqueous potassium laurate at the critical micelle concentration. These authors used an equilibrium method, the drop volume method, and their result is quite close to the value of 1.8 dyne/cm. predicted by the theory. In this laboratory, poly(methyl methacrylate) latexes swollen with the monomer gave 4.9 dyne/cm. interfacial tension according to the theory. The experimental interfacial tension between the monomer-saturated latex and the water-saturated monomer was 11.0 dyne/cm. by the ring method. It is likely that the drop volume method would have given a lower interfacial tension and better agreement with the theory.

Swelling of latex particles with a blend of two monomers is described in Table VI. The monomers were styrene and ethyl acrylate, whose solubility parameters (8.7 and 8.4 cal.<sup>0.5</sup>/cc.<sup>0.5</sup>) and molar volumes (115 and 109 cc./mole) are very similar.<sup>31</sup> For this case it is justifiable to set  $\chi_{1p} = \chi_{2p}$ ,  $\chi_{12} = 0$ , and  $j = 1$ . Substitution in eqs. (7), (10), and (11) gives  $K = 1$ . The footnote of Table VI shows that this theoretical expectation is fulfilled. Though blends richer in ethyl acrylate swell the particles more than those richer in styrene, there is no preferential enrichment of ethyl acrylate in the latex particles. It would be desirable to obtain latex swelling data with a blend of two very dissimilar solvents for which the theory predicts  $K$  values differing from unity, but such data are as yet unavailable.

### Results Relevant to the Kinetics of Emulsion Polymerization

In developing a theory of emulsion polymerization, Medvedev et al.<sup>38,39</sup> assumed that all unconverted monomer is absorbed into the latex particles from the beginning of the reaction, that the surface area between the monomer-swollen latex particles and the aqueous phase is constant throughout the reaction, and that the propagation rate is controlled by the diffusion

of monomer to the surface of the particles. These assumptions would hold only if the latex particles absorbed large quantities of monomer; below 10% conversion a swell ratio larger than ten would be required. The experimental data and theoretical considerations presented above show that these assumptions are not realistic.

Parts I and III<sup>1,3</sup> assumed that, during emulsion polymerization,  $\phi_m$  is constant in intervals I and II, i.e., until separate monomer phase is present. The validity of this assumption would require that the equilibrium value of  $\phi_m$  corresponding to saturation must be independent of particle size within the range of particle size variation during emulsion polymerization. Evidently, this assumption cannot accurately correspond to facts. In this context two questions are pertinent: (1) If  $\phi_m$  varies with conversion, how does this affect the precision of theoretical predictions? (2) How much in reality does  $\phi_m$  vary with conversion?

Parts I and II showed that particle nucleation is completed at low conversion. During the interval of particle nucleation (interval I) the lowest possible particle radius would be the radius of a micelle, approximately  $2.5 \times 10^{-7}$  cm.<sup>40</sup> The theory also predicts that for most monomers and most practical recipes the particle radius at the completion of particle nucleation should be less than  $2.5 \times 10^{-6}$  cm. During interval I the particle surfaces are saturated with soap so that the interfacial tension must be low, only few dyne/cm. It is also safe to assume  $\chi$  values less than 0.5 for most monomers. Inspection of Figure 1 reveals that, under such conditions,  $\phi_m$  may, at most, increase 1.5-fold during interval I.

The most sensitive test for the particle nucleation theory is the comparison of calculated and experimental particle radii. The theoretical equation for particle radii [eq. (12) of Part II] contains  $\phi_m$  in the form  $[\phi_m/(1 - \phi_m)]^{0.133}$ . Even if the  $\phi_m$  values used in calculations according to this equation were 50% in error, the error in most calculated particle radius values would be less than 15%.

Another important equation of the theory for interval I predicts that the conversion at the completion of particle nucleation ( $P_{cr}$ ) is proportional to  $\phi_m^{0.2}(1 - \phi_m)^{0.8}$ . If the value of  $\phi_m$  used in calculating  $P_{cr}$  is over-estimated by 50%, the error in  $P_{cr}$  is likely to be less than 15%.

In interval II the monomer-swollen particles continue to grow, and at the end of this interval they attain approximately the same size as that of the fully polymerized particles. In most kinetic experiments interval II is completed below 50% conversion. It should also be kept in mind that meaningful kinetic data cannot be obtained below 1% conversion. Thus during the kinetic measurements the average particle volume can change at most 50-fold and the average particle radius can change at most 4-fold. It is likely that for most practical systems  $\phi_m > 0.4$ , and  $r_0 > 1 \times 10^6$  cm. at the beginning of interval II. Since at the beginning of interval II the particle surfaces are saturated with soap, the value of  $\gamma$  should not exceed 10 dyne/cm. If  $\chi < 0.5$ , Figure 1 predicts that  $\phi_m$  should increase by less than 25% during interval II at constant  $\gamma$ . However, in reality such

variation in  $\phi_m$  hardly takes place. As the particles grow, their surfaces become partially saturated with soap and the interfacial tension increases. This increase in  $\gamma$  may reduce  $\phi_m$  and compensate for the effect of increasing  $r_0$  which, in itself, would cause an increase in  $\phi_m$ . Experimental results obtained by Van der Hoff<sup>41</sup> and by Herzfeld et al.<sup>42</sup> suggest that  $\phi_m$  decreases by at most 25% during interval II of the emulsion polymerization of styrene. In this laboratory, the emulsion polymerization of methyl methacrylate was short-stopped at various conversions, more monomer was added to the latex and  $\phi_m$  at saturation was then determined by static centrifugation. The  $\phi_m$  values were almost constant and varied randomly between 0.70 and 0.73.

According to the theory of interval II, independent parameters can predict the values of  $B$ , a constant in the conversion-time relationship  $P = At^2 + Bt$ , and of the molecular weight,  $M_{SE}$ , which would be obtained at infinitely fast termination. The pertinent equations [eqs. (7) and (17) of Part IV] are influenced by  $\phi_m$  through the term  $\phi_m^{0.6}(1 - \phi_m)^{0.4}$ . This term is relatively insensitive to the value of  $\phi_m$ , and even an unlikely 50% error in the value of  $\phi_m$  would cause only few per cent error in predicting  $B$  and  $M_{SE}$ .

In summary, theoretical predictions and experimental data indicate that, during intervals I and II, the monomer concentration in the particles varies little with conversion as long as a swelling equilibrium corresponding to saturation is maintained. The expected variation in the  $\phi_m$  values does not cause significant error in the theoretical predictions concerning the kinetics, particle size, and molecular weight.

### Some Notes on Copolymerization in Latex Systems

The classical theory of homogeneous copolymerization gives the ratio of two monomers incorporated into the polymer as a function of the ratio of the amounts of unconverted monomers. The theory uses two parameters, the reactivity ratios  $r_{12}$  and  $r_{21}$ .

In emulsion copolymerization the ratio of unconverted monomers, determined experimentally, is characteristic of all monomers present, to those dissolved in latex particles and in water, and those present in the binary monomer phase. However, only the ratio of monomer concentrations at the locus of polymerization, within the latex particles, influences the copolymerization. If the solubility of the two comonomers in water is low, and if the conversion is also low, the experimentally determined ratio of two monomers approximately equals the ratio of monomers in the binary monomer phase,  $v_1/v_2$ . The ratio of monomer concentrations in the latex particles is then  $\phi_1/\phi_2 = Kv_1/v_2$  [cf. eqs. (7)–(11)]. Under these conditions, the effective reactivity ratios,  $r_{12}^*$  and  $r_{21}^*$  are:<sup>32</sup>

$$r_{12}^* = K r_{12}$$

$$r_{21}^* = r_{21}/K$$

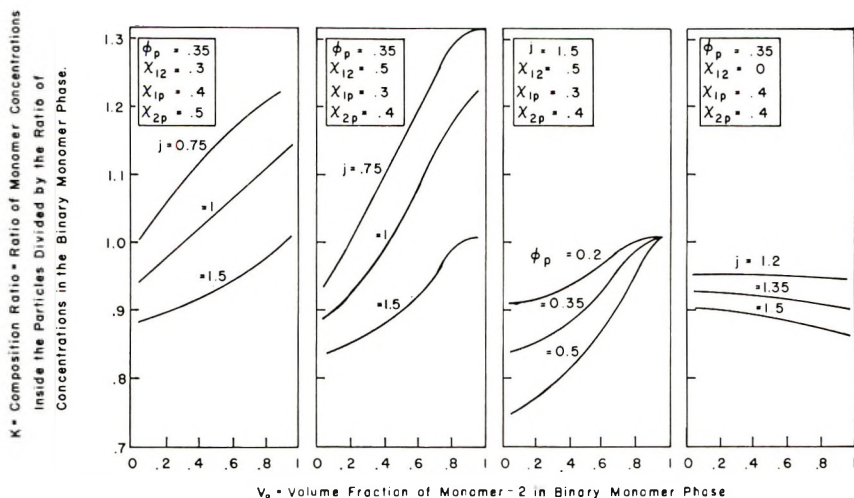


Fig. 3. Composition ratios calculated according to the Krigbaum-Carpenter theory. By definition  $K$  is larger than unity if there is a relative enrichment of monomer 1 in the particles.

At the other extreme, at high conversions in interval III, the monomers are entirely within the latex particles (if the solubility of monomer in water is low). The experimentally determined ratio of unconverted monomers then equals that at the polymerization locus.

It is evident that the maximum deviation from the reactivity ratio scheme during intervals I and II is measured by the deviation of  $K$  from unity. Figure 3 shows that  $K$  should not deviate from unity by more than 40%. Consequently, preferential enrichment of one monomer in the latex particles is not likely to cause more than 40% discrepancy between the reactivity ratios determined by homogeneous and by emulsion polymerization. The reported reactivity ratios, determined either by emulsion or by homogeneous polymerization, often lack precision and can be associated with experimental errors larger than 40%. Within the accuracy of the available data, copolymerization in emulsion and homogeneous medium should therefore define comparable reactivity ratios. This prediction is confirmed by data obtained before 1955, reviewed by Bovey et al.,<sup>32</sup> and by more recent data.<sup>43,44</sup> For highly water-soluble monomers, such as acrylonitrile, a correction for solubility in water must be applied.

Bovey et al.<sup>32</sup> showed that in the emulsion copolymerization of styrene and butadiene the styrene content of the copolymer may occasionally pass through a minimum with increasing conversion. This result is inconsistent with the reactivity ratio theory, and Bovey et al.<sup>32</sup> explain it by assuming that diffusion of the monomer to the polymerization locus was controlling the rate of polymerization. An alternate interpretation is suggested by the results of Figure 3 and the foregoing discussion: the minimum may be caused by the variation in the values of  $K$ ,  $r_{12}^*$ , and  $r_{21}^*$  with increasing conversion.

The thermodynamic theory predicts that only two comonomers with equal molar volumes, equal solubility parameters, and equal polarity, i.e., with identical solvent properties, should obey strictly the reactivity ratio scheme in emulsion polymerization. Only such comonomers are associated with  $K$  values equal to unity irrespective of their concentrations.

The latex samples of Table VII were supplied by Mr. C. F. Ryan and their swelling in pyridine was determined by Mrs. F. B. Farnum. The other experimental work was carried out by Mr. E. M. Young.

### References

1. J. L. Gardon, *J. Polym. Sci. A-1*, **6**, 623 (1968) (Part I).
2. J. L. Gardon, *J. Polym. Sci. A-1*, **6**, 643 (1968) (Part II).
3. J. L. Gardon, *J. Polym. Sci. A-1*, **6**, 665 (1968) (Part III).
4. J. L. Gardon, *J. Polym. Sci. A-1*, **6**, 687 (1968) (Part IV).
5. M. Morton, S. Kaizerman, and M. W. Altier, *J. Colloid Sci.*, **9**, 300 (1954).
6. C. A. Johnson, *Surface Sci.*, **3**, 429 (1965).
7. P. J. Flory, *Principles of Polymer Chemistry*, Cornell Univ. Press, Ithaca, N.Y., 1953, pp. 511-518, 576-581.
8. E. Vanzo, R. H. Marchessault, and V. Stannett, *J. Colloid Sci.*, **20**, 62 (1965).
9. P. J. Flory and J. Rehner, *J. Chem. Phys.*, **11**, 521 (1943).
10. W. R. Krigbaum and D. K. Carpenter, *J. Polym. Sci.*, **14**, 241 (1954).
11. Rohm and Haas Co., *Special Products Bulletins* SP-229 and SP-60 (June 1, 1964).
12. M. Morton, J. A. Cala, and M. W. Altier, *J. Polym. Sci.*, **19**, 547 (1956).
13. Z. Manyasek and A. Rezabek, *J. Polym. Sci.*, **56**, 47 (1962).
14. H. Wiener, *J. Polym. Sci.*, **7**, 1 (1951).
15. H. Gerrens, W. Fink, and E. Kohnlein, in *Macromolecular Chemistry*, Prague, 1965; *J. Polymer Sci. C*, **16**, 2781 (1967).
16. H. Finkentscher and K. Herrle, *Angew. Chem.*, **59**, 174 (1947).
17. M. Morton, P. P. Salatiello, and H. Landfield, *J. Polym. Sci.*, **8**, 279 (1952).
18. E. J. Meehan, *J. Amer. Chem. Soc.*, **71**, 628 (1949).
19. M. Morton, P. P. Salatiello, and H. Landfield, *J. Polym. Sci.*, **8**, 215 (1952).
20. D. M. French, *J. Polym. Sci.*, **33**, 395 (1958).
21. D. H. Napper and A. G. Parts, *J. Polym. Sci.*, **61**, 113 (1962).
22. D. Hummel, G. Ley, and C. Schneider, *Advan. Chem. Ser.*, **34**, 60 (1962).
23. D. Hummel, *Angew. Chem.*, **75**, 330 (1963).
24. H. Gerrens and E. Kohnlein, *Z. Elektrochem.*, **64**, 1199 (1960).
25. K. P. Paoletti and F. W. Billmeyer, *J. Polym. Sci. A*, **2**, 2049 (1964).
26. W. V. Smith, *J. Amer. Chem. Soc.*, **70**, 3695 (1948).
27. B. M. E. Van der Hoff, *J. Polym. Sci.*, **44**, 241 (1960).
28. J. W. Vanderhoff, E. B. Bradford, H. L. Tarkowski, and B. W. Wilkinson, *J. Polym. Sci.*, **50**, 265 (1961).
29. E. Barthelomé, H. Gerrens, R. Harbeck, and H. M. Witz, *Z. Elektrochem.*, **60**, 334 (1956).
30. W. D. Harkins, *J. Amer. Chem. Soc.*, **69**, 1428 (1947).
31. J. L. Gardon, in *Encyclopedia of Polymer Science and Technology*, H. F. Mark, N. G. Gaylord, and N. Bikales, Eds., Interscience, New York, 1966, Volume III, pp. 833-862.
32. F. A. Bovey, I. M. Kolthoff, A. I. Medalia, and E. J. Meehan, *Emulsion Polymerization*, Interscience, New York, 1955, pp. 251-269.
33. J. Rehner, *J. Polym. Sci.*, **46**, 550 (1960).
34. G. M. Bristow and F. M. Watson, *Trans. Faraday Soc.*, **54**, 1742 (1958).
35. M. L. Huggins, *Ann. N.Y. Acad. Sci.*, **44**, 431 (1943).
36. C. E. H. Bawn, R. F. S. Freeman, and A. R. Kamaliddin, *Trans. Faraday Soc.*, **46**, 677 (1950).

37. C. P. Roe and P. D. Brass, *J. Colloid Sci.*, **9**, 602 (1954).
38. G. D. Berezhnoi, P. M. Khomikovskii, and S. S. Medvedev, *Vysokomol. Soedin.*, **2**, 141 (1960).
39. S. S. Medvedev, *Proc. Int. Symp. Macromol. Chem., Prague, 1957*, Pergamon Press, New York, pp. 174-190.
40. B. M. E. Van der Hoff, *Advan. Chem. Ser.*, **34**, 6 (1962).
41. B. M. E. Van der Hoff, *J. Phys. Chem.*, **60**, 1250 (1956).
42. S. H. Herzfeld, A. Roginsky, M. L. Corrin, and W. D. Harkins, *J. Polym. Sci.*, **5**, 207 (1950).
43. Z. Machacek, *Z. Chem. Listy*, **48**, 477 (1954).
44. B. G. Elgood and B. J. Sauntson, *Chem. Ind. (London)*, **1965**, 1558.

Received December 28, 1967

Revised February 13, 1968

## Effect of Acetylene on the $\gamma$ -Radiation-Induced Polymerization of Ethylene

HIROSHI MITSUI, FUMIO HOSOI, MIYUKI HAGIWARA, and  
TSUTOMU KAGIYA, *Japan Atomic Energy Research Institute,  
Takasaki Radiation Chemistry Research Establishment, Takasaki,  
Gunma, Japan*

### Synopsis

The effects of acetylene on the  $\gamma$ -radiation-induced polymerization of ethylene were studied from the viewpoint of the gaseous products and polymer structure. The experiments were carried out under a pressure of 400 kg/cm<sup>2</sup>; the temperature was 30°C; the dose rate was  $1.1 \times 10^5$  rad/hr; and the acetylene content was 0–20%. The solid polymer was obtained in the polymerization of ethylene containing 2.2% acetylene, while the monomer containing 19.7% acetylene gave a yellowish viscous oil. The polymer yield and molecular weight decreased remarkably with acetylene content. The main gaseous product was hydrogen, and trace amounts of butane, butene-1, butadiene-1,3, and benzene and its derivatives were also observed. The rate of formation of hydrogen was almost independent of acetylene content and there was no difference in acetylene contents before and after the irradiation was found. The infrared spectra of the polymers showed the presence of vinylidene, *trans*-vinylene, and terminal vinyl unsaturations, 1,4-disubstituted benzene, and carbonyl groups. The contents of *trans*-vinylene, terminal vinyl, and methyl groups increased with acetylene content, and that of vinylidene was independent of acetylene content. The monomer reactivity ratios of ethylene and acetylene were evaluated as 45.5 and 66.0, respectively. On the basis of the results, the effects of acetylene on the  $\gamma$ -radiation-induced polymerization of ethylene were discussed.

### INTRODUCTION

In the previous papers,<sup>1,2</sup> we reported that hydrogen and acetylene are formed as by-products in the  $\gamma$ -radiation-induced polymerization of ethylene under high pressure. Munari et al.<sup>3</sup> studied the effects of acetylene on the ethylene polymerization under a low pressure of 45 kg/cm<sup>2</sup>, and reported that the polymer yield, molecular weight, and melting point decrease markedly with acetylene concentration, the number of methyl groups per 1000 carbon atoms of the polymer increases, and the number of unsaturations is little affected by acetylene.

The purpose of this paper is to elucidate the role of acetylene in the polymerization under a high pressure of 400 kg/cm<sup>2</sup> from the viewpoint of the gaseous products and the structure of the polymer formed in the polymerization of ethylene containing acetylene.

## EXPERIMENTAL

The reaction apparatus, ethylene monomer, and irradiation facilities were the same as described in the previous paper.<sup>4</sup> Commercially available acetylene (99.9% pure) was used. After the reaction vessel was evacuated and filled five times with a premixed ethylene-acetylene mixture containing the desired amount of acetylene to about 20 kg/cm<sup>2</sup>, the vessel was charged with the mixture to a pressure of 400 kg/cm<sup>2</sup> at 30°C. The experiments were carried out under an initial pressure of 400 kg/cm<sup>2</sup>; the temperature was  $30 \pm 1^\circ\text{C}$ , and the dose rate was  $1.1 \times 10^5$  rad/hr.

Hydrogen, methane, and ethane were determined by the same methods as described in the previous paper.<sup>4</sup> Acetylene was determined at 170°C by using a Hitachi KGL-2A gas chromatograph provided with a 7 m column packed with squalane (20%) and with higher aliphatic hydrocarbons at 80°C by using the same gas chromatograph. A Shimadzu GC-1B gas chromatograph provided with a 3-m tricresyl phosphate (30%) column was used at 100°C for detection of benzene and its derivatives.

The molecular weight of solid polymer was determined from the intrinsic viscosity measurement<sup>5</sup> and that of the greaselike polymer from the reduced osmotic pressure measurement in tetralin solution at 110°C by using a high-speed membrane osmometer, Model 502 (Mechrolab Co.) provided with OS-gel cellophane film (S & S Co.).

The infrared spectral measurement was made with films (about 0.2 mm thickness) for solid polymers, and with the use of NaCl cells (0.05 mm thickness) for the greaselike and oily polymers. The measurements were made with a Nippon-Bunko Model DS-301 infrared spectrophotometer using NaCl optics. The double bond and methyl group contents of the polymer were determined from the infrared spectrum as described by Cernia et al.<sup>6</sup> and Bryant et al.,<sup>7</sup> respectively.

## RESULTS AND DISCUSSION

### Effects of Acetylene on the Polymer Yield and Molecular Weight

All experimental results are summarized in Table I. The ethylene containing 0–2.21% acetylene gives solid polymer as a main product, and the monomers containing 12.9 and 19.7% acetylene give a colorless grease and a yellowish, viscous oil, respectively.

Both polymer yield and molecular weight decrease remarkably with increasing acetylene content (Fig. 1). In Figure 1, the extent of the reduction of polymer yield is much larger than that of molecular weight at the acetylene content below about 0.4%, while, though the difference is small, the situation is reversed when the acetylene concentration is increased more than about 0.4% because the molecular weight is depressed more than the polymer yield. As the result, the number of moles of polymer chain (defined as the ratio of the polymer yield to the molecular weight) decreases

TABLE I  
Experimental Results of the Polymerization Using the  
Monomer Containing Acetylene<sup>a</sup>

	Run 1	Run 2	Run 3	Run 4	Run 5	Run 6	Run 7
Reaction time, hr.	2	2	2	2	2	30	150
C <sub>2</sub> H <sub>2</sub> , %							
Initial	0.00	0.18	0.64	1.26	2.22	12.9	19.7
Final	$2.6 \times 10^{-3}$	0.19	0.68	1.42	2.12	12.7	19.7
Polymer yield, g/l	54.04	20.22	13.57	6.69	4.13	4.03 <sup>b</sup>	12.03 <sup>c</sup>
Molecular weight $\times 10^{-4}$	25.0	19.5	13.8	4.4	1.9	0.45 <sup>d</sup>	—
Number of polymer chains $\times 10^4$ , mol/l	2.16	1.04	0.98	1.52	2.17	8.96	—
Gaseous product, ppm							
H <sub>2</sub>	12	10	13	12	13	77	671
C <sub>4</sub> H <sub>10</sub>	0	0	0	0	0	trace	94
C <sub>4</sub> H <sub>8</sub> -1	0	0	0	0	0	trace	91
C <sub>4</sub> H <sub>6</sub> -1,3	0	0	0	0	0	trace	62
Benzene and its derivatives, ppm	0	0	0	0	0	trace	trace
Double bonds in polymer per 1000 carbon atoms							
R—CH=CH <sub>2</sub>	0.00	0.01	0.04	0.1	0.33	8.28	16.90
R—CH=CH—R' (trans)	0.00	0.00	0.06	0.15	0.37	8.86	22.35
R,R'C=CH <sub>2</sub>	0.04	0.05	0.03	0.05	0.07	1.31	1.86
Methyl groups in polymer, per 1000 carbon atoms	2.58	3.04	5.70	7.24	12.37	72.8	146.8
Benzene structure	—	—	—	—	—	trace	trace

<sup>a</sup> Reaction conditions: pressure, 400 kg/cm<sup>2</sup>; temperature, 30°C; dose rate,  $1.1 \times 10^5$  rad/hr; reactor volume, 100 ml.

<sup>b</sup> Colorless grease.

<sup>c</sup> Yellowish viscous oil.

<sup>d</sup> Determined from the critical osmotic pressure.

markedly with a small amount of acetylene, passes a minimum at near 0.4%, and thereafter increases (Fig. 2).

From these results, it is concluded that the polymerization is retarded by the addition of acetylene, and the retardation can be at least considered to be caused by the marked decrease in the rate of propagation. The marked decrease in the number of moles of polymer chain with a small amount of acetylene suggests the occurrence of a reaction which reduces the number of polymer chains, such as bimolecular termination or crosslinking of polymers with acetylene. The increase of the number of moles of polymer chain observed at an acetylene content more than about 0.4% is attributed to the increase of the rates of initiation and/or transfer. The results given in Figure 2 may indicate that the rate of the reaction reducing the number of polymer chains exceeds the rates of initiation and/or transfer in the range of acetylene content less than about 0.4%, while the latter becomes larger than the former with further addition of acetylene.

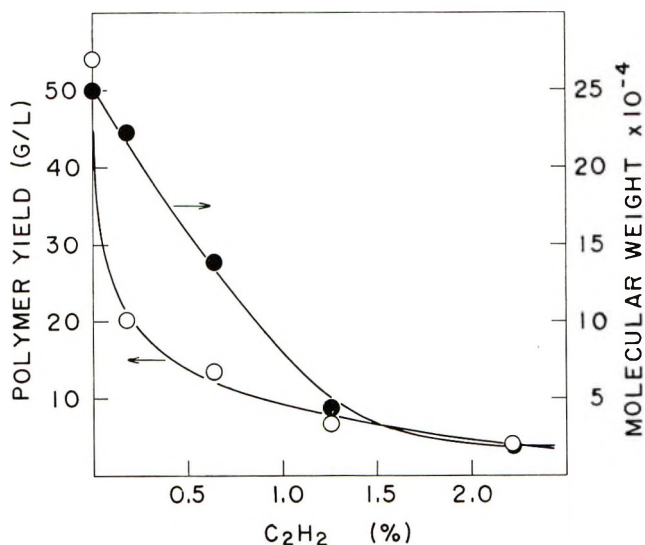


Fig. 1. Effects of acetylene content on (○) the polymer yield and (●) the molecular weight. Reaction pressure, 400 kg/cm<sup>2</sup>; temperature, 30°C; time, 2 hr; dose rate,  $1.1 \times 10^5$  rad/hr; reactor volume, 100 ml.

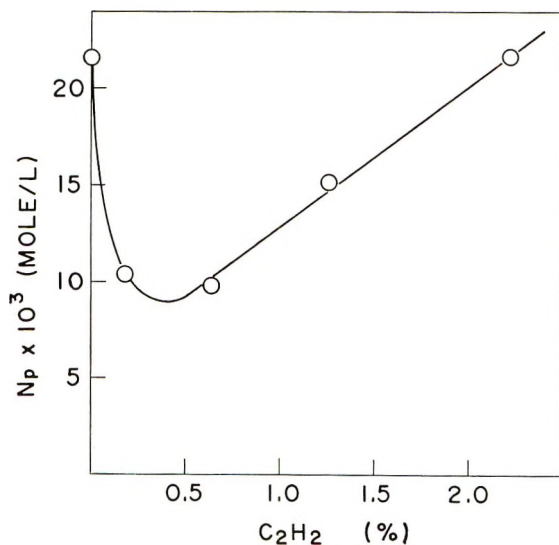


Fig. 2. Relation between the number of moles of polymer chain  $N_p$  and acetylene content. Reaction conditions same as given for Figure 1.

### Effects of Acetylene on the Gaseous Products

As can be seen in Table I and Figure 3, no marked difference in acetylene contents before and after the irradiation is observed. Hydrogen formation is, however, clearly observed, and its amount is independent of acetylene content. This result indicates that the reaction of formation of hydrogen

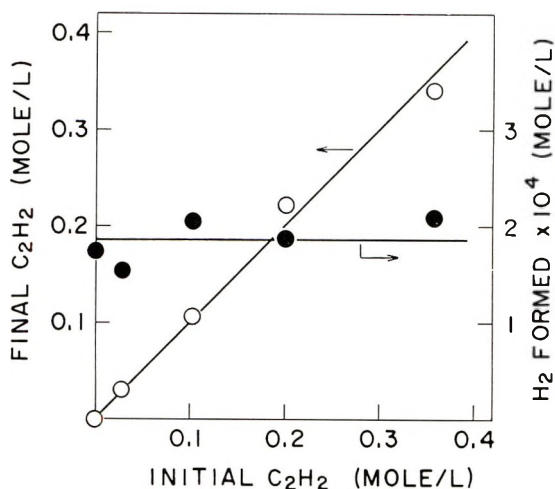


Fig. 3. Relation of (○) acetylene contents determined before and after irradiation and (●) the effects of acetylene content on the hydrogen formation. Reaction conditions same as given for Figure 1.

proposed in previous paper<sup>2</sup> is not affected by adding acetylene. Further, the results of runs 6 and 7 show that the trace amounts of butane, butene-1, butadiene-1,3 and benzene and its derivatives are also formed during irradiation. This result indicates that acetylene acts as a terminator, and that cyclization of acetylene trimer takes place.

### Effects of Acetylene on the Polymer Structure

Figure 4 shows the infrared spectra of the polymers obtained by runs 1 (polymer A), 6 (polymer B), and 7 (polymer C) given in Table I. The band attributed to the triple bonds ( $2140\text{--}2100$  and  $2260\text{--}2190\text{ cm}^{-1}$ ) are not observed in the spectra of polymers A, B, and C. This means no initiation from the radical having a triple bond formed by radiolysis of acetylene takes place. A peak near  $1640\text{ cm}^{-1}$ , assigned to nonconjugated  $\text{C}=\text{C}$  stretching vibration, is observed, while a peak for conjugated  $\text{C}=\text{C}$  (near  $1600\text{ cm}^{-1}$ ) is not observed. The absorption bands near  $1165$ ,  $1040$ ,  $1015$ , and  $810\text{ cm}^{-1}$  in polymers B and C show the presence of a 1,4-disubstituted benzene structure in these polymers. Further, the carbonyl group band (near  $1720\text{ cm}^{-1}$ ) observed in both spectra of polymers B and C suggests that these polymers contain structures which are readily oxidized.

Table I and Figure 4 show that polymer A lacks both unsaturations of terminal vinyl ( $908$  and  $990\text{ cm}^{-1}$ ) and *trans*-vinylene ( $964\text{ cm}^{-1}$ ), and has only a small amount of vinylidene ( $888\text{ cm}^{-1}$ ), while polymers B and C have relatively large amounts of terminal vinyl and *trans*-vinylene groups. As shown in Figure 5, contents of both the terminal vinyl and *trans*-vinylene types increase almost equally with acetylene content. From the results, it is concluded that the terminal vinyl and *trans*-vinylene groups are formed

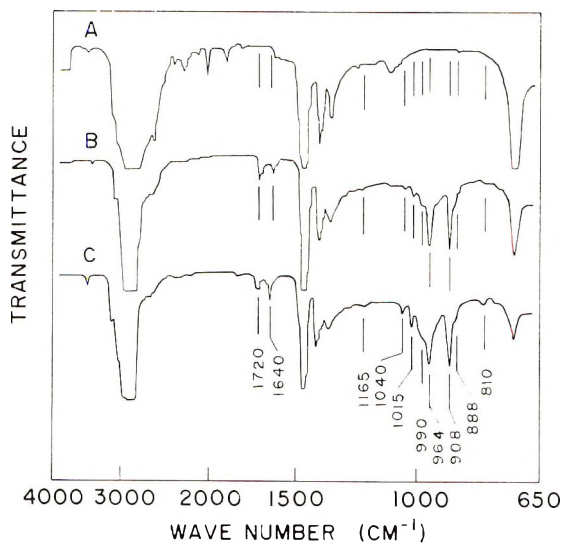


Fig. 4. Infrared spectra of polymers formed by  $\gamma$ -radiation-induced polymerization of (A) pure ethylene at 2 hr (polymer A, film 2 mm thickness), (B) ethylene containing 12.9% acetylene at 30 hr (polymer B, NaCl cell, 0.05 mm thickness), and (C) ethylene containing 19.7% acetylene at 150 hr (polymer C, NaCl cell, 0.05 mm thickness). Reaction pressure, 400 kg/cm<sup>2</sup>; temperature, 30°C; dose rate,  $1.1 \times 10^5$  rad/hr; reactor volume, 100 ml.

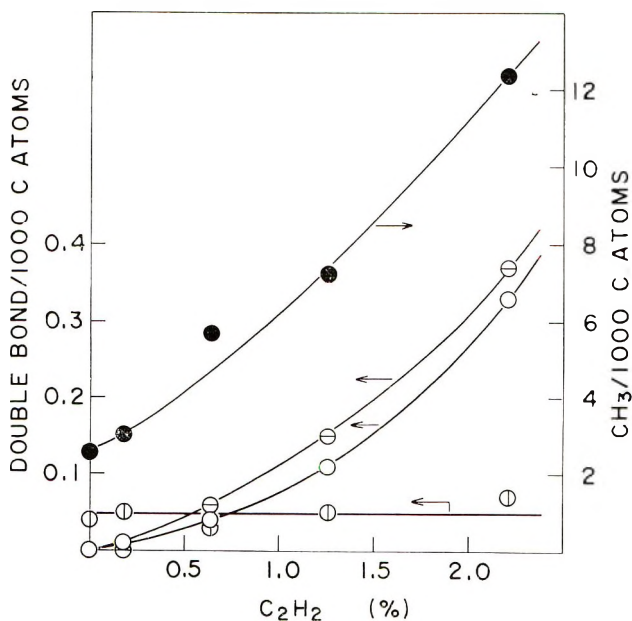


Fig. 5. Effects of acetylene content on the contents of unsaturations and methyl group in the polymers formed: (○) terminal vinyl group; (⊖) *trans*-vinylene group; (⊕) vinylidene group; (●) methyl group. Reaction conditions same as given for Figure 1.



Revised February 9, 1968

## Study on Modification of Polymers with the Aid of the Schmidt Reaction

A. RAVVE, *Corporate R&E, Continental Can Company, Chicago, Illinois, 60620*

### Synopsis

A study of the Schmidt reaction on several polymers with pendant carboxylic and ketone moieties was carried out. Four polymers were used as starting materials: (1) poly(methyl vinyl ketone), (2) poly(acrylic acid), (3) a copolymer of methyl vinyl ketone and acrylic acid, and (4) a copolymer of styrene and acrylic acid. Most reactions were conducted in an acetic acid medium with the exception of one reaction on poly(acrylic acid) which was done in dioxane and another on copolymer of styrene and acrylic acid done in chloroform. It was found that a Schmidt reaction on poly(acrylic acid) in acetic acid solution will lead to intermolecular reactions of the intermediate with the solvent in preference to reactions with neighboring carboxyl groups on the polymer backbone. A tendency of poly(acrylic acid) to form cyclic anhydrides under these reaction conditions interferes with the yield of acetamide units.

Smets and co-workers<sup>1</sup> demonstrated that the Curtius and Lossen rearrangements on poly(acrylyl chloride) lead to fairly regular polyampholytes. This was also found to be true when the Hoffman reaction was carried out on polyacrylamide.<sup>2</sup>

The Schmidt reaction on poly(acrylic acid) was not investigated. It is commonly assumed that this rearrangement goes through similar intermediates and may be expected to yield similar products.

Aldehydes and ketones are more reactive towards hydrazoic acid than are carboxylic acids.<sup>3</sup> A Schmidt reaction on a polyketone was reported by Van Paesschen,<sup>4</sup> who formed poly(*p*-acetamino-styrene) from polyacetylstyrene. Also, Michel and Murphey<sup>5</sup> carried out intramolecular rearrangement on polyketones to form polyamides.

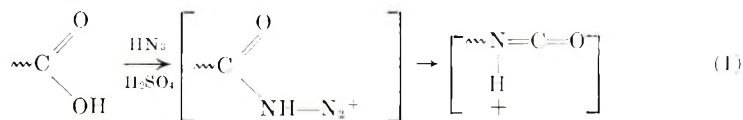
The work by Van Paesschen<sup>4</sup> is particularly significant because he found that acetic acid is a good solvent medium for this reaction on polyketones. No difficulty was apparently encountered from the fact that the carboxylic groups of acetic acid may themselves be reactive towards hydrazoic acid and are present in large excess.

This paper describes results from carrying out the Schmidt reaction on four polymers: (1) poly(methyl vinyl ketone); (2) poly(acrylic acid); (3) a copolymer of methyl vinyl ketone and acrylic acid; and (4) a copolymer of styrene and acrylic acid.

## RESULTS AND DISCUSSION

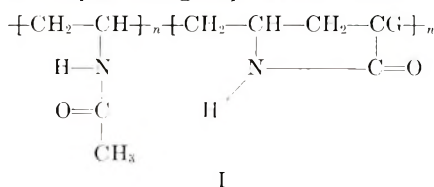
The mechanisms of reactions of hydrazoic acid with carboxylic acids and with ketones were adequately described elsewhere.<sup>6</sup> When the ketones are unsymmetrical (as would be the case of macromolecules with pendant reactive moieties), then the bulkier of the R groups are usually expected to migrate preferentially.<sup>6</sup> It appears that this type of migration was actually observed by Van Paesschen.<sup>4</sup> The same should probably be expected in rearrangement of poly(methyl vinyl ketone) to poly(*N*-acetyl vinyl-amine).

With respect to reactivity of carboxylic acids, the Schmidt reaction is presumed to differ slightly from the Curtius reaction in that it involves a protonated intermediate.<sup>6,7</sup>



Also, in this case the lower homologs appear to be less reactive. Thus, acetic acid was found to give poor yields of methylamine.<sup>6</sup> Some dicarboxylic acids like succinic and its lower homologs also fail to give good yields of diamines.<sup>6</sup> On the other hand, others, like adipic acid, give satisfactory high yields.<sup>6</sup>

In carrying out the reaction on poly(acrylic acid), one might expect that functional interaction of neighboring isocyanate groups with carboxylic acid groups should lead to formation of large amounts of lactam rings. At the same time, if the reaction is carried out in acetic acid solvent, as done by Van Paesschen,<sup>4</sup> then formation of acetamide structures might turn out to be competitive with formation of lactams. The reaction product might then have pendant groups as shown in I



as well as, perhaps, some unreacted carboxyl groups, depending upon the yield.

On the other hand, an all-poly(vinyl acetamide) structure should be identical to one produced from the Schmidt reaction on poly(vinyl methyl ketone), provided that very high conversions are possible in the latter case.

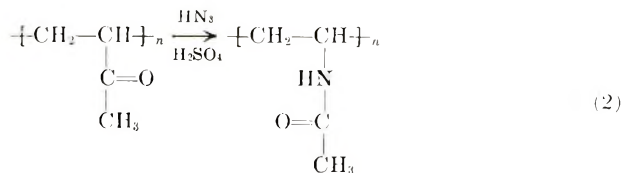


TABLE I  
Summary of Results From Carrying Out Schmidt Reaction on Polymer I

Reaction product	Nitrogen content, %	Ketone groups converted based on nitrogen, %	IR analysis		Group analysis by NMR spectroscopy	
			$\mu$	Interpretation	Ab-sorption position of protons, ppm	Interpretation
Polymer II	6.96	42.2	3.01(m)	NH stretching (H bond)	1.45	Methylene, $\text{—}\overset{\text{H}}{\underset{\text{H}}{\text{C}}}\text{—}$
			6.00(s)	Amide I ( $\nu$ C=O)	2.75	Methyl ketone, $\text{H—}\overset{\text{O}}{\underset{\text{H}}{\text{C}}}\text{—}$
			6.51(w)	Amide II ( $\delta$ NH)	3.70	Backbone tertiary hydrogen, $\text{—}\overset{\text{H}}{\underset{\text{H}}{\text{C}}}\text{—}$
			7.31(m)	sym $\text{CH}_3$ deformation of $\text{CH}_3\text{CO}$ group		$\alpha$ to acetamide group, $\text{—}\overset{\text{O}}{\underset{\text{H}}{\text{C}}}\text{—}\overset{\text{H}}{\underset{\text{H}}{\text{C}}}\text{—}\overset{\text{O}}{\underset{\text{H}}{\text{C}}}\text{—}\text{CH}_3$
					7.70	Amide hydrogen, $\text{—}\overset{\text{O}}{\underset{\text{H}}{\text{C}}}\text{—}\overset{\text{H}}{\underset{\text{H}}{\text{C}}}\text{—}\text{CH}_3$
						5-9 $J_{\text{ab}}$ (cps) no resolution

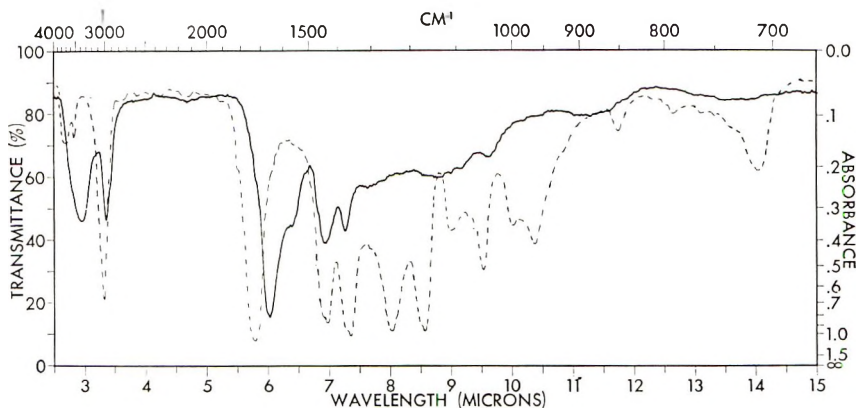


Fig. 1. Infrared spectra of (—) polymer II and (---) polymer I.

So, presumably one might arrive at polymers with similar structures by starting with two different macromolecules via this rearrangement. This will, of course, only be true if the conversions are high and in the reaction of poly(acrylic acid), the isocyanate intermediate reacts preferentially with acetic acid and not intramolecularly.

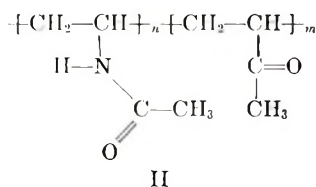
The reaction was, therefore, first carried out on poly(vinyl methyl ketone), polymer I, by employing conditions used by Van Paesschen.<sup>4</sup> Only a 42.2% conversion (based on nitrogen) was achieved. The data on the product, polymer II, are summarized in Table I.

Infrared spectrum of polymer II is shown in Figure 1 with the assignment of the significant peaks given in Table I.

Further information on the structure of the product is indicated from the nuclear magnetic resonance spectrum shown in Figure 2 and summarized in Table I. Both newly formed acetamide groups and unreacted methyl ketone groups appear present.

Although reactions of hydrazoic acid with ketones can often lead to tetrazole formations, especially when there is an excess of the reagent,<sup>6</sup> no indication of such structures can be detected from NMR spectra.

Thus, we can conclude that the structure of polymer II is as shown



Poly(acrylic acid), polymer III, was reacted in two different solvents, in dioxane and in glacial acetic acid. The results are summarized in Table II. The conversion in dioxane was considerably poorer than in acetic acid, as judged from the nitrogen content of the product, polymer IV. Both reactions were carried out at 60°C. The best results were obtained in

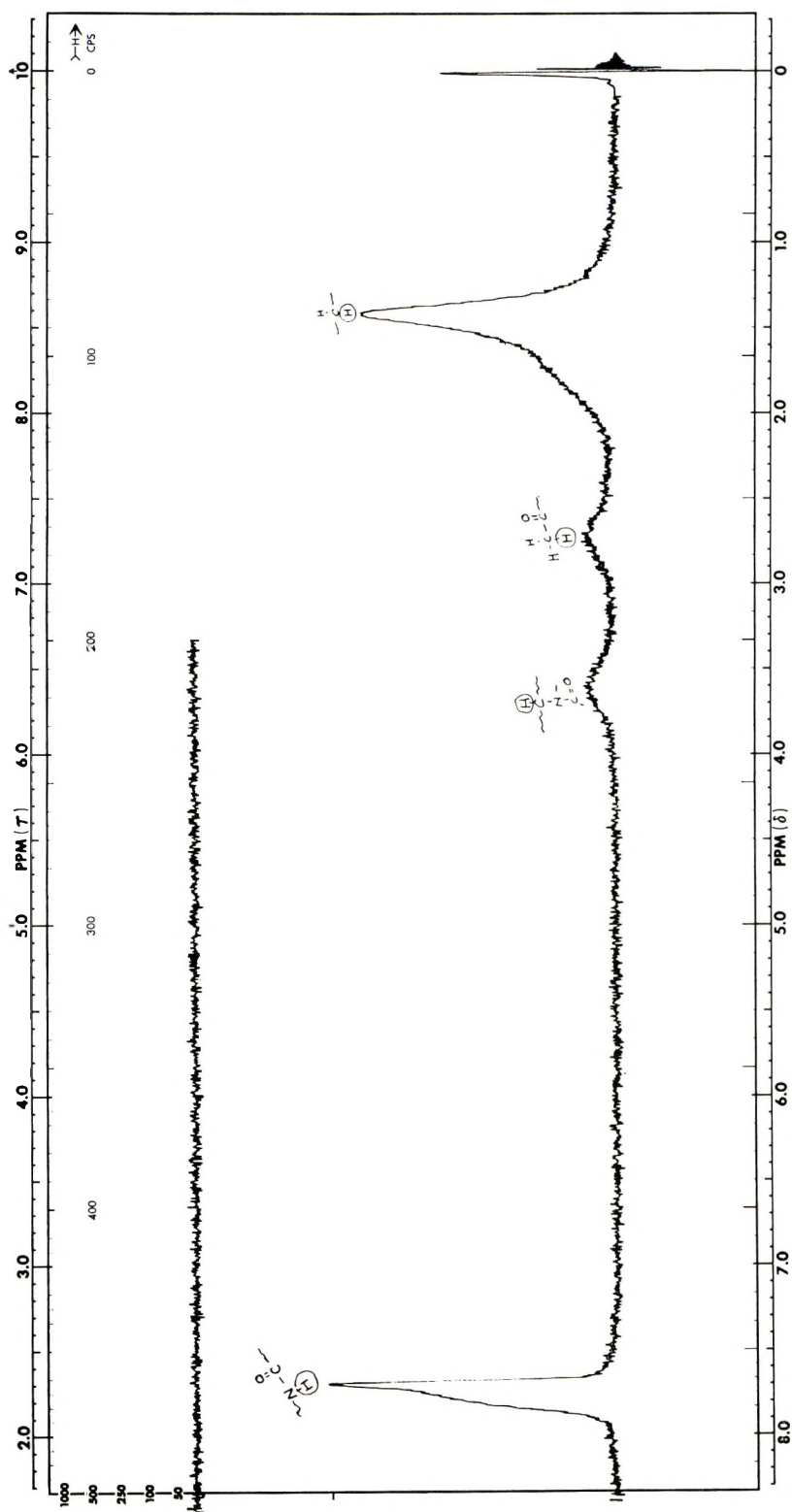


Fig. 2. NMR spectrum of polymer II.

TABLE II  
Summary of Results From Carrying Out Schmidt Reaction on Polymer III

Reaction product	Nitrogen content, %	Reaction solvent	Reaction temperature, °C	IR analysis	
				$\mu$	Interpretation
Polymer IV	2.7	Dioxane	60	5.75(s)	C=O from carboxyl or from anhydride
Polymer V	9.1	Acetic acid	60	6.05-6.10	Secondary amide, Amide I ( $\nu$ C=O)
				6.00(s)	Amide I ( $\nu$ C=O)
				6.45(m)	Amide II ( $\delta$ NH)
Polymer VI Polymer VII	Trace 7.48	Acetic acid Acetic acid	20 60	8.70(s)	cyclic $\beta$ hydride
				—	
				5.75(s)	C=O from carboxyl or from anhydride
Polymer VIII	4.08	Acetic acid	121	6.00(w)	Amide I ( $\nu$ C=O)
				6.51(w)	Amide II ( $\delta$ NH)
				7.70(s)	cyclic anhydride
Polymer IX	None	Acetic acid and acetic anhydride	60	5.70-5.75	C=O from carboxyl or from anhydride
				6.15(w)	Amide I ( $\nu$ C=O)
				—	

preparing polymers V and VII at that temperature in acetic acid. It is significant that when the reaction was carried out at higher temperatures to obtain polymer VIII, lower conversions resulted. Also, when this was done at room temperature to obtain polymer VI, the yield again was very poor. When some acetic acid was replaced by acetic anhydride, no apparent conversion took place. Instead, poly(acrylic acid) appeared to convert in part to poly(acrylic anhydride), yielding polymer VIII. The fact that hydrazoic acid reacted preferentially with the polymer rather than with acetic acid, which is in great excess, is significant as well. This might perhaps be attributed to a neighboring group effect in addition to poor reactivity of acetic acid. Thus, when this reaction was attempted in the presence of an equimolar quantity of glutaric acid, which possesses the same number of carbons between the carboxylic groups as does polyacrylic

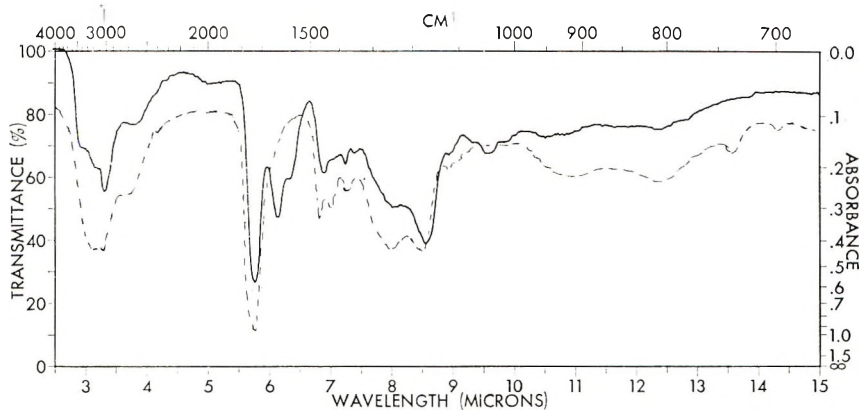


Fig. 3. Infrared spectra of (—) polymer V and (---) polymer III.

acid, completely unreacted polymer was recovered. No attempt was made to isolate the product from glutaric acid.

The infrared spectrum of polymer V is shown in Figure 3. Interpretation of this spectrum and all other products from poly(acrylic acid) is given in Table II.

It is hard to determine from the spectra alone whether the amide absorptions at  $6.05\ \mu$  were due to cyclic structures or due to acetamide groups. Presence of unreacted carboxyl groups in the product complicate the picture as carbonyl absorption from  $\gamma$  lactams was observed at  $5.7\text{--}5.9\ \mu$ , in the same place as the  $\text{C}=\text{O}$  absorption from carboxyl groups.<sup>8</sup>

It was possible to obtain NMR spectrum from polymer IX due to its solubility in perfluoroacetone. This is shown in Figure 4. A strong chemical shift at 5.3 ppm appears to be due to methylene protons of a cyclic anhydride group, though such a group would normally be expected to yield a doublet. Such a doublet, however, might be beyond the resolution capabilities of the instrument.

TABLE III  
Summary of Results From Carrying Out Schmidt Reaction on Polymers X and XI

Reaction product	Nitrogen content, %	Reacted carboxyl groups % (by KOH titration)	Ketone groups converted, % (based on nitrogen and acid conversion)	IR analysis		Group analysis by NMR spectroscopy	
				$\mu$	Interpretation	Absorption, ppm	Interpretation
Polymer XI	6.10	35.7	36.6	3.01(m)	NH stretching (H bond) O		
				5.80(s) 6.10(s) 7.30	C=O from $\text{--}\overset{\text{O}}{\underset{\text{O}}{\text{C}}}\text{--OH}$ Amide I ( $\nu\text{C=O}$ ) sym $\text{CH}_3$ deformation of $\text{CH}_3\text{C=O}$ group.		
				5.80(s) 6.05(m)	C=O from $\text{--}\overset{\text{O}}{\underset{\text{O}}{\text{C}}}\text{--OH}$ Amide I ( $\nu\text{C=O}$ )		
Polymer XIII	8.13	—	—	7.30	sym $\text{CH}_3$ deformation of $\text{CH}_3\text{C=O}$ group	2.15	methyl ketone, $\text{H} \begin{array}{c} \text{O} \\ \parallel \\ \text{H} - \text{C} - \text{C}^{\text{mw}} - \text{H} \end{array}$

2.85	$  \begin{array}{c}  \diagup \\  \text{methyl of acetamide,} \\  \diagdown  \end{array}  $	$  \begin{array}{c}  \text{H} \\    \\  \text{H}^+ - \text{C} - \text{C} - \text{N}^{\sim} \\     \quad   \\  \text{H} \quad \text{O} \quad \text{H}  \end{array}  $
3.00		
3.15		
5.48	anhydride,	$  \begin{array}{c}  \text{H}^+ \\    \\  \text{CH} - \text{C} - \text{CH} \\    \quad   \quad   \\  \text{CH} \quad \text{C} \quad \text{C} \\     \quad    \quad    \\  \text{O} \quad \text{O} \quad \text{O}  \end{array}  $
8.05	amide hydrogen,	$  \begin{array}{c}  \sim \\    \\  \text{C} - \text{N} - \text{C} - \text{CH}_3 \\     \quad   \\  \text{O} \quad \text{H}^+  \end{array}  $

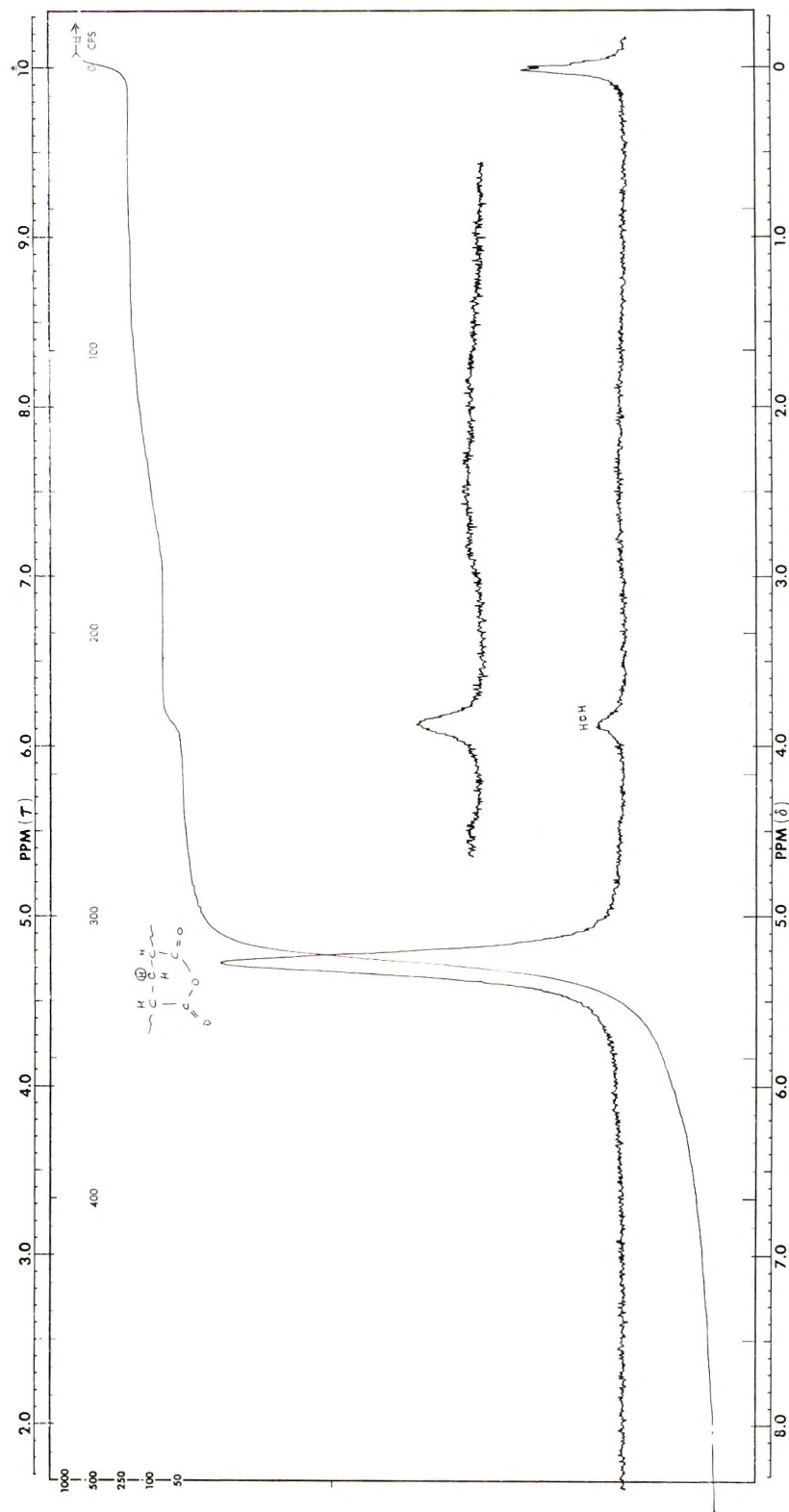


Fig. 4. NMR spectrum of polymer IX.

The presence of this group is further indicated in the infrared spectrum shown in Figure 5. The new peak at  $8.7\ \mu$  is commonly associated with C—O stretching of cyclic anhydrides in which ring strain is involved.<sup>8-10</sup>

Because the products from Schmidt reactions on poly(acrylic acid) were quite insoluble and, therefore, difficult to study, two copolymers were prepared with methyl vinyl ketone. The first one contained 71.8% methyl vinyl ketone, polymer X, and the second 40% of methyl vinyl ketone,

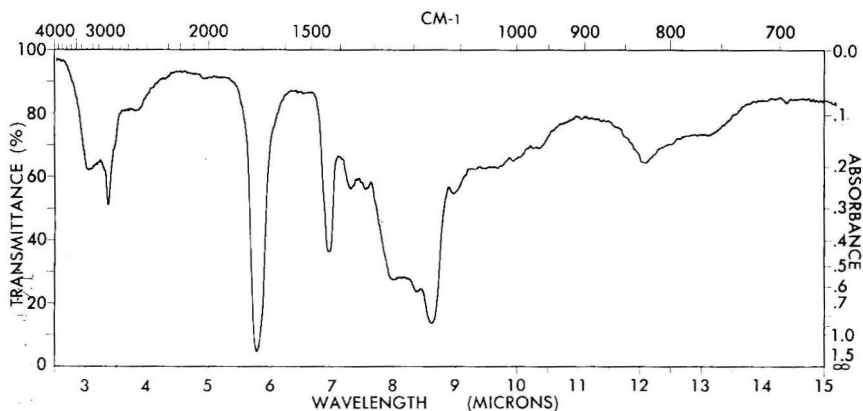


Fig. 5. Infrared spectrum of polymer IX.

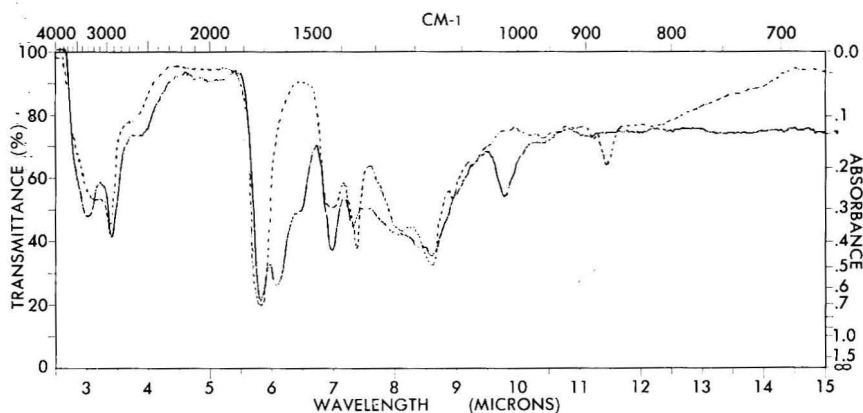


Fig. 6. Infrared spectra of (—) polymer XII and (---) polymer X.

polymer XI. Sufficient quantities of hydrazoic acid were used in the rearrangements to react with all pendant ketones and carboxyl groups on the backbones. The results are summarized in Table III.

Infrared spectra of polymer XII, the product from reaction on polymer X, are shown in Figure 6.

The NMR spectra of polymer XI and its product, polymer XIII, are shown in Figures 7 and 8. The shift at 3.5 ppm seen in Figure 7 appears to be due to presence of moisture.<sup>11</sup>

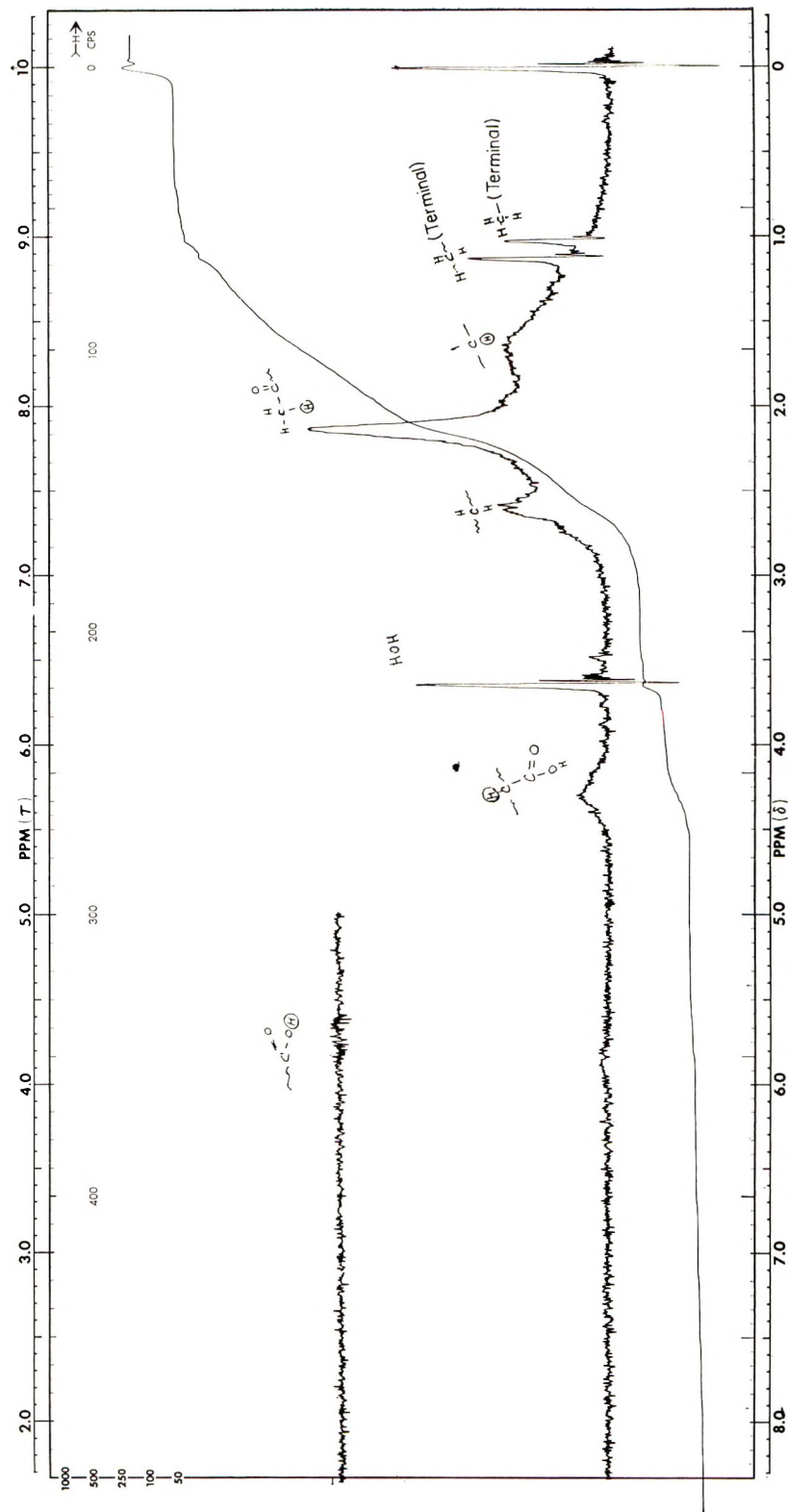


Fig. 7. NMR spectrum of polymer XI.

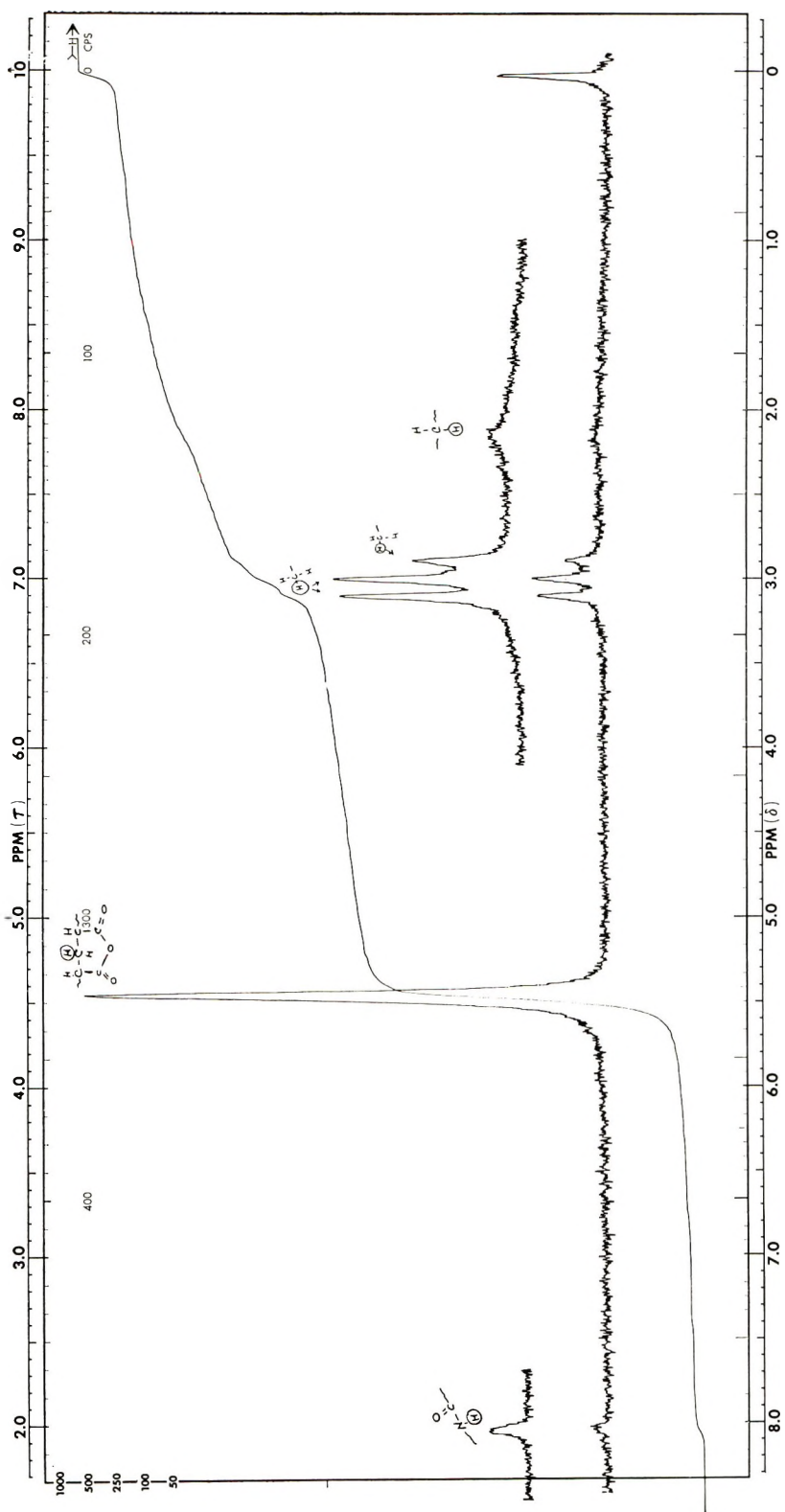
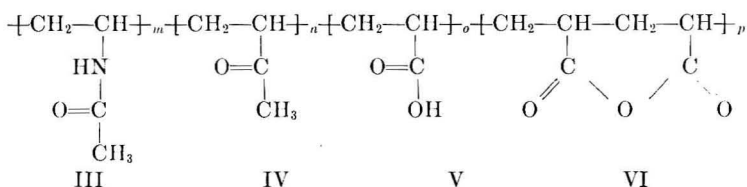


Figure 8 indicates the presence of two different types of methyl group in polymer XIII, at 2.1 ppm, and a doublet at 3.0 ppm and at 3.1 ppm.<sup>10</sup> The peak due to chemical shift at 5.5 ppm is quite similar to the anhydride peak of polymer IX, shown in Figure 4. The chemical shift at 8.1 ppm appears to be due to an amide hydrogen.<sup>11</sup> Thus, it appears the Polymer XIII may have only the structures III-VI present:



Chloroform and benzene are two solvents originally recommended for carrying out the Schmidt reaction on carboxylic acids.<sup>6</sup> Because polyacrylic acid is virtually insoluble in these solvents, a 8:2 copolymer of styrene and acrylic acid, polymer XIV, was prepared. The rearrangement was then carried out in chloroform to yield polymer XV. The results are shown in Table IV. Infrared spectrum of polymer XV is shown in Figure

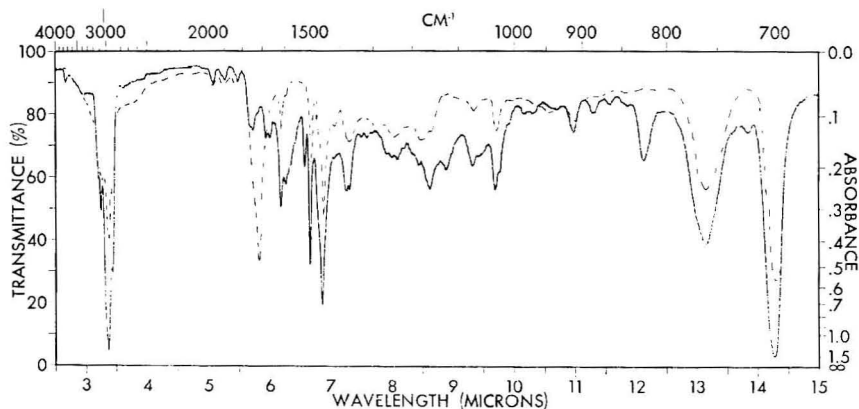


Fig. 9. Infrared spectra of (—) polymer XV and (---) polymer XIV.

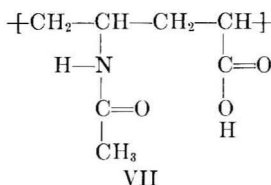
9. The C=O absorption of the carboxyl group is almost all gone and replaced by amide C=O absorption at 6.1  $\mu$ . As the combustion analysis indicates that there are approximately as many oxygens as nitrogens present, it appears that in this case ampholyte structures did form similarly to Curtius and Lossen rearrangements carried out by Smets.<sup>1</sup>

The above considerations fail to resolve the structure of the product obtained by carrying out the Schmidt reaction on polyacrylic acid in acetic acid solution. Some additional light can perhaps be shed on the composition of the products by combustion analysis. Polymer V was found to have the following analysis: C, 50.11%; H, 8.06%; N, 9.10%; O, 31.45%. Polymer VII was found to have the analysis: C, 50.30%; H, 7.75%; N,

TABLE IV  
Summary of Results From Carrying Out Schmidt Reaction on Polymer XIV

Reaction product	Nitrogen content, %	Con- version of carboxyl groups to lactam, %	IR analysis		
			$\mu$		Interpretation
Poly- mer XV	1.78	93	5.65(w)	C=O	from carboxyl or from anhydride, or lactam secondary amide, Amide I ( $\nu$ C=O)
			5.80(w)		
			6.00(w)		

7.70%; O, 34.25%. A possible polymer structure of one acetamide group to one carboxyl group (VII)



would have the composition: VII C, 53.51%; H, 7.20%; N, 9.15%; O, 31.21%. All other structures containing lactams and acid anhydrides would raise the carbon content and lower the nitrogen content. On the basis of these considerations, it appears that a Schmidt reaction on poly-(acrylic acid) in acetic acid solution will lead to predominantly intermolecular reactions of the isocyanate intermediate. At the same time, the tendency to form cyclic anhydrides under these conditions when sulfuric acid is present is competitive and lowers the yields.

The reasons for the lack of reactivity on the part of poly(acrylic anhydride) to hydrazoic acid is not clear. It was shown that such a reaction can take place with some low molecular weight anhydrides and leads to good yields of diamines.<sup>6</sup> Here, however, we may be dealing with steric hindrance.

## EXPERIMENTAL

### Preparation of Polymers

**Preparation of Poly(vinyl Methyl Ketone), Polymer I.** Freshly distilled (methyl vinyl ketone) monomer,  $n_D^{20} = 1.486$ , was polymerized at 80°C in benzene solution, with the use of 1% benzoyl peroxide initiator, inert atmosphere, and mechanical stirring for 8 hr. The solution was then cooled and poured into a large excess of methyl alcohol causing the polymer

to precipitate. The precipitate was washed with an additional quantity of methyl alcohol and dried.

ANAL. Found: C, 68.56%; H, 8.57%.

**Schmidt Reaction on Polymer I (Polymer II).** Polymer I (8 g) was dissolved in 400 ml of glacial acetic acid, and 30 ml of concentrated sulfuric acid was added. The temperature was then raised to 60°C. While the reaction was stirred, 13 g of sodium azide was added in small portions. The agitation and above temperature were maintained for 4 hr. A dark-brown resin separated while nitrogen evolved from the reaction mixture. The product was separated, washed thoroughly with water, and then dried *in vacuo*.

ANAL. Found: C, 67.60%; H, 8.07%; O (direct), 17.38%; N, 6.96%.

**Preparation of Poly(acrylic Acid), Polymer III.** Freshly distilled acrylic acid monomer was polymerized in 2:1 isopropyl alcohol-toluene mixture, with the use of 1% benzoyl peroxide initiator, at reflux temperature of the solvent mixture, with stirring, and under nitrogen atmosphere. After the reaction proceeded for 8 hr, the solution was cooled and then poured into dry acetone, causing the polymer to precipitate. The polymer was washed thoroughly with dry acetone and dried.

ANAL. Found: C, 50.36%; H, 5.45%; O (direct), 44.56%.

**Preparation of Polymer IV.** This was carried out in a manner similar to that for polymer II, except that dioxane was used as the reaction solvent and the temperature was maintained at 60°C. Upon completion of the reaction the polymer, which was still soluble, was precipitated by addition of hexane. The polymer was then redissolved in tetrahydrofuran and shaken with an anionic ion-exchange resin, Rohm and Haas Company, Amberlite IRF-59 to remove all sulfuric acid. The polymer was then reprecipitated with hexane and dried.

ANAL. Found: N, 2.71%.

**Preparation of Polymers V, VI, VII, and VIII.** These preparations were carried out in the same manner as polymer II, using glacial acetic acid as solvent. Polymers V and VII were prepared at 60°C, while polymer VI was prepared at room temperature and polymer VIII at reflux temperature of the solvent, 118°C. In all cases the products were precipitated by addition of hexane then redissolved in methyl alcohol and treated with an anionic ion-exchange resin, Rohm and Haas, IR-410. The alcohol was then removed *in vacuo*.

ANAL. Found for polymer V: C, 50.11%; H, 8.06%; N, 9.10%; O, 31.45%. For polymer VI: C, 51.60%; H, 6.91%; N, 0.50%. For polymer VII: C, 50.30%; H, 7.75%; N, 7.70%; O, 34.25%. For polymer VIII: C, 51.50%; H, 6.46%; N, 4.08%.

**Preparation of Polymer IX.** Polymer IX was prepared as polymer VI, except that instead of using glacial acetic acid as the reaction medium, the solvent was a 90:10 acetic acid-acetic anhydride mixture.

ANAL. Found: C, 52.16%; H, 7.78%; O, 40.11%.

**Preparation of Polymers X and XI.** This was carried out by copolymerizing, respectively, 0.8:1 and 1.55:1 mixtures of acrylic acid and methyl vinyl ketone monomers; 1% benzoyl peroxide was used as the initiator in both cases. The reaction mixtures were stirred under N<sub>2</sub> atmosphere at 60°C for 8 hr. The products were then precipitated with hexane, washed, and dried.

ANAL. Found for polymer X: C, 59.66%; H, 7.61%; O, 32.81%; by titration with 0.1N alcoholic KOH, 28.15% acrylic acid.

For polymer XI: C, 55.42%; H, 6.68%; O, 36.54%; by titration with 0.1N alcoholic KOH, 60.19% acrylic acid.

**Preparation of Polymers XII and XIII.** These preparations were carried out in the same manner as for polymers V and VII.

ANAL. Found for polymer XII: C, 62.24%; H, 7.50%; N, 6.10%; O, 24.29%; by titration with 0.1N alcoholic KOH, 18.0% acrylic acid.

For polymer XIII: C 55.46%; H, 7.28%; N, 8.13%.

**Preparation of Polymer XIV.** This was carried out on toluene solution with a 9:1 mixture of styrene and acrylic acid. The polymerization was carried out with 0.75% benzoyl peroxide as the initiator. After stirring under N<sub>2</sub> atmosphere at 100°C for 8 hr, the product was precipitated by addition to a large excess of methanol, washed, and dried.

ANAL. Found: C, 85.40%; H, 7.41%; O, 7.18%. Calcd. (for 20% acrylic acid): C, 85.82%; H, 7.36%; O, 6.58%.

**Preparation of Polymer XV.** Preparation of this polymer was carried out with 10 g of polymer XIV in 300 ml of chloroform. A 10 ml portion of concentrated H<sub>2</sub>SO<sub>4</sub> was added, and while the reaction mixture was stirred and maintained at 45–50°C, 5 g of sodium azide was added in small increments. The reaction mixture was stirred and heated for additional 2.5 hr. Then product was precipitated with water, washed free from acid, and dried.

ANAL. Found: C, 88.50%; H, 8.22%; N, 1.94%; O, 2.48%.

### Infrared Spectra

All infrared spectra were obtained with a Perkin-Elmer model 137 spectrophotometer. The polymers were examined as thin films on sodium chloride plates.

### Nuclear Magnetic Resonance Spectra

All NMR data was obtained with a Varian A-60 high-resolution spectrometer at 60 Mcps. Determinations were carried out at room temperature.

### References

1. M. Vrancken and G. Smets, *J. Polym. Sci.*, **14**, 521 (1954).
2. M. Mullier and G. Smets, *J. Polym. Sci.*, **23**, 915 (1957).
3. P. A. S. Smith, *The Chemistry of Open-Chain Organic Nitrogen Compounds*, Vol. 1, W. A. Benjamin, New York, 1965.
4. G. Van Paesschen, *Makromol. Chem.*, **63**, 123 (1963).
5. R. H. Michel and W. A. Murphey, *J. Polym. Sci.*, **55**, 741 (1961).
6. H. Wolff, *Organic Reactions*, Vol. III, Wiley, New York, 1946, Chap. 8.
7. E. S. Gould, *Mechanism and Structure in Organic Chemistry*, Holt, Rinehart and Winston, New York, 1959.
8. J. P. Phillips, *Spectra-Structure Correlation*, Academic Press, New York, 1964.
9. J. R. Dyer, *Applications of Absorption Spectroscopy of Organic Compounds*, Prentice-Hall, Englewood Cliffs, N. J. 1965.
10. L. J. Bellamy, *Infra-red Spectra of Complex Molecules*, Wiley, New York, 1958.
11. R. H. Bible, Jr., *Interpretation of NMR Spectra*, Plenum Press, New York, 1965.

Received February 22, 1968

## Photo and Thermal Polymerization Sensitized by Donor-Acceptor Interaction. I. *N*-Vinylcarbazole-Acrylonitrile and Related Systems

SHIGEO TAZUKE and SEIZO OKAMURA, *Department of Polymer Chemistry, Kyoto University, Kyoto, Japan*

### Synopsis

Spontaneous photo and thermal polymerization of *N*-vinylcarbazole (VCZ)-acrylonitrile (AN), VCZ-acetonitrile, AN-*N*-ethylcarbazole, and AN-ferrocene were studied. These combinations of electron donor with acceptor were thermally rather stable but showed prominent photopolymerizability when the systems were irradiated by near ultraviolet light. The VCZ-AN system showed multireactivity producing VCZ polymer and a copolymer of VCZ with AN. The composition of copolymer was approximately the same as that of polymer produced in radical copolymerization. The effects of additives (DPPH, NH<sub>3</sub>, H<sub>2</sub>O, air) indicated simultaneous occurrence of cationic and radical polymerization in the AN-VCZ and acetonitrile-VCZ systems. The results were interpreted on the assumption of initial formation of a cation radical-anion radical pair. The ratio of cationic to radical polymerization differed for photo and thermal polymerization. In no case was anionic polymerization detected.

### INTRODUCTION

Polymerizations initiated by charge-transfer interaction between donor and acceptor have been extensively studied by various researchers with special reference to *N*-vinylcarbazole (VCZ), as reviewed by Hatano et al.<sup>1</sup> Factual knowledge has been accumulated on the polymerization of VCZ in combination with various organic as well as inorganic acceptors. Natures of initiating and propagating species are, however, still the subject of controversy. Ellinger has suggested that the polymerization of VCZ by a weak electron acceptor such as acrylonitrile (AN) or methyl methacrylate is initiated by mesomeric polarization without formation of an ion-radical resulting from complete electron transfer.<sup>2</sup> The state of incomplete charge transfer (mesomeric polarization) was claimed to control the propagation step as well, resulting in the formation of VCZ homopolymer alone in spite of the presence of another polymerizable monomer, such as acrylonitrile or methyl methacrylate. Later, Ellinger<sup>3</sup> found thermal copolymerization of VCZ with methyl methacrylate, which seemed to contradict his previous concept. An alternative mechanism may be initiation by ion-radicals. For the strong donor-strong acceptor combination, dissociation of the charge transfer pair to ion-radicals is easily conceivable. For a weak acceptor-

VCZ system, it is, however, questionable as to whether complete electron transfer is energetically accessible. Formation of the ion-radical has been confirmed by ESR spectroscopy for polymerization of VCZ by inorganic acceptors<sup>4</sup> and oxidizing metal salts.<sup>5</sup> Although this seems to be a good support for ion-radical initiation, the same ESR spectra were observed for pairs of *N*-ethylcarbazole and oxidizing metal salts.<sup>5</sup> The identity of the paramagnetic species with the initiating species is therefore an unsolved problem.

Even if the polymerization were initiated by an ion-radical, the propagating species could not be an ion-radical since the ion-radical conjugation system is separated into ion and radical after the first addition of monomer. Also, prior to addition of monomer, a cation-radical paired with an anion-radical might couple to diradical or cation-anion. Such coupling of ion-radicals was suggested as intermediate in the 1,2-cycloaddition between donor and acceptor ethylenic compounds.<sup>6</sup>

Confirmation of ion-radical initiation may be achieved if one proves simultaneous propagation of both ion and radical. The authors have already reported that a single oxidizing metal salt can initiate cationic or radical polymerization of VCZ or 4-vinylpyridine, respectively, and proposed electron transfer initiation via an ion-radical for both systems.<sup>7</sup> In the present study simultaneous propagation of cation and radical is confirmed for photo and thermal polymerization of VCZ-AN system.

The photochemistry of charge transfer polymerization is an interesting subject which has been little examined. Since ion-radical formation or mesomeric polarization is caused by charge separation in a donor-acceptor pair, photoexcitation would be a powerful method for promoting initiation. Even a thermally stable charge-transfer pair such as VCZ-nitrobenzene could be easily brought into polymerization by photoirradiation.<sup>8</sup> In addition, photochemically produced active species would be expected to have a different reactivity from a similar thermally produced one because of the Franck-Condon principle.

## EXPERIMENTAL

### Materials

VCZ (Koch-Light Lab.) was recrystallized once from *n*-hexane; mp 65.2°C.

Styrene and acrylonitrile were washed with alkali and acid then repeatedly with water, dried, and distilled twice over calcium hydride.

*N*-Ethylcarbazole as received (commercial reagent, chemical pure grade) was by no means pure and was purified by repeated recrystallization from methanol after decolorizing the methanol solution by activated charcoal.

Acetonitrile was distilled twice over calcium hydride.

Ammonia was prepared by warming concentrated aqueous ammonia. The evolved ammonia was dried by being passed through a barium oxide

column, purified by trap-to-trap distillations, and finally transferred to the reaction vessel under high vacuum.

All other reagents were commercial materials and used without further purification.

### Light Source and Polymerization

The apparatus for photoirradiation was the same as described in the previous report.<sup>8</sup> Polymerization was carried out in a glass reaction tube of 12 mm diameter. The glass tubes absorbed 98.0–99.9% of light at 290 m $\mu$ . Small differences in absorption by reaction vessel were not serious problems for polymerization systems which have strong absorption at wavelengths over 300 m $\mu$ , such as those systems containing VCZ or ECZ. Depending upon the transparency of the reaction vessels in the near-ultraviolet region, however, considerable fluctuation of polymer yield was observed for the photopolymerization of pure AN, which showed absorption only up to 280 m $\mu$ . Since the reaction vessel does not have a flat surface, it was not possible to determine absolute amount of photoenergy absorbed by the reaction system. As a relative measure, the photoreduction of potassium ferrioxalate solution<sup>9</sup> was examined in the same reaction vessel. The rate of reaction was  $7.15 \times 10^{-5}$ – $7.60 \times 10^{-5}$  mol/l-sec when the initial concentration of Fe<sup>III</sup> was  $6 \times 10^{-3}M$ .

The reaction tube was sealed either in the presence of air or after degassing at a pressure of  $10^{-4}$  mm Hg by several freeze-thaw cycles.

When polymerization was to be carried out in dark, the reaction tube was wrapped with aluminum foil to ensure complete darkness.

Polymerizations of AN–VCZ, AN–ECZ, VCZ–CH<sub>3</sub>CN systems in bulk and some copolymerizations, depending upon monomer feed ratio, proceeded as precipitation polymerization. In particular, the VCZ–AN polymer formed on the glass wall of the reaction tube was partly insoluble even in dimethyl-formamide and dimethyl sulfoxide. Viscosity measurements were therefore not attempted.

The polymerization mixtures were poured into methanol, filtered, and washed with the precipitant.

### Fractionation of Polymers Obtained in VCZ–AN System

The polymerization products of VCZ–AN system were fractionated by benzene extraction at 60°C for 3 days. The benzene extract was precipitated in methanol, and the precipitate was confirmed as polyvinyl-carbazole by infrared spectroscopy.

Extraction of polymer by saturated zinc chloride aqueous solution at boiling point was used to determine the presence of polyacrylonitrile. Polyacrylonitrile prepared by ordinary radical polymerization was completely soluble in such a zinc chloride solution.

### Determination of Polymer Composition

Copolymer compositions of AN-VCZ and AN-St were determined by both elemental analysis and infrared spectroscopy. The key bands for infrared spectroscopy were  $2240\text{ cm}^{-1}$  for AN and  $920\text{--}930\text{ cm}^{-1}$  for VCZ and St. Results by both methods agreed well, and in later studies, determination by infrared spectroscopy was mainly used.

## RESULTS AND DISCUSSION

### AN-VCZ System

Thermal polymerization of this system was first studied by Ellinger<sup>2</sup> and was reported to produce polyvinylcarbazole alone. His results are, however, reproducible only for thermal polymerization in the presence of air. Results of polymerization are shown in Figures 1 and 2 and Table I. Acceleration by photoirradiation is striking. Benzene extraction yields two fractions. The benzene-soluble part was confirmed to be polyvinylcarbazole (PVCZ). The weight fraction of PVCZ depends very much on reaction conditions and additives. In photopolymerization, addition of ammonia completely suppresses the formation of PVCZ (Table I) whereas the total polymer yield increases, as shown in Figure 3. On the other hand,

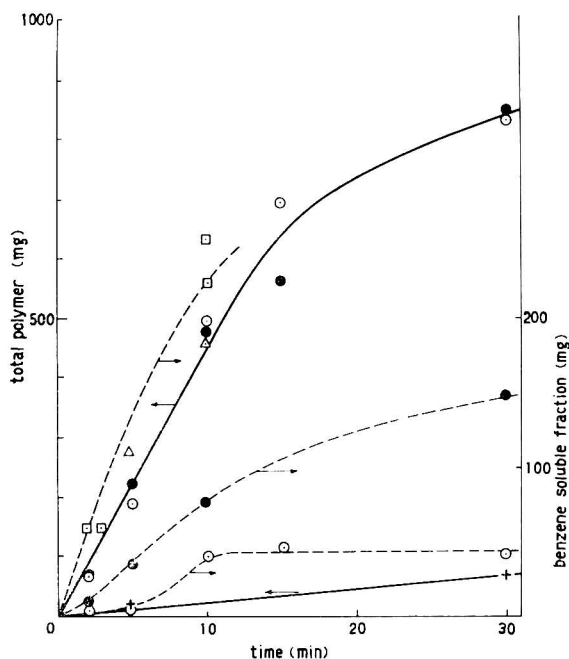


Fig. 1. Plots of (—) total yield and (---) benzene-soluble fraction for photopolymerization of VCZ-AN systems at  $30^{\circ}\text{C}$ : ( $\bigcirc$ ) *in vacuo*; ( $\bullet$ ) in air; ( $\Delta$ ) in  $\text{CO}_2$ ; ( $\square$ ) *in vacuo*,  $[\text{H}_2\text{O}] = 0.1M$ ; ( $+$ ) *in vacuo*,  $[\text{DPPH}] = 10^{-3}M$ .  $[\text{VCZ}] = 1M$  in AN; volume of solution: 3 ml; VCZ 582 mg, AN 2070 mg.

TABLE I  
 Polymerization of VCZ-AN System<sup>a</sup>

Polymeri- zation	Atmosphere	Additive	Time, min	Yield, mg	$D_{220}/D_{930}$ <sup>b</sup>	VCZ in total polymer, mole-%	Benzene- soluble fraction wt-% <sup>c</sup>
Photo	Vacuum	None	10	490	4.05	20.8	8.3
"	Air	"	10	477	2.72	28.1	16.3
"	Vacuum	H <sub>2</sub> O, 0.1 <i>M</i>	3	149	1.16	48.2	
"	"	"	10	630	1.96	36.8	35.6
"	"	DPPH, 10 <sup>-3</sup> <i>M</i>	5	18	0.453	73.0	
"	"	"	30	68	0.601	66.2	41.0
"	"	NH <sub>3</sub> , 0.047 ml	5	400	4.39	19.4	0
Thermal	Vacuum	None	480	77	0.573	67.8	
"	Air	"	480	56	0.0	100	
"	Vacuum	H <sub>2</sub> O, 0.1 <i>M</i>	311	59	0.437	74.1	
"	"	DPPH, 10 <sup>-3</sup> <i>M</i>	311	—	—	—	
"	"	NH <sub>3</sub> , 0.025 ml	2880	47	5.12	17.1	

<sup>a</sup> [VCZ] = 1.0*M* in AN, volume of solution: 3 ml; VCZ 582 mg, AN 2.07 g; Reaction at 30°C for photopolymerization and at 60°C for thermal polymerization.

<sup>b</sup> Intensity ratio of infrared spectra at 2240 cm<sup>-1</sup> and 930 cm<sup>-1</sup>.

<sup>c</sup> Extracted fraction after treating the total polymer with benzene at 60°C for 3 days.

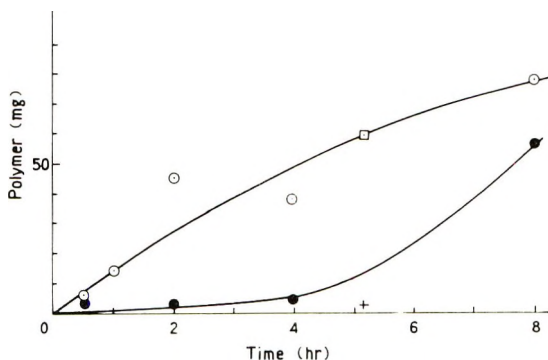


Fig. 2. Thermal polymerization of VCZ-AN systems in the dark at 60°C: (○) *in vacuo*, (●) in air, (◻) *in vacuo*,  $[H_2O] = 0.1M$ ; (+) *in vacuo*,  $[DPPH] = 10^{-3}M$ . VCZ 582 mg, AN 2070 mg.

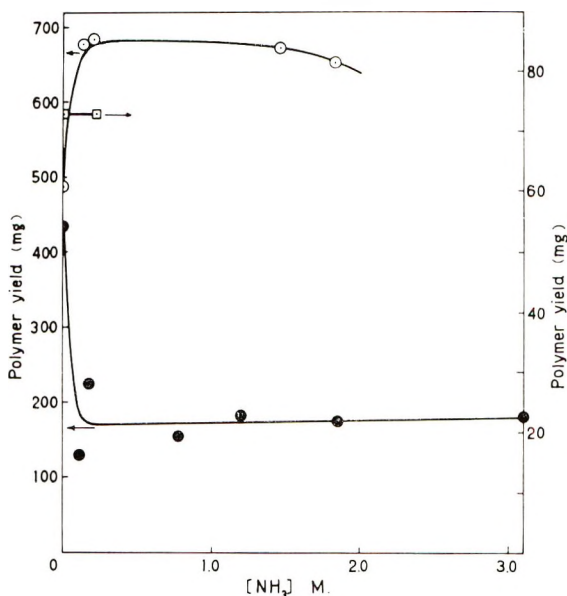


Fig. 3. Effect of ammonia on yield in photopolymerization at 30°C *in vacuo*: (○) VCZ-AN (VCZ 582 mg, AN 2070 mg), polymerization for 10 min; (●) VCZ- $CH_3CN$  (VCZ 582 mg,  $CH_3CN$  2.58 ml), polymerization for 60 min; (◻) VCZ-AN (VCZ 582 mg, AN 2070 mg, azobisisobutyronitrile  $10^{-3}M$ ), dark polymerization at 60°C for 30 min.

addition of 2,2-diphenyl-1-picrylhydrazyl (DPPH) reduces the total polymer yield and increases the VCZ fraction in the polymer.

These findings would indicate that there are at least two simultaneous polymerization mechanisms, which lead to formation of PVCZ and VCZ-AN copolymer. PVCZ is very likely to be formed by a cationic mechanism and the copolymer is by radical mechanism. The presence of air does not hinder polymerization, the yield of PVCZ being higher than in the vacuum system. This result and the similar finding that the rate of polymerization

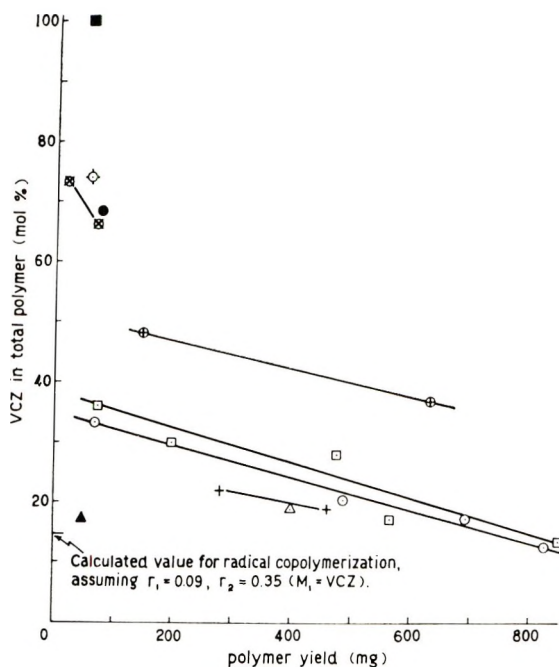
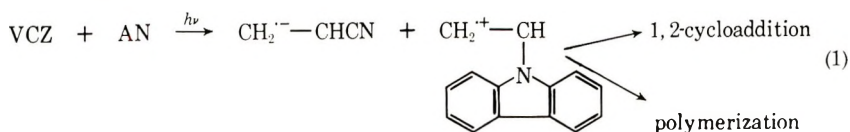


Fig. 4. Plots of content of VCZ in product vs. polymer yield: (□)  $h\nu$ , in air; (○)  $h\nu$ , in vacuo; (⊕)  $h\nu$ , in vacuo,  $[H_2O] = 0.1M$ ; (⊞)  $h\nu$ , in vacuo,  $[DPPH] = 10^{-3}M$ ; (Δ)  $h\nu$ , in vacuo,  $[NH_3] = 0.4-0.75M$ ; (+)  $h\nu$ , in  $CO_2$ ; (⊕) thermal, in vacuo,  $[H_2O] = 0.1M$ ; (▲) thermal, in vacuo,  $[NH_3] = 0.176M$ ; (■) thermal, in air; (●) thermal, in vacuo. VCZ 582 mg, AN 2.07 g; 30°C for photopolymerization, 60°C for thermal polymerization.

increases whereas formation of PVCZ is inhibited in the presence of ammonia, are difficult to explain if one assumes cationic and radical initiating species to be independent of each other. Air and ammonia would not influence the conventional cation and radical, respectively. The most likely explanation is given by the assumption of ion-radical initiation. Ion-radical pairs [eq. (1)] would either initiate polymerization or couple to cyclobutane derivatives. Although products of 1,2-cycloaddition have not been isolated in the present system, the occurrence is very probable by analogy to the reaction between donor vinyl compounds such as vinyl ethers and acceptor ethylenic compounds such as tetracyanoethylene.<sup>6</sup> The present results of additive effect seem to indicate multireactivity of initiating species. These ion-radicals could act as both radical and ionic initiators. It is well conceivable that additives would enhance the initiating efficiency of the ion-radical by converting it to an ordinary radical or ion which might be otherwise totally lost by 1,2-cycloaddition:



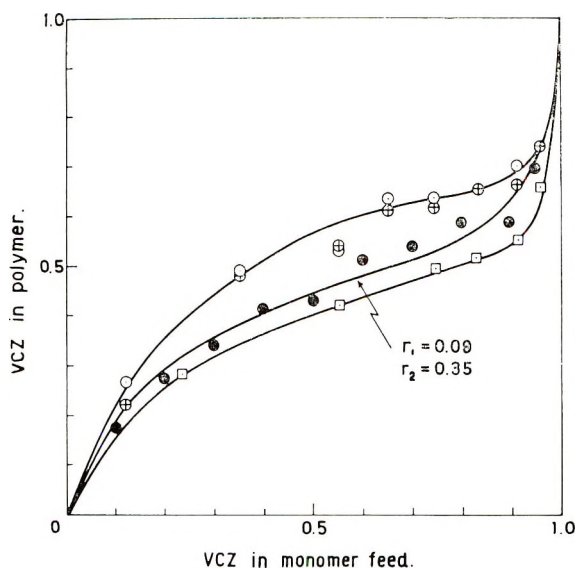


Fig. 5. Composition of polymers from VCZ-AN system: ( $\oplus$ ) photopolymerization in air, 30°C,  $[\text{VCZ}] + [\text{AN}] = 5 \times 10^{-3}$  mol, 2 ml benzene, from N content; ( $\circ$ ) photopolymerization in air, 30°C,  $[\text{VCZ}] + [\text{AN}] = 5 \times 10^{-3}$  mol, 2 ml benzene, from infrared spectrum; ( $\square$ ) photopolymerization in dark, 60°C,  $[\text{VCZ}] + [\text{AN}] = 2.5M$ ,  $\text{AIBN} = 10^{-2}M$ , from infrared spectrum.

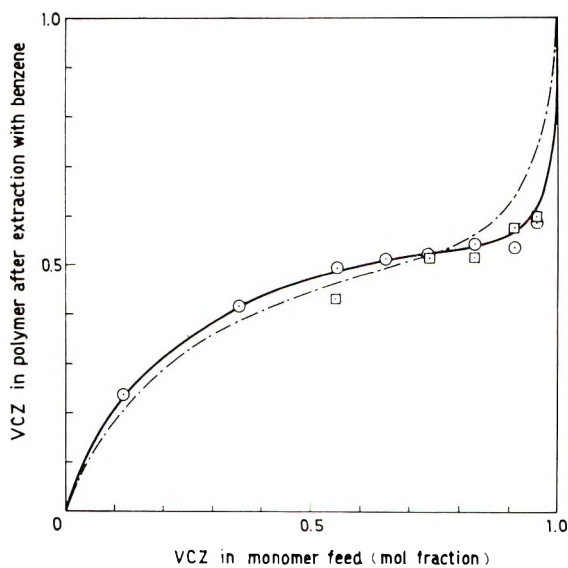


Fig. 6. Composition of photopolymer after benzene extraction: ( $\circ, \square$ ) same as in Fig. 5; (---) radical polymerization at 60°C.

In support of the view mentioned above, ammonia acts as retarder for polymerization of the VCZ-acetonitrile system, in which 1,2-cycloaddition is not expected.

The content of VCZ in polymer under various polymerization conditions is shown in Figure 4 as a function of conversion. These results are understandable if radical and cationic polymerizations occur simultaneously. The effect of water needs to be explained. For an extremely basic monomer such as VCZ, water does not inhibit cationic polymerization but acts as chain-transfer agent. VCZ can be even polymerized by acid in aqueous suspension. Consequently, water might change the cationic activity of the initial ion-radical pair by promoting conversion to proton through chain transfer.

Although formation of anionic polymer is expected, a fraction extractable by saturated zinc chloride solution is not detected; homopolymer of AN does not therefore seem to be formed.

To confirm the polymerization mechanism, the copolymerization of VCZ-AN in benzene was studied. Polymerization was stopped at less than 10% (in most cases, less than 5%) conversion. As shown in Figure 5, there are considerable discrepancies between radical copolymerization and photopolymerization without initiator, in particular in air. The difference is far too large to be attributed to the difference in polymerization temperature (30°C for photopolymerization and 60°C for thermal polymerization). Copolymers by photopolymerization apparently consist of two fractions. After benzene extraction, photopolymers produced in air show decreased content of VCZ and the compositions are nearly identical to photopolymer produced *in vacuo*. The composition curves are close to that of polymer obtained in radical polymerization, as shown in Figure 6.

### AN-ECZ System

In the preceding section, both donor and acceptor are vinyl compounds. It is obvious that polymerization of VCZ is initiated by AN. However, VCZ might as well initiate polymerization of AN. To confirm the action of donor on the polymerization of AN, ECZ was chosen as a nonpolymerizable donor.

Results in Table II indicate that ECZ is an effective photosensitizer for radical polymerization of AN although the system is thermally very stable. The retarding effect of hydrochloric acid might, however, indicate contribution of an anionic species. Copolymerization of AN with styrene initiated by donor confirms the radical mechanism as shown in Figure 7. Donors other than ECZ can be also used. Ferrocene is known to be a strong donor, forming a charge-transfer complex with tetracyanoethylene and other compounds.<sup>10</sup> Photopolymerization of AN is sensitized by ferrocene, as shown in Figure 8. However, charge-transfer interaction between AN and ferrocene is uncertain, since ferrocene is also active for polymerization of styrene. The relative ratio of ferrocene-initiated polymerization of AN to that of styrene is about 6, which is about equal to the

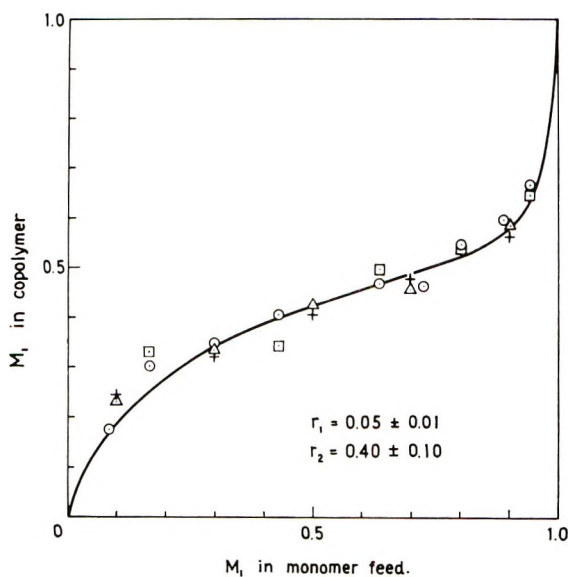


Fig. 7. Composition of photopolymers from AN-styrene at 30°C in bulk: (○) AN-St-AIBN ( $10^{-2}M$ ); (●) AN-St-ferrocene ( $10^{-3}M$ ); (+) AN-St-ECZ, in air,  $[AN] + [St] = 2 \times 10^{-2}M$ , ECZ 0.35 g; ( $\Delta$ ) AN-St-ECZ *in vacuo*,  $[AN] + [St] = 2 \times 10^{-2}$  mol, ECZ 0.35 g.

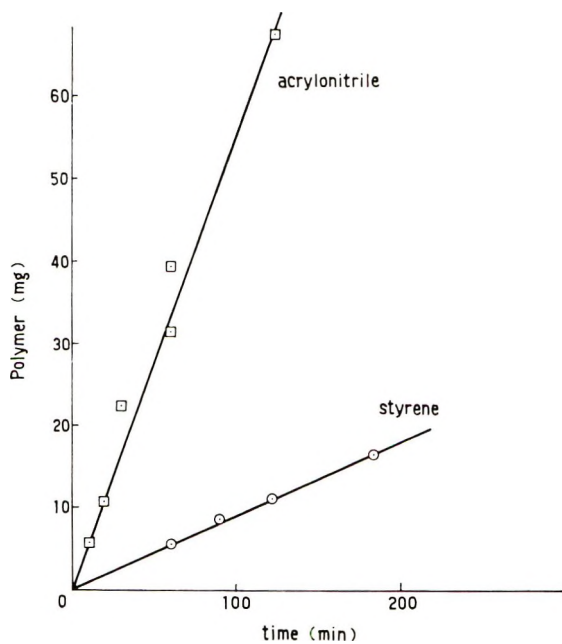


Fig. 8. Photopolymerization of AN and styrene sensitized by ferrocene at 30°C *in vacuo*.  $[Ferrocene] = 1.0 \times 10^{-3}M$ , monomer 1.5 ml.

TABLE II  
Polymerization of AN-*N*-Ethylcarbazole (ECZ) System<sup>a</sup>

Polymerization	Atmosphere	Additive	Time, min	Yield, mg
Photo	Vacuum	None	60	245, 234
"	Air	"	60	112, 105
"	Vacuum	DPPH, $10^{-3}M$	60	20, 31
"	Air	"	60	15, 12
"	Vacuum	HCl, 0.1 <i>M</i>	60	71, 75
"	Air	"	60	11, 14
Thermal	Vacuum	None	360	0
"	Air	"	2900	0

<sup>a</sup> AN 1.5 ml, ECZ 0.35 g; 30°C for photopolymerization, 60°C for thermal polymerization.

ratio  $k_p/k_t^{1/2}$  for AN to that for styrene. There seems to be no special preference to AN when ferrocene is used as sensitizer. For polymerization sensitized by ECZ, the rate ratio of AN to styrene is over 20, to judge by data in Tables II and IV.

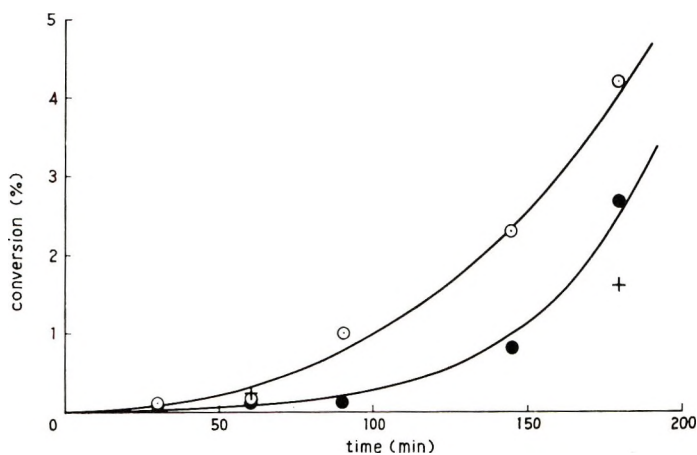


Fig. 9. Photopolymerization of styrene in the presence of ECZ and  $\text{CH}_3\text{CN}$  at 30°C: (○) in air, styrene 2 ml,  $\text{CH}_3\text{CN}$  0.16 ml, ECZ 600 mg; (●) *in vacuo*; (+) styrene alone *in vacuo*.

### VCZ-Acetonitrile System

When the nitrile compound has no vinyl group, polymerization of VCZ is also easily induced by photo irradiation, as shown in Table III. Thermal polymerization is extremely slow, and it is difficult to compare the rates. Thermal polymerization seems to be cationic as judged by effects of additives. The retarding effect of DPPH and ammonia (Fig. 3) supports a radical cationic mechanism of photopolymerization. The effect of DPPH in the photopolymerization system, however, might in part be due to a

TABLE III  
 Polymerization of VCZ-Acetonitrile System<sup>a</sup>

Polymerization	Atmosphere	Additive	Time, min	Yield, mg
Photo	Vacuum	None	60	432
"	Air	"	60	445
"	Vacuum	H <sub>2</sub> O, 0.1 <i>M</i>	60	441
"	"	DPPH, 10 <sup>-3</sup> <i>M</i>	60	4.7
Thermal	Vacuum	None	200	4.5
"	"	"	1440	15.5
"	Air	"	200	6.0
"	"	"	1440	16.4
"	Vacuum	H <sub>2</sub> O, 0.1 <i>M</i>	1440	1.6
"	"	DPPH, 10 <sup>-3</sup> <i>M</i>	180	3.7
"	"	"	1440	13.1
"	"	NH <sub>3</sub> , 0.045 ml	1440	5.7
"	"	NH <sub>3</sub> , 0.015 ml	1440	4.8

<sup>a</sup> [VCZ] = 1.0*M* in acetonitrile, volume of solution 3 ml; VCZ = 582 mg, acetonitrile = 2.58 ml; 30°C for photopolymerization, 60°C for thermal polymerization.

filter effect which would reduce the intensity of light absorbed by the charge-transfer pair, since DPPH has strong absorption bands in the region above 320 m $\mu$  which is employed in the present experiment.

### Polymerization Systems Not Containing Donor or Acceptor

Since photo and thermal polymerizations of vinyl compounds may be brought about by prolonged irradiation or heating without donor-acceptor combination, several sets of reaction systems were examined for their polymerizability as described in Table IV.

 TABLE IV  
 Slow Polymerization Systems without Charge Transfer Interaction<sup>a</sup>

Polymerization system	Polymerization	Atmosphere	Time, min	Yield, mg
VCZ (0.3 g)-benzene (1.0 ml)	Thermal	Air	140	2.7
" "	Photo	"	150	10.0
VCZ (0.3 g)-styrene (1.0 ml)	Thermal	"	270	0.4
" "	Photo	"	300	69.3
ECZ (0.35 g)-styrene (1.5 ml)	Photo	Vacuum	61	10.7
" "	Photo	"	61	3.6
Styrene (0.34 ml)-CH <sub>3</sub> CN (2.58 ml)	Photo	"	460	0
" "	Thermal	"	460	0
AN (1.5 ml)	Photo	"	60	15 $\pm$ 15
Styrene (2.0 ml)-ECZ (600 mg)-CH <sub>3</sub> CN (0.16 ml)	Thermal	"	1920	39.0
" "	"	Air	1920	34.2
Styrene (2.0 ml)	"	Vacuum	1920	52.7

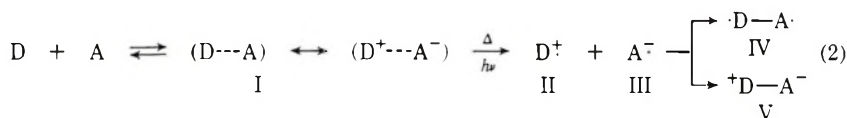
<sup>a</sup> 30°C for photopolymerization, 60°C for thermal polymerization.

Both VCZ and AN are stable to heat and light when the counterpart of the charge transfer pair is absent. Combination of VCZ with styrene shows very low sensitivity towards thermal and photo reaction. When both of donor and acceptor lack a vinyl group, the donor-acceptor pair does not show photosensitivity. The ECZ-acetonitrile pair is an inefficient initiator for polymerization of styrene, as shown in Figure 9.

It is concluded that the presence of a donor-acceptor pair, at least one of which is a polymerizable monomer, is a necessary condition for rapid photopolymerization.

### Polymerization Mechanism

Coexistence of cationic and radical polymerization is clearly shown by the results mentioned above. Formation of initiating species would be as shown in eq. (2):



State I indicates mesomeric polarization which has been claimed as initiator by Ellinger.<sup>2</sup> Although there is no evidence in support of or against the possibility of initiation by I, consideration of I alone as the initiating species is apparently insufficient to explain the whole of polymerization. Assumption of ion-radicals in pairs would be more reasonable to interpret the fact that cationic and radical active species are interrelated. However, the fate of anionic species is still unknown and should be studied under rigorously dry conditions in future.

Further reaction of II and III would yield diradical or cation-anion. Contribution of the diradical in the initiation process, as mentioned by Zutty et al.,<sup>11</sup> is probable in the autocatalytic copolymerization of norbornene with sulfur dioxide, but uncertain for the present system. More than 10 years ago, Gilbert et al.<sup>12</sup> claimed the coexistence of cation and anion in the autocatalytic ionic polymerization of vinylidene cyanide and vinyl ethers. This description is too brief for further comments on the mechanism.

The nature of the initiating species in thermal and photopolymerization is qualitatively the same, since cationic and radical polymerizations are observed for both systems. However, the radical nature of polymerization seems to predominate over the cationic one in photopolymerization compared to the thermal system, although the absolute yield of PVCZ in photopolymerization is much higher than that in thermal polymerization. This might indicate a difference in reactivity of the photoexcited ion-radical pair from the thermally produced one.

### References

1. M. Hatano, H. Nomuri, and N. Tamura, *High Polymers*, **18**, 823, 905 (1967).
2. L. P. Ellinger, *Polymer*, **5**, 559 (1964).
3. L. P. Ellinger, *Polymer*, **6**, 549 (1965).
4. M. Nishii, K. Tsuji, K. Takakura, K. Hayashi, and S. Okamura, *Kabunshi Kagaku*, **23**, 254 (1966).
5. S. Tazuke, T. B. Tjoa, and S. Okamura, *J. Polym. Sci. A-1*, **5**, 1911 (1967).
6. E. M. Kosower, *Progr. Phys. Org. Chem.*, **3**, 112 (1965).
7. S. Tazuke, K. Nakagawa, and S. Okamura, *J. Polym. Sci. B*, **3**, 923 (1965).
8. S. Tazuke, M. Asai, S. Ikeda, and S. Okamura, *J. Polym. Sci. B*, **5**, 453 (1967).
9. C. G. Hatchard and C. A. Parker, *Proc. Roy. Soc. (London)*, **A235**, 518 (1956).
10. M. Rosenblum, R. W. Fish, and C. Bennet, *J. Amer. Chem. Soc.*, **86**, 5166 (1964).
11. N. L. Zutty, C. W. Wilson III, G. H. Porter, and D. C. Priest, *J. Polym. Sci.*, **49**, 143 (1963).
12. H. Gilbert, F. F. Miller, S. J. Averill, E. J. Carlson, V. L. Folt, H. J. Heller, F. D. Stewart, R. F. Schmidt, and H. L. Trumbull, *J. Amer. Chem. Soc.*, **78**, 1669 (1956).

Received November 6, 1967

Revised March 4, 1968

## Photodegradation of Polyethylene Film

JAMES F. HEACOCK, FRANK B. MALLORY,\* and FRANK P. GAY,†  
*Film Department, Experimental Station Laboratory,  
E. I. du Pont de Nemours & Company, Inc., Wilmington, Delaware 19898*

### Synopsis

A structure occurs in radical-polymerized polyethylene which leads to formation of a triene on ultraviolet radiation. An inhibition of oxidative processes is observed while the triene or its precursor are being consumed. Subsequent formation of oxygenated products—hydroxyl, carbonyl, and carboxyl—is well behaved and arises from short wavelength light. A crosslinking reaction is initiated by light of  $\sim 4000 \text{ \AA}$  wavelength.

### Introduction

Exposure of clear, low-density polyethylene films to air and natural or simulated sunlight leads to the uptake of oxygen, the formation of carbonyl, hydroxyl, and vinyl groups, the evolution of acetone, acetaldehyde, water, and oxides of carbon, an increase in brittleness, the formation of crosslinks, and the physical failure of the films. An increase in density and a competition between scission and crosslinking is reported.<sup>1-16</sup>

The thermal oxidation of similar polyethylenes has also been extensively studied.<sup>3,4,8,9-15</sup> The polymers have been observed to undergo changes similar to those found in photodegradation studies except that during thermal degradation vinyl groups are not observed, and carboxyl groups constitute a considerably smaller fraction of the carbonyl groups that are formed.

We have examined the early stages of photodegradation kinetically. These stages should be informative with regard to the chemical processes occurring and are important because functional failure can occur at low oxidation levels.

### Experimental

Films were prepared in the thickness range 25–250  $\mu$ , with most experiments performed on samples of  $150 \pm 5 \mu$  (6 mils). The major studies were on a branched polyethylene of density 0.919 g/cc with 37 methyls, 0.1 vinyl, 0.06 *trans* olefins, and 0.32 vinylidene groups/2000 carbon atoms.

\* Present address: Department of Chemistry, Bryn Mawr College, Bryn Mawr, Pa. Work done on summer appointment, 1958.

† To whom inquiries should be addressed.

Unterzaucher oxygen analysis gave initial (or blank) oxygen content of 0.15%. The number-average molecular weight was 23 000. Laboratory-prepared branched polyethylenes were of comparable viscosity and density. Linear polyethylene was prepared with titanium tetrachloride/aluminum alkyl catalysis with  $\rho = 0.96$ ,  $\eta_{inh} = 1.5$ , and ash  $< 200$  ppm. Polypropylene films were pressed from hexane-extracted commercial resin, Hercules Profax.

Film samples were mounted on a cylindrical rack which was rotated concentrically around ten Westinghouse fluorescent sunlamps.<sup>17</sup> These lamps emit principally in the 2800–3900 Å region with an integrated intensity of  $1.5 \times 10^{-5}$  einsteins/hr-cm<sup>2</sup> at the film-sample distance as measured by uranyl oxalate actinometry.<sup>18</sup> New lamps were washed and operated for 100 hr before use in kinetic runs; lamps were replaced after 1000 hr of use. The sample-to-lamp distance was 3 in. and the distance between adjacent fluorescent tubes was 2.5 in. The entire assembly was housed in an insulated chamber which was maintained within  $\pm 0.8^\circ\text{C}$  at one of five fixed temperatures between 50 and  $90^\circ\text{C}$  by means of compressed air which was passed through a thermostatically controlled furnace and then blown into the chamber. The relative humidity within the chamber was undetectable ( $< 2\%$ ) at all five temperatures.

Infrared absorption spectra of the photodegradation products in the films were obtained with a Perkin-Elmer Model 21 spectrophotometer with a sample of unexposed control film in the reference beam. Absorbance measurements were made at 2.9 (OH), 5.8 (CO), and 11.0 (vinyl)  $\mu$ . The infrared data for each exposure time at each temperature were obtained as averages from at least four film samples which had been exposed during different stages of the 1000-hr lifetimes of the light sources and at different physical locations on the rack. Within a set of replicate samples the mean deviation from the average absorbance at each of the wavelengths was  $< \pm 7\%$ . The thicknesses used caused interference fringes at longer wavelengths and it was necessary to obtain the base line value for the measurements of the vinyl absorbance at 11.0  $\mu$  by drawing in the fringes in accordance with the pattern on both sides of 11.0  $\mu$ .

The peak at 5.8  $\mu$  in the spectra of photodegraded polyethylene films has been assigned to carboxylic acids, ketones, and aldehydes. A procedure was developed<sup>19</sup> to determine carboxyl groups separately from the other carbonyl groups by treatment of the photodegraded films with sulfur tetrafluoride gas at  $80^\circ\text{C}$ . Control experiments on ethylene-methacrylic acid copolymer, ethylene-carbon monoxide copolymer, and polymethacrolein showed that this treatment quantitatively converts carboxylic acids into acid fluorides without affecting ketones or aldehydes. Thus, the absorbance of the peak at 5.8  $\mu$  in the spectra of the photodegraded film samples which had been treated with sulfur tetrafluoride was used as a measure of the concentration of ketones and aldehydes in the samples. The absorbance of carboxyl groups in the films was determined both by the difference in the absorbance at 5.8  $\mu$  before and after treatment with sulfur

tetrafluoride and by the absorbance of the acid fluoride peak at  $5.45\ \mu$  in the spectra of the treated films. The acid fluorides could be hydrolyzed quantitatively back to carboxylic acids by exposure of the treated films to steam for 6–8 hr.

Ultraviolet spectra were obtained by using a Cary Model 14 spectrophotometer.

Crystallinity index and crystalline perfection were determined by x-ray diffraction.

Density was determined in a density gradient column with the use of an ethanol–water system.

Zero strength temperature was determined by placing  $1/4$  in. wide film strips under a load of 25 g against a bar at various temperatures. The time to break at a series of temperatures is plotted and zero strength temperature determined graphically as the temperature for 5 sec to break.

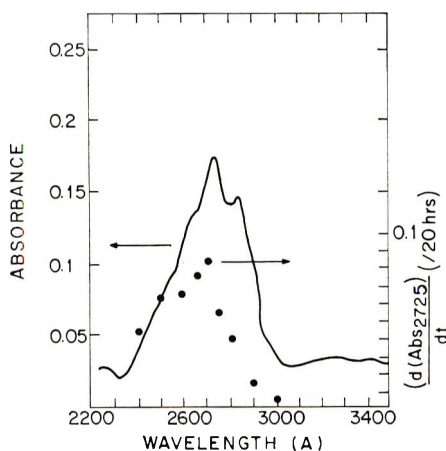


Fig. 1. Triene formation: (—) ultraviolet absorption of ultraviolet-irradiated 150  $\mu$  polyethylene after 2 hr; (●) rate of formation of absorbance at 2725 Å as a function of exposure wavelength with normalized incident energy.

## Results

The first observable change in branched polyethylene caused by irradiation with fluorescent sunlamps is the appearance of a group of peaks in the vicinity of 2725 Å in the absorption spectrum (Fig. 1). No absorption change was detected in the infrared spectrum. The absorbance at 2725 Å reached a maximum value of 0.15 in 150  $\mu$  film after a 2-hr exposure at 50°C. The initial rate at which the absorbance of this multiplet developed was temperature-independent between 50 and 90°C and was the same *in vacuo*, nitrogen, air, and oxygen, indicating no oxygen dependence or a low enough requirement to be satisfied by dissolved oxygen. The rate was half order in incident light. Continued exposure caused a decrease in the intensity of the multiplet. The rate of disappearance of the multiplet was

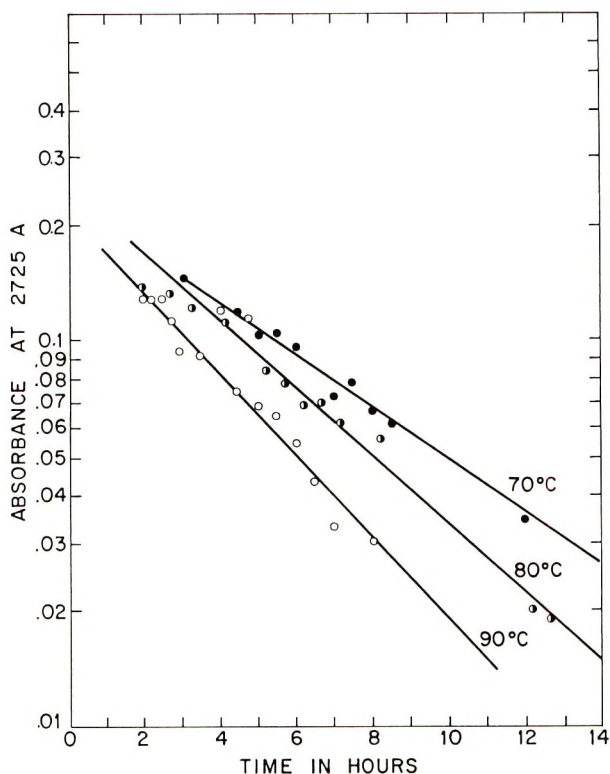


Fig. 2. Destruction of triene on irradiation at 70, 80, and 90°C.

first order in multiplet and was temperature-dependent with a 5.6 kcal/mole activation energy (Fig. 2). The exposure time required for complete disappearance of the multiplet at each temperature corresponded roughly to the induction time for onset of formation of hydroxyl, carbonyl, carboxyl, and vinyl groups.

The formation of the multiplet was observed after irradiation in films of additive-free polyethylene which had been prepared both with peroxide and with azo initiators. No multiplet formation was observed in an experiment with linear polyethylene. Soxhlet extraction of the polyethylene with various liquids prior to irradiation did not prevent formation of the multiplet.

By using a Beckman DU as a monochromator and normalizing the photon flux (determined by uranyl oxalate actinometry) for the various wavelengths, the activation spectrum was obtained for formation of the multiplet (Fig. 1). The rate of formation of multiplet is at a maximum at 2750 Å, decreases with shorter and longer wavelengths, and becomes negligible at 3000–3100 Å. By use of cut-off filters, exposure of the film to the 3900–4100 Å region was shown to destroy a precursor of the multiplet by some path not involving the multiplet. Thus, the formation of the multiplet was not observed when the film was exposed to direct sunlight or carbon arc

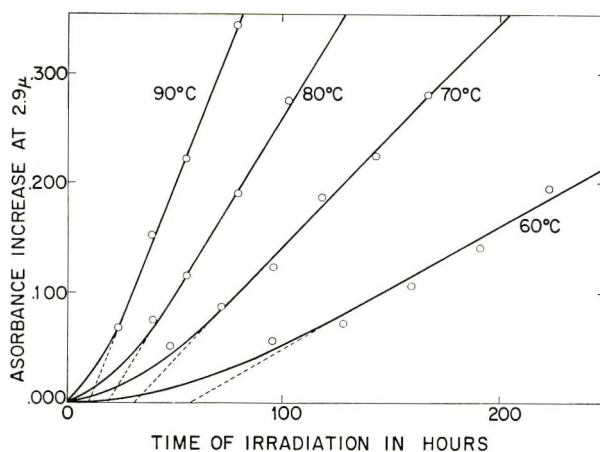


Fig. 3. Hydroxyl content of photodegraded polyethylene film.

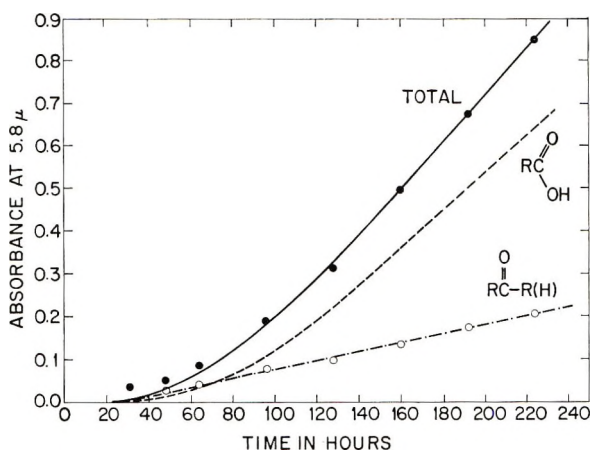


Fig. 4. Formation of carboxyl and carbonyl at 60°C.

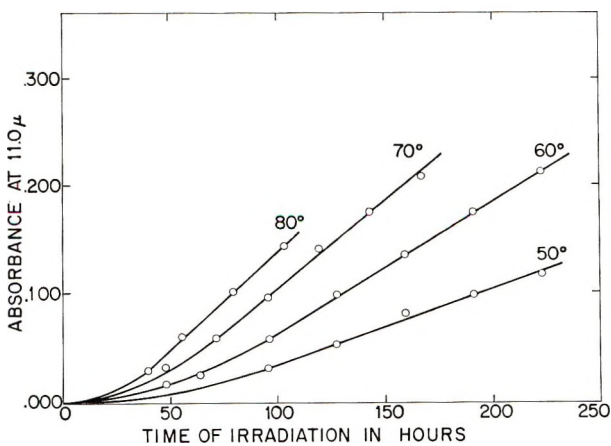


Fig. 5. Vinyl content of photodegraded polyethylene film.

TABLE I  
Rate Parameters for Functional Group Formation

Temperature, °C	$(dA/dt)(\text{CO})$ $\times 10^{3a}$	$t_0^b$	$(dA/dt)(\text{OH})$ $\times 10^{3a}$	$t_0^b$	$(dA/dt)(\text{C}=\text{C})$ $\times 10^{3a}$	$t_0^b$	$1/2(d^2A/dt^2)-$ $(\text{CO}_2\text{H})$ $\times 10^5$	$t_0^b$
50	0.44	63	c	c	0.70	51	0.78	60
60	1.1	30	1.11	57	1.19	50	2.3	30
70	2.8	22	2.05	31	1.63	36	6.0	22
80	5.2	15	3.19	19	1.80	23	15.0	15
90	10.1	10	4.93	10	(1.70)	12	32.0	10
$E^\ddagger$ , kcal/mole	19.2		10.9				22.6	

<sup>a</sup> In absorbance units per hour.

<sup>b</sup> Back extrapolated effective zero time.

<sup>c</sup> Absorbance at 2.9  $\mu$  did not develop enough for accurate evaluation.

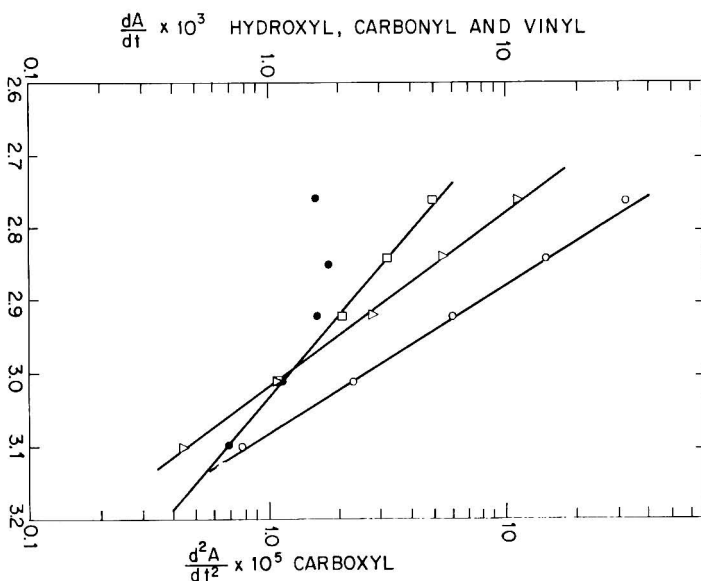


Fig. 6. Arrhenius plots of functional group formation: (O) carboxyl; ( $\Delta$ ) carbonyl; ( $\square$ ) hydroxyl; ( $\bullet$ ) vinyl.

radiation. The rate of destruction of the multiplet itself (formed by irradiation for 2 hr with fluorescent sunlamps) with 3900–4100 Å radiation was slow, demonstrating that the mechanism for the destruction of the precursor, under these conditions, does not include the species responsible for the multiplet as an intermediate. After a 20–30 hr exposure to carbon arc radiation or direct sunlight, no multiplet was formed on subsequent irradiation with fluorescent sunlamps. Treatment with bromine vapor also suppressed formation of the multiplet.

Figure 3 shows the formation of hydroxyl (absorbance at 2.9  $\mu$ ) as a function of exposure time at several different temperatures. Figure 4 demonstrates the increase in absorbance at 5.8  $\mu$ , as a function of exposure time at 60°C, along with the division of this absorbance into its carboxyl and carbonyl components. Curves for the vinyl group formation were similar to the hydroxyl curves (Fig. 5). The data for the hydroxyl and vinyl group showed an eventual decrease in  $dA/dt$  in the 90°C experiment. The ketone absorbance may show a similar trend at high oxidation levels. All three absorbances follow a rate law of  $A_x = k_x(t - t_0)$ , where  $t_0$  is an extrapolated zero time (= induction period). The carboxyl absorbances can be broken into two parts. The first part holds to moderately high oxidation levels (2–4% oxygen) and is of the form  $A_c = k_c(t - t_0)^2$  and the second part is a linear function,  $A_c = k_c'(t - t_0')$ . On heavier gauge films (150  $\mu$ ) the linear portion of the carboxyl curve is only evident on samples aged at 50 and 60°C, but in thin films (50  $\mu$ ) where the absorbance can be followed to higher oxidation levels, the carboxyl absorbance apparently becomes linear during the aging at 70, 80, and 90°C.

The rates in terms of absorbance units are given in Table I. Arrhenius plots of these data, in Figure 6, give reasonable straight lines and the activation energies,  $E^\ddagger$ , are also tabulated in Table I.

Using the extinction coefficients: ketone  $\sim 190$ , hydroxyl  $\sim 55$ , vinyl  $\sim 150$ , and carboxyl  $\sim 500$  l./mol-cm, we can calculate the approximate composition of a polyethylene film after a typical run of 244 hr at  $60^\circ\text{C}$ . The polymer contains about one hydroxyl per 300 carbon atoms, one carboxyl per 900 carbon atoms, one ketone or aldehyde per 1000 carbon atoms and one vinyl group per 700 carbon atoms. Calculated oxygen content was  $\sim 0.7\%$  while measured content was  $0.85\%$ .

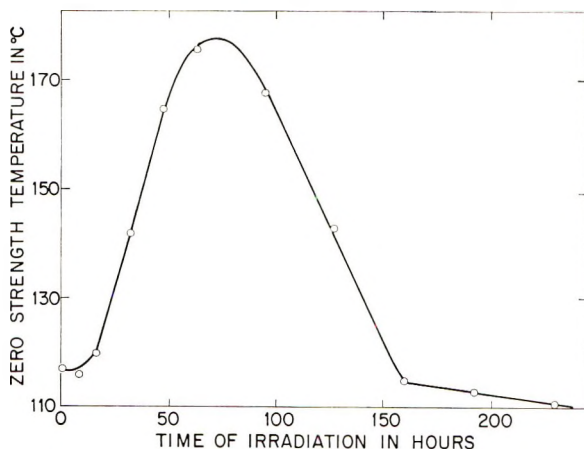


Fig. 7. Zero strength temperature of polyethylene film photodegraded at  $60^\circ\text{C}$ .

Measurements of the ultraviolet spectra of the photodegraded films after multiplet destruction showed the absorbance at various wavelengths in the  $260\text{--}360\text{ m}\mu$  region was linear with exposure time at each temperature; the slopes increased with temperature. Except for the transient peaks of the multiplet, no distinct maxima were observed in the ultraviolet.

Plots of the percentage oxygen (Unterzaucher) in the films against the exposure time at each temperature gave a family of curves qualitatively similar to the curves for the carbonyl and hydroxyl data. The activation energy for overall oxygen incorporation was  $\sim 5$  kcal/mol compared to an activation energy for oxygen diffusion of  $9.8$  kcal/mole.<sup>20</sup> As a further check on diffusion control, in 200 hr at  $60^\circ\text{C}$ ,  $1\text{ cm}^2$  of  $150\text{ }\mu$  thick film picks up  $\sim 1.4 \times 10^{-4}$  g oxygen compared to an oxygen flux of  $\sim 3 \times 10^{-3}$  g, calculated by using the room temperature permeability coefficient. The maximum oxygen content to which the degradation was carried was  $4.4\%$  after 104 hr at  $90^\circ\text{C}$ .

Plots of the density of the photodegraded films against exposure time at each temperature also resembled the plots for the carbonyl and hydroxyl data except for anomalous behavior during early stages of exposure. The measured density of the unexposed virgin film was  $0.9189\text{ g/cc}$ , but only the

density data for the films photodegraded at 60 and 70°C appeared to extrapolate back to this value at zero exposure time. The 50°C data extrapolated to about 0.915 g/cc, whereas the 80 and 90°C data extrapolated to about 0.921 g and 0.922 g/cc, respectively. The maximum density observed in this work was 0.9640 g/cc (after 104 hr at 90°C). The crystallinity index and crystalline perfection increased as density increased.

Plots of the values of the zero strength temperature (ZST) for the photodegraded films against exposure time at each temperature gave a well-behaved family of curves of the type shown in Figure 7. These curves were characterized by a maximum zero strength temperature  $Z_{\max}$  and by a sharp inflection point which was reached after a longer exposure time. The values of these parameters are given in Table II.

TABLE II  
Parameters from Zero Strength Temperature Measurements

Temperature °C	$Z_{\max}$ , °C	$t_{Z_{\max}}$ , hr	$t_{Z_{\text{inflection}}}$ , hr
50	147	105	242
60	178	72	160
70	204	58	130
80	210	39	106
90	216	26	81

Cut-off filter experiments show that the reactions can proceed at wavelengths between 3900 and 4100 Å. At these wavelengths, in the absence of short wavelength radiation, the ZST approaches a limiting value with time rather than passing through a maximum. The limiting value is near 300°C.

Film samples which had been previously photodegraded to various extents at 80°C were heated for a further 138 hr at 80°C in the dark, other conditions remaining constant. The samples developed an additional absorbance at 5.8  $\mu$  equivalent to only an additional 11 hr light exposure. The vinyl group absorbance at 11.0  $\mu$  decreased slightly as has been observed previously for thermal degradation.<sup>4</sup>

Addition of antioxidants inhibits the degradation of polyethylene by 4000 Å light and by heat alone, but does not have a strong effect on polymer irradiated by 2750 Å light. Some degradation proceeds through the multiplet with 2750 Å light, while radical species are scavenged by the antioxidant.

### Discussion

In this discussion 2750 Å light will refer to a broad band centered at 2750 Å; similarly 4000 Å light will refer to a broad band centered at 4000 Å.

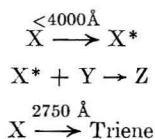
The course of the photodegradation separates naturally into an initial and a later stage. The following observations on the initial stage were detailed in the previous section and are now considered further: (1) initial radiation of polyethylene with light of 2750 Å yields a multiplet in

the 2750 Å region, while thermal treatment and 4000 Å light do not cause formation of the multiplet; (2) radiation of polyethylene by 4000 Å light stops formation of the multiplet by subsequent 2750 Å radiation; (3) the multiplet disappears in a thermal reaction with a low enthalpy of activation, 5.6 kcal/mol; and (4) only after disappearance of the multiplet or its precursor(s) do the rates of formation of carbonyl, hydroxyl, and carboxyl groups become well behaved.

The multiplet is the first product of the photolysis of polyethylene by 2750 Å light which allows analysis. The structure responsible for these peaks is assigned to conjugated triene because of its close spectral resemblance to many trienes.<sup>21,22</sup> If the *trans* configuration is assumed for all double bonds, the 2840, 2725, and 2630 Å peaks of the multiplet are shifted about 50 Å to longer wavelengths than expected for the internal triene. Either an additional alkyl substituent or a replacement of a *trans* by a *cis* double bond would accommodate the spectrum of the multiplet. A similar structure has been observed<sup>1</sup> on electron irradiation of polyethylene.<sup>23</sup>

Some information on the triene's precursor is available. First, heat and 4000 Å light do not cause formation of triene. Either the precursor does not exist under these circumstances or it reacts differently than it does with 2750 Å light. A difference between thermal and photochemical reactions is not surprising. To find a complete change in reactions between 2750 and 4000 Å light is surprising. Since initial 4000 Å radiation precludes triene formation, failure to absorb 4000 Å is eliminated as a rationale. Failure of 4000 Å radiation rapidly to destroy preformed triene eliminates the possibility of only a small undetected triene concentration being present. We conclude that the action of the 4000 Å light is upon a species prior to the immediate precursor of the triene.

We consider the following a likely but unproven hypothesis. All species which absorb 4000 Å also absorb 2750 Å light. The absorption at long wavelengths may be accounted for by an oxygen collision complex of the type described by Evans.<sup>24</sup> (If so, the precursor may resemble a diene.) The absorption results in the formation of an oxygen adduct. With the long wavelength light, the adduct rearranges to a stable product which is involved in the crosslinking reactions. With the shorter wavelength light, the adduct is unstable and the net chemistry is dehydrogenation to form the conjugated triene as one product. In the latter case a competitive situation obtains, in the former case the structure is simply destroyed. In the simplest case:



A second piece of information concerning the precursor is its minimum concentration. Since both the rates of appearance and disappearance of the triene are known, the maximum absorbance of the triene (in the hy-

pothetical absence of triene loss) can be calculated. This maximum absorbance is 0.205 at 2725 Å in the case of samples used. Using a triene extinction coefficient at 2725 Å of  $\sim 6 \times 10^4$  l./mol-cm, a concentration of  $\sim 1$  triene unit per 300,000 carbons or about 1/13 chain was calculated for our sample. This must be a minimum concentration of the precursor.

A third piece of information on the precursor is available. The origin of the precursor is in the radical-polymerized polyethylene. It is not in additives since triene formation was observed in additive-free polyethylene initiated with peroxide or azo compounds. Failure to remove the precursor by extraction of the polymer indicates it is chemically bonded to the chain. Failure to generate triene during the photolysis of linear polyethylene restricts the origin of the precursor to a radical polymerization.

In summary a structure occurs in radical-polymerized polyethylene which is converted to triene after light absorption. It also scavenges radicals generated from other sources. The triene disappears by a reaction of low activation energy.

Approximately at the time of triene disappearance the normal oxidation processes became well behaved and more rapid. We believe the two events are related. In our simple scheme the end of the induction period would coincide with the disappearance of the radical-scavenging precursor and implies that photooxidation occurs in restricted locales of the polymer. The debris from the triene (or precursor) decomposition may be involved in subsequent events.

Before proceeding to a discussion of the oxidative processes, the assignment of the 2.9  $\mu$  absorption peak predominantly to alcoholic hydroxyl will be considered. The O—H stretching vibration in carboxylic acids usually occurs in the 3.3–3.6  $\mu$  region rather than at 2.9  $\mu$ . The former region was not accessible for accurate measurements because of the intense C—H absorption of the polymer; however, absorption here did increase as the carboxyl content increased. The assignment for alcoholic hydroxyl groups was supported by the apparent formation of 3,5-dinitrobenzoate esters which were attached to the polymer when a Decalin solution of the oxidized polymer was treated with 3,5-dinitrobenzoyl chloride in the presence of pyridine. Although hydroperoxides and perhaps peracids are intermediates in the photodegradation of polyethylene, the concentrations of these groups are believed insufficient to account for the 2.9  $\mu$  absorption. Free and associated hydroperoxide groups in polyethylene are reported to absorb at 2.81<sup>4,12,14</sup> and 2.97  $\mu$ <sup>12</sup> respectively. The fact that the 2.9  $\mu$  band did not decrease after treatment at 200°C argues against a major contribution of hydroperoxides.

After the triene disappearance, the following salient features develop. The concentrations of hydroxyl and carbonyl groups increase linearly with time with activation energies of 11 and 19 kcal/mol, respectively. The carboxyl content increased linearly as a function of time squared with an activation energy of 23 kcal/mol. Structureless ultraviolet absorption increased in the 2600–3600 Å region. Oxygen uptake, density, crystallin-

ity, and crystalline perfection increase parallel with carbonyl and hydroxyl concentration. The zero strength temperature reaches a maximum which is followed by an inflection point.

The increased rate of production of oxygen-containing groups with the disappearance of triene has already been considered speculatively. The steady rate of their appearance was not anticipated because the quantity of absorbed light increases over the long period of constant rate. An explanation can be devised for this finding but elaboration is not considered fruitful. The increase in density (over that caused by oxygen uptake), crystallinity, and perfection of crystallinity indicates that the reactions occur in the disordered regions. This means that the amorphous regions may contain as much as 20% oxygen by the end of a 90°C run, if the initial crystalline fraction is of the order of 70%.

The locus of attack may be inferred from the behavior of linear polyethylene and polypropylene under the same exposure conditions. Linear polyethylene fails physically quite rapidly but the rate of oxidation to form hydroxyl and carbonyl groups is much slower than observed in branched polyethylene. On the other hand, polypropylene also fails rapidly but the rate of oxidation is much higher. In this case growth of hydroxyl is greater than carbonyl, both being greater than seen in branched polyethylene. Taken in conjunction with the density and crystallinity data, these observations lead to the conclusion that attack occurs predominantly at branch points. Since we know of no data indicating solubility of diffusion of oxygen in the well ordered crystalline fractions of these polymers, coincidence of these branch points in the disordered regions and attack are consistent.<sup>25-27</sup> The oxidation results primarily in destruction of the accessible amorphous regions which are also the regions subject to physical stress. Thus, highly crystalline linear polyethylene would be expected to and does fail physically at very low oxidation levels.

The formation of carboxyl groups does not parallel that of hydroxyl and carbonyl groups. If we postulate a photooxidation of an aldehyde, then the calculated enthalpy of activation is that of aldehyde formation from a secondary source such as peroxy or its precursor. We do not find evidence for a significant concentration of aldehyde so an efficient photochemical conversion to carboxyl must exist. Thermal treatment should either not yield carboxyl or should yield it in much reduced quantities, which is consonant with our results and reports on thermal oxidation.<sup>4</sup>

If one assumes zero strength temperature  $Z$  can be related to melt viscosity, we can calculate a crosslink density of the polymer. The initial increase in  $Z$  with exposure time is attributed to the formation of crosslinks, tentatively peroxidic. Peroxidic crosslinks have been postulated in polyethylene after high energy radiation in the presence of oxygen. The limiting value of 300°C of  $Z$  with long wavelength irradiation is compatible with values for polyethylenes crosslinked in other manners.

The decrease in  $Z$  is attributed to chain scission reactions. Since vinyl and carboxyl formation parallel the decrease, a direct correlation is prob-

able. The difference in magnitudes of the two is attributed to the relative insensitivity of the viscosity to increasingly larger numbers of smaller fragments in the presence of a relatively constant number of large chains from the crystalline regions. The inflection is associated with a "no strength" melt caused by severe degradation.

The crosslinking was shown to occur on exposure to 4000 Å radiation and to be relatively independent of carbonyl and hydroxyl formation. We conclude that a different set of reaction paths is dominant in the two different wavelength regions. The set at higher wavelengths is associated with the formation of crosslinks. The set at lower wavelengths is associated with the formation of triene, carbonyl, and hydroxyl groups. At least in the early stages, the longer wavelength reactions are more inhibited by antioxidants than the latter. Reactions originating from the 4000 Å species are interfered with by the 2750 Å product set since crosslink formation is slowed and the zero strength temperature passes through a maximum in the presence of an ultraviolet continuum. These effects can be seen on comparison of functional groups generated in exposures to various wavelength sources such as sunshine, xenon lamps, or carbon arcs.

The overall photodegradative process has the characteristics of a photo-initiated thermal decomposition. The product distribution differs from straight thermal degradation because of the nature of the initiating species. The photoreactions are of two types: the first is peculiar to long wavelengths and yields primarily crosslinking; the second occurs at shorter wavelengths and gives the mixture of chemical products usually examined.

### References

1. A. W. Pross and R. M. Black, *J. Soc. Chem. Ind.* (London), **69**, 113 (1950).
2. A. R. Burgess, *Nat. Bur. Std. (U. S.) Circ.*, **No. 525**, 149.
3. L. H. Cross, R. B. Richards, and H. A. Willis, *Discussions Faraday Soc.*, **9**, 235 (1950).
4. F. M. Rugg, J. J. Smith, and R. C. Bacon, *J. Polym. Sci.*, **13**, 535 (1954).
5. V. T. Wallder, W. J. Clarke, J. B. DeCoste, and J. B. Howard, *Ind. Eng. Chem.*, **42**, 2320 (1950).
6. G. Oster, G. K. Oster, and H. Moroson, *J. Polym. Sci.*, **34**, 671 (1959).
7. H. Wilski, *Angew. Chem.*, **71**, 612 (1959).
8. B. S. Biggs, *Nat. Bur. Std. (U. S.) Circ.* **No. 525**, 137.
9. C. S. Myers, *Ind. Eng. Chem.*, **44**, 1095 (1952).
10. B. S. Biggs, and W. L. Hawkins, *Mod. Plastics*, **31**, No. 1, 121 (1953).
11. J. E. Wilson, *Ind. Eng. Chem.*, **47**, 2201 (1955).
12. J. D. Burnett, R. G. J. Miller, and H. A. Willis, *J. Polym. Sci.*, **15**, 592 (1955).
13. H. C. Beachell and S. P. Nemphos, *J. Polym. Sci.*, **21**, 113 (1956).
14. J. P. Luongo, *J. Polym. Sci.*, **42**, 139 (1960).
15. H. C. Beachell, and G. W. Tarbet, *J. Polym. Sci.*, **45**, 451 (1960).
16. E. Turi, L. G. Roldan, F. Rahl, and H. J. Oswald, paper presented at Meeting of American Chemical Society, Chicago, 1964; *Polymer Preprints*, **5**, No. 2, 558 (1964).
17. Westinghouse Data Sheet No. ASC-502.
18. K. R. Osborn, *J. Polym. Sci.*, **38**, 357 (1959).
19. J. F. Heacock, *J. Appl. Polym. Sci.*, **7**, 2319 (1963).
20. H. J. Bixler, Dissertation, MIT, Cambridge, Mass.

21. L. Crombie and J. L. Tayler, *J. Chem. Soc.*, **1954**, 2816.
22. C. Y. Hopkins and M. J. Chisholm, *Can. J. Chem.*, **40**, 2078 (1962).
23. D. M. Bodily and M. Dole, *J. Chem. Phys.*, **45**, 1428 (1966).
24. D. F. Evans, *J. Chem. Soc.*, **1960**, 1735.
25. W. L. Hawkins, W. Matreyek, and F. H. Winslow, *J. Polym. Sci.*, **41**, 1 (1959).
26. F. H. Winslow, W. Matreyek, and S. M. Stills, paper presented at American Chemical Society Meeting, Phoenix, 1966; *Polymer Preprints*, **7**, No. 1, 390 (1966).
27. M. P. Schard and C. A. Russell, *J. Appl. Polym. Sci.*, **8**, 985 (1964).

Received March 5, 1968

## NOTES

*Preparation and Polymerization of 2-Pyridyl Methacrylate*

In the course of our study on the reactivities of methacrylate monomers, we prepared 2-pyridyl methacrylate, in which an electron-attracting heterocyclic ring is attached to the ester group, and examined its polymerizabilities in radical and anionic polymerizations. In this note, we wish to report those results briefly.

**Preparation of Monomer**

Methacrylic chloride and anhydrous sodium 2-pyridinolates, prepared via the diazonium salt of commercial 2-aminopyridine,<sup>1</sup> were reacted in benzene suspension with ice cooling. 2-Pyridyl methacrylate, boiling at 90–93°C/4 mm Hg, was obtained in 60% yield. Other physical properties of this monomer are: mp ca. –15°C,  $d_{20}^{20}$  1.5168, insoluble in water but soluble in usual organic solvents. The structure was identified by the infrared spectrum, which showed  $\nu_{C=O}$  1742 cm<sup>-1</sup>,  $\nu_{C=C}$  1638 cm<sup>-1</sup>,  $\nu_{C=N}$  of ring 1593, 1574 cm<sup>-1</sup>,  $\delta_{CH}$  (1,2-substd. ring) 773 cm<sup>-1</sup>, and by the NMR spectrum showing, besides methacrylic protons at 8.02, 4.27, and 3.67  $\tau$ , ABCD type complex multiplets at 1.6–3.1  $\tau$ , which is very similar to those for 2-picoline and 2-aminopyridine.

The electron-attracting property of the 2-pyridyl group is exemplified by the higher carbonyl-stretching vibration (Table I) and is comparable to that of the *p*-nitrophenyl group.

TABLE I  
 $\nu_{C=O}$  of Methacrylates

Ester group	$\sigma^*$	$\nu_{C=O}$ , cm <sup>-1a</sup>
Methyl	0.00	1716
Phenyl	+0.60	1728
<i>p</i> -Nitrophenyl	+0.78 <sup>b</sup>	1742 <sup>c</sup>
2-Pyridyl	—	1742

<sup>a</sup> In CCl<sub>4</sub> solution.

<sup>b</sup>  $\sigma_p$  value.

<sup>c</sup> In CHCl<sub>3</sub> solution.

**Radical Homopolymerization**

2-Pyridyl methacrylate gives white powdery polymer with azobisisobutyronitrile between –78°C (with the aid of sunlight) and +180°C in bulk or solution. Specific viscosities of the polymers ranged from 0.5 to 0.1 dl/g (0.5% pyridine solution at 30°C). The white polymer is likely to take on a light-brown color on drying. Pyridine is the only solvent for the polymer we have found; benzene, chloroform, acetone and even dimethylformamide and dimethyl sulfoxide have no solvent power. The PMT (polymer melt temperature)<sup>2</sup> was 100–110°C. The polymer structure was identified by infrared and NMR spectra. The  $\alpha$ -methyl protons in the NMR spectrum do not show triad-splitting; however, the spectrum obtained after the polymer was hydrolyzed in concentrated sulfuric acid and reesterified with diazomethane was the same as that obtained for poly(methyl methacrylate). We were able to calculate the activation parameter dif-

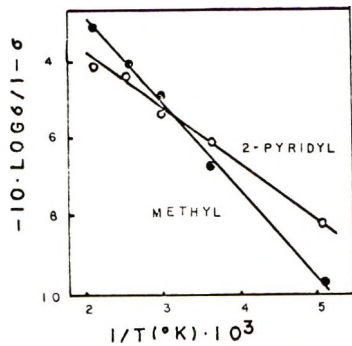


Fig. 1. Bovey plots for (●) methyl methacrylate and (○) 2-pyridyl methacrylate.

ferences between isotactic and syndiotactic propagation according to Bovey's equation:<sup>3</sup>

$$2.30 \log \sigma / 1 - \sigma = \Delta S_i^{\ddagger} - \Delta S_s^{\ddagger} / R + \Delta H_i^{\ddagger} - \Delta H_s^{\ddagger} / RT$$

The results are shown in Figure 1 and Table II. Here we found a smaller activation enthalpy difference for 2-pyridyl methacrylate than for methyl methacrylate.

TABLE II  
Activation Parameter Differences for Methyl and 2-Pyridyl Methacrylates

Ester group	$\Delta H_i^{\ddagger} - \Delta H_s^{\ddagger}$ , kcal/mol	$\Delta S_i^{\ddagger} - \Delta S_s^{\ddagger}$ , eu
Methyl	1.03	0.7
2-Pyridyl	0.64	-0.5

Radical Copolymerization

Copolymerization experiments were carried out at 60°C with azobisisobutyronitrile as initiator. Methyl methacrylate or styrene was chosen as comonomer (M<sub>1</sub>). Co-

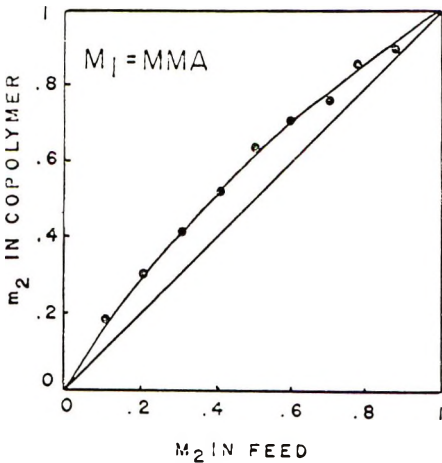


Fig. 2. Copolymerization of 2-pyridyl methacrylate with methyl methacrylate.

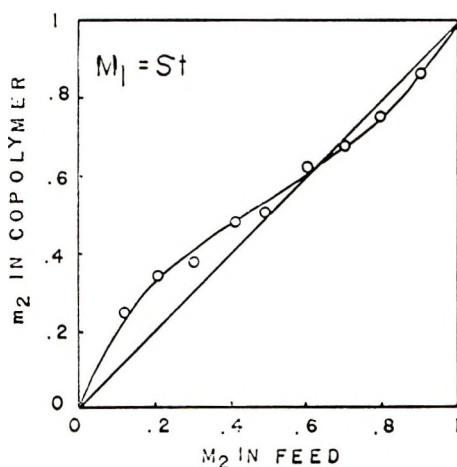


Fig. 3. Copolymerization of 2-pyridyl methacrylate with styrene.

polymer compositions were calculated from nitrogen assays. Monomer reactivity ratios were calculated by the Fineman-Ross equation, and the experimental errors were calculated at the confidence level of 95%. The results are shown graphically in Figures 2 and 3 and Table III. Although the discrepancy between two sets of  $Q$ ,  $e$  parameters is not small, the relatively large  $Q_2$  and  $e_2$  values are compatible with the electron-attracting property of 2-pyridyl group when compared to those values of methacrylate monomers.<sup>4</sup>

TABLE III  
Monomer Reactivity Ratios and  $Q$ ,  $e$  Values of 2-Pyridyl Methacrylate (M)

$M_1$	$r_1$	$r_2$	$Q_2$	$e_2$
Methyl methacrylate	$0.60 \pm 0.05$	$1.4 \pm 0.15$	1.5	+0.8
Styrene	$0.35 \pm 0.03$	$0.62 \pm 0.11$	1.1	+0.5

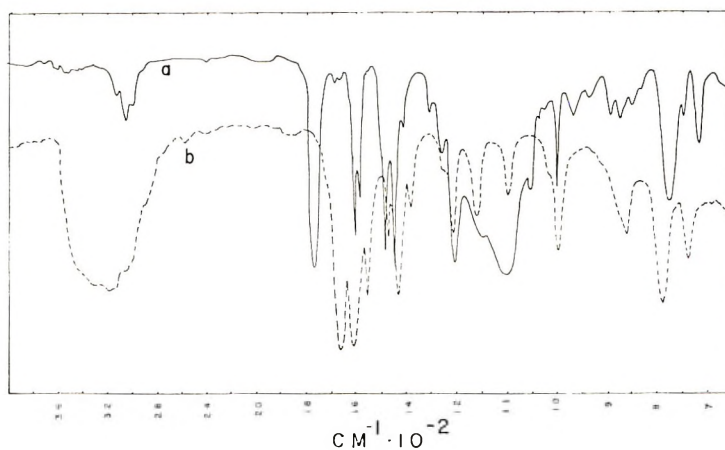


Fig. 4. Infrared spectra of polymers obtained (a) with AIBN and (b) with phenylmagnesium bromide.

### Anionic Polymerization

Attempted anionic homopolymerization with phenylmagnesium bromide or *n*-butyllithium in toluene at  $-78$  and  $0^{\circ}\text{C}$  gave a small amount of methanol-soluble but ether-insoluble solid. Its infrared spectrum (Fig. 4*b*) was of primary amide and quite different from that of the radical polymer (Fig. 4*a*). No methyl and methylene signals appeared in the NMR spectrum. The infrared spectra showed it to be identical with  $\alpha$ -pyridone prepared by acidifying anhydrous sodium 2-pyridinol. There is apparently cleavage of the very labile 2-pyridyl ester group and the resulting 2-pyridinol was converted to its tautomer,  $\alpha$ -pyridone, and isolated. The yield of  $\alpha$ -pyridone roughly corresponded to the amount of catalyst used. The unreacted monomer could be recovered from the ether-soluble portion after evaporation.

### References

1. W. T. Caldwell, F. T. Tyson, and L. Lauer, *J. Amer. Chem. Soc.* **66**, 1479 (1944).
2. W. R. Sorenson and T. W. Campbell, *Preparative Methods of Polymer Chemistry*, Interscience, New York, 1961, p. 49.
3. F. A. Bovey, *J. Polym. Sci.*, **46**, 59 (1960).
4. T. Otsu, T. Ito, and M. Imoto, *J. Polym. Sci. B*, **3**, 113 (1965).

KENJI YOKOTA  
MASAAKI SASAKI  
YOSHIO ISHII

Department of Synthetic Chemistry  
Faculty of Engineering  
Nagoya University  
Nagoya, Japan

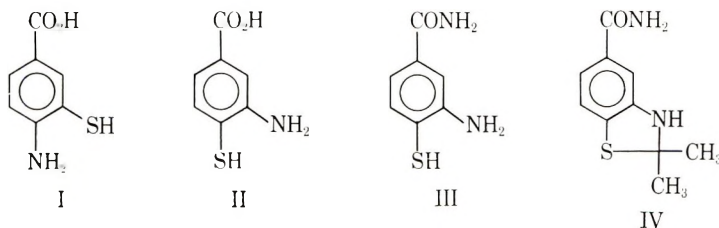
Received March 15, 1967  
Revised February 27, 1968

### Polybenzothiazoles. III. A-B Polymers

#### Introduction

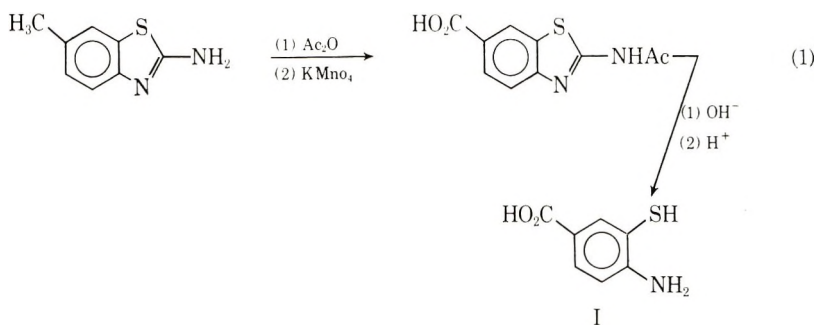
The successful synthesis of high molecular weight, thermally stable polybenzothiazoles (PBT) from AA-BB type reactants has been reported.<sup>1-3</sup> In addition, Imai and co-workers<sup>4</sup> have reported the successful polymerization of an A-B monomer, 3-mercapto-4-aminobenzoic acid hydrochloride, in polyphosphoric acid (PPA) to a high molecular weight thermally stable PBT. Kiprianov and Mushkalo<sup>5</sup> had previously attempted the preparation of PBT by melt condensation of two A-B monomers, 3-mercapto-4-aminobenzoic acid and its methyl ester, but failed due to decomposition during the polymerization.

This communication describes work on the preparation and subsequent polymerization of four A-B monomers: 3-mercapto-4-aminobenzoic acid (I), 3-amino-4-mercaptobenzoic acid (II), 3-amino-4-mercaptobenzamide (III), and 2,2-dimethylbenzothiazoline-5-carboxamide (IV).

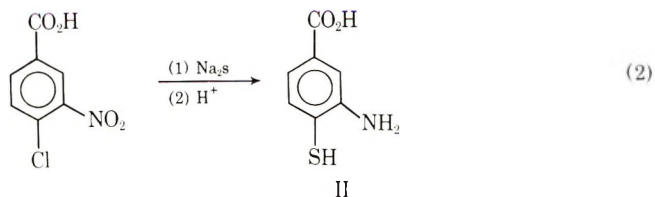


#### Discussion

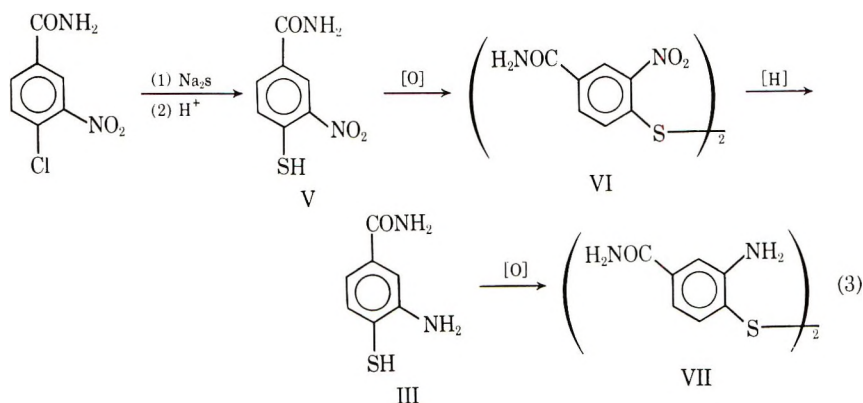
**Monomers.** 3-Mercapto-4-aminobenzoic acid (I) was prepared following Schubert's<sup>6</sup> method [eq. (1)].



3-Amino-4-mercaptobenzoic acid (II) was obtained in poor overall yields (20%) by the reaction of 3-nitro-4-chlorobenzoic acid with sodium sulfide [eq. (2)]:



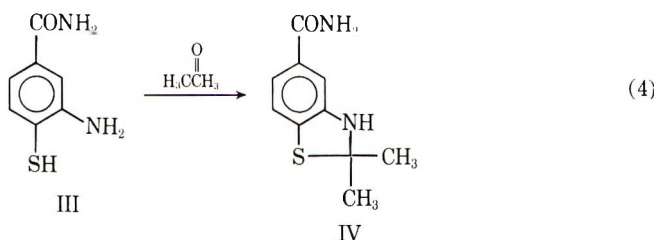
The major synthetic effort involved the preparation of 3-amino-4-mercaptobenzamide (III), a suspected processable A-B monomer, as shown in eq. (3):



Various reaction parameters were studied in an attempt to replace the chloro group of 3-nitro-4-chlorobenzamide using sodium sulfide followed by reduction of the nitro group to the desired A-B monomer without isolating the intermediate, 3-nitro-4-mercaptobenzamide (V) or its disulfide form (VI).

Complete replacement of the chloro group prior to reduction was unsuccessful and resulted in a crude product which was difficult to purify. Good overall yield (50%) of 3-amino-4-mercaptobenzamide (III) was obtained by isolating and purifying the intermediate, bis(2-nitro-4-carbamylphenyl) disulfide (VI), prior to hydrogenation in methanol, using platinum dioxide as catalyst. Although 3-mercapto-4-aminobenzoic acid displayed good stability toward air oxidation, extreme care was necessary to maintain 3-amino-4-mercaptobenzoic acid and its amide, once isolated, in an inert atmosphere because of the tendency to undergo air oxidation to the corresponding disulfide.

2,2-Dimethylbenzothiazoline-5-carboxamide was readily prepared by refluxing 3-amino-4-mercaptobenzamide (III) in acetone [eq. (4)]:



Characterization of the monomers and intermediate compounds is given in Table I.

**Polymers.** The A-B monomers were polymerized by melt and solution techniques. Melt polycondensations were performed by introducing a polymerization tube, containing the monomer under an argon atmosphere, into a preheated oil bath at a temperature about 30°C above the melting point of the monomer. A clear melt readily formed with the evolution of volatiles as the bath temperature was increased to 250°C during 1 hr and maintained at 250°C for 1 hr.

The resulting yellow to light brown intermediate polymers were removed from the polymerization tube, pulverized, and recharged. Heating was continued from 300°C to 400°C during 2 hr and at 400°C for 1 hr under argon. Decarboxylation was observed during the polymerization of the two carboxylic acid monomers as evidenced by passing the exit gases through an aqueous solution of barium hydroxide. Monomer I exhibited more decarboxylation than Monomer II although decarboxylation was slight in both cases. 3-Amino-4-mercaptobenzamide (III) was expected to yield a processable pre-polymer which could be subsequently advanced to high molecular weight polymer.

TABLE I  
Characterization of Monomers and Intermediates

Compound	Melting point, <sup>a</sup> °C	Formula	Elemental analysis <sup>b</sup>			
			% C	% H	% N	% S
I	204-205	C <sub>7</sub> H <sub>7</sub> N <sub>2</sub> O <sub>2</sub> S	49.71 (49.80)	4.23 (4.17)	8.15 (8.51)	19.14 (18.95)
II	149-150	C <sub>7</sub> H <sub>7</sub> N <sub>2</sub> O <sub>3</sub> S	49.66 (49.80)	4.17 (4.17)	8.27 (8.51)	19.06 (18.95)
III	153-154	C <sub>7</sub> H <sub>8</sub> N <sub>2</sub> OS	50.03 (49.98)	4.83 (4.79)	16.52 (16.66)	18.89 (19.06)
IV	144-144.5	C <sub>10</sub> H <sub>12</sub> N <sub>2</sub> OS	57.78 (57.76)	5.80 (5.76)	13.21 (13.45)	15.49 (15.40)
V	146-149	C <sub>7</sub> H <sub>6</sub> N <sub>2</sub> O <sub>3</sub> S	44.27 (42.41)	3.39 (3.05)	13.52 (14.14)	15.65 (16.18)
VI	259-262	C <sub>14</sub> H <sub>10</sub> N <sub>4</sub> O <sub>8</sub> S <sub>2</sub>	42.40 (42.63)	2.69 (2.56)	14.38 (14.21)	16.09 (16.26)
VII	265-267	C <sub>14</sub> H <sub>14</sub> N <sub>4</sub> O <sub>8</sub> S <sub>2</sub>	49.78 (50.01)	4.66 (4.23)	16.56 (16.80)	18.92 (19.20)

<sup>a</sup> Sealed tube.

<sup>b</sup> Calculated values in parentheses.

However, solidification occurred early in the initial heating phase to yield a yellow solid which exhibited very poor solubility and no true polymer melt temperature although slight softening above 300°C was observed. Employing phenol as a flux during the initial condensation stage failed to improve the tractability of the intermediate polymer. Monomer IV underwent self condensation to form a clear pale yellow melt which also rapidly resolidified to provide an intractable polymer. The molecular weight of the polymers prepared via the melt technique was relatively low as indicated by inherent viscosities of 0.23–0.31.

Solution polymerization of the four monomers was attempted in a variety of solvents such as *m*-cresol, *N,N*-dimethylacetamide, and PPA. Condensation in all solvents except PPA provided intractable yellow solids with inherent viscosities of 0.15–0.25. High molecular weight polymer was obtained in PPA by the following general procedure. Commercial grade PPA (100 g) was deoxygenated by bubbling argon through the acid at 170°C. The monomer (0.010 mol) was added to the cooled deoxygenated PPA under argon and stirred to 250°C during 2 hr and maintained at 250°C for 1 hr. The resulting viscous solution was poured into water in a Waring Blendor to precipitate a yellow solid which was thoroughly washed with aqueous sodium carbonate and water. A quantitative yield of polymer was obtained of substantially high molecular weight as indicated by inherent viscosities  $\sim 1.0$  dl/g.

Since the isolation of a processable system was unsuccessful, polymer characterization was limited to inherent viscosity, elemental analysis, and thermogravimetric analysis as reported in Table II. The thermal stabilities of the A-B polymers were excellent as

TABLE II  
Characterization of Polymers

Mono- mer	Method of preparation	$\eta_{inh.}$ dl/g <sup>a</sup>	PDT, <sup>b</sup> °C		Elemental analysis <sup>c</sup>			
			Air	Helium	% C	% H	% N	% S
I	Melt	0.23	575	640	—	—	—	—
	PPA	1.08	535	690	—	—	—	—
II	Melt	0.29	585	650	—	—	—	—
	PPA	1.29	540	680	—	—	—	—
III	Melt	0.31	600	675	62.85	2.40	10.66	23.89
	PPA	1.33	550	685	62.91	2.39	10.58	24.02
IV	Melt	0.24	580	640	62.96	2.31	10.61	23.96
	PPA	0.91	550	630	63.01	2.25	10.48	23.76

<sup>a</sup> Inherent viscosity (0.5% H<sub>2</sub>SO<sub>4</sub> at 25°C).

<sup>b</sup> Polymer decomposition temperature determined on Stanton Thermobalance at  $\Delta T$  of 6.67°C/min.

<sup>c</sup> Calculated for (C<sub>7</sub>H<sub>3</sub>NS)<sub>n</sub>: C, 63.13%; H, 2.27%; N, 10.52%; S, 24.08%.

indicated by polymer decomposition temperature (PDT) in air and in helium respectively of about 560°C and 650°C. As indicated by Marvel,<sup>7</sup> the thermal stability in air of polymers prepared in commercial grade PPA are adversely effected by impurities present in the PPA. This is further evidenced by the lower PDT of the A-B polymers prepared via solution polymerization in PPA versus melt polymerization.

This work was supported by the United States Navy under Contracts N0w 64-0524-c and N0w 66-0144-c monitored by the Bureau of Naval Weapons, Washington, D.C., and Contract N60921-67-C-0221 monitored by the Naval Ordnance Laboratory, Silver Springs, Maryland. The experimental work reported herein was conducted at Narmco Research and Development Division of Whittaker Corporation.

## References

1. P. M. Hergenrother, W. Wrasidlo, and H. H. Levine, *J. Polymer Sci. A*, **3**, 1665 (1965).
2. Y. Imai, I. Taska, K. Uno, and Y. Iwakura, *Makromol. Chem.*, **83**, 167 (1965).
3. P. M. Hergenrother and H. H. Levine, *J. Polymer Sci. A-1*, **4**, 2341 (1966).
4. Y. Imai, K. Uno, and Y. Iwakura, *Makromol. Chem.*, **83**, 179 (1965).
5. A. I. Kiprianov and I. L. Mushkalo, *J. Gen. Chem. (USSR)*, **32**, 4040 (1962).
6. M. Shubert, *Lieb. Ann. Chem.*, **558**, 29 (1947).
7. C. S. Marvel, private communication.

PAUL M. HERGENROTHER\*

Boeing Scientific Research Laboratories  
Seattle, Washington 98124

HAROLD H. LEVINE

Narmco Research & Development Division  
San Diego, California 92123

\* Address inquiries to this author.